Standard Model Extensions with an Extra Higgs Singlet:
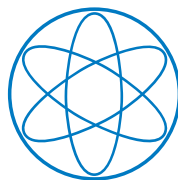
One-Loop Renormalization and Collider Phenomenology

Cyril Patrick Pietsch

Max-Planck-Institut für Physik
(Werner-Heisenberg-Institut)

München 2018

Technische Universität München
Max-Planck-Institut für Physik
(Werner-Heisenberg-Institut)

Standard Model Extensions with an Extra Higgs Singlet: One-Loop Renormalization and Collider Phenomenology

Cyril Patrick Pietsch

Vollständiger Abdruck der
von der Fakultät für Physik
der Technischen Universität München
zur Erlangung des akademischen Grades eines
Doktors der Naturwissenschaften (Dr. rer. nat.)
genehmigten Dissertation.

Vorsitzender: Prof. Dr. Lothar Oberauer
Prüfer der Dissertation: 1. Hon.-Prof. Dr. Wolfgang Hollik
                         2. Prof. Dr. Nora Brambilla

Die Dissertation wurde am 09.05.2018
bei der Technischen Universität München eingereicht und
durch die Fakultät für Physik am 18.06.2018 angenommen.

Abstract

In this thesis, the extension of the Standard Model by an extra Higgs singlet (EHS) Φ_h is investigated. The singlet exclusively couples to the standard sector via a renormalizable quartic Higgs-portal interaction term in the modified Higgs potential. Three scenarios are studied which differ by the related non-standard symmetry group under which Φ_h transforms. In the complex-Φ_h extension the scenarios are considered where Φ_h is charged under a local (EHSL model) or global (EHSG model) non-standard U(1) symmetry group. In the ab-initio real-Φ_h extension the scenario is considered where Φ_h transforms under a discrete non-standard $\mathcal{Z}_2$ symmetry group (EHSD model). In any case, the underlying non-standard symmetry is spontaneously broken by the non-vanishing vacuum expectation value of Φ_h.

A massive non-standard Abelian gauge field is part of the physical content of the EHSL model. It does not couple directly to the standard sector owing to an additionally postulated $\mathcal{Z}_2$ symmetry. In the EHSG model the imaginary part of Φ_h is a physical non-standard Goldstone boson. In each of the three considered models the real part of Φ_h mixes with the real part of the neutral component of the standard Higgs doublet due to the non-vanishing vacuum expectation value of Φ_h in the presence of the Higgs-portal coupling. It is assumed that one of the two associated scalar mass eigenstates is responsible for the resonance detected around 125 GeV by the experiments at the CERN Large Hadron Collider.

The Lagrangians of the three models are elaborated, full one-loop renormalization is performed, and a complete list of corresponding Feynman rules is established. Within the scope of perturbative unitarity theoretical bounds for the free model parameters are derived. In order to test the models by means of experimental measurements precise predictions for important observables accessible at collider experiments are calculated including one-loop quantum effects. Explicit results are provided for the most sensitive electroweak precision observables as well as for the significant Higgs observables: the partial decay widths, the total decay width and the branching ratios of the standard-like Higgs boson. With these, the free parameters of the three EHS models can be considerably constrained by comparing with experimental data.

Zusammenfassung

Diese Doktorarbeit befasst sich mit der Erweiterung des Standardmodells mit einem extra Higgs-Singlett (EHS) Φ_h. Das Singlett-Feld wechselwirkt mit dem Standardsektor ausschließlich über einen renormierbaren biquadratischen Higgs-Portal-Term im modifizierten Higgs-Potential. Es werden drei Szenarien analysiert, welche sich in der zugehörigen Nichtstandard-Symmetriegrupen unterscheiden, unter welcher Φ_h sich transformiert. In der Erweiterung mit komplexem Φ_h wird eine Nichtstandard-U(1)-Symmetriegruppe mit den beiden Varianten einer globalen U(1)-Symmetrie (EHSG-Modell) und einer lokalen U(1)-Eichsymmetrie (EHSL-Modell) betrachtet. In der Erweiterung mit einem ab-initio-reellen Feld Φ_h wird das Szenario betrachtet, in welchem Φ_h unter einer diskreten Nichtstandard-$\mathcal{Z}_2$-Symmetriegruppe transformiert (EHSD-Modell). In jedem Fall wird die zugrunde liegende Nichtstandard-Symmetrie spontan durch den nicht verschwindenden Vakuumerwartungswert von Φ_h gebrochen.

Zum physikalischen Inhalt des EHSL-Modells gehört ein massives Abelsches Nichtstandard-Eichfeld. Aufgrund einer zusätzlich postulierten $\mathcal{Z}_2$-Symmetrie koppelt dieses nicht direkt an den Standardsektor. Im EHSG-Modell liefert das komplexe Feld Φ_h ein physikalisches Nichtstandard-Goldstone-Boson. Wegen des nicht verschwindenden Vakuumerwartungswerts von Φ_h mischen sich in jedem der drei betrachteten Modelle der Realteil von Φ_h und der Realteil der neutralen Komponente des Standard-Higgs-Dubletts in Anwesenheit der Higgs-Portal-Kopplung. Es wird davon ausgegangen, dass einer der beiden zugehörigen skalaren Masse-Eigenzustände für die an den Experimenten am CERN Large Hadron Collider entdeckte Resonanz bei 125 GeV verantwortlich ist.

Die Lagrange-Dichten der drei Modelle werden ausgearbeitet, die zugehörige vollständige Renormierung auf dem Einschleifen-Niveau durchgeführt und eine Liste der kompletten Feynman-Regeln erstellt. Im Rahmen von perturbativer Unitarität werden theoretische Grenzen für die freien Modellparameter hergeleitet. Um die Modelle anhand von experimentellen Messungen zu testen, werden präzise Vorhersagen für relevante Observablen einschließlich der Einschleifen-Quantenkorrekturen berechnet und diskutiert. Für die sensitivsten elektroschwachen Präzisionsobservablen sowie für die signifikanten partiellen Zerfallsbreiten, die Gesamtzerfallsbreite und die Verzweigungsverhältnisse des standardartigen Higgs-Bosons werden explizit Ergebnisse bereitgestellt. Hiermit können die freien Parameter der drei betrachteten EHS-Modelle durch Vergleich mit experimentellen Daten deutlich eingeschränkt werden.

Contents

Chapter 1

Introduction

The ambitious and extensive search for a consistent theory of the fundamental interactions between the elementary constituents of matter has led to the contemporary formulation of the Standard Model (SM) of particle physics [1–10]. This renowned relativistic quantum field theory (QFT) is based on the gauge theories of the strong and electroweak interaction and incorporates spontaneous symmetry breaking in the electroweak sector according to the Higgs mechanism [6,7,11–15]. As a renormalizable QFT the SM allows to make precise predictions for measurable quantities. With remarkable success it has been validated by many experiments from low to high energy scales. After the discovery of a Higgs-like particle at the CERN Large Hadron Collider (LHC) by the ATLAS and CMS collaboration [16,17] in July 2012 it soon became clear that the observed state behaves like the SM Higgs boson [18]. This ground-breaking discovery corresponds to a milestone step towards a deeper understanding of the mechanism providing masses to the fundamental particles. With the accurately measured mass of the Higgs boson, $M_H^{\text{exp}} = 125.09 \pm 0.24$ GeV [19], the entire input of the SM is determined and the sensitivity to physics beyond the SM is increased.

In fact, physics beyond the SM is required in order to address remaining unresolved problems of crucial importance in elementary particle physics which subsist both from a theoretical and an experimental point of view: the missing link to gravity, the size of the observed baryon asymmetry in the universe [20], the strong CP problem [21], the origin of dark matter [22,23] and dark energy [24]. There are also some secondary issues like e.g. a potential instability of the electroweak vacuum [25] in the SM with reference to the measured values of the Higgs-boson and top-quark mass. In order to tackle these issues theorists both seek for a more fundamental theory (which incorporates the SM as an effective theory in the low energy limit) and investigate the phenomenological impact of extensions of the SM.

Since the Higgs sector is currently the least understood part of the SM, even after the discovery in 2012, extensions of the SM naturally go along with modifications of the scalar sector still compatible with experimental data. The minimal extensions of the SM with an augmentation of the Higgs sector are of the type "Higgs portal" and involve an extra scalar field. The minimal Higgs-portal extensions of the SM just involve an additional Higgs singlet [26–77]. In that context, it is assumed that the observed spin-

zero particle brings along modified couplings to the well-known standard sector and/or new couplings to a hidden (non-standard) sector. The standard-like scalar might be produced and decay in more involved ways but nevertheless pretend to be the SM Higgs boson within the current limits of experimental accuracy. Precise predictions for ongoing and future experimental investigations are required for testing the theoretical concepts.

In this thesis, the minimal extension of the SM Higgs sector by one additional scalar singlet field Φ_h is investigated up to the one-loop level in various classes of models with different realizations of the hidden sector associated with the singlet Φ_h. The extra Higgs singlet (EHS) is assumed to be "hidden", i.e. completely neutral with respect to the symmetry group of the SM. The only coupling to the standard sector occurs via a renormalizable quartic interaction term of the form $(\Phi_s^\dagger \Phi_s)(\Phi_h^\dagger \Phi_h)$, the portal, with the standard doublet Φ_s in the enlarged Higgs potential.

Three distinct scenarios are studied which differ by the underlying non-standard symmetry group (the hidden symmetry) and the corresponding particle content. It is assumed that the hidden symmetry is spontaneously broken by a non-zero vacuum expectation value (vev) v_h of the scalar singlet Φ_h. The singlet field itself can be complex or real; accordingly, the hidden symmetry is either continuous or discrete. For these two settings the simplest non-standard symmetry groups under which Φ_h can transform are examined.

Regarding the version with a complex Φ_h, the scenario is studied where v_h spontaneously breaks a hidden U(1) symmetry group $\mathrm{U}(1)_{Y_h}$. The hidden hypercharge Y_h can be considered the generator of either a global or a local $\mathrm{U}(1)_{Y_h}$. The scenario with the global symmetry is denoted as EHSG model, the other one with the local symmetry as EHSL model. In the version where the field Φ_h is real, the hidden symmetry under which Φ_h transforms is restricted to be a discrete one. This third scenario is called EHSD model and the related discrete hidden symmetry group is denoted as $\mathcal{Z}_2^{\mathrm{D}}$.

In the EHSL scenario, with a broken local $\mathrm{U}(1)_{Y_h}$ gauge symmetry, an extra non-standard gauge field Z' appears which is neutral under the SM gauge group. Kinetic mixing with the standard B-field is basically possible and would yield another connection to the standard sector. It is prevented when invariance of the Lagrangian under a non-standard $\mathcal{Z}_2$ symmetry group, labeled as $\mathcal{Z}_2^{\mathrm{L}}$, is imposed.

The three models have different physical contents. In the EHSG model the breaking of the global $\mathrm{U}(1)_{Y_h}$ symmetry leads to a massless Goldstone boson, described by the imaginary part φ_h of Φ_h. In the EHSL model the field φ_h is unphysical as it can be gauged away by means of the local $\mathrm{U}(1)_{Y_h}$. It yields the longitudinal polarization state of the Z' boson by the Higgs mechanism, providing also a mass $M_{Z'}$ which will be treated as a free parameter. Finally, neither the Z' nor the φ_h boson exists in the EHSD model where Φ_h is real ab initio.

Still, there is a significant characteristic feature the three models have in common. Due to the non-vanishing hidden vev v_h in each of these models the real part of Φ_h mixes with the real part of the neutral component of Φ_s in the case of a coupled hidden sector. Therefore, the two associated scalar mass eigenstates H_1 and H_2 with corresponding masses M_{H_1} and M_{H_2} both consist of a standard and a non-standard field component.

The intrinsic mixing is parametrized by an angle α and vanishes in the decoupling limit $\alpha \to 0$ which brings us back to the SM phenomenology. The field H_1 is chosen to be the standard-like scalar found by the LHC experiments and consequently its mass is fixed to $M_{H_1} = M_H^{\text{exp}}$. In each of the three models the non-standard parameters α, M_{H_2} and v_{h} are treated as free parameters.

At the cost of a few extra parameters these EHS extensions could solve some of the open questions of the SM. This in particular holds for the EHSL model. By absence of kinetic mixing it provides a stable dark-matter candidate, the Z' boson which is compatible with the established experimental constraints for dark matter [42]. The EHSL model is even capable of simultaneously generating a strong first-order electroweak phase transition as required for effective electroweak baryogenesis [42] — an especially promising explanation of baryon asymmetry in our universe. Furthermore, the instability or metastability of the electroweak vacuum can be eliminated by the EHSL model [43]. Consequently, the EHSL model is a paradigm of a promising minimal SM extension by which future discoveries at collider experiments could also be related to important aspects of cosmology.

In either of the three considered models the second (non-standard type) Higgs boson H_2 does not represent a stable dark-matter candidate unless tiny mixing angles α are considered. For such miniscule mixing, however, the models become less interesting from a phenomenological point of view. Still, also in the absence of a gauged non-standard sector the singlet extension of the SM remains attractive and may likewise account for the stabilization of the electroweak vacuum [35, 39], for improved fits with the experimental data and for future discoveries. The respective models may also be considered as part of more involved extensions of the SM. Hence, a comparison of the EHSL, EHSG and EHSD model predictions for observables beyond the leading order (LO) in perturbation theory is desirable for higher precision. In this work, we carry out this task for the first time.

At LO in perturbation theory the EHSL and EHSD models have been studied earlier with primary focus on constraints from perturbativity, vacuum stability, dark-matter and collider phenomenology [27–43]. Models with a real singlet have been studied at the one-loop level [51–53]. The one-loop renormalization of the EHSD model has been addressed in [51].

Here, we work out the Lagrangians of the EHSL, EHSG and EHSD models with particular focus on gauge invariance, respectively BRS invariance and quantization. Furthermore, we derive corresponding exclusion bounds from tree-level perturbative unitarity. In this thesis we establish new one-loop renormalization schemes for the EHSL, EHSG and EHSD models which enable a convenient comparison of corresponding next-to-leading order (NLO) predictions. Our renormalization schemes moreover cover the associated unphysical sectors such that all the Green functions are properly renormalized. The complete list of corresponding Feynman rules including counterterms is specified in the appendix. Related `FeynArts` [78] model files for automatic calculations in the three models have been created.

The non-standard parameter space associated with an extended Higgs sector can often be constrained indirectly from experimental precision data by exploring the impact

of associated non-standard quantum effects. In the EHSD model it has been shown that the prediction for the W-boson mass M_W is quite sensitive to non-standard one-loop contributions of the extended scalar sector [52]. The related impact on further electroweak precision observables (EWPOs) has been discussed in [53]. In that regard, only the non-standard parameters α and M_{H_2} play a role. At the one-loop level the fields Z' and $\varphi_{\rm h}$ do not contribute to EWPOs, hence the corresponding predictions are the same in the three models under consideration. We improve the calculation of EWPOs by taking into account the feedback on the standard contributions from the shift in M_W due to non-standard contributions in the loop terms. We furthermore take into account the (so far neglected) non-standard one-loop effects in the couplings of the Z boson to fermions. We perform a $\Delta\chi^2$ analysis which combines our non-standard NLO predictions for the most sensitive EWPOs M_W, $\sin^2\theta_{\rm eff}^{\rm lep}$ (effective leptonic mixing angle) and $A_{\rm FB}^{0,b}$ (forward-backward pole asymmetry of the Z decay into a pair of b quarks) and hereby obtain bounds complementary to the constraints from unitarity.

Finally, we focus on observables related to the decays of the H_1 boson in the three models and apply our renormalization schemes to calculate the one-loop contributions to the relevant decay rates that are studied by the LHC experiments. In this way we obtain new NLO predictions for the significant fermionic two-body partial widths $\Gamma(H_1 \to b\bar{b})$, $\Gamma(H_1 \to c\bar{c})$ and $\Gamma(H_1 \to \tau\bar{\tau})$ into b quarks, c quarks and τ leptons. Moreover, we provide new predictions for the inclusive four-body partial widths $\Gamma(H_1 \to VV \to 4f)$ into fermion pairs via the exchange of two standard gauge bosons $V = W, Z$. A new (basically model-independent) formula is derived in order to include the dominant non-standard one-loop corrections which stem from the associated renormalized H_1VV-vertex corrections.

Besides these decay modes of the H_1 boson into SM particles, there are also decay channels into non-standard particles, depending in detail on the specific type of the EHS models. For masses $M_{H_2} < M_{H_1}/2$ the decay channel $H_1 \to H_2H_2$ is open in all three model classes. For the EHSG model with a physical Goldstone boson the decay $H_1 \to \varphi_{\rm h}\varphi_{\rm h}$ is always possible for non-zero mixing. In the EHSL model with gauged $\mathrm{U}(1)_{Y_{\rm h}}$ symmetry the hidden Goldstone bosons are unphysical, instead, the decay mode $H_1 \to Z'Z'$ occurs for sufficiently low masses of the $\mathrm{U}(1)_{Y_{\rm h}}$ gauge boson Z'. For all these cases we calculate the partial widths including the one-loop contributions in the specific models for the first time.

The heavy-to-light Higgs partial width $\Gamma(H_1 \to H_2H_2)$ has already been studied at the one-loop level in the EHSD model [51]. Here, we complete the NLO contributions by including the residual loops arising in the models EHSL and EHSG and show that associated one-loop effects from the EHSL non-standard gauge sector are in general non-negligible.

The new decay channels $H_1 \to Z'Z'$ and $H_1 \to \varphi_{\rm h}\varphi_{\rm h}$ occur only in the EHSL and EHSG models. The partial width $\Gamma(H_1 \to Z'Z')$ in the limit of massless Z' bosons turns into the partial width $\Gamma(H_1 \to \varphi_{\rm h}\varphi_{\rm h})$ as a consequence of the equivalence theorem. An explicit calculation and comparison confirms this limit at the NLO level, and thus underlines the consistency of our renormalization schemes.

Summing up all the individual decay channels yields the total width $\Gamma_{\rm tot}^{H_1}$ of the

H_1 boson, including the respective one-loop contributions. Finally, we provide new one-loop predictions for $\Gamma_{\text{tot}}^{H_1}$ and the branching ratios $\text{BR}(H_1 \to \text{X}_i)$ into the various standard-particle final states ($\text{X}_i = ZZ, WW, AA, AZ, gg, \tau\bar{\tau}, b\bar{b}, c\bar{c}$), including also photons A and gluons g. Together with recent experimental bounds for the total width and signal strengths of the standard-like Higgs boson [79] these results can be used to considerably constrain the non-standard parameter ranges associated with the EHSL, EHSG and EHSD models.

This work is structured in the following way: In Chapter 2 we recall the formulation of the electroweak Standard Model. In Chapter 3 we describe the theoretical frameworks of the EHSL, EHSG and EHSD models. Proceeding from the Lagrangian of the EHSL model we emphasize the differences between the three models and highlight their interconnection. In Chapter 4 we derive the bounds for the non-standard parameters from tree-level perturbative unitarity. The one-loop renormalization of the three models is worked out in Chapter 5. We examine the impact of associated non-standard one-loop contributions on the predictions for EWPOs in Chapter 6. The decays of H_1 are presented and discussed in Chapter 7. Conclusions are given in Chapter 8. In Appendix A we provide the full list of Feynman rules for the one-loop renormalized EHSL, EHSG and EHSD models. A distinguished set of Ward identities from the hidden U(1) is specified in Appendix B. It contains relations between scalar n-point vertex functions and counterterms for checks of consistency in the EHSG model and in the limiting case of a vanishing hidden gauge coupling in the EHSL model. Appendix C collects further numerical results for the H_1-decay observables in completion of those discussed in Chapter 7.

Chapter 2

The electroweak Standard Model

In this chapter the theoretical framework of the electroweak Standard Model (in the following abbreviated by SM) is summarized. Here, we do not intend to describe the latter in detail but rather want to illustrate the conventions we use in this work with respect to the standard sector. For a more extensive treatment of the SM see e.g. [80–83].

2.1 The classical Lagrangian

The SM describes the electroweak interactions within the framework of a QFT which is gauge invariant under the symmetry group $SU(2)_W \times U(1)_Y$. This symmetry group is spontaneously broken by the Higgs mechanism, which among others predicts a physical massive scalar particle − the infamous Higgs boson. As a consequence of electroweak symmetry breaking, the desired mass terms for the gauge bosons of the broken subgroups are generated, as well as mass terms for the fundamental fermions via Yukawa couplings. The Lorentz- and gauge-invariant classical Lagrangian $\mathcal{L}_{SM}^{cl}$ of the SM is made up of a gauge part $\mathcal{L}_{SM}^{G}$, a fermionic part $\mathcal{L}_{SM}^{F}$ and a Higgs part $\mathcal{L}_{SM}^{\Phi}$,

$$\mathcal{L}_{SM}^{cl} = \mathcal{L}_{SM}^{G} + \mathcal{L}_{SM}^{F} + \mathcal{L}_{SM}^{\Phi}, \tag{2.1.1}$$

which will be defined one by one in the following.

2.1.1 Gauge part

The non-Abelian gauge group $SU(2)_W \times U(1)_Y$ is generated by the weak isospin operators I^a ($a = 1, 2, 3$) and the weak hypercharge operator Y.[1] For each of those generators there exists a dedicated vector field which transforms according to the adjoint representation of the corresponding gauge group. Accordingly, we introduce a triplet of vector fields W_μ^a associated with I^a and a singlet vector field B_μ belonging to Y. In the following, g_2 and g_1 represent the gauge coupling constants of $SU(2)_W$

---

[1] With I^a and Y acting on a field X, the corresponding representation matrices I_X^a and weak hypercharge Y_X are obtained.

and $\mathrm{U}(1)_Y$. Furthermore, ϵ^{abc} are the structure constants corresponding to the Lie algebra of $\mathrm{SU}(2)_\mathrm{W}$. The above-mentioned vector fields form the associated field strength tensors, defined as

$$
\begin{aligned}
W^a_{\mu\nu} &= \partial_\mu W^a_\nu - \partial_\nu W^a_\mu + g_2\epsilon^{abc}W^b_\mu W^c_\nu, \\
B_{\mu\nu} &= \partial_\mu B_\nu - \partial_\nu B_\mu,
\end{aligned}
\tag{2.1.2}
$$

such that the gauge part of the classical Lagrangian can be written as

$$
\mathcal{L}^\mathrm{G}_\mathrm{SM} = -\frac{1}{4}W^a_{\mu\nu}W^{a,\mu\nu} - \frac{1}{4}B_{\mu\nu}B^{\mu\nu}.
\tag{2.1.3}
$$

According to the principle of minimal substitution, the covariant derivative

$$
D_\mu = \partial_\mu - ig_2 I^a W^a_\mu + ig_1 \frac{Y}{2}B_\mu
\tag{2.1.4}
$$

determines the interaction of the gauge fields with fields corresponding to $\mathcal{L}^\mathrm{F}_\mathrm{SM}$ and $\mathcal{L}^\Phi_\mathrm{SM}$, as shown in the following.

2.1.2   Fermionic part

The left-handed leptons (L'_i) and quarks (Q'_i) of each generation i are doublets,

$$
L'^\mathrm{L}_i = \omega_- L'_i = \begin{pmatrix} \nu'^\mathrm{L}_i \\ l'^\mathrm{L}_i \end{pmatrix}, \qquad Q'^\mathrm{L}_i = \omega_- Q'_i = \begin{pmatrix} u'^\mathrm{L}_i \\ d'^\mathrm{L}_i \end{pmatrix},
\tag{2.1.5}
$$

the right-handed fermions are singlets,

$$
l'^\mathrm{R}_i = \omega_+ l'_i, \qquad u'^\mathrm{R}_i = \omega_+ u'_i, \qquad d'^\mathrm{R}_i = \omega_+ d'_i,
\tag{2.1.6}
$$

under $\mathrm{SU}(2)_\mathrm{W}$. Here, $\omega_\pm = \frac{1\pm\gamma_5}{2}$ are the projectors on the right- and left-handed fields. The fermion fields introduced in (2.1.5) and (2.1.6) are weak eigenstates, which is marked by the prime index. The symbol ν stands for a neutrino, l for a charged lepton, u for an up-type and d for a down-type quark. These fundamental fermions are classified by the quantum numbers of the weak isospin I, its third component I^3 and the weak hypercharge Y. The latter is chosen such that for each fermion the associated electric charge can be derived from the Gell-Mann-Nishijima relation

$$
Q = I^3 + \frac{Y}{2},
\tag{2.1.7}
$$

which defines the generator of the electric charge Q. The left-handed (right-handed) fermion fields are related to the fundamental (trivial) representation of $\mathrm{SU}(2)_\mathrm{W}$ with $I^a = \tau^a/2$ ($I^a = 0$), where τ^a are the Pauli matrices. Here, we consider the minimal formulation of the SM in which no right-handed neutrinos are considered. Therefore, all the neutrinos remain massless after electroweak symmetry breaking. The kinetic terms of the fermions as well as the couplings of the fermions to the gauge sector are comprised in the fermionic part $\mathcal{L}^\mathrm{F}_\mathrm{SM}$ of the classical Lagrangian, which reads (Feynman slash notation)

$$
\mathcal{L}^\mathrm{F}_\mathrm{SM} = \sum_i \left(\overline{L}_i'^\mathrm{L} i\!\!\not{D} L_i'^\mathrm{L} + \overline{Q}_i'^\mathrm{L} i\!\!\not{D} Q_i'^\mathrm{L} + \overline{l}_i'^\mathrm{R} i\!\!\not{D} l_i'^\mathrm{R} + \overline{u}_i'^\mathrm{R} i\!\!\not{D} u_i'^\mathrm{R} + \overline{d}_i'^\mathrm{R} i\!\!\not{D} d_i'^\mathrm{R} \right),
\tag{2.1.8}
$$

with D_μ specified by (2.1.4).

2.1.3 Higgs part

In order to obtain massless photons but massive W and Z bosons, we have to break the $\mathrm{SU}(2)_\mathrm{W} \times \mathrm{U}(1)_Y$ gauge symmetry such that the electromagnetic subgroup $\mathrm{U}(1)_\mathrm{em}$ remains unbroken. In order to achieve this target one applies the Higgs mechanism, which in turn also generates the masses of the fermions as soon as the above-mentioned Yukawa couplings are introduced. Hence, the desired mass terms for the gauge bosons and fermions are obtained by adding the Higgs part

$$
\begin{aligned}
\mathcal{L}_\mathrm{SM}^\Phi = {} & (D_\mu \Phi)^\dagger (D^\mu \Phi) - V(\Phi) \\
& - \sum_{i,j} \left(\overline{L}_i'^\mathrm{L} G_{ij}^l l_j'^\mathrm{R} \Phi + \overline{Q}_i'^\mathrm{L} G_{ij}^u u_j'^\mathrm{R} \tilde{\Phi} + \overline{Q}_i'^\mathrm{L} G_{ij}^d d_j'^\mathrm{R} \Phi + \mathrm{h.c.} \right)
\end{aligned}
\tag{2.1.9}
$$

to the classical Lagrangian. At this point a weak-isospin doublet

$$
\Phi(x) = \begin{pmatrix} \phi^+(x) \\ \phi^0(x) \end{pmatrix}
\tag{2.1.10}
$$

with hypercharge $Y = 1$ is introduced. The Higgs doublet Φ is composed of two complex scalar fields ϕ^+ and ϕ^0. The charge conjugated Higgs doublet $\tilde{\Phi}$ is defined by $\tilde{\Phi} = i\tau^2 \Phi^*$. More explicitly, the Higgs potential $V(\Phi)$ in (2.1.9) reads

$$
V(\Phi) = -\mu^2 \Phi^\dagger \Phi + \frac{\lambda}{4} \left(\Phi^\dagger \Phi \right)^2, \qquad \mu^2, \lambda > 0.
\tag{2.1.11}
$$

In this parametrization, the coupling λ must be positive in order to confine the energy from below and the mass parameter μ^2 has to be positive such that Φ acquires a non-vanishing vacuum expectation value (vev) by minimizing (2.1.11):

$$
\langle \Phi \rangle = \frac{1}{\sqrt{2}} \begin{pmatrix} 0 \\ v \end{pmatrix}, \qquad v = \frac{2\mu}{\sqrt{\lambda}}.
\tag{2.1.12}
$$

This non-vanishing vev v is essential for the desired electroweak symmetry breaking. Expanded around this ground state we can write Φ as

$$
\Phi(x) = \begin{pmatrix} \phi^+(x) \\ \frac{1}{\sqrt{2}} \left[v + H(x) + i\varphi(x) \right] \end{pmatrix},
\tag{2.1.13}
$$

where the component fields $H(x)$, $\phi^+(x)$ and $\varphi(x)$ have a vanishing vev. In the following, $\phi^-(x)$ represents the adjoint of $\phi^+(x)$. The fields $\phi^\pm(x)$ and $\varphi(x)$ are the would-be Goldstone bosons $-$ unphysical degrees of freedom, since these fields can be removed by a gauge transformation. In contrast, the Higgs field $H(x)$ describes physical scalar particles that are neutral with respect to the electric charge and have corresponding mass

$$
M_H = \sqrt{2}\mu.
\tag{2.1.14}
$$

The scalar fields $H, \phi^\pm$ and φ have triple and quartic self-couplings determined by the potential (2.1.11). The couplings of the fields $H, \phi^\pm$ and φ to the gauge fields are

determined by the first term in (2.1.9), namely the kinetic term of Φ, according to minimal substitution. In the second line of (2.1.9) the Yukawa part of $\mathcal{L}_{\mathrm{SM}}^{\Phi}$ is specified. It consists of terms involving the Yukawa-coupling matrices G^f $(f = l, u, d)$ which provide couplings of the scalar component fields to the fermion sector as well as mass terms for the up-type quarks, the down-type quarks and the charged leptons.

2.1.4   Gauge invariance

The classical Lagrangian $\mathcal{L}_{\mathrm{SM}}^{\mathrm{cl}}$ as given above is invariant under the gauge transformations

$$\mathbf{T}_{\mathrm{W}}(x) = \exp\left[i\frac{\tau^a}{2}\theta^a(x)\right], \qquad \mathbf{T}_Y(x) = \exp\left[-i\frac{Y}{2}\theta^Y(x)\right], \tag{2.1.15}$$

with the local transformation parameters θ^a and θ^Y corresponding to $\mathrm{SU}(2)_{\mathrm{W}}$ and $\mathrm{U}(1)_Y$. Under the (combined) transformations (2.1.15) the Higgs doublet behaves like

$$\Phi(x) \rightarrow \mathbf{T}_{\mathrm{W}}(x)\mathbf{T}_Y(x)\Phi(x), \tag{2.1.16}$$

and the left-handed and right-handed fermions transform according to

$$\begin{aligned}
\Psi_i'^{\mathrm{L}}(x) &\rightarrow \mathbf{T}_{\mathrm{W}}(x)\mathbf{T}_Y(x)\Psi_i'^{\mathrm{L}}(x), \qquad (\Psi_i' = L_i', Q_i'), \\
\psi_i'^{\mathrm{R}}(x) &\rightarrow \mathbf{T}_Y(x)\psi_i'^{\mathrm{R}}(x), \qquad (\psi_i' = l_i', u_i', d_i').
\end{aligned} \tag{2.1.17}$$

Finally, the vector bosons act as

$$\begin{aligned}
B_\mu(x)\frac{Y}{2} &\rightarrow \mathbf{T}_Y(x)\left[B_\mu(x)\frac{Y}{2} - i\frac{1}{g_1}\partial_\mu\right]\mathbf{T}_Y^{\dagger}(x), \\
W_\mu^a(x)\frac{\tau^a}{2} &\rightarrow \mathbf{T}_{\mathrm{W}}(x)\left[W_\mu^a(x)\frac{\tau^a}{2} + i\frac{1}{g_2}\partial_\mu\right]\mathbf{T}_W^{\dagger}(x),
\end{aligned} \tag{2.1.18}$$

according to the rule of minimal substitution. In infinitesimal form (2.1.16), (2.1.17) and (2.1.18) read

$$\begin{aligned}
\Phi(x) &\rightarrow \left[1 - i\frac{1}{2}\delta\theta^Y(x) + i\frac{\tau^a}{2}\delta\theta^a(x)\right]\Phi(x), \\
\Psi_i'^{\mathrm{L}}(x) &\rightarrow \left[1 - i\frac{Y}{2}\delta\theta^Y(x) + i\frac{\tau^a}{2}\delta\theta^a(x)\right]\Psi_i'^{\mathrm{L}}(x), \\
\psi_i'^{\mathrm{R}}(x) &\rightarrow \left[1 - i\frac{Y}{2}\delta\theta^Y(x)\right]\psi_i'^{\mathrm{R}}(x), \\
B_\mu(x) &\rightarrow B_\mu(x) + \frac{1}{g_1}\partial_\mu\delta\theta^Y(x), \\
W_\mu^a(x) &\rightarrow W_\mu^a(x) + \frac{1}{g_2}\partial_\mu\delta\theta^a(x) + \epsilon^{abc}W_\mu^b(x)\delta\theta^c(x).
\end{aligned} \tag{2.1.19}$$

2.1.5 Physical basis

As specified above, the classical Lagrangian $\mathcal{L}_{\mathrm{SM}}^{\mathrm{cl}}$ depends on the following set of original parameters: the gauge coupling constants g_1 and g_2, the Yukawa coupling constants G_{ij}^f and the Higgs-potential parameters μ^2 and λ. This set can be replaced by an equivalent set of physical parameters corresponding to the physical fields of the theory. In order to identify the latter, the mass matrices for the gauge fields as well as for the charged leptons, the up-type and the down-type quarks have to be diagonalized.

Mass-eigenstate basis of the gauge bosons

For the gauge sector we obtain the mass eigenstates $W_\mu^\pm$, Z_μ and A_μ as a linear combination of the original gauge fields W_μ^a $(a = 1, 2, 3)$ and B_μ from

$$W_\mu^\pm = \frac{1}{\sqrt{2}} \left(W_\mu^1 \mp i W_\mu^2 \right) \tag{2.1.20}$$

and

$$\begin{pmatrix} Z_\mu \\ A_\mu \end{pmatrix} = \begin{pmatrix} \cos\theta_W & \sin\theta_W \\ -\sin\theta_W & \cos\theta_W \end{pmatrix} \begin{pmatrix} W_\mu^3 \\ B_\mu \end{pmatrix}. \tag{2.1.21}$$

The resulting masses for the physical W bosons $(W_\mu^\pm)$, Z bosons (Z_μ) and photons (A_μ) are

$$M_W = \frac{v}{2} g_2, \qquad M_Z = \frac{v}{2} \sqrt{g_1^2 + g_2^2}, \qquad M_A = 0. \tag{2.1.22}$$

The electroweak mixing angle θ_W introduced in (2.1.21) is related to the masses of the W and Z bosons as follows,

$$\cos\theta_W = \frac{g_2}{\sqrt{g_1^2 + g_2^2}} = \frac{M_W}{M_Z}. \tag{2.1.23}$$

We also have

$$\sin\theta_W = \frac{g_1}{\sqrt{g_1^2 + g_2^2}}, \tag{2.1.24}$$

and for convenience the abbreviations $s_W \equiv \sin\theta_W$ and $c_W \equiv \cos\theta_W$ are used in the following. Matching to QED, the elementary electric charge $e = \sqrt{4\pi\alpha_{\mathrm{em}}}$ can be related to g_1 and g_2 as

$$e = \frac{g_1 g_2}{\sqrt{g_1^2 + g_2^2}}. \tag{2.1.25}$$

Mass-eigenstate basis of the fermions

With the help of a bi-unitary transformation $U_{ij}^{f,\mathrm{L/R}}$ of the left/right-handed fermion fields, the mass matrices for charged leptons l_i', up-type quarks u_i' and down-type quarks d_i' can be diagonalized. As a result, we obtain the fermion mass eigenstates

$$f_i^{\mathrm{L}} = \sum_j U_{ij}^{f,\mathrm{L}} f_j'^{\mathrm{L}}, \qquad f_i^{\mathrm{R}} = \sum_j U_{ij}^{f,\mathrm{R}} f_j'^{\mathrm{R}}, \tag{2.1.26}$$

with corresponding masses

$$m_{f,i} = \frac{v}{\sqrt{2}} \sum_{j,k} U_{ij}^{f,\mathrm{L}} G_{jk}^f U_{ki}^{f,\mathrm{R}\dagger}. \tag{2.1.27}$$

In order to denote fermionic mass eigenstates, we stick to the notation for the related weak eigenstates introduced in (2.1.5) and (2.1.6) but drop the corresponding prime index.

As already stated before, the neutrinos remain massless since no right-handed neutrinos are present in the minimal formulation of $\mathcal{L}_{\mathrm{SM}}^{\mathrm{cl}}$. Due to this zero-mass degeneracy in the neutrino sector we are free to choose the corresponding transformation $U_{ij}^{\nu,\mathrm{L}}$ such that related charged-current interactions are diagonal. This defines the physical neutrino states

$$\nu_i^{\mathrm{L}} = \sum_j U_{ij}^{l,\mathrm{L}} \nu_j'^{\mathrm{L}}. \tag{2.1.28}$$

Transforming into the fermionic mass-eigenstate basis generates one remaining non-trivial 3×3 matrix, the quark-mixing matrix $\mathbf{V}$ [10], given by

$$\mathbf{V} = U^{u,\mathrm{L}} U^{d,\mathrm{L}\dagger}. \tag{2.1.29}$$

At the tree-level $\mathbf{V}$ only appears in the charged-current interaction between quarks and the W boson. Tree-level interactions between fermions and the neutral gauge bosons cannot trigger flavour-changing neutral currents since the unitary transformation matrices $U^{f,\mathrm{L/R}}$ drop out in the associated vertices.

Gauge transformations of the mass eigenstates

For the sake of completeness, we also provide the infinitesimal gauge transformations listed in (2.1.19) in the physical basis. Introducing the related fields and parameters as specified above, we obtain the corresponding transformations of the scalar component fields,

$$
\begin{aligned}
H &\to H + \frac{e}{2s_W c_W} \varphi \, \delta\theta^Z + \frac{ie}{2s_W} \left[\phi^+ \delta\theta^- - \phi^- \delta\theta^+ \right], \\
\varphi &\to \varphi - \frac{e}{2s_W c_W} [v + H] \, \delta\theta^Z + \frac{e}{2s_W} \left[\phi^+ \delta\theta^- + \phi^- \delta\theta^+ \right], \\
\phi^\pm &\to \phi^\pm \mp ie \, \phi^\pm \left[\delta\theta^A + \frac{s_W^2 - c_W^2}{2s_W c_W} \delta\theta^Z \right] \pm \frac{ie}{2s_W} [v + H \pm i\varphi] \, \delta\theta^\pm,
\end{aligned}
\tag{2.1.30}
$$

of the left- and right-handed fermion fields $\psi_{i,\pm}^{\mathrm{L}}$ and ψ_i^{R} with associated electric charges $Q_{\psi_{i,\pm}^{\mathrm{L}}}$ and $Q_{\psi_i^{\mathrm{R}}}$,

$$
\begin{aligned}
\psi_{i,\pm}^{\mathrm{L}} \to \psi_{i,\pm}^{\mathrm{L}} - ie \left[Q_{\psi_{i,\pm}^{\mathrm{L}}} \delta\theta^A + \frac{s_W}{c_W} \left(Q_{\psi_{i,\pm}^{\mathrm{L}}} \mp \frac{1}{2s_W^2} \right) \delta\theta^Z \right] \psi_{i,\pm}^{\mathrm{L}} & \\
+ \frac{ie}{\sqrt{2}s_W} \delta\theta^\pm v_{ij}^\pm \psi_{j,\mp}^{\mathrm{L}}, \qquad (\Psi_i^{\mathrm{L}} \equiv (\psi_{i,+}^{\mathrm{L}}, \psi_{i,-}^{\mathrm{L}})^{\mathsf{T}} = L_i^{\mathrm{L}}, Q_i^{\mathrm{L}}), & \quad (2.1.31) \\
\psi_i^{\mathrm{R}} \to \psi_i^{\mathrm{R}} - ie\, Q_{\psi_i^{\mathrm{R}}} \left(\delta\theta^A + \frac{s_W}{c_W} \delta\theta^Z \right) \psi_i^{\mathrm{R}}, \qquad (\psi_i^{\mathrm{R}} = u_i^{\mathrm{R}}, d_i^{\mathrm{R}}, l_i^{\mathrm{R}}), &
\end{aligned}
$$

as well as of the gauge bosons,

$$
\begin{aligned}
A_\mu &\to A_\mu + \partial_\mu \delta\theta^A + ie \left[W_\mu^+ \delta\theta^- - W_\mu^- \delta\theta^+ \right], \\
Z_\mu &\to Z_\mu + \partial_\mu \delta\theta^Z - ie\frac{c_W}{s_W} \left[W_\mu^+ \delta\theta^- - W_\mu^- \delta\theta^+ \right], \\
W_\mu^\pm &\to W_\mu^\pm + \partial_\mu \delta\theta^\pm \mp \frac{ie}{s_W} \left[W_\mu^\pm \left(s_W \delta\theta^A - c_W \delta\theta^Z \right) - \left(s_W A_\mu - c_W Z_\mu \right) \delta\theta^\pm \right],
\end{aligned} \qquad (2.1.32)
$$

with

$$
\begin{aligned}
\delta\theta^\pm &= \frac{1}{\sqrt{2}} \frac{1}{g_2} \left(\delta\theta^1 \mp i\delta\theta^2 \right), \\
\delta\theta^A &= \frac{1}{g_1} c_W \delta\theta^Y - \frac{1}{g_2} s_W \delta\theta^3, \\
\delta\theta^Z &= \frac{1}{g_2} c_W \delta\theta^3 + \frac{1}{g_1} s_W \delta\theta^Y,
\end{aligned} \qquad (2.1.33)
$$

and (δ_{ij} is the Kronecker delta)

$$
v_{ij}^{-\dagger} = v_{ij}^+ = \begin{cases} \mathbf{V}_{ij}, & \text{for quarks,} \\ \delta_{ij}, & \text{for leptons.} \end{cases} \qquad (2.1.34)
$$

Equipped with (2.1.12), (2.1.14), (2.1.22), (2.1.25), (2.1.27) and (2.1.29) the original parameters of $\mathcal{L}_{\mathrm{SM}}^{\mathrm{cl}}$, namely g_1, g_2, λ, μ^2 and G_{ij}^f, can be replaced by the equivalent set of physical parameters e, M_W, M_Z, M_H, $m_{f,i}$ and $\mathbf{V}_{ij}$. The latter ones can be measured directly by suitable experiments.

2.2 Quantization

A characteristic feature of a non-Abelian gauge theory like the SM is that for proper quantization a gauge-fixing term $\mathcal{L}_{\mathrm{SM}}^{\mathrm{fix}}$ and a related Faddeev-Popov term $\mathcal{L}_{\mathrm{SM}}^{\mathrm{ghost}}$ have to be added to $\mathcal{L}_{\mathrm{SM}}^{\mathrm{cl}}$ [84]. The gauge-fixing term $\mathcal{L}_{\mathrm{SM}}^{\mathrm{fix}}$ is required in order to eliminate unphysical degrees of freedom which originate from the invariance of $\mathcal{L}_{\mathrm{SM}}^{\mathrm{cl}}$ under the gauge transformations specified in (2.1.19) and (2.1.30), (2.1.31), (2.1.32). However, just adding $\mathcal{L}_{\mathrm{SM}}^{\mathrm{fix}}$ to $\mathcal{L}_{\mathrm{SM}}^{\mathrm{cl}}$ still leaves some remaining unphysical contributions. This is

why, additionally, the term $\mathcal{L}_{\mathrm{SM}}^{\mathrm{ghost}}$ has to be introduced. It cancels these remaining unphysical contributions originating from the gauge-fixing term.

For higher-order calculations, choosing a renormalizable gauge is of importance. In this regard, a convenient choice is the class of the R_ξ gauges in which the gauge-fixing term of the SM reads

$$\mathcal{L}_{\mathrm{SM}}^{\mathrm{fix}} = -\frac{1}{2\xi_A}\left(F^A\right)^2 - \frac{1}{2\xi_Z}\left(F^Z\right)^2 - \frac{1}{\xi_W}F^+F^-, \tag{2.2.1}$$

with the linear gauge-fixing operators

$$\begin{aligned}
F^A &= \partial^\mu A_\mu, \\
F^Z &= \partial^\mu Z_\mu - M_Z\xi_Z'\varphi, \\
F^\pm &= \partial^\mu W_\mu^\pm \mp iM_W\xi_W'\phi^\pm,
\end{aligned} \tag{2.2.2}$$

and the five independent gauge parameters, namely ξ_a ($a = A, Z, \pm$) and ξ_a' ($a = Z, \pm$), where $\xi_\pm^{(\prime)} = \xi_W^{(\prime)}$. Introducing such a general linear gauge-fixing term leads to the gauge-boson propagators

$$i\Delta_{\mu\nu}^{V^a}(k) = -\frac{i}{k^2 - M_a^2}g_{\mu\nu}^{\mathrm{T}} - \frac{i\xi_a}{k^2 - \xi_a M_a^2}g_{\mu\nu}^{\mathrm{L}}, \tag{2.2.3}$$

which behave as $1/k^2$ for large k^2. The term proportional to

$$g_{\mu\nu}^{\mathrm{T}} = g_{\mu\nu} - \frac{k_\mu k_\nu}{k^2} \tag{2.2.4}$$

represents the transverse part; the term proportional to

$$g_{\mu\nu}^{\mathrm{L}} = \frac{k_\mu k_\nu}{k^2} \tag{2.2.5}$$

stands for the longitudinal part of the propagator, and we use the notation $V^a = A, Z, W^\pm$ for $a = A, Z, \pm$, where $M_\pm = M_W$.

As mentioned above, additionally we have to consider the Faddeev-Popov part, which reads

$$\mathcal{L}_{\mathrm{SM}}^{\mathrm{ghost}} = -\int \mathrm{d}^4z\,\mathrm{d}^4y\,\bar{u}^a(x)\left[\frac{\delta F^a(x)}{\delta\phi^c(z)}\frac{\delta\phi^c(z)}{\delta\theta^b(y)} + \frac{\delta F^a(x)}{\delta V_\nu^c(z)}\frac{\delta V_\nu^c(z)}{\delta\theta^b(y)}\right]u^b(y), \tag{2.2.6}$$

and introduces the Faddeev-Popov ghost and anti-ghost fields $u^a(x)$ and $\bar{u}^a(x)$. Here, we have $a, b, c \in \{A, Z, \pm\}$, with $\phi^Z \equiv \varphi$ and $\phi^A \equiv 0$. As can be seen from (2.2.6), the dynamics of the ghost fields including associated tree-level couplings to the vector and scalar bosons is completely determined by the variation of the linear gauge-fixing operators (2.2.2) under the infinitesimal transformations $\delta\varphi$, $\delta\phi^\pm$, δA_μ, δZ_μ and $\delta W_\mu^\pm$, specified in (2.1.30) and (2.1.32).

Within the 't Hooft gauge [85, 86], where $\xi_a' = \xi_a$ is chosen for $a = Z, \pm$, we do not have to consider mixing terms of the form $V_\mu^a\partial^\mu\phi^a$. The latter generally stem from the

kinetic term of Φ in (2.1.9) as a consequence of electroweak symmetry breaking. These terms, together with the corresponding mixing terms introduced by $\mathcal{L}_{\mathrm{SM}}^{\mathrm{fix}}$ in the 't Hooft gauge, form a four-derivative which leaves the action invariant. This is how we get rid of such undesired terms in the Lagrangian. In the 't Hooft gauge, the propagators of the would-be Goldstone bosons read

$$i\Delta^{\phi^a}(k) = \frac{i}{k^2 - \xi_a M_a^2}, \quad (a = Z, \pm), \tag{2.2.7}$$

and similarly, the propagators of the ghost fields are given by

$$i\Delta^{u^a}(k) = \frac{i}{k^2 - \xi_a M_a^2}, \quad (a = A, Z, \pm). \tag{2.2.8}$$

The ξ_a-dependence of the corresponding masses emphasizes that these fields correspond to the unphysical sector. Generally, the ghost field u^A remains massless, since $M_A = 0$. The would-be Goldstone bosons φ and $\phi^\pm$ as well as the other ghost fields u^Z and $u^\pm$ have propagator poles which coincide with the poles we obtain for the longitudinal parts of the associated gauge-boson propagators specified in (2.2.3). This is crucial for a proper cancellation of unphysical poles in S-matrix elements.

For convenience, we mostly consider the 't Hooft-Feynman gauge, where all the gauge parameters introduced above are set to unity ($\xi_A = 1$, and $\xi_a = \xi_a' = 1$, for $a = Z, \pm$). According to the considerations above, the 't Hooft-Feynman gauge provides gauge-boson propagators which are particularly simple (in fact directly proportional to the Minkowski metric $g_{\mu\nu}$) as well as masses for the unphysical fields $\phi^\pm$, $u^\pm$, φ, u^Z and u^A, which are equal to the related gauge-boson masses (2.1.22).

Altogether, the complete Lagrangian of the (quantized) SM can be written as the sum

$$\mathcal{L}_{\mathrm{SM}} = \mathcal{L}_{\mathrm{SM}}^{\mathrm{cl}} + \mathcal{L}_{\mathrm{SM}}^{\mathrm{fix}} + \mathcal{L}_{\mathrm{SM}}^{\mathrm{ghost}}. \tag{2.2.9}$$

A list of corresponding Feynman rules can be found e.g. in [82].

2.3   BRS invariance

Normal gauge invariance is destroyed by adding the gauge-fixing and Faddeev-Popov part to the classical Lagrangian of a gauge theory like the SM. However, a wider symmetry of the Lagrangian can be reestablished by defining the transformation behaviour of the ghost and anti-ghost fields appropriately. This symmetry is called BRS symmetry [87–89], named after Becchi, Rouet and Stora. Regarding the introduction of the ghost fields in (2.2.6), the BRS symmetry provides a deeper motivation. Furthermore, the concept of BRS invariance is essential for the general proof of renormalizability of non-Abelian gauge theories [85, 86, 90–92]. This is because the continuous BRS symmetry leads to the Slavnov-Taylor identities [93, 94] between Green functions.

The BRS transformations of the scalar fields, fermions and gauge bosons in the SM follow from (2.1.30), (2.1.31) and (2.1.32) by replacing the corresponding infinitesimal

transformation parameters (2.1.33) according to

$$\delta\theta^A = \delta\lambda\, u^A, \qquad \delta\theta^Z = \delta\lambda\, u^Z, \qquad \delta\theta^\pm = \delta\lambda\, u^\pm, \tag{2.3.1}$$

where $\delta\lambda$ is a Grassmann-valued, infinitesimal constant which anticommutes with the ghost and anti-ghost fields. Therefore, we can directly conclude that $\mathcal{L}_{\mathrm{SM}}^{\mathrm{cl}}$ is BRS invariant. In this context, it is convenient to introduce the BRS operator $\boldsymbol{s}$ which is defined by the BRS transformation of a generic field X according to

$$\mathrm{X} \longrightarrow \mathrm{X} + \delta_{\mathrm{BRS}}\mathrm{X} \equiv \mathrm{X} + \delta\lambda\,\boldsymbol{s}\mathrm{X}. \tag{2.3.2}$$

Note that for the two generic products of fields $\mathcal{A}$ and $\mathcal{B}$ we have the product rule

$$\boldsymbol{s}\left(\mathcal{A}\mathcal{B}\right) = \left(\boldsymbol{s}\mathcal{A}\right)\mathcal{B} \pm \mathcal{A}\left(\boldsymbol{s}\mathcal{B}\right), \tag{2.3.3}$$

with the plus (minus) sign for the case in which $\mathcal{A}$ contains an even (odd) number of Grassmann variables. Taking into account (2.1.30), (2.1.31), (2.1.32), (2.1.34), (2.3.1) and (2.3.2), we obtain the BRS transformations of the scalar component fields,

$$\begin{aligned}
\boldsymbol{s}H &= \frac{e}{2s_W c_W}\varphi\, u^Z + \frac{ie}{2s_W}\left[\phi^+ u^- - \phi^- u^+\right], \\
\boldsymbol{s}\varphi &= -\frac{e}{2s_W c_W}\left[v + H\right] u^Z + \frac{e}{2s_W}\left[\phi^+ u^- + \phi^- u^+\right], \\
\boldsymbol{s}\phi^\pm &= \mp ie\,\phi^\pm\left[u^A + \frac{s_W^2 - c_W^2}{2s_W c_W}u^Z\right] \pm \frac{ie}{2s_W}\left[v + H \pm i\varphi\right]u^\pm,
\end{aligned} \tag{2.3.4}$$

of the left- and right-handed fermion fields,

$$\begin{aligned}
\boldsymbol{s}\psi_{i,\pm}^{\mathrm{L}} &= -ie\left[Q_{\psi_{i,\pm}^{\mathrm{L}}}u^A + \frac{s_W}{c_W}\left(Q_{\psi_{i,\pm}^{\mathrm{L}}} \mp \frac{1}{2s_W^2}\right)u^Z\right]\psi_{i,\pm}^{\mathrm{L}} + \frac{ie}{\sqrt{2}s_W}u^\pm v_{ij}^\pm\,\psi_{j,\mp}^{\mathrm{L}}, \\
\boldsymbol{s}\psi_i^{\mathrm{R}} &= -ie\,Q_{\psi_i^{\mathrm{R}}}\left(u^A + \frac{s_W}{c_W}u^Z\right)\psi_i^{\mathrm{R}},
\end{aligned} \tag{2.3.5}$$

as well as of the gauge bosons,

$$\begin{aligned}
\boldsymbol{s}A_\mu &= \partial_\mu u^A + ie\left[W_\mu^+ u^- - W_\mu^- u^+\right], \\
\boldsymbol{s}Z_\mu &= \partial_\mu u^Z - ie\frac{c_W}{s_W}\left[W_\mu^+ u^- - W_\mu^- u^+\right], \\
\boldsymbol{s}W_\mu^\pm &= \partial_\mu u^\pm \mp ie\left[W_\mu^\pm\left(u^A - \frac{c_W}{s_W}u^Z\right) - \left(A_\mu - \frac{c_W}{s_W}Z_\mu\right)u^\pm\right].
\end{aligned} \tag{2.3.6}$$

The BRS transformations of u^a and $\bar{u}^a$ can be defined in such a way that $\mathcal{L}_{\mathrm{SM}}^{\mathrm{fix}} + \mathcal{L}_{\mathrm{SM}}^{\mathrm{ghost}}$ is BRS invariant:

$$\begin{aligned}
\boldsymbol{s}u^A &= ie\, u^- u^+, & \boldsymbol{s}\bar{u}^A &= -\frac{1}{\xi_A}F^A, \\
\boldsymbol{s}u^Z &= -ie\frac{c_W}{s_W}\, u^- u^+, & \boldsymbol{s}\bar{u}^Z &= -\frac{1}{\xi_Z}F^Z, \\
\boldsymbol{s}u^\pm &= \pm i\frac{e}{s_W}u^\pm\left(s_W u^A - c_W u^Z\right), & \boldsymbol{s}\bar{u}^\pm &= -\frac{1}{\xi_W}F^\mp.
\end{aligned} \tag{2.3.7}$$

Consequently, the aim of a BRS-invariant total Lagrangian $\mathcal{L}_{\mathrm{SM}}$ is achieved.

Chapter 3

The model with an extra Higgs singlet

As already pointed out in the introduction, in this work we investigate the extension of the SM Higgs sector (see Subsect. 2.1.3) by one additional scalar singlet $\Phi_{\rm h}$. In the class of models under consideration the extra Higgs singlet (EHS) $\Phi_{\rm h}$ exclusively couples to the standard sector through a renormalizable quartic interaction term of the form $(\Phi_{\rm s}^\dagger \Phi_{\rm s})(\Phi_{\rm h}^\dagger \Phi_{\rm h})$ in the extended Higgs potential. From now on $\Phi_{\rm s}$ denotes the standard Higgs-doublet field which as usually only transforms under the gauge group $\mathrm{SU}(2)_{\rm W} \times \mathrm{U}(1)_Y$ of the SM. With respect to the latter, the scalar field $\Phi_{\rm h}$ is completely neutral. The singlet $\Phi_{\rm h}$, however, transforms under a symmetry group associated with the hidden (non-standard) sector.[1] Depending on whether the complex-$\Phi_{\rm h}$ or the real-$\Phi_{\rm h}$ extension is considered, the hidden symmetry under which $\Phi_{\rm h}$ transforms is either continuous or discrete. In any case the underlying hidden symmetry is spontaneously broken by the non-vanishing vev $v_{\rm h}$ which corresponds to $\Phi_{\rm h}$.

For the complex-$\Phi_{\rm h}$ extension we study the case where $v_{\rm h}$ spontaneously breaks a hidden $\mathrm{U}(1)$ symmetry group, which we denote by $\mathrm{U}(1)_{Y_{\rm h}}$. The hidden hypercharge $Y_{\rm h}$ either generates

- a global $\mathrm{U}(1)_{Y_{\rm h}}$, denoted as scenario EHSG, or

- a local $\mathrm{U}(1)_{Y_{\rm h}}$, denoted as scenario EHSL.

For the (ab-initio) real-$\Phi_{\rm h}$ extension we examine the case where $v_{\rm h}$ spontaneously breaks a discrete hidden $\mathcal{Z}_2$ symmetry group $\mathcal{Z}_2^{\rm D}$, which acts on the field $\Phi_{\rm h}$ as

$$\Phi_{\rm h} \to -\Phi_{\rm h}. \tag{3.0.1}$$

Accordingly, the last scenario is named EHSD model.

Only in the EHSL model with a spontaneously broken local $\mathrm{U}(1)_{Y_{\rm h}}$ the non-standard gauge boson Z' appears. In order to prevent kinetic mixing with the standard sector we impose the invariance of the EHSL Lagrangian under a non-standard $\mathcal{Z}_2$ symmetry group denoted as $\mathcal{Z}_2^{\rm L}$. The hidden vev $v_{\rm h}$ leaves the $\mathcal{Z}_2^{\rm L}$ unbroken. In the EHSL model

---

[1]In this regard, the appended lower index s (h) of a given field marks the affiliation with the standard (hidden) sector.

model	Φ_{h}	$v_{\mathrm{h}} \neq 0$ spontaneously breaks	Z'	φ_{h}
EHSL	complex	local $\mathrm{U}(1)_{Y_{\mathrm{h}}}$	✓	unphysical
EHSG	complex	global $\mathrm{U}(1)_{Y_{\mathrm{h}}}$	–	physical
EHSD	real	discrete $\mathcal{Z}_2^{\mathrm{D}}$	–	–

Table 3.1: Short overview of the models under consideration.

the degree of freedom which goes into the longitudinal polarization of the massive Z' boson is given by the imaginary part of Φ_{h}, here denoted as φ_{h}, according to the Higgs mechanism. Thus, in the EHSL model the field φ_{h} is unphysical and plays the role of a hidden would-be Goldstone boson. In contrast, in the EHSG model where the $\mathrm{U}(1)_{Y_{\mathrm{h}}}$ is global, φ_{h} is a physical massless scalar field. Finally, neither the Z' boson nor the field φ_{h} exists in the EHSD model where Φ_{h} is real. In Tab. 3.1 we give a summary of the three considered scenarios.

In this chapter we establish the theoretical framework of the three model classes. We start with the EHSL model as the most general case. The theoretical framework of the EHSG model is obtained by taking the limit of a vanishing hidden gauge-coupling constant. Subsequently removing the imaginary part φ_{h} of Φ_{h} by hand finally provides us with the theoretical framework of the EHSD model.

3.1   The extended classical Lagrangian

In this section we survey the classical Lagrangian of the model with an EHS Φ_{h}. We focus on the classification according to the EHSL, EHSG and EHSD models. While in the EHSG model and in the EHSD model only the Higgs part of $\mathcal{L}_{\mathrm{SM}}^{\mathrm{cl}}$ is extended, the EHSL model furthermore takes into account an extended gauge sector. Throughout this work, it is assumed that fermions have no interactions with the hidden sector, hence the fermionic part of $\mathcal{L}_{\mathrm{SM}}^{\mathrm{cl}}$ is left untouched. Accordingly, the classical Lagrangian corresponding to the extension of the SM by an EHS Φ_{h} can be written as

$$\mathcal{L}_{\mathrm{EHS}}^{\mathrm{cl}} = \mathcal{L}_{\mathrm{SM}}^{\mathrm{G}} + \mathcal{L}_{\mathrm{SM}}^{\mathrm{F}} + \mathcal{L}_{\mathrm{EHSL}}^{Z'} + \mathcal{L}_{\mathrm{EHS}}^{\Phi_{\mathrm{s/h}}}, \tag{3.1.1}$$

where the entire Higgs part is summarized in $\mathcal{L}_{\mathrm{EHS}}^{\Phi_{\mathrm{s/h}}}$ and the non-standard gauge part of the EHSL model is given by $\mathcal{L}_{\mathrm{EHSL}}^{Z'}$. Hence, the third term on the right-hand side of (3.1.1) is absent in the EHSG and EHSD models. The gauge part $\mathcal{L}_{\mathrm{SM}}^{\mathrm{G}}$ and the fermionic part $\mathcal{L}_{\mathrm{SM}}^{\mathrm{F}}$ of the SM are already defined in Subsects. 2.1.1 and 2.1.2.

3.1.1   Higgs and gauge part

In its compact form the Lagrangian of the extended Higgs sector reads

$$\begin{aligned}
\mathcal{L}_{\mathrm{EHS}}^{\Phi_{\mathrm{s/h}}} = &\left(D_\mu \Phi_{\mathrm{s}}\right)^\dagger \left(D^\mu \Phi_{\mathrm{s}}\right) + \left(D_{\mathrm{h},\mu}\Phi_{\mathrm{h}}\right)^\dagger \left(D_{\mathrm{h}}^\mu \Phi_{\mathrm{h}}\right) - V(\Phi_{\mathrm{s}}, \Phi_{\mathrm{h}}) \\
&- \sum_{i,j}\left(\overline{L}_i^{\prime \mathrm{L}} G_{ij}^l l_j^{\prime \mathrm{R}}\Phi_{\mathrm{s}} + \overline{Q}_i^{\prime \mathrm{L}} G_{ij}^u u_j^{\prime \mathrm{R}}\tilde{\Phi}_{\mathrm{s}} + \overline{Q}_i^{\prime \mathrm{L}} G_{ij}^d d_j^{\prime \mathrm{R}}\Phi_{\mathrm{s}} + \mathrm{h.c.}\right),
\end{aligned} \tag{3.1.2}$$

with the scalar fields Φ_s and Φ_h introduced in the beginning of this chapter. The first two terms on the right-hand side of (3.1.2) are the corresponding kinetic terms. The standard doublet Φ_s is only charged under the gauge group $\mathrm{SU}(2)_W \times \mathrm{U}(1)_Y$ of the SM and carries the corresponding hypercharge $Y = 1$. Therefore, the standard covariant derivative D_μ is the one already given in (2.1.4). The kinetic term of Φ_h contains the non-standard covariant derivative

$$D_{h,\mu} = \partial_\mu + ig_h' \frac{Y_h}{2} Z_\mu', \qquad (3.1.3)$$

which is effective in the EHSL model according to the principle of minimal substitution. The hidden gauge-coupling constant g_h' as well as the non-standard spin-one field Z_μ' is associated with the local $\mathrm{U}(1)_{Y_h}$ of the EHSL model. In the following, we substitute the hidden hypercharge Y_h into g_h according to

$$g_h \equiv g_h' \frac{Y_h}{2}. \qquad (3.1.4)$$

In the EHSG and EHSD models the field Φ_h does not carry quantum numbers of any gauge group and consequently the non-standard covariant derivative $D_{h,\mu}$ in (3.1.2) then simply has to be replaced by the four-derivative ∂_μ.

With the third term on the right-hand side of (3.1.2) the renormalizable modified Higgs potential

$$\begin{aligned} V(\Phi_s, \Phi_h) = \; & -\mu_s^2 \, \Phi_s^\dagger \Phi_s + \frac{\lambda_s}{4} (\Phi_s^\dagger \Phi_s)^2 \\ & -\mu_h^2 \, \Phi_h^\dagger \Phi_h + \frac{\lambda_h}{4} (\Phi_h^\dagger \Phi_h)^2 + \eta \, (\Phi_s^\dagger \Phi_s)(\Phi_h^\dagger \Phi_h) \end{aligned} \qquad (3.1.5)$$

is introduced, with the real-valued parameters μ_s^2, μ_h^2, λ_s, λ_h and η. We demand that the modified Higgs potential provides the two non-vanishing vevs v_s for Φ_s and v_h for Φ_h. Minimizing the potential (3.1.5) and requiring that both the standard vev v_s and the hidden vev v_h is positive definite yields

$$v_s = \sqrt{\frac{4\mu_s^2 \lambda_h - 8\eta\mu_h^2}{\lambda_s \lambda_h - 4\eta^2}}, \qquad v_h = \sqrt{\frac{4\mu_h^2 \lambda_s - 8\eta\mu_s^2}{\lambda_s \lambda_h - 4\eta^2}}. \qquad (3.1.6)$$

The last term in (3.1.5) is proportional to the Higgs-portal coupling η and gives rise to the interaction between the standard and the hidden sector. Additional terms in (3.1.5) are forbidden by the requirement of renormalization and the $\mathrm{U}(1)_{Y_h}$ symmetry of the EHSL and EHSG models, respectively the $\mathcal{Z}_2^D$ symmetry of the EHSD model.[2] Hence, it is important to note that in each of the three models under consideration the modified Higgs potential is given by (3.1.5).

The fields Φ_s and Φ_h can be expanded around the respective vevs v_s and v_h yielding

$$\Phi_s(x) = \begin{pmatrix} \phi^+(x) \\ \frac{1}{\sqrt{2}} \left[v_s + H(x) + i\varphi_s(x) \right] \end{pmatrix}, \qquad \Phi_h(x) = \frac{1}{\sqrt{2}} \left[v_h + \chi(x) + i\varphi_h(x) \right]. \qquad (3.1.7)$$

---

[2]In the real-Φ_h extension without the $\mathcal{Z}_2^D$ the hidden vev v_h becomes irrelevant as it can be shifted away by means of a reparametrization of the Higgs-potential parameters [50].

We write the Higgs doublet in analogy to the SM (cf. Subsect. 2.1.3) but attach the lower index s to the corresponding vev and to the associated neutral would-be Goldstone boson in order to distinguish these quantities from the related counterparts in the hidden sector. So, the component fields $\phi^\pm$ and φ_s represent the charged and neutral would-be Goldstone bosons of the standard sector. Since Φ_h is real in the EHSD model the component field φ_h is only present in the EHSL and EHSG models. Therefore, in the EHSD model we set $\varphi_h \equiv 0$. The role of the fields H, χ and φ_h in the Φ_h extension of the SM is discussed in the next section where we introduce the physical basis.

The second line of (3.1.2) depicts the Yukawa part of $\mathcal{L}_{\text{EHS}}^{\Phi_{s/h}}$. Its structure is identical to the Yukawa part of $\mathcal{L}_{\text{SM}}^{\Phi}$ in the SM (cf. Subsect. 2.1.3). Only the doublet Φ_s couples to the fermion sector via standard Yukawa-interaction terms where $\tilde{\Phi}_s = i\tau^2 \Phi_s^*$. Hence, the hidden vev v_h does not contribute to the generation of fermion masses. Couplings of Φ_h to the fermions are forbidden due to standard and non-standard symmetry.

We still have to specify the non-standard gauge part $\mathcal{L}_{\text{EHSL}}^{Z'}$ corresponding to the EHSL model. Relating to the above-mentioned $\mathcal{Z}_2^{\text{L}}$ the fields of the standard sector are neutral but the non-standard fields transform as

$$\Phi_h \rightarrow \Phi_h^\dagger, \quad Z'_\mu \rightarrow -Z'_\mu. \tag{3.1.8}$$

Consequently, the term $B^{\mu\nu} Z'_{\mu\nu}$ involving just one power of the non-standard field strength tensor $Z'_{\mu\nu} = \partial_\mu Z'_\nu - \partial_\nu Z'_\mu$ violates the $\mathcal{Z}_2^{\text{L}}$ and therefore kinetic mixing between the Abelian standard and non-standard gauge fields is forbidden (cf. Subsect. 2.1.1). As indicated in [70] this also holds at higher orders. Kinetic mixing is not generated radiatively in the EHSL model. With respect to the $\mathcal{Z}_2^{\text{L}}$ the field Φ_h has to transform as specified in (3.1.8) such that the kinetic term of Φ_h in (3.1.2) is allowed. Hence, the non-standard gauge part in (3.1.1) is given by

$$\mathcal{L}_{\text{EHSL}}^{Z'} = -\frac{1}{4} Z'_{\mu\nu} Z'^{\mu\nu}. \tag{3.1.9}$$

Having specified the complete classical Lagrangian (3.1.1) we emphasize that in each of the three models the Higgs-portal term proportional to the coupling η in (3.1.5) is the exclusive source of interaction between the standard and the hidden sector. The limit of a vanishing Higgs-portal coupling $\eta \rightarrow 0$ inevitably leads to the decoupling of the entire hidden sector and thus brings us back to the phenomenology of the SM.

3.1.2 Gauge invariance

At this point, let us have a closer look at the underlying symmetries of $\mathcal{L}_{\text{EHS}}^{\text{cl}}$ in the three models under consideration. The classical Lagrangian $\mathcal{L}_{\text{EHS}}^{\text{cl}}$ is invariant under the gauge transformations (2.1.15) specified for the SM. Since Φ_s only carries quantum numbers of the SM gauge group we have

$$\Phi_s(x) \rightarrow \mathbf{T}_{\text{W}}(x) \mathbf{T}_Y(x) \Phi_s(x), \tag{3.1.10}$$

in analogy to (2.1.16). The singlet Φ_h transforms trivially under $\text{SU}(2)_{\text{W}} \times \text{U}(1)_Y$ and the same holds for the non-standard gauge field Z'_μ.

In the EHSL model, the field $\Phi_{\rm h}$ transforms as follows

$$\Phi_{\rm h}(x) \to \mathbf{T}_{Y_{\rm h}}(x)\Phi_{\rm h}(x), \tag{3.1.11}$$

with

$$\mathbf{T}_{Y_{\rm h}}(x) = \exp\left[-i\frac{Y_{\rm h}}{2}\theta^{Y_{\rm h}}(x)\right], \tag{3.1.12}$$

whereas the Z'_μ transforms as

$$Z'_\mu(x)\frac{Y_{\rm h}}{2} \to \mathbf{T}_{Y_{\rm h}}(x)\left[Z'_\mu(x)\frac{Y_{\rm h}}{2} - i\frac{1}{g'_{\rm h}}\partial_\mu\right]\mathbf{T}^\dagger_{Y_{\rm h}}(x), \tag{3.1.13}$$

according to the convention of minimal substitution (cf. Subsect. 2.1.4). In infinitesimal form, the gauge transformations (3.1.10), (3.1.11) and (3.1.13) read

$$\Phi_{\rm s}(x) \to \left[1 - i\frac{1}{2}\delta\theta^Y(x) + i\frac{\tau^a}{2}\delta\theta^a(x)\right]\Phi_{\rm s}(x),$$

$$\Phi_{\rm h}(x) \to \left[1 - i\frac{Y_{\rm h}}{2}\delta\theta^{Y_{\rm h}}(x)\right]\Phi_{\rm h}(x), \tag{3.1.14}$$

$$Z'_\mu(x) \to Z'_\mu(x) + \frac{1}{g'_{\rm h}}\partial_\mu\delta\theta^{Y_{\rm h}}(x).$$

In the EHSG model (where no Z'_μ appears) the transformation of $\Phi_{\rm h}$ can be written as in (3.1.11), (3.1.12) and (3.1.14) but with a global $\mathbf{T}_{Y_{\rm h}}$ (i.e. in the EHSG model $\mathbf{T}_{Y_{\rm h}}$ or rather $\theta^{Y_{\rm h}}$ has no space-time dependence). In the EHSD model with the discrete $\mathcal{Z}_2^{\rm D}$ (3.0.1) there is no infinitesimal transformation of $\Phi_{\rm h}$.

In each of the three models the associated transformations of the left-handed and right-handed fermion fields as well as of the standard gauge fields are identical to those of the SM. The corresponding expressions are already given in (2.1.17), (2.1.18) and (2.1.19).

3.1.3 Physical basis

Rewriting (3.1.5) in terms of the scalar component fields introduced in (3.1.7) yields

$$
\begin{aligned}
V(\Phi_{\rm s}, \Phi_{\rm h}) =& -t_H H - t_\chi\chi - \frac{t_H}{v_{\rm s}}\phi^+\phi^- - \frac{t_H}{2v_{\rm s}}\varphi_{\rm s}^2 - \frac{t_\chi}{2v_{\rm h}}\varphi_{\rm h}^2 + \frac{1}{2}\left(H,\chi\right)\mathcal{M}^2\begin{pmatrix}H\\\chi\end{pmatrix} \\
&+ \frac{\lambda_{\rm s}v_{\rm s}}{4}H^3 + \frac{\lambda_{\rm h}v_{\rm h}}{4}\chi^3 + \frac{\eta v_{\rm s}}{2}H\chi^2 + \frac{\eta v_{\rm h}}{2}H^2\chi + \frac{\lambda_{\rm s}v_{\rm s}}{2}H\phi^-\phi^+ \\
&+ \eta v_{\rm h}\chi\phi^-\phi^+ + \frac{\lambda_{\rm s}v_{\rm s}}{4}H\varphi_{\rm s}^2 + \frac{\lambda_{\rm h}v_{\rm h}}{4}\chi\varphi_{\rm h}^2 + \frac{\eta v_{\rm s}}{2}H\varphi_{\rm h}^2 + \frac{\eta v_{\rm h}}{2}\chi\varphi_{\rm s}^2 \\
&+ \frac{\lambda_{\rm s}}{16}H^4 + \frac{\lambda_{\rm h}}{16}\chi^4 + \frac{\eta}{4}H^2\chi^2 + \frac{\lambda_{\rm s}}{4}H^2\phi^-\phi^+ + \frac{\eta}{2}\chi^2\phi^-\phi^+ \\
&+ \frac{\lambda_{\rm s}}{8}H^2\varphi_{\rm s}^2 + \frac{\eta}{4}\chi^2\varphi_{\rm s}^2 + \frac{\eta}{4}H^2\varphi_{\rm h}^2 + \frac{\lambda_{\rm h}}{8}\chi^2\varphi_{\rm h}^2 + \frac{\lambda_{\rm s}}{4}\left(\phi^-\phi^+\right)^2 \\
&+ \frac{\lambda_{\rm s}}{4}\phi^-\phi^+\varphi_{\rm s}^2 + \frac{\eta}{2}\phi^-\phi^+\varphi_{\rm h}^2 + \frac{\lambda_{\rm s}}{16}\varphi_{\rm s}^4 + \frac{\eta}{4}\varphi_{\rm s}^2\varphi_{\rm h}^2 + \frac{\lambda_{\rm h}}{16}\varphi_{\rm h}^4,
\end{aligned}
\tag{3.1.15}
$$

with the tadpole coefficients

$$t_H = \mu_{\mathrm{s}}^2 v_{\mathrm{s}} - \frac{1}{4}\lambda_{\mathrm{s}} v_{\mathrm{s}}^3 - \frac{1}{2}\eta v_{\mathrm{s}} v_{\mathrm{h}}^2, \qquad t_\chi = \mu_{\mathrm{h}}^2 v_{\mathrm{h}} - \frac{1}{4}\lambda_{\mathrm{h}} v_{\mathrm{h}}^3 - \frac{1}{2}\eta v_{\mathrm{h}} v_{\mathrm{s}}^2, \tag{3.1.16}$$

and the symmetric but non-diagonal squared-mass matrix

$$\mathcal{M}^2 = \begin{pmatrix} -\mu_{\mathrm{s}}^2 + \frac{3}{4}\lambda_{\mathrm{s}} v_{\mathrm{s}}^2 + \frac{1}{2}\eta v_{\mathrm{h}}^2 & \eta v_{\mathrm{s}} v_{\mathrm{h}} \\ \eta v_{\mathrm{s}} v_{\mathrm{h}} & -\mu_{\mathrm{h}}^2 + \frac{3}{4}\lambda_{\mathrm{h}} v_{\mathrm{h}}^2 + \frac{1}{2}\eta v_{\mathrm{s}}^2 \end{pmatrix} \tag{3.1.17}$$

of the fields H and χ. The terms involving the field φ_{h} in (3.1.15) are only present in the complex-Φ_{h} extension of the SM and have to be set to zero when considering the EHSD model. In the last five lines of (3.1.15) the resulting cubic and quartic scalar self-coupling terms are listed. Without exception the terms involving both standard and hidden component fields are proportional to the portal coupling η. The tadpole coefficients t_H and t_χ vanish at LO according to the minimum conditions (3.1.6). Consequently, at LO the mass matrix (3.1.17) further simplifies to

$$\mathcal{M}_{\mathrm{LO}}^2 = \begin{pmatrix} \frac{1}{2}\lambda_{\mathrm{s}} v_{\mathrm{s}}^2 & \eta v_{\mathrm{s}} v_{\mathrm{h}} \\ \eta v_{\mathrm{s}} v_{\mathrm{h}} & \frac{1}{2}\lambda_{\mathrm{h}} v_{\mathrm{h}}^2 \end{pmatrix}, \tag{3.1.18}$$

and the mass terms of $\phi^{\pm}$, φ_{s} and φ_{h} in (3.1.15) vanish.

Mass-eigenstate basis of the scalar fields

Due to the non-vanishing v_{h} a mixing between H and χ occurs in the presence of the Higgs-portal coupling η in each of the three models; hence, neither the field H nor the field χ is a mass eigenstate. We switch to the related mass-eigenstate basis by diagonalizing the symmetric squared-mass matrix (3.1.18). This is achieved by means of the rotation

$$\mathcal{T}^{-1}\mathcal{M}_{\mathrm{LO}}^2 \mathcal{T} = \begin{pmatrix} M_{H_1}^2 & 0 \\ 0 & M_{H_2}^2 \end{pmatrix}, \qquad \mathcal{T} = \begin{pmatrix} c_\alpha & -s_\alpha \\ s_\alpha & c_\alpha \end{pmatrix}, \tag{3.1.19}$$

with the notation $c_\alpha \equiv \cos\alpha$ and $s_\alpha \equiv \sin\alpha$ and with the corresponding mixing angle α which obeys the relation

$$\tan 2\alpha = \frac{4\eta v_{\mathrm{s}} v_{\mathrm{h}}}{\lambda_{\mathrm{s}} v_{\mathrm{s}}^2 - \lambda_{\mathrm{h}} v_{\mathrm{h}}^2}. \tag{3.1.20}$$

The physical scalar fields H_1 and H_2 for the mass eigenstates can be written as a linear combination of the original scalar fields H and χ,

$$\begin{pmatrix} H_1 \\ H_2 \end{pmatrix} = \begin{pmatrix} c_\alpha & s_\alpha \\ -s_\alpha & c_\alpha \end{pmatrix} \begin{pmatrix} H \\ \chi \end{pmatrix}, \tag{3.1.21}$$

with corresponding mass eigenvalues

$$M_{H_{1/2}}^2 = \frac{1}{4}\left(\lambda_{\mathrm{s}} v_{\mathrm{s}}^2 + \lambda_{\mathrm{h}} v_{\mathrm{h}}^2\right) \pm \frac{1}{4}\left(\lambda_{\mathrm{s}} v_{\mathrm{s}}^2 - \lambda_{\mathrm{h}} v_{\mathrm{h}}^2\right)\sqrt{1 + \tan^2 2\alpha}. \tag{3.1.22}$$

Inversion of (3.1.21) allows us to rewrite the original scalar fields H and χ as linear combinations of the mass eigenstates H_1 and H_2. Therefore, e.g. the tadpole coefficients t_{H_1} and t_{H_2} of the fields H_1 and H_2 are simply given by the linear combinations

$$
\begin{aligned}
t_{H_1} &= c_\alpha t_H + s_\alpha t_\chi, \\
t_{H_2} &= -s_\alpha t_H + c_\alpha t_\chi,
\end{aligned}
\tag{3.1.23}
$$

and thus vanish at LO, too. The original Higgs-potential parameters $\lambda_{\rm s}$, $\lambda_{\rm h}$ and η can be replaced by the parameters α, M_{H_1}, M_{H_2}, $v_{\rm s}$ and $v_{\rm h}$ according to

$$
\begin{aligned}
\lambda_{\rm s} &= \frac{M_{H_1}^2 + M_{H_2}^2 + \left(M_{H_1}^2 - M_{H_2}^2\right) c_{2\alpha}}{v_{\rm s}^2}, \\
\lambda_{\rm h} &= \frac{M_{H_1}^2 + M_{H_2}^2 - \left(M_{H_1}^2 - M_{H_2}^2\right) c_{2\alpha}}{v_{\rm h}^2}, \\
\eta &= \frac{\left(M_{H_1}^2 - M_{H_2}^2\right) s_{2\alpha}}{2 v_{\rm s} v_{\rm h}},
\end{aligned}
\tag{3.1.24}
$$

which follows from (3.1.20) and (3.1.22). Equipped with (3.1.15), (3.1.21) and (3.1.24) it is straightforward to derive the cubic and quartic scalar self-coupling terms in the mass-eigenstate basis. The corresponding Feynman rules are listed in Appendix A.

From (3.1.20) we can deduce that only the domain

$$
-\frac{\pi}{4} < \alpha < +\frac{\pi}{4}
\tag{3.1.25}
$$

has to be considered. With (3.1.25) there is no hierarchy of M_{H_1} and M_{H_2}, i.e. we take into account both $M_{H_2} > M_{H_1}$ and $M_{H_2} < M_{H_1}$. From (3.1.21) it follows that the limit $\alpha \to 0$ provides us with the situation in which the field H_1 is equal to the standard Higgs field H and in which the field H_2 is equal to the hidden component field χ. Taking into account (3.1.20) and the positive definite $v_{\rm s/h}$ we see that the limit $\alpha \to 0$ requires $\eta \to 0$ which leads to a decoupling of the hidden sector as explained above. Thus, without exception, the limit $\alpha \to 0$ brings us back to the phenomenology of the SM. As already stated before, in this work we treat the field H_1 to be responsible for the resonance detected around 125 GeV at the LHC [16, 17] and we fix the mass M_{H_1} accordingly.

Non-standard couplings to the standard gauge bosons

With $\Phi_{\rm s}$ given in (3.1.7), expansion of the corresponding kinetic term yields

$$
\begin{aligned}
\left(D_\mu \Phi_{\rm s}\right)^\dagger \left(D^\mu \Phi_{\rm s}\right) &= \frac{1}{2}(\partial_\mu H)(\partial^\mu H) + M_W^2 W_\mu^- W^{+\mu} \left(1 + \frac{2}{v_{\rm s}} H + \frac{1}{v_{\rm s}^2} H^2\right) \\
&\quad + \frac{1}{2} M_Z^2 Z_\mu Z^\mu \left(1 + \frac{2}{v_s} H + \frac{1}{v_s^2} H^2\right) + \ldots,
\end{aligned}
\tag{3.1.26}
$$

where the dots summarize the remaining terms which appear analogously to the SM and involve couplings with the standard would-be Goldstone bosons $\phi^\pm$ and $\varphi_{\rm s}$ as well

as the kinetic terms of the latter. Analogously to the SM (cf. Subsect. 2.1.5), for the standard gauge bosons $W_\mu^\pm$, Z_μ and A_μ we obtain the corresponding masses

$$M_W = \frac{v_\mathrm{s}}{2} g_2, \qquad M_Z = \frac{v_\mathrm{s}}{2} \sqrt{g_1^2 + g_2^2}, \qquad M_A = 0. \tag{3.1.27}$$

Sometimes in this work, we use the relation

$$v_\mathrm{s} = \frac{2 s_W M_W}{e}, \tag{3.1.28}$$

which follows from (2.1.24), (2.1.25) and (3.1.27). Obviously, the hidden vev v_h does not contribute to electroweak symmetry breaking in the standard sector.

Due to the mixing (3.1.21) of H and χ both the physical standard-like scalar field H_1 and the physical non-standard-like scalar field H_2 couple to the massive standard gauge bosons $W_\mu^\pm$ and Z_μ at the tree-level. Analogously to the SM, there exist no tree-level couplings of the standard Higgs field H to the photon field A_μ. Therefore, the mass eigenstates $H_{1/2}$ do not directly couple to the photon either. The resulting standard and non-standard couplings in the mass-eigenstate basis can be found in terms of corresponding Feynman rules in Appendix A. Note that the non-standard fields Z' and φ_h do not couple to the standard gauge bosons at the tree-level.

Couplings to the non-standard gauge bosons

With Φ_h given in (3.1.7), expansion of the corresponding kinetic term in the EHSL model yields

$$\begin{aligned}
(D_{\mathrm{h},\mu} \Phi_\mathrm{h})^\dagger (D_\mathrm{h}^\mu \Phi_\mathrm{h}) = {}& \frac{1}{2} (\partial_\mu \chi)(\partial^\mu \chi) + \frac{1}{2} (\partial_\mu \varphi_\mathrm{h})(\partial^\mu \varphi_\mathrm{h}) + \frac{1}{2} (g_\mathrm{h} v_\mathrm{h})^2 Z'_\mu Z'^\mu \\
& + g_\mathrm{h} v_\mathrm{h} Z'_\mu (\partial^\mu \varphi_\mathrm{h}) - g_\mathrm{h} (\partial_\mu \chi) Z'^\mu \varphi_\mathrm{h} + g_\mathrm{h} (\partial_\mu \varphi_\mathrm{h}) Z'^\mu \chi \quad (3.1.29) \\
& + g_\mathrm{h}^2 v_\mathrm{h} \chi Z'_\mu Z'^\mu + \frac{1}{2} g_\mathrm{h}^2 \chi^2 Z'_\mu Z'^\mu + \frac{1}{2} g_\mathrm{h}^2 \varphi_\mathrm{h}^2 Z'_\mu Z'^\mu.
\end{aligned}$$

The first two terms in (3.1.29) are the kinetic terms of the non-standard component fields χ and φ_h. According to the Higgs mechanism the third term on the right-hand side of (3.1.29) generates a mass $M_{Z'}$ for the non-standard gauge boson Z'_μ,

$$M_{Z'} = g_\mathrm{h} v_\mathrm{h}, \tag{3.1.30}$$

as a consequence of the non-vanishing vev v_h which spontaneously breaks the local $\mathrm{U}(1)_{Y_\mathrm{h}}$ in the EHSL model. Accordingly, in the EHSL model the field φ_h plays the role of a hidden would-be Goldstone boson which constitutes the longitudinal degree of freedom of the massive Z'_μ.

The first term in the second line of (3.1.29) is a mixing term between Z'_μ and its corresponding would-be Goldstone boson φ_h. Analogously to the SM, we get rid of this term by a suitable gauge-fixing choice which is introduced in the following section.

The remaining terms in (3.1.29) are the emerging triple and quartic interaction terms between the Z' boson and the non-standard scalar fields χ and φ_h. Note that

due to the mixing (3.1.21) in the third line of (3.1.29) the first term provides the tree-level couplings $H_i Z' Z'$ and the second term provides the tree-level couplings $H_i H_j Z' Z'$, where $i, j \in \{1, 2\}$. These couplings are of particular interest both in the context of collider signatures of the fields H_1, H_2, Z'_μ and in the context of astrophysical topics like e.g. vector dark-matter relic abundance in the EHSL model [42, 43, 70]. Relating to collider signatures of the standard-like Higgs boson H_1, one may not forget about the corresponding decay channel $H_1 \to Z' Z'$ in the non-standard parameter region $M_{Z'} < M_{H_1}/2$. In Chapter 7 we give the first NLO prediction for the corresponding partial width $\Gamma(H_1 \to Z' Z')$ and investigate its potential impact on further H_1-decay observables.

From (3.1.29) we can conclude that the limit $g_\mathrm{h} \to 0$ provides us with the situation of a decoupled massless Z' boson and hence with the EHSG model where the field φ_h is the Goldstone boson of the spontaneously broken global $\mathrm{U}(1)_{Y_\mathrm{h}}$. Recall that the term quadratic in the field φ_h in (3.1.15) is proportional to the tadpole coefficient t_χ and thus vanishes at LO according to the minimum condition (3.1.6). The zero-mass of φ_h is furthermore protected from radiative corrections as a consequence of the global $\mathrm{U}(1)_{Y_\mathrm{h}}$ symmetry. The corresponding $\mathrm{U}(1)_{Y_\mathrm{h}}$ Ward identity is listed in relation (B.2.1) of Appendix B. In the EHSG model (3.1.29) only consists of the two kinetic terms corresponding to χ and φ_h. Additionally removing the component field φ_h in the limit of vanishing g_h provides us with the phenomenology of the EHSD model, where (3.1.29) is only given by the kinetic term of the real component field χ.

Non-standard couplings to the fermions

From the Yukawa part of $\mathcal{L}_\mathrm{EHS}^{\Phi_\mathrm{s/h}}$ specified in the second line of (3.1.2) we obtain the fermion mass eigenstates (2.1.26) and (2.1.28) already introduced in the context of the SM. Analogously to (2.1.27) the masses for the charged fermion fields read

$$m_{f,i} = \frac{v_\mathrm{s}}{\sqrt{2}} \sum_{j,k} U_{ij}^{f,\mathrm{L}} G_{jk}^f U_{ki}^{f,\mathrm{R}\dagger}. \tag{3.1.31}$$

The non-vanishing hidden vev v_h does not contribute to the mass generation in the fermion sector.

The resulting couplings of the scalar component fields H, $\phi^\pm$ and φ_s to the fermion fields are identical with those appearing in the SM. Here, we obtain non-standard tree-level couplings of the scalar fields H_1 and H_2 to the massive fermion fields due to the mixing (3.1.21) of H and χ. The non-standard fields Z' and φ_h, however, do not couple to the fermion fields.

Gauge transformations of the mass eigenstates

Next, we provide the infinitesimal gauge transformations of the fields corresponding to the extended Higgs and non-standard gauge sector of the EHSL model in the mass-eigenstate basis. Taking into account (3.1.14) and (3.1.28), we introduce the physical

fields and parameters as defined in this section and obtain

$$H_1 \to H_1 + c_\alpha \left(\frac{M_Z}{v_s} \varphi_s \, \delta\theta^Z + i \frac{M_W}{v_s} \left[\phi^+ \delta\theta^- - \phi^- \delta\theta^+ \right] \right) + s_\alpha \frac{M_{Z'}}{v_h} \varphi_h \, \delta\theta^{Z'},$$

$$H_2 \to H_2 - s_\alpha \left(\frac{M_Z}{v_s} \varphi_s \, \delta\theta^Z + i \frac{M_W}{v_s} \left[\phi^+ \delta\theta^- - \phi^- \delta\theta^+ \right] \right) + c_\alpha \frac{M_{Z'}}{v_h} \varphi_h \, \delta\theta^{Z'},$$

$$\phi^\pm \to \phi^\pm \mp i e \phi^\pm \left[\delta\theta^A + \frac{s_W^2 - c_W^2}{2 s_W c_W} \delta\theta^Z \right] \pm i \frac{M_W}{v_s} \left[v_s + c_\alpha H_1 - s_\alpha H_2 \pm i \varphi_s \right] \delta\theta^\pm,$$

$$\varphi_s \to \varphi_s - \frac{M_Z}{v_s} \left[v_s + c_\alpha H_1 - s_\alpha H_2 \right] \delta\theta^Z + \frac{M_W}{v_s} \left[\phi^+ \delta\theta^- + \phi^- \delta\theta^+ \right],$$

$$\varphi_h \to \varphi_h - \frac{M_{Z'}}{v_h} \left[v_h + s_\alpha H_1 + c_\alpha H_2 \right] \delta\theta^{Z'},$$

$$Z'_\mu \to Z'_\mu + \partial_\mu \delta\theta^{Z'},$$

$$\text{(3.1.32)}$$

with the infinitesimal local transformation parameter

$$\delta\theta^{Z'}(x) = \frac{1}{g'_h} \delta\theta^{Y_h}(x) \tag{3.1.33}$$

corresponding to the hidden gauge sector of the EHSL model (cf. Subsect. 2.1.5). The infinitesimal $SU(2)_W \times U(1)_Y$ gauge transformations of $\phi^\pm$ and φ_s in (3.1.32) are the same in the EHSG and EHSD models. For the three models the infinitesimal $SU(2)_W \times U(1)_Y$ gauge transformations of the fermion fields and of the standard gauge bosons are already specified in (2.1.31) and (2.1.32).

The infinitesimal gauge transformations of the fields H_1, H_2 and φ_h in the EHSG model are obtained from the respective ones in (3.1.32) by taking the limit $g'_h \to 0$ after a consistent reintroduction of the parameter g'_h according to (3.1.4), (3.1.30) and (3.1.33), which yields

$$H_1 \to H_1 + c_\alpha \left(\frac{M_Z}{v_s} \varphi_s \, \delta\theta^Z + i \frac{M_W}{v_s} \left[\phi^+ \delta\theta^- - \phi^- \delta\theta^+ \right] \right) + s_\alpha \varphi_h \delta\theta_h,$$

$$H_2 \to H_2 - s_\alpha \left(\frac{M_Z}{v_s} \varphi_s \, \delta\theta^Z + i \frac{M_W}{v_s} \left[\phi^+ \delta\theta^- - \phi^- \delta\theta^+ \right] \right) + c_\alpha \varphi_h \delta\theta_h, \tag{3.1.34}$$

$$\varphi_h \to \varphi_h - \left[v_h + s_\alpha H_1 + c_\alpha H_2 \right] \delta\theta_h,$$

with the infinitesimal global transformation parameter

$$\delta\theta_h = \frac{Y_h}{2} \delta\theta^{Y_h}. \tag{3.1.35}$$

In the EHSD model there are no infinitesimal non-standard transformations and the infinitesimal $SU(2)_W \times U(1)_Y$ gauge transformations of H_1 and H_2 read

$$H_1 \to H_1 + c_\alpha \left(\frac{M_Z}{v_s} \varphi_s \, \delta\theta^Z + i \frac{M_W}{v_s} \left[\phi^+ \delta\theta^- - \phi^- \delta\theta^+ \right] \right),$$

$$H_2 \to H_2 - s_\alpha \left(\frac{M_Z}{v_s} \varphi_s \, \delta\theta^Z + i \frac{M_W}{v_s} \left[\phi^+ \delta\theta^- - \phi^- \delta\theta^+ \right] \right). \tag{3.1.36}$$

3.2   Quantization

In the EHSL model the gauge-fixing and the Faddeev-Popov Lagrangian of the SM have to be extended due to the presence of the associated $\mathrm{U}(1)_{Y_\mathrm{h}}$ gauge sector.[3] Therefore, in order to obtain the quantized Lagrangian for the Φ_h extension of the SM, we define a proper gauge-fixing term $\mathcal{L}_\mathrm{EHS}^\mathrm{fix}$ and a related Faddeev-Popov term $\mathcal{L}_\mathrm{EHS}^\mathrm{ghost}$ in the following.

A suitable gauge-fixing Lagrangian is given by

$$\mathcal{L}_\mathrm{EHS}^\mathrm{fix} = -\frac{1}{2\xi_A}\left(F^A\right)^2 - \frac{1}{2\xi_Z}\left(F^Z\right)^2 - \frac{1}{\xi_W}F^+F^- - \frac{1}{2\xi_{Z'}}(F^{Z'})^2, \tag{3.2.1}$$

where the first three terms are identified with the standard gauge-fixing operators

$$F^A = \partial^\mu A_\mu, \qquad F^Z = \partial^\mu Z_\mu - M_Z\xi'_Z\varphi_\mathrm{s}, \qquad F^\pm = \partial^\mu W_\mu^\pm \mp iM_W\xi'_W\phi^\pm, \tag{3.2.2}$$

and thus correspond to the gauge-fixing part of the standard sector which is treated analogously to the SM (cf. Sect. 2.2). In the EHSG and EHSD models alongside the gauge symmetries of the standard sector no additional gauge symmetry is imposed. Consequently, in the EHSG and EHSD models we do not have to extend the gauge-fixing part of the SM and the corresponding gauge-fixing Lagrangian is just given by the first three terms on the right-hand side of (3.2.1). The last term in (3.2.1) has to be considered only in the EHSL model and introduces the linear gauge-fixing operator

$$F^{Z'} = \partial^\mu Z'_\mu - M_{Z'}\xi'_{Z'}\varphi_\mathrm{h}, \tag{3.2.3}$$

which is associated with the corresponding $\mathrm{U}(1)_{Y_\mathrm{h}}$ gauge sector. All in all we have seven independent gauge parameters in the EHSL model, the five standard gauge parameters ξ_a $(a = A, Z, W)$ and ξ'_a $(a = Z, W)$, and the two non-standard gauge parameters $\xi_{Z'}$ and $\xi'_{Z'}$.

Next, we specify the corresponding Faddeev-Popov part which reads

$$\mathcal{L}_\mathrm{EHS}^\mathrm{ghost} = -\int \mathrm{d}^4z\,\mathrm{d}^4y\,\bar{u}^a(x)\left[\frac{\delta F^a(x)}{\delta\phi^c(z)}\frac{\delta\phi^c(z)}{\delta\theta^b(y)} + \frac{\delta F^a(x)}{\delta V_\nu^c(z)}\frac{\delta V_\nu^c(z)}{\delta\theta^b(y)}\right]u^b(y), \tag{3.2.4}$$

and introduces the Faddeev-Popov ghost and anti-ghost fields $u^a(x)$ and $\bar{u}^a(x)$, respectively, with $a, b, c \in \{A, Z, \pm, Z'\}$. We have $\phi^A \equiv 0$, $\phi^Z \equiv \varphi_\mathrm{s}$, $\phi^{Z'} \equiv \varphi_\mathrm{h}$ and $V^a = A, Z, W^\pm, Z'$ for $a = A, Z, \pm, Z'$. The structure of $\mathcal{L}_\mathrm{EHS}^\mathrm{ghost}$ extends the structure of $\mathcal{L}_\mathrm{SM}^\mathrm{ghost}$ specified in (2.2.6) by the hidden gauge sector with non-standard ghost and anti-ghost fields $u^{Z'}(x)$ and $\bar{u}^{Z'}(x)$. These fields cancel unphysical degrees of freedom associated with the non-standard gauge sector and only couple via the trilinear vertices $H_i\,u^{Z'}\bar{u}^{Z'}$, $i = 1, 2$ (cf. App. A.18). Compared to the SM (cf. Sect. 2.2), in the model with an EHS Φ_h the ghost fields u^A, u^Z and $u^\pm$ (and their overlined counterparts) have similar couplings. The only difference is that due to the mixing of the original scalar

---

[3]Regarding the quantization of the standard gauge sector we closely follow the conventions established for the SM in [83].

fields H and χ, in each of the three models under consideration couplings of the fields H_1 and H_2 to the ghost fields of the standard sector emerge.

The couplings involving standard and non-standard Faddeev-Popov fields are derived from (3.2.4) with the variation of the linear gauge-fixing operators (3.2.2) and (3.2.3) under the infinitesimal gauge transformations δA_μ, δZ_μ, $\delta W_\mu^\pm$, $\delta\varphi_{\rm s}$, $\delta\phi^\pm$, $\delta Z_\mu'$ and $\delta\varphi_{\rm h}$ specified in (2.1.32) and (3.1.32). The same holds for the propagators of the Faddeev-Popov ghosts. Corresponding Feynman rules ('t Hooft-Feynman gauge) are listed in Appendix A. Therein, furthermore the associated one-loop counterterms are listed. We refer to Sect. 5.3 where we amongst others introduce the renormalization of the unphysical sector.

Unless stated otherwise in this work we stick to the 't Hooft-Feynman gauge, such that $\xi_a = 1$ ($a = A, Z, W, Z'$) and $\xi_a' = 1$ ($a = Z, W, Z'$). Accordingly, the standard and non-standard mixing terms $Z_\mu\partial^\mu\varphi_{\rm s}$, $W_\mu^\pm\partial^\mu\phi^\pm$ and $Z_\mu'\partial^\mu\varphi_{\rm h}$ from the kinetic terms (3.1.26) and (3.1.29) are cancelled (cf. Sect. 2.2), the propagators of the gauge bosons have the simplest form, and the masses of the would-be Goldstone bosons and ghosts are equal to the masses of the related gauge bosons. Only in the context of renormalization we treat the seven distinct gauge-fixing parameters as independent quantities.

Closely related to the associated non-standard gauge sector, in the EHSL model the fields $u^{Z'}$ and $\bar{u}^{Z'}$ decouple in the limit $g_{\rm h} \to 0$. Note that according to (3.1.30) for a fixed value of the hidden vev $v_{\rm h}$ the limit $g_{\rm h} \to 0$ implies $M_{Z'} \to 0$ which results in $M_{\varphi_{\rm h}} \to 0$. Hence, also at the quantized level the limit $g_{\rm h} \to 0$ properly brings us back to the phenomenology of the EHSG model, where $\varphi_{\rm h}$ is a physical massless scalar field.

Finally, the complete Lagrangian of the (quantized) $\Phi_{\rm h}$ extension of the SM can be written as the sum

$$\mathcal{L}_{\rm EHS} = \mathcal{L}_{\rm EHS}^{\rm cl} + \mathcal{L}_{\rm EHS}^{\rm fix} + \mathcal{L}_{\rm EHS}^{\rm ghost}\,, \tag{3.2.5}$$

with $\mathcal{L}_{\rm EHS}^{\rm cl}$, $\mathcal{L}_{\rm EHS}^{\rm fix}$ and $\mathcal{L}_{\rm EHS}^{\rm ghost}$ specified in (3.1.1), (3.2.1) and (3.2.4).

3.3   BRS invariance

As already mentioned in the context of the SM, conventional gauge invariance is destructed once the inevitable gauge-fixing and Faddeev-Popov part has been added to the classical Lagrangian. Therefore, in $\mathcal{L}_{\rm EHS}$ we have lost the invariance under the local transformations defined in (2.1.15) and (3.1.12) for the EHSL model, respectively in (2.1.15) for the EHSG and EHSD models. The extended BRS symmetry can be found in analogy to Sect. 2.3 and provides the fundamental framework for the derivation of useful Slavnov-Taylor identities in the model with an EHS $\Phi_{\rm h}$. In the EHSL model we have to treat the $\mathrm{U}(1)_{Y_{\rm h}}$ symmetry, which is broken by the introduction of $\mathcal{L}_{\rm EHS}^{\rm fix}$, accordingly. Therefore, we have to define a suitable transformation behaviour of the associated non-standard ghost and anti-ghost fields $u^{Z'}$ and $\bar{u}^{Z'}$.

In the model with an EHS $\Phi_{\rm h}$ the infinitesimal $\mathrm{SU}(2)_{\rm W} \times \mathrm{U}(1)_Y$ gauge transformations of the fermions and standard gauge bosons are the same as in the SM. Consequently, the BRS transformations of the fermions, standard gauge bosons and standard

ghost and anti-ghost fields do not change compared to the SM and are thus already given in (2.3.5), (2.3.6) and (2.3.7).

The remaining BRS transformations in the EHSL model can be derived from (3.1.32), with the infinitesimal transformation parameters $\delta\theta^A$, $\delta\theta^Z$ and $\delta\theta^\pm$ replaced according to (2.3.1) and with $\delta\theta^{Z'}$ replaced according to

$$\delta\theta^{Z'} = \delta\lambda\, u^{Z'}. \tag{3.3.1}$$

The Grassmann-valued, infinitesimal constant $\delta\lambda$ in (2.3.1) and (3.3.1) anticommutes with the ghost fields of the standard and the hidden sector. We obtain the BRS transformations

$$\begin{aligned}
\boldsymbol{s}H_1 &= c_\alpha \left(\frac{M_Z}{v_{\rm s}} \varphi_{\rm s} u^Z + i\frac{M_W}{v_{\rm s}} \left[\phi^+ u^- - \phi^- u^+ \right] \right) + s_\alpha \frac{M_{Z'}}{v_{\rm h}} \varphi_{\rm h} u^{Z'}, \\
\boldsymbol{s}H_2 &= -s_\alpha \left(\frac{M_Z}{v_{\rm s}} \varphi_{\rm s} u^Z + i\frac{M_W}{v_{\rm s}} \left[\phi^+ u^- - \phi^- u^+ \right] \right) + c_\alpha \frac{M_{Z'}}{v_{\rm h}} \varphi_{\rm h} u^{Z'}, \\
\boldsymbol{s}\phi^\pm &= \mp ie\phi^\pm \left[u^A + \frac{s_W^2 - c_W^2}{2 s_W c_W} u^Z \right] \pm i\frac{M_W}{v_{\rm s}} \left[v_{\rm s} + c_\alpha H_1 - s_\alpha H_2 \pm i\varphi_{\rm s} \right] u^\pm, \\
\boldsymbol{s}\varphi_{\rm s} &= -\frac{M_Z}{v_{\rm s}} \left[v_{\rm s} + c_\alpha H_1 - s_\alpha H_2 \right] u^Z + \frac{M_W}{v_{\rm s}} \left[\phi^+ u^- + \phi^- u^+ \right], \\
\boldsymbol{s}\varphi_{\rm h} &= -\frac{M_{Z'}}{v_{\rm h}} \left[v_{\rm h} + s_\alpha H_1 + c_\alpha H_2 \right] u^{Z'}, \\
\boldsymbol{s}Z'_\mu &= \partial_\mu u^{Z'},
\end{aligned} \tag{3.3.2}$$

making use of the BRS operator $\boldsymbol{s}$ which is defined in (2.3.2). The BRS transformations of the non-standard ghost $u^{Z'}$ and anti-ghost $\bar{u}^{Z'}$ are defined such that the requirement $\delta_{\rm BRS}(\mathcal{L}_{\rm EHS}^{\rm fix} + \mathcal{L}_{\rm EHS}^{\rm ghost}) = 0$ is fulfilled. In this way, for general $\xi_{Z'}$ and $\xi'_{Z'}$ we obtain the BRS transformations

$$\boldsymbol{s}u^{Z'} = 0, \qquad \boldsymbol{s}\bar{u}^{Z'} = -\frac{1}{\xi_{Z'}} F^{Z'}. \tag{3.3.3}$$

The $\mathrm{SU}(2)_{\rm W} \times \mathrm{U}(1)_Y$ BRS transformations of $\phi^\pm$ and $\varphi_{\rm s}$ in (3.3.2) also apply to the EHSG and EHSD models. In the EHSG model there is no BRS transformation for the global $\mathrm{U}(1)_{Y_{\rm h}}$ symmetry and according to (2.3.1) and (3.1.34) the non-standard scalar fields transform as

$$\begin{aligned}
H_1 &\to H_1 + c_\alpha \left(\frac{M_Z}{v_{\rm s}} \varphi_{\rm s}\, \delta\lambda\, u^Z + i\frac{M_W}{v_{\rm s}} \left[\phi^+ \delta\lambda\, u^- - \phi^- \delta\lambda\, u^+ \right] \right) + s_\alpha \varphi_{\rm h} \delta\theta_{\rm h}, \\
H_2 &\to H_2 - s_\alpha \left(\frac{M_Z}{v_{\rm s}} \varphi_{\rm s}\, \delta\lambda\, u^Z + i\frac{M_W}{v_{\rm s}} \left[\phi^+ \delta\lambda\, u^- - \phi^- \delta\lambda\, u^+ \right] \right) + c_\alpha \varphi_{\rm h} \delta\theta_{\rm h}, \\
\varphi_{\rm h} &\to \varphi_{\rm h} - \left[v_{\rm h} + s_\alpha H_1 + c_\alpha H_2 \right] \delta\theta_{\rm h},
\end{aligned} \tag{3.3.4}$$

with the infinitesimal global transformation parameter $\delta\theta_{\rm h}$ specified in (3.1.35).

In the EHSD model the $\mathrm{SU}(2)_{\rm W} \times \mathrm{U}(1)_Y$ BRS transformations of H_1 and H_2 follow

from (2.3.1) and (3.1.36) and read

$$
\begin{aligned}
\boldsymbol{s}H_1 &= c_\alpha \left(\frac{M_Z}{v_{\mathrm{s}}} \varphi_{\mathrm{s}} u^Z + i\frac{M_W}{v_{\mathrm{s}}} \left[\phi^+ u^- - \phi^- u^+ \right] \right), \\
\boldsymbol{s}H_2 &= -s_\alpha \left(\frac{M_Z}{v_{\mathrm{s}}} \varphi_{\mathrm{s}} u^Z + i\frac{M_W}{v_{\mathrm{s}}} \left[\phi^+ u^- - \phi^- u^+ \right] \right).
\end{aligned}
\tag{3.3.5}
$$

The $\mathrm{SU}(2)_{\mathrm{W}} \times \mathrm{U}(1)_Y$ BRS transformations in the real-Φ_{h} extension of the SM have already been given in [51].

In Appendix B we utilize the global $\mathrm{U}(1)_{Y_{\mathrm{h}}}$ transformations in (3.3.4) in order to derive a helpful set of Ward identities between scalar vertex functions from the global $\mathrm{U}(1)_{Y_{\mathrm{h}}}$ invariance of the generating vertex functional (cf. App. B.1). These $\mathrm{U}(1)_{Y_{\mathrm{h}}}$ Ward identities can be used for consistency checks, in particular with regard to the one-loop renormalization of the EHSG model which is discussed in Chapter 5.

Slavnov-Taylor identities between Green functions

The Slavnov-Taylor identities between Green functions of spontaneously broken gauge theories can be written in the generic form [83]

$$
0 = \frac{\delta_{\mathrm{BRS}}}{\delta\lambda} \left\langle T \prod_l \Psi_{I_l} \right\rangle = \boldsymbol{s} \left\langle T \prod_l \Psi_{I_l} \right\rangle,
\tag{3.3.6}
$$

where the Green functions are written as vevs $\langle \dots \rangle$ of time-ordered products of fields. Here, a generic field Ψ_{I_l} (with the index I containing the possibly occurring indices) stands for one of the fields $W_\mu^\pm$, Z_μ, A_μ, $\psi_{i,\pm}^{\mathrm{L}}$, $\overline{\psi}_{i,\pm}^{\mathrm{L}}$, ψ_i^{R}, $\overline{\psi}_i^{\mathrm{R}}$, H_1, H_2, Z_μ', $\phi^\pm$, φ_{s}, φ_{h}, u^a and $\overline{u}^a$, or for one of the gauge-fixing operators F^a ($a = A, Z, \pm, Z'$). For on-shell asymptotic fields we denote the corresponding physical components by $\Psi_{I_l}^{\mathrm{phys}}$. According to [95–97] the BRS variation of the latter must vanish, i.e.

$$
\boldsymbol{s}\Psi_{I_l}^{\mathrm{phys}} = 0.
\tag{3.3.7}
$$

In Chapter 7 we make use of (3.3.6) and (3.3.7) in order to confirm the Goldstone-boson equivalence theorem in the limit of massless Z' bosons at the one-loop level.

Chapter 4

Perturbative unitarity

In order to obtain a detailed overview over the regions of interest in non-standard parameter space, i.e. about those regions where the model with an EHS Φ_h is reliable on perturbative grounds, we study the related issue of (tree-level) perturbative unitarity in this chapter. The EHSL and EHSD models have already been discussed earlier in this context in [29] and [39]. The authors followed the guideline of [98] in which an upper bound for the Higgs mass in the SM was derived from tree-level perturbative unitarity for the first time. Here, we perform a similar analysis in order to obtain bounds for the non-standard parameters α, M_{H_2} and v_h. We obtain more compact and easy-to-handle expressions for the set of inequalities which represent the bounds from tree-level perturbative unitarity in the complex-Φ_h and in the real-Φ_h extension of the SM. This is achieved with the help of orthogonal transformation matrices which convert the scattering matrices in the high-energy limit from the basis of the original scalar fields H and χ into the corresponding mass-eigenstate basis and vice versa.

4.1   Concept

The framework of [98] can be extended in order to obtain constraints for models with more involved Higgs sectors.[1] For such an analysis several (model-dependent) bosonic $2 \rightarrow 2$ scattering processes have to be considered. Analogously to the SM, a partial wave analysis shows that only the $l = 0$ partial waves (angular momentum l) for the scattering channels involving the associated physical scalar bosons and longitudinal vector bosons in the external legs are relevant for unitarity considerations. According to the Goldstone-boson equivalence theorem (cf. Subsect. 7.2.7), in the high-energy limit the external longitudinally-polarized gauge bosons can be replaced by the associated would-be Goldstone bosons. Thus, only pure scalar high-energy $2 \rightarrow 2$ scattering processes have to be considered with regard to this analysis of perturbative unitarity.

For the EHS models the relevant processes can be summarized in terms of respective

---

[1]In the same way e.g. the two-Higgs-doublet model has been discussed in [99]. Furthermore, we refer to [60] where the real-Φ_h extension of the SM without $\mathcal{Z}_2^D$ symmetry in the SM limit is examined in a similar manner.

scattering matrices. Propagator-suppressed processes can be neglected in the high-energy limit. Consequently, each element of a given scattering matrix is determined just by one of the tree-level quartic scalar self-couplings emerging from the modified Higgs potential (3.1.5). We thus have to distinguish between two distinct sets of quartic scalar self-couplings − the one corresponding to the complex-Φ_h extension and the one corresponding to the real-Φ_h extension of the SM. The high-energy scattering matrix for the EHSL model is identical to the one for the EHSG model and from this analysis we hence obtain identical bounds for these two models.[2] For the real-Φ_h extension of the SM we obtain different bounds due to the absence of the imaginary part φ_h.

Equipped with the two pure scalar high-energy scattering matrices for the complex-Φ_h and real-Φ_h extensions of the SM, we derive the bounds in the following way: for each of the two-particle initial states we require that the probability of scattering into the sum of accessible two-particle final states is less or equal to one. From this requirement we obtain upper bounds for the eigenvalues of the two scattering matrices which depend on the free original parameters λ_s, λ_h and η associated with the modified Higgs potential (3.1.5). With the help of (3.1.24) these constraints can be translated into corresponding bounds for the free parameters α, M_{H_2} and v_h.

For the numerical analysis in this chapter, the standard vev v_s is approximated by the value 246 GeV, according to $v_s^2 \approx 1/(\sqrt{2}G_F) \approx (246\,\text{GeV})^2$, with the Fermi constant G_F [100, 101]. Throughout in this work, we fix the mass of the standard-like Higgs boson M_{H_1} to the current experimental central value of 125.09 GeV [19].

4.2 Calculation

Performing a partial wave decomposition of the matrix element $\mathcal{M}$ which corresponds to the generic scalar scattering process $S_1 S_2 \to S_3 S_4$ yields

$$\mathcal{M}(s, \theta) = 16\pi \sum_{l=0}^{\infty} (2l+1) P_l(\cos\theta) a_l(s), \qquad (4.2.1)$$

with the Mandelstam variable s (center-of-mass energy squared), the partial wave amplitudes a_l and the Legendre polynomials P_l which depend on the cosine of the scattering angle θ. In the center-of-mass system the corresponding differential cross section can be written as

$$\frac{d\sigma}{d\Omega} = \frac{1}{64\pi^2 s} |\mathcal{M}|^2. \qquad (4.2.2)$$

Exploiting the orthogonality of the P_l, we obtain the total cross section

$$\sigma = \int_0^{2\pi} \int_{-1}^{+1} d(\cos\theta) \frac{d\sigma}{d\Omega} = \frac{16\pi}{s} \sum_{l=0}^{\infty} (2l+1) |a_l|^2 \qquad (4.2.3)$$

---

[2]This is because, similarly to [29], we desist from considering non-standard parameter regions in the EHSL model where the corresponding (g_h-dependent) transverse amplitudes might be non-negligible.

of the generic scattering process $S_1 S_2 \to S_3 S_4$. With the help of the optical theorem we can relate (4.2.3) to the imaginary part of the corresponding forward scattering amplitude, which yields

$$|a_l|^2 = \operatorname{Re}(a_l)^2 + \operatorname{Im}(a_l)^2 \overset{!}{=} \operatorname{Im}(a_l) \tag{4.2.4}$$

and leads us to the unitarity constraint

$$|\operatorname{Re}(a_l)| \le \frac{1}{2} \tag{4.2.5}$$

for the partial wave amplitudes.[3] The partial wave amplitudes a_l in (4.2.5) can be written as

$$a_l(s) = \frac{1}{32\pi} \int_{-1}^{+1} d(\cos\theta) \, P_l(\cos\theta) \, \mathcal{M}(s, \theta), \tag{4.2.6}$$

which follows from inversion of (4.2.1).

For an analysis of the significant scattering amplitudes in the limit $s \to \infty$ it is sufficient to restrict us to the $l = 0$ partial waves and to neglect processes mediated by internal propagators. Accordingly, the matrix element in (4.2.6) reduces to the generic quartic scalar self-coupling $C_{S_1 S_2 S_3 S_4}$ which corresponds to the underlying tree-level scattering process $S_1 S_2 \to S_3 S_4$ and the constraint (4.2.5) can be converted into

$$|C_{S_1 S_2 S_3 S_4}| \le 8\pi. \tag{4.2.7}$$

The constraint (4.2.7) already constitutes an upper bound for the quartic scalar self-couplings $C_{S_1 S_2 S_3 S_4}$ which stem from the modified Higgs potential (3.1.5). In the EHSL and EHSG models we have $S_1, S_2, S_3, S_4 \in \{H_1, H_2, \varphi_{\rm s}, \phi^{\pm}, \varphi_{\rm h}\}$, in the EHSD model we have $S_1, S_2, S_3, S_4 \in \{H_1, H_2, \varphi_{\rm s}, \phi^{\pm}\}$. The couplings $C_{S_1 S_2 S_3 S_4}$ which are listed in App. A.11 depend on the free parameters α, M_{H_2} and $v_{\rm h}$. Thus, (4.2.7) already puts a constraint on the latter.

So far, we treated the distinct $2 \to 2$ scatterings separately. More stringent bounds for the non-standard parameters α, M_{H_2} and $v_{\rm h}$ are obtained by the requirement that the probability of scattering into the sum of accessible two-particle final states is less or equal to one for each of the two-particle initial states. This corresponds to the requirement that the eigenvalues of the scattering matrices obey the constraint (4.2.7) initially imposed on the individual quartic scalar self-couplings of the EHS models.

The 15×15 scattering matrix $\boldsymbol{M}_{15 \times 15}^{H_1 H_2}$ for the complex-$\Phi_{\rm h}$ extension of the SM is defined in the basis

$$\begin{aligned} &(\phi^+ \phi^-, \varphi_{\rm s}\varphi_{\rm s}/\sqrt{2}, \varphi_{\rm h}\varphi_{\rm h}/\sqrt{2}, H_1 H_1/\sqrt{2}, H_2 H_2/\sqrt{2}, H_1 H_2, \\ &\phi^+ H_1, \phi^+ H_2, \phi^+ \varphi_{\rm s}, \phi^+ \varphi_{\rm h}, \varphi_{\rm s} H_1, \varphi_{\rm s} H_2, \varphi_{\rm h} H_1, \varphi_{\rm h} H_2, \varphi_{\rm h} \varphi_{\rm s}), \end{aligned} \tag{4.2.8}$$

where the fields $\phi^{\pm}$ and $\varphi_{\rm s}$ stand for the longitudinal $W_\mu^{\pm}$ and Z_μ, and the field $\varphi_{\rm h}$ either stands for the longitudinal Z'_μ (EHSL model) or for the physical non-standard

---

[3]We can also derive a less stringent bound $|a_l| \le 1$ from (4.2.4) just by exploiting the fact that $\operatorname{Im}(a_l) \le |a_l|$. However, here we consider the stronger bound (4.2.5) which can be deduced by a graphical consideration of (4.2.4).

Goldstone boson φ_h (EHSG model). We take into account normalization factors $1/\sqrt{2}$ for identical fields in the initial and final states of the scattering processes. More explicitly, the block-diagonal scattering matrix $\boldsymbol{M}^{H_1 H_2}_{15\times 15}$ can be written as

$$\boldsymbol{M}^{H_1 H_2}_{15\times 15} = \begin{pmatrix} \boldsymbol{A}^{H_1 H_2}_{6\times 6} & & \\ & \boldsymbol{B}^{H_1 H_2}_{4\times 4} & \\ & & \boldsymbol{C}^{H_1 H_2}_{5\times 5} \end{pmatrix}, \tag{4.2.9}$$

with the submatrix

$$\boldsymbol{A}^{H_1 H_2}_{6\times 6} = \begin{pmatrix} C_{\phi^4} & \frac{C_{\phi^2 \varphi_\mathrm{s}^2}}{\sqrt{2}} & \frac{C_{\phi^2 \varphi_\mathrm{h}^2}}{\sqrt{2}} & \frac{C_{H_1^2 \phi^2}}{\sqrt{2}} & \frac{C_{H_2^2 \phi^2}}{\sqrt{2}} & C_{H_1 H_2 \phi^2} \\ \frac{C_{\phi^2 \varphi_\mathrm{s}^2}}{\sqrt{2}} & \frac{C_{\varphi_\mathrm{s}^4}}{2} & \frac{C_{\varphi_\mathrm{s}^2 \varphi_\mathrm{h}^2}}{2} & \frac{C_{H_1^2 \varphi_\mathrm{s}^2}}{2} & \frac{C_{H_2^2 \varphi_\mathrm{s}^2}}{2} & \frac{C_{H_1 H_2 \varphi_\mathrm{s}^2}}{\sqrt{2}} \\ \frac{C_{\phi^2 \varphi_\mathrm{h}^2}}{\sqrt{2}} & \frac{C_{\varphi_\mathrm{s}^2 \varphi_\mathrm{h}^2}}{2} & \frac{C_{\varphi_\mathrm{h}^4}}{2} & \frac{C_{H_1^2 \varphi_\mathrm{h}^2}}{2} & \frac{C_{H_2^2 \varphi_\mathrm{h}^2}}{2} & \frac{C_{H_1 H_2 \varphi_\mathrm{h}^2}}{\sqrt{2}} \\ \frac{C_{H_1^2 \phi^2}}{\sqrt{2}} & \frac{C_{H_1^2 \varphi_\mathrm{s}^2}}{2} & \frac{C_{H_1^2 \varphi_\mathrm{h}^2}}{2} & \frac{C_{H_1^4}}{2} & \frac{C_{H_1^2 H_2^2}}{2} & \frac{C_{H_1^3 H_2}}{\sqrt{2}} \\ \frac{C_{H_2^2 \phi^2}}{\sqrt{2}} & \frac{C_{H_2^2 \varphi_\mathrm{s}^2}}{2} & \frac{C_{H_2^2 \varphi_\mathrm{h}^2}}{2} & \frac{C_{H_1^2 H_2^2}}{2} & \frac{C_{H_2^4}}{2} & \frac{C_{H_1 H_2^3}}{\sqrt{2}} \\ C_{H_1 H_2 \phi^2} & \frac{C_{H_1 H_2 \varphi_\mathrm{s}^2}}{\sqrt{2}} & \frac{C_{H_1 H_2 \varphi_\mathrm{h}^2}}{\sqrt{2}} & \frac{C_{H_1^3 H_2}}{\sqrt{2}} & \frac{C_{H_1 H_2^3}}{\sqrt{2}} & C_{H_1^2 H_2^2} \end{pmatrix}, \tag{4.2.10}$$

the submatrix

$$\boldsymbol{B}^{H_1 H_2}_{4\times 4} = \begin{pmatrix} C_{H_1^2 \phi^2} & C_{H_1 H_2 \phi^2} & 0 & 0 \\ C_{H_1 H_2 \phi^2} & C_{H_2^2 \phi^2} & 0 & 0 \\ 0 & 0 & C_{\phi^2 \varphi_\mathrm{s}^2} & 0 \\ 0 & 0 & 0 & C_{\phi^2 \varphi_\mathrm{h}^2} \end{pmatrix}, \tag{4.2.11}$$

and the submatrix

$$\boldsymbol{C}^{H_1 H_2}_{5\times 5} = \begin{pmatrix} C_{H_1^2 \varphi_\mathrm{s}^2} & C_{H_1 H_2 \varphi_\mathrm{s}^2} & 0 & 0 & 0 \\ C_{H_1 H_2 \varphi_\mathrm{s}^2} & C_{H_2^2 \varphi_\mathrm{s}^2} & 0 & 0 & 0 \\ 0 & 0 & C_{H_1^2 \varphi_\mathrm{h}^2} & C_{H_1 H_2 \varphi_\mathrm{h}^2} & 0 \\ 0 & 0 & C_{H_1 H_2 \varphi_\mathrm{h}^2} & C_{H_2^2 \varphi_\mathrm{h}^2} & 0 \\ 0 & 0 & 0 & 0 & C_{\varphi_\mathrm{s}^2 \varphi_\mathrm{h}^2} \end{pmatrix}. \tag{4.2.12}$$

As a short notation, we introduced the powers of multiply occurring fields in the index of a quartic scalar self-coupling, with $\phi = \phi^\pm$ having regard to conservation of electric charge. A direct calculation of the eigenvalues of $\boldsymbol{M}^{H_1 H_2}_{15\times 15}$ is quite involved and results in bulky analytic expressions which are unsuitable for our purpose. We therefore introduce the transformation matrix $\boldsymbol{U}_\alpha$ which converts $\boldsymbol{M}^{H_1 H_2}_{15\times 15}$ into the related scattering matrix $\boldsymbol{M}^{H\chi}_{15\times 15}$ defined in the basis of the original scalar fields H and χ,

$$\begin{aligned} &(\phi^+ \phi^-, \varphi_\mathrm{s} \varphi_\mathrm{s}/\sqrt{2}, \varphi_\mathrm{h} \varphi_\mathrm{h}/\sqrt{2}, HH/\sqrt{2}, \chi\chi/\sqrt{2}, H\chi, \\ &\phi^+ H, \phi^+ \chi, \phi^+ \varphi_\mathrm{s}, \phi^+ \varphi_\mathrm{h}, \varphi_\mathrm{s} H, \varphi_\mathrm{s} \chi, \varphi_\mathrm{h} H, \varphi_\mathrm{h} \chi, \varphi_\mathrm{h} \varphi_\mathrm{s}), \end{aligned} \tag{4.2.13}$$

according to

$$\boldsymbol{M}^{H_1 H_2}_{15\times 15} = \boldsymbol{U}^\mathsf{T}_\alpha \boldsymbol{M}^{H\chi}_{15\times 15} \boldsymbol{U}_\alpha. \tag{4.2.14}$$

In other words, the real-valued block-diagonal matrix $\boldsymbol{U}_\alpha$ transforms the basis vector (4.2.8) into the basis vector (4.2.13) and can thus be written as follows,

$$\boldsymbol{U}_\alpha = \begin{pmatrix} \boldsymbol{A}_{3\times3} & & \\ & \boldsymbol{B}_{5\times5} & \\ & & \boldsymbol{C}_{7\times7} \end{pmatrix}, \qquad (4.2.15)$$

where $\boldsymbol{A}_{3\times3} = \mathbb{1}_{3\times3}$ and the submatrices $\boldsymbol{B}_{5\times5}$ and $\boldsymbol{C}_{7\times7}$ are given by

$$\boldsymbol{B}_{5\times5} = \begin{pmatrix} c_\alpha^2 & s_\alpha^2 & -\sqrt{2}s_\alpha c_\alpha & 0 & 0 \\ s_\alpha^2 & c_\alpha^2 & \sqrt{2}s_\alpha c_\alpha & 0 & 0 \\ \sqrt{2}s_\alpha c_\alpha & -\sqrt{2}s_\alpha c_\alpha & c_{2\alpha} & 0 & 0 \\ 0 & 0 & 0 & c_\alpha & -s_\alpha \\ 0 & 0 & 0 & s_\alpha & c_\alpha \end{pmatrix} \qquad (4.2.16)$$

and

$$\boldsymbol{C}_{7\times7} = \begin{pmatrix} 1 & 0 & 0 & 0 & 0 & 0 & 0 \\ 0 & 1 & 0 & 0 & 0 & 0 & 0 \\ 0 & 0 & c_\alpha & -s_\alpha & 0 & 0 & 0 \\ 0 & 0 & s_\alpha & c_\alpha & 0 & 0 & 0 \\ 0 & 0 & 0 & 0 & c_\alpha & -s_\alpha & 0 \\ 0 & 0 & 0 & 0 & s_\alpha & c_\alpha & 0 \\ 0 & 0 & 0 & 0 & 0 & 0 & 1 \end{pmatrix}. \qquad (4.2.17)$$

Equipped with (4.2.15)−(4.2.17) it is straightforward to verify that $\boldsymbol{U}_\alpha^\mathsf{T}\boldsymbol{U}_\alpha = \mathbb{1}_{15\times15}$, i.e. $\boldsymbol{U}_\alpha$ is orthogonal. Note that the normalization factors $1/\sqrt{2}$ for identical fields in (4.2.8) and (4.2.13) are crucial in order to find an orthonormal $\boldsymbol{U}_\alpha$.[4] Because $\boldsymbol{U}_\alpha$ is orthonormal the eigenvalues of $\boldsymbol{M}_{15\times15}^{H\chi}$ are identical to the eigenvalues of $\boldsymbol{M}_{15\times15}^{H_1 H_2}$. Therefore, we are free to calculate these from the considerably less complex scattering matrix $\boldsymbol{M}_{15\times15}^{H\chi}$. More explicitly, we have

$$\boldsymbol{M}_{15\times15}^{H\chi} = \begin{pmatrix} \boldsymbol{A}_{5\times5}^{H\chi} & \\ & \boldsymbol{B}_{10\times10}^{H\chi} \end{pmatrix}, \qquad (4.2.18)$$

with the submatrix

$$\boldsymbol{A}_{5\times5}^{H\chi} = \begin{pmatrix} C_{\phi^4} & \frac{C_{\phi^2\varphi_{\mathrm{s}}^2}}{\sqrt{2}} & \frac{C_{\phi^2\varphi_{\mathrm{h}}^2}}{\sqrt{2}} & \frac{C_{H^2\phi^2}}{\sqrt{2}} & \frac{C_{\chi^2\phi^2}}{\sqrt{2}} \\ \frac{C_{\phi^2\varphi_{\mathrm{s}}^2}}{\sqrt{2}} & \frac{C_{\varphi_{\mathrm{s}}^4}}{2} & \frac{C_{\varphi_{\mathrm{s}}^2\varphi_{\mathrm{h}}^2}}{2} & \frac{C_{H^2\varphi_{\mathrm{s}}^2}}{2} & \frac{C_{\chi^2\varphi_{\mathrm{s}}^2}}{2} \\ \frac{C_{\phi^2\varphi_{\mathrm{h}}^2}}{\sqrt{2}} & \frac{C_{\varphi_{\mathrm{s}}^2\varphi_{\mathrm{h}}^2}}{2} & \frac{C_{\varphi_{\mathrm{h}}^4}}{2} & \frac{C_{H^2\varphi_{\mathrm{h}}^2}}{2} & \frac{C_{\chi^2\varphi_{\mathrm{h}}^2}}{2} \\ \frac{C_{H^2\phi^2}}{\sqrt{2}} & \frac{C_{H^2\varphi_{\mathrm{s}}^2}}{2} & \frac{C_{H^2\varphi_{\mathrm{h}}^2}}{2} & \frac{C_{H^4}}{2} & \frac{C_{H^2\chi^2}}{2} \\ \frac{C_{\chi^2\phi^2}}{\sqrt{2}} & \frac{C_{\chi^2\varphi_{\mathrm{s}}^2}}{2} & \frac{C_{\chi^2\varphi_{\mathrm{h}}^2}}{2} & \frac{C_{H^2\chi^2}}{2} & \frac{C_{\chi^4}}{2} \end{pmatrix}, \qquad (4.2.19)$$

and the diagonal submatrix

$$\begin{aligned} \boldsymbol{B}_{10\times10}^{H\chi} = \operatorname{diag}(&C_{H^2\chi^2}, C_{H^2\phi^2}, C_{\chi^2\phi^2}, C_{\phi^2\varphi_{\mathrm{s}}^2}, C_{\phi^2\varphi_{\mathrm{h}}^2}, \\ &C_{H^2\varphi_{\mathrm{s}}^2}, C_{\chi^2\varphi_{\mathrm{s}}^2}, C_{H^2\varphi_{\mathrm{h}}^2}, C_{\chi^2\varphi_{\mathrm{h}}^2}, C_{\varphi_{\mathrm{s}}^2\varphi_{\mathrm{h}}^2}). \end{aligned} \qquad (4.2.20)$$

---

[4]As indicated in [60] these normalization factors are often ignored in the literature.

The quartic couplings which determine the non-trivial entries of the scattering matrix $\boldsymbol{M}^{H\chi}_{15\times15}$ (summarized in the submatrices $\boldsymbol{A}^{H\chi}_{5\times5}$ and $\boldsymbol{B}^{H\chi}_{10\times10}$) are derived from the quartic interaction terms listed in the last three lines of (3.1.15). The entries of $\boldsymbol{M}^{H\chi}_{15\times15}$ thus exhibit a very simple structure, in particular in terms of the original parameters λ_s, λ_h and η. The corresponding submatrices (4.2.19) and (4.2.20) provide us with the five distinct eigenvalues

$$
\begin{aligned}
e^\mathrm{c}_\mathrm{s} = \frac{\lambda_\mathrm{s}}{2}, \qquad\qquad e^\mathrm{c}_\mathrm{h} &= \frac{\lambda_\mathrm{h}}{2}, \qquad\qquad e^\mathrm{c}_\eta = \eta, \\
e^\mathrm{c}_\pm = \frac{1}{4}\left(3\lambda_\mathrm{s} + 2\lambda_\mathrm{h} \pm \sqrt{32\eta^2 + (2\lambda_\mathrm{h} - 3\lambda_\mathrm{s})^2}\right)&,
\end{aligned}
\tag{4.2.21}
$$

where the upper index c denotes the affiliation with the complex-Φ_h extension of the SM. As already mentioned above, the bounds from perturbative unitarity are obtained from the requirement

$$
\left|e^\mathrm{c}_\mathrm{s}\right|, \left|e^\mathrm{c}_\mathrm{h}\right|, \left|e^\mathrm{c}_\eta\right|, \left|e^\mathrm{c}_\pm\right| \leq 8\pi.
\tag{4.2.22}
$$

The same procedure (4.2.8)$-$(4.2.22) can be performed for the real-Φ_h extension of the SM. The two bases are then obtained from (4.2.8) and (4.2.13) by erasing the entries involving the non-standard Goldstone boson φ_h. Analogously to (4.2.14) we find an orthogonal matrix which transforms the corresponding 10×10 scattering matrix from one basis into the other. Following the same approach we obtain the four distinct eigenvalues

$$
e^\mathrm{r}_\mathrm{s} = \frac{\lambda_\mathrm{s}}{2}, \quad e^\mathrm{r}_\eta = \eta, \quad e^\mathrm{r}_\pm = \frac{1}{8}\left(6\lambda_\mathrm{s} + 3\lambda_\mathrm{h} \pm \sqrt{64\eta^2 + 9(\lambda_\mathrm{h} - 2\lambda_\mathrm{s})^2}\right),
\tag{4.2.23}
$$

where the upper index r denotes the affiliation with the real-Φ_h extension of the SM. Again, we require

$$
|e^\mathrm{r}_\mathrm{s}|, |e^\mathrm{r}_\eta|, |e^\mathrm{r}_\pm| \leq 8\pi
\tag{4.2.24}
$$

in order to obtain the bounds from perturbative unitarity.

Taking into account (3.1.24), the bounds (4.2.22) and (4.2.24) for the complex-Φ_h and real-Φ_h extensions of the SM can be translated into appropriate constraints for the non-standard parameters α, M_{H_2} and v_h. In the following, we survey these constraints numerically within the non-standard parameter region $|\alpha| \leq \pi/6$ (cf. Sect. 6.1) and $1\ \mathrm{GeV} \leq M_{H_2} \leq 5\ \mathrm{TeV}$.

4.3   Numerical results

In Figs. 4.1a,b the bounds (4.2.22) for the complex-Φ_h extension (left side) and the bounds (4.2.24) for the real-Φ_h extension (right side) are depicted in the plane α and M_{H_2} for different v_h. The red ($v_\mathrm{h} = 100\ \mathrm{GeV}$), orange ($v_\mathrm{h} = 280\ \mathrm{GeV}$), brown ($v_\mathrm{h} = 500$ GeV), blue ($v_\mathrm{h} = 1\ \mathrm{TeV}$) and green ($v_\mathrm{h} = 10\ \mathrm{TeV}$) boundary lines represent the upper bounds for M_{H_2} (i.e. the maximally allowed M_{H_2}).

The results for the complex-Φ_h extension (EHSL and EHSG models) exhibit the same behaviour as those for the real-Φ_h extension (EHSD model). It becomes obvious
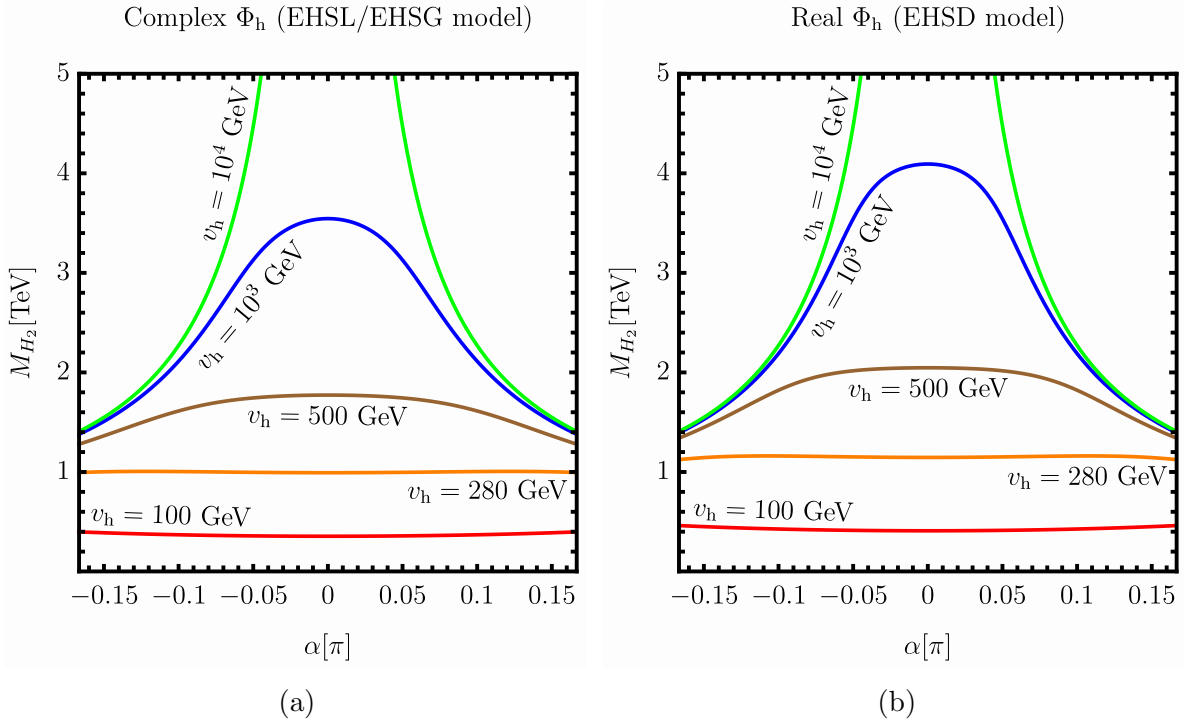
Figure 4.1: Exclusion bounds from tree-level perturbative unitarity for the complex-Φ_h extension of the SM (left side) and for the real-Φ_h extension of the SM (right side) in the plane α and M_{H_2} for different v_h. Excluded regions lie above the displayed boundary lines. The results on the left apply to the EHSL and EHSG models, the results on the right apply to the EHSD model.

that smaller v_h lead to stronger bounds from perturbative unitarity. For large $v_h \gtrsim 10$ TeV we obtain the weakest unitarity bounds. In this large-v_h region the variation of the input parameter v_h becomes irrelevant. This is because v_h only appears in the denominators of the quartic scalar self-couplings which involve fields carrying non-standard components. The other non-standard parameters which enter the analysis, namely α and M_{H_2}, only appear in the numerators of the quartic scalar self-couplings (cf. App. A.11). Our numerical results show that for $v_h \gtrsim 10$ TeV the hidden vev is large enough to sufficiently suppress associated parts in the quartic scalar self-couplings such that corresponding unitarity bounds are not anymore v_h-sensitive. Consequently, the green exclusion bounds furthermore can be interpreted as the bounds which depict the maximally allowed M_{H_2} for $v_h \gtrsim 10$ TeV. Moreover, the consideration above explains why the bounds from perturbative unitarity become stronger for smaller v_h.

A comparison of the exclusion bounds for $v_h \leq 1$ TeV in Figs. 4.1a,b shows that stronger bounds from perturbative unitarity are obtained in the complex-Φ_h extension. This is what we expect because compared to the latter fewer scattering channels have to be taken into account in the real-Φ_h extension. However, comparing the green exclusion bounds in Figs. 4.1a,b we conclude that in the $v_h \gtrsim 10$ TeV region constraints from perturbative unitarity for the parameters α, M_{H_2} and v_h are in good approximation

the same in the EHSL, EHSG and EHSD models. We can explain this observation by taking a closer look at those quartic scalar self-couplings in the scattering matrix $\boldsymbol{M}_{15\times15}^{H_1H_2}$ which involve the hidden Goldstone boson φ_h and which are thus responsible for the extra scattering channels we have to consider in the complex-Φ_h extension. These couplings are always proportional to at least one power of v_h^{-1} and hence negligible for sufficiently large v_h.

We conclude that for $v_\mathrm{h} = 280$ GeV in each of the three models values of M_{H_2} up to about 1 TeV are allowed by perturbative unitarity for all α. For very small $v_\mathrm{h} = 100$ GeV we are even capable to put constraints on moderate M_{H_2} way below the TeV scale. For larger v_h well above the electroweak scale, small mixing angles can compensate for a non-perturbative blow-up of the quartic couplings such that very large M_{H_2} up to several TeV cannot be excluded by perturbative unitarity.

Chapter 5

Renormalization

Higher-order calculations are necessary in order to keep up with the precision of present and future collider experiments. Moreover, the exploration of quantum effects contributing to related physical observables often leads to significant indirect constraints for the free parameters of a given model. For a meaningful prediction beyond the tree-graph approximation the theory first has to be renormalized.

Renormalization is required because higher-order Feynman diagrams give rise to ultraviolet (UV) divergences which, without a proper treatment, spoil the calculations. The procedure of renormalization basically consists of a suitable redefinition of the original parameters and fields such that in the end, all the UV divergences are eliminated in the renormalized Green functions and S-matrix elements. In a renormalizable theory this is achievable at all orders of perturbation theory. For the general proof of renormalizability of gauge theories we refer to [91, 102, 103].

The SM is a renormalizable theory and the same holds for the extensions we consider in this work. In the model with an EHS Φ_{h} the renormalization of the extended sector has to be established with care, such that all the UV-divergent standard and non-standard higher-order contributions are properly absorbed without infringing the symmetries of the theory. The one-loop renormalization of the EHSD model has already been discussed in [51]. Furthermore, we refer to [54, 56] where the one-loop renormalization of the real-Φ_{h} extension without the $\mathcal{Z}_2^{\mathrm{D}}$ symmetry has been constructed.

In this chapter we establish a new complete one-loop renormalization scheme for the EHSL model such that the limit $g_{\mathrm{h}} \to 0$ provides a smooth transition to the renormalized EHSG model. From the latter the renormalized EHSD model is obtained just by subsequently removing the component field φ_{h}. Thus, the renormalization scheme we construct in this chapter enables a convenient comparison of NLO predictions of these three extensions of the SM. Within the context of Chapter 7 this feature among others provides us with a test of gauge invariance regarding our renormalization scheme. Moreover, our renormalization scheme treats the unphysical sector such that the entire set of Green functions is properly renormalized.[1]

---

[1] We checked this analytically for every single one-loop vertex function with the help of the `Mathematica` packages `FeynArts` [78] and `FormCalc` [104].

5.1   Concept of one-loop calculations

In general, the LO relations between observables and the original bare parameters of a gauge theory are changed by higher-order corrections. Furthermore, beyond the LO the bare parameters become divergent. These divergent higher-order contributions either have UV, infrared or collinear origin. Collinear singularities emerge from the vanishing momentum-squares of external legs which are directly coupled to two internal massless propagators. Infrared singularities originate from the virtual exchange of certain massless particles (like e.g. photons). At this point, we emphasize that the virtual exchange of massless φ_{h} in the EHSG model does not lead to infrared divergences due to the structure of the corresponding scalar self-couplings. We do not further discuss infrared and collinear singularities because mass singularities are not important in this thesis. Here, we are concerned with UV singularities.

The four-momenta of the fields inside the loops of corresponding Feynman diagrams are not determined by momentum conservation. Consequently, we have to integrate over all these possible loop momenta − and this integration yields UV-divergent results. In order to deal with that problem, we first have to make the divergent Feynman integrals well-defined. This is achieved by adopting a suitable regularization scheme which restores the original theory in a certain limit. In the following, we restrict ourselves to the one-loop order for which the entire basis of master integrals is well-known, together with corresponding analytic solutions.

In the model with an EHS Φ_{h} the Lorentz- and gauge-invariant dimensional regularization scheme [103, 105] is eminently suitable and used throughout this work. In dimensional regularization we make use of the fact that the emerging UV-divergent four-dimensional (space-time) loop integrals are convergent if the dimension is reduced to $D = 4 - 2\epsilon$. Therefore, the dimension of the loop integrals is changed according to the transformation

$$\int \frac{d^4 q}{(2\pi)^4} \to \mu^{4-D} \int \frac{d^D q}{(2\pi)^D}, \tag{5.1.1}$$

where the arbitrary mass scale μ is introduced in order to retain the original mass dimension of the integrals. Furthermore, some identities have to be modified which involve the dirac matrices, the Levi-Civita and the metric tensor, such that the Clifford algebra is valid as well in D dimensions. In the dimensional regularization scheme we work with the scalar n-point ($n = 1, 2, 3, \dots$) one-loop integrals A_0, B_0, C_0, ... and with the scalar coefficient functions B_1, B_{00}, B_{11}, C_1, C_2, C_{00}, C_{11}, C_{12}, C_{22}, ... of the n-point ($n = 2, 3, \dots$) one-loop tensor integrals B_μ, $B_{\mu\nu}$, C_μ, $C_{\mu\nu}$, ... according to the conventions of [82]. The emerging one-loop integrals are described by these functions which can be split into terms independent of ϵ, terms proportional to ϵ and terms proportional to $1/\epsilon$. In the limit $D \to 4$ the original singularities reappear as

$$\Delta = \frac{1}{\epsilon} - \gamma_{\mathrm{E}} + \log 4\pi, \tag{5.1.2}$$

with the constant combination $-\gamma_{\mathrm{E}} + \log 4\pi$ (Euler's constant γ_{E}) characteristic for dimensional regularization. Renormalization consists of properly subtracting these $1/\epsilon$ terms by means of a suitable redefinition of the original parameters of the theory.

We use the method of multiplicative renormalization, where the parameters c_i and fields ψ_i of the original Lagrangian are replaced by the corresponding bare quantities $c_{i,0}$ and $\psi_{i,0}$ according to

$$c_i \to c_{i,0} \equiv Z_{c_i} c_i = (1 + \delta Z_{c_i}) c_i = c_i + \delta c_i, \qquad (5.1.3)$$

and

$$\psi_i \to \psi_{i,0} \equiv \sqrt{Z_{\psi_i}} \psi_i = \sqrt{1 + \delta Z_{\psi_i}} \psi_i. \qquad (5.1.4)$$

The multiplicative quantities Z_{c_i} and Z_{ψ_i} in front of the resulting renormalized parameters c_i and renormalized fields ψ_i introduce the associated renormalization constants δc_i and δZ_{ψ_i} into which, finally, the $1/\epsilon$ terms are absorbed. After the transformations (5.1.3) and (5.1.4) the bare Lagrangian can be separated into the original part, which is now written in terms of renormalized c_i and ψ_i, and into the related counterterm part, which collects the corresponding renormalization constants. The counterterm part of the bare Lagrangian gives rise to counterterm vertices which extend our set of Feynman rules and ensure that all Green functions and S-matrix elements are properly renormalized, i.e. UV finite in the limit $\epsilon \to 0$. The advantage of multiplicative renormalization is that underlying symmetry relations, e.g. the Slavnov-Taylor identities (3.3.6), also include the corresponding counterterms which provides a deeper insight into the UV-divergence structure of the theory.

The finite parts of the renormalization constants still have to be fixed. Therefore, suitable renormalization conditions are imposed on particular renormalized vertex functions evaluated at specific momenta. Within the scope of this thesis two renormalization schemes are used, namely the modified minimal-subtraction ($\overline{\mathrm{MS}}$) scheme and the on-shell scheme. In the $\overline{\mathrm{MS}}$ scheme, in addition to the singular $1/\epsilon$ terms of the bare parameters and fields just the terms proportional to the constant combination $-\gamma_{\mathrm{E}} + \log 4\pi$ are absorbed in the renormalization constants. As a result, $\overline{\mathrm{MS}}$-renormalized parameters and fields still depend on the regularization scale μ introduced in (5.1.1) and obey renormalization-group equations [106, 107], which determine the μ running of couplings and masses. This is different in the on-shell scheme, where further finite parts are absorbed in the renormalization constants such that the on-shell renormalized fields and parameters are independent of the scale μ. Hence, an advantage of the on-shell scheme is that it provides a direct relation between the renormalized parameters and physical observables.

According to the LSZ reduction formula [108–111] (named after Lehmann, Symanzik and Zimmermann) we furthermore have to take care about a correct normalization of the involved external wave functions when calculating S-matrix elements beyond the tree-level approximation. A properly normalized S-matrix element is obtained from the related renormalized truncated Green function by multiplying the latter with a renormalized LSZ factor $\hat{R}_{\Psi}^{1/2}$ for each external field Ψ in the process. The wave-function renormalization constant $\hat{R}_{\Psi}$ is defined by the residue of the renormalized Ψ propagator at the corresponding physical mass. While we require $\hat{R}_{\Psi} = 1$ for on-shell renormalized Ψ, these factors are non-trivial for $\overline{\mathrm{MS}}$ renormalized Ψ.

5.2   Standard on-shell conditions

The renormalization constants corresponding to the parameters and fields of the standard parts $\mathcal{L}_{\mathrm{SM}}^{\mathrm{G}}$ and $\mathcal{L}_{\mathrm{SM}}^{\mathrm{F}}$ in $\mathcal{L}_{\mathrm{EHS}}^{\mathrm{cl}}$ (3.1.1) can be directly adopted from the on-shell renormalization scheme of the SM [82,83,112–123], following the conventions of [82,83].

We first introduce the renormalized physical parameters M_W, M_Z, e, $m_{f,i}$ and $\mathbf{V}_{ij}$ with the corresponding bare parameters decomposed as follows,

$$
\begin{aligned}
M_{W,0}^2 &= M_W^2 + \delta M_W^2, \\
M_{Z,0}^2 &= M_Z^2 + \delta M_Z^2, \\
e_0 &= e + \delta e, \\
m_{f,i,0} &= m_{f,i} + \delta m_{f,i},
\end{aligned}
\tag{5.2.1}
$$

and

$$
\mathbf{V}_{ij,0} = \mathbf{V}_{ij} + \delta \mathbf{V}_{ij}.
\tag{5.2.2}
$$

Moreover, it is convenient to define the auxiliary renormalized quantities c_W and s_W as

$$
c_{W,0} = c_W + \delta c_W, \qquad\qquad s_{W,0} = s_W + \delta s_W,
\tag{5.2.3}
$$

with corresponding renormalization constants determined by

$$
\frac{\delta c_W}{c_W} = \frac{1}{2}\left(\frac{\delta M_W^2}{M_W^2} - \frac{\delta M_Z^2}{M_Z^2}\right), \qquad\qquad \frac{\delta s_W}{s_W} = -\frac{c_W^2}{s_W^2}\frac{\delta c_W}{c_W},
\tag{5.2.4}
$$

according to a first-order expansion in the bare version of (2.1.23).

In first-order approximation the renormalized physical fields $W_\mu^\pm$, Z_μ, A_μ, f_i^{L} and f_i^{R} (cf. Subsect. 2.1.5) are related to the corresponding bare fields as follows,

$$
\begin{aligned}
W_{\mu,0}^\pm &= \left(1 + \frac{1}{2}\delta Z_{WW}\right) W_\mu^\pm, \\
\begin{pmatrix} Z_{\mu,0} \\ A_{\mu,0} \end{pmatrix} &= \begin{pmatrix} 1 + \frac{1}{2}\delta Z_{ZZ} & \frac{1}{2}\delta Z_{ZA} \\ \frac{1}{2}\delta Z_{AZ} & 1 + \frac{1}{2}\delta Z_{AA} \end{pmatrix} \begin{pmatrix} Z_\mu \\ A_\mu \end{pmatrix}, \\
f_{i,0}^{\mathrm{L}} &= \left(\delta_{ij} + \frac{1}{2}\delta Z_{ij}^{f,\mathrm{L}}\right) f_j^{\mathrm{L}}, \\
f_{i,0}^{\mathrm{R}} &= \left(\delta_{ij} + \frac{1}{2}\delta Z_{ij}^{f,\mathrm{R}}\right) f_j^{\mathrm{R}}.
\end{aligned}
\tag{5.2.5}
$$

In order to fix the renormalization constants introduced above, we specify first the renormalized one-particle irreducible (OPI) two-point functions of the standard gauge bosons and fermions ('t Hooft-Feynman gauge),

$$
\begin{aligned}
\hat{\Gamma}_{\mu\nu}^{WW}(k) &= -ig_{\mu\nu}\left(k^2 - M_W^2\right) - ig_{\mu\nu}^{\mathrm{T}}\hat{\Sigma}_{\mathrm{T}}^{WW}(k^2) - ig_{\mu\nu}^{\mathrm{L}}\hat{\Sigma}_{\mathrm{L}}^{WW}(k^2), \\
\hat{\Gamma}_{\mu\nu}^{ab}(k) &= -ig_{\mu\nu}\left(k^2 - M_a^2\right)\delta_{ab} - ig_{\mu\nu}^{\mathrm{T}}\hat{\Sigma}_{\mathrm{T}}^{ab}(k^2) - ig_{\mu\nu}^{\mathrm{L}}\hat{\Sigma}_{\mathrm{L}}^{ab}(k^2), \\
&\qquad\qquad (a,b = A, Z \text{ and } M_A = 0), \\
\hat{\Gamma}_{ij}^{f}(k) &= i\left(\slashed{k} - m_i\right)\delta_{ij} \\
&\quad + i\left[\slashed{k}\omega_-\hat{\Sigma}_{ij}^{f,\mathrm{L}}(k^2) + \slashed{k}\omega_+\hat{\Sigma}_{ij}^{f,\mathrm{R}}(k^2) + \left(m_{f,i}\omega_- + m_{f,j}\omega_+\right)\hat{\Sigma}_{ij}^{f,\mathrm{S}}(k^2)\right],
\end{aligned}
\tag{5.2.6}
$$

from which the related renormalized propagators can be obtained by inversion. The tensors $g_{\mu\nu}^{\mathrm{T}}$ and $g_{\mu\nu}^{\mathrm{L}}$ are already defined in (2.2.4) and (2.2.5).

In this work the "hat" on top of a given one-loop quantity denotes that it is properly renormalized, i.e. that the corresponding one-loop counterterm is included. Thus, e.g. a renormalized one-loop self-energy $\hat{\Sigma}(k^2)$ always can be split into the associated unrenormalized part $\Sigma(k^2)$ and into the corresponding counterterm part Σ_{CT} according to

$$\hat{\Sigma}(k^2) = \Sigma(k^2) + \Sigma_{\mathrm{CT}}. \tag{5.2.7}$$

In (5.2.6) the lower indices T and L denote the transverse and longitudinal parts of the standard gauge-boson self-energies Σ^{WW} and Σ^{ab}, whereas the upper indices L, R and S characterize the left-handed, right-handed and scalar parts of the fermion self-energies Σ_{ij}^{f}. In each case the explicit form of Σ_{CT} in terms of basic renormalization constants can be derived from the Feynman rules specified in Appendix A.

In the on-shell scheme we require that on-shell fields do not mix and that the corresponding renormalized masses match the physical ones. Accordingly, the squared renormalized masses are set to the real parts of the poles of the corresponding renormalized (diagonal) propagators and the real parts of the residues of these renormalized propagators are set to unity. Translating the on-shell renormalization conditions into corresponding conditions for the fermionic and bosonic OPI two-point functions in (5.2.6) provides us with the explicit form of the related mass and field renormalization constants,

$$
\begin{aligned}
\delta m_{f,i} &= \frac{m_{f,i}}{2}\widetilde{\mathrm{Re}}\left[\Sigma_{ii}^{f,\mathrm{L}}(m_{f,i}^2) + \Sigma_{ii}^{f,\mathrm{R}}(m_{f,i}^2) + 2\Sigma_{ii}^{f,\mathrm{S}}(m_{f,i}^2)\right], \\
\delta Z_{ii}^{f,\mathrm{L}} &= -\widetilde{\mathrm{Re}}\Sigma_{ii}^{f,\mathrm{L}}(m_{f,i}^2) \\
&\quad - m_{f,i}^2\frac{\partial}{\partial k^2}\widetilde{\mathrm{Re}}\left[\Sigma_{ii}^{f,\mathrm{L}}(k^2) + \Sigma_{ii}^{f,\mathrm{R}}(k^2) + 2\Sigma_{ii}^{f,\mathrm{S}}(k^2)\right]\bigg|_{k^2=m_{f,i}^2}, \\
\delta Z_{ii}^{f,\mathrm{R}} &= -\widetilde{\mathrm{Re}}\Sigma_{ii}^{f,\mathrm{R}}(m_{f,i}^2) \\
&\quad - m_{f,i}^2\frac{\partial}{\partial k^2}\widetilde{\mathrm{Re}}\left[\Sigma_{ii}^{f,\mathrm{L}}(k^2) + \Sigma_{ii}^{f,\mathrm{R}}(k^2) + 2\Sigma_{ii}^{f,\mathrm{S}}(k^2)\right]\bigg|_{k^2=m_{f,i}^2}, \\
\delta Z_{ij}^{f,\mathrm{L}} &= \frac{2}{m_{f,i}^2 - m_{f,j}^2}\widetilde{\mathrm{Re}}\left[m_{f,j}^2\Sigma_{ij}^{f,\mathrm{L}}(m_{f,j}^2) + m_{f,i}m_{f,j}\Sigma_{ij}^{f,\mathrm{R}}(m_{f,j}^2)\right. \\
&\qquad\qquad\qquad\qquad\qquad \left. + \left(m_{f,i}^2 + m_{f,j}^2\right)\Sigma_{ij}^{f,\mathrm{S}}(m_{f,j}^2)\right], \qquad i \neq j, \\
\delta Z_{ij}^{f,\mathrm{R}} &= \frac{2}{m_{f,i}^2 - m_{f,j}^2}\widetilde{\mathrm{Re}}\left[m_{f,j}^2\Sigma_{ij}^{f,\mathrm{R}}(m_{f,j}^2) + m_{f,i}m_{f,j}\Sigma_{ij}^{f,\mathrm{L}}(m_{f,j}^2)\right. \\
&\qquad\qquad\qquad\qquad\qquad \left. + 2m_{f,i}m_{f,j}\Sigma_{ij}^{f,\mathrm{S}}(m_{f,j}^2)\right], \qquad i \neq j,
\end{aligned}
\tag{5.2.8}
$$

and

$$\delta M_V^2 = \widetilde{\mathrm{Re}} \Sigma_{\mathrm{T}}^{VV}(M_V^2), \qquad (V = W, Z),$$

$$\delta Z_{VV} = -\widetilde{\mathrm{Re}} \frac{\partial \Sigma_{\mathrm{T}}^{VV}(k^2)}{\partial k^2}\bigg|_{k^2 = M_V^2}, \qquad (V = W, Z, A), \tag{5.2.9}$$

$$\delta Z_{AZ} = -2\widetilde{\mathrm{Re}} \frac{\Sigma_{\mathrm{T}}^{AZ}(M_Z^2)}{M_Z^2}, \qquad \delta Z_{ZA} = 2 \frac{\Sigma_{\mathrm{T}}^{AZ}(0)}{M_Z^2}.$$

Here, $\widetilde{\mathrm{Re}}$ means that the real part of the one-loop integrals in the self-energies is taken leaving the quark-mixing matrix elements $\mathbf{V}_{ij}$ unchanged. As a consequence of transversality the longitudinal gauge-boson self-energies in (5.2.6) do not play a role in the fixing of the renormalization constants. According to (5.2.4), with (5.2.9) also the renormalization constants δc_W and δs_W are determined.

A further renormalization condition is needed in order to fix the renormalization constant δe. For this purpose, it is convenient to define the renormalized electric charge e by the full electron-electron-photon vertex for on-shell external fields in the limit of vanishing photon momentum (Thomson limit), which results in

$$\frac{\delta e}{e} = -\frac{1}{2}\delta Z_{AA} - \frac{1}{2}\frac{s_W}{c_W}\delta Z_{ZA} = \frac{1}{2}\frac{\partial \Sigma_{\mathrm{T}}^{AA}(k^2)}{\partial k^2}\bigg|_{k^2 = 0} - \frac{s_W}{c_W}\frac{\Sigma_{\mathrm{T}}^{AZ}(0)}{M_Z^2}. \tag{5.2.10}$$

For completeness we mention that the renormalized quark-mixing matrix $\mathbf{V}$ is defined in analogy to (2.1.26) and (2.1.29) by the unitary transformation matrices relating the renormalized fermionic weak eigenstates to the renormalized fermionic mass eigenstates. This fixes the renormalization constants $\delta \mathbf{V}_{ij}$ in terms of fermionic field renormalization constants

$$\delta \mathbf{V}_{ij} = \frac{1}{4}\left[\left(\delta Z_{ik}^{u,\mathrm{L}} - \delta Z_{ik}^{u,\mathrm{L}\dagger}\right)\mathbf{V}_{kj} - \mathbf{V}_{ik}\left(\delta Z_{kj}^{d,\mathrm{L}} - \delta Z_{kj}^{d,\mathrm{L}\dagger}\right)\right]. \tag{5.2.11}$$

Note that most of the one-loop renormalization constants specified above depend on the free non-standard parameters α and M_{H_2} due to the tree-level mixing (3.1.21) in the scalar sector. As there exist no tree-level couplings of the fields Z' and φ_{h} to the standard gauge bosons and fermions the explicit expressions of the one-loop renormalization constants specified within this section are the same for the EHSL, EHSG and EHSD models.

5.3   Extended sector

In this section we perform the renormalization of the remaining fields and parameters, which are associated with the Higgs part $\mathcal{L}_{\mathrm{EHS}}^{\Phi_{\mathrm{s/h}}}$ (3.1.2), with the non-standard gauge part $\mathcal{L}_{\mathrm{EHSL}}^{Z'}$ (3.1.9), with the gauge-fixing part $\mathcal{L}_{\mathrm{EHS}}^{\mathrm{fix}}$ (3.2.1), and with the Faddeev-Popov part $\mathcal{L}_{\mathrm{EHS}}^{\mathrm{ghost}}$ (3.2.4). This completes the renormalization of the physical and unphysical sectors of the three EHS models.

5.3.1 Renormalization transformations

Extended scalar sector

We introduce the entire set of renormalization constants corresponding to the fields and parameters in $\mathcal{L}_{\mathrm{EHS}}^{\Phi_{\mathrm{s/h}}}$ before rotating to the mass-eigenstate basis via (3.1.21).

According to (5.1.4), both Φ_{s} and Φ_{h} obtain multiplicative field renormalization constants,

$$\Phi_{\mathrm{s},0} = \sqrt{Z_{\Phi_{\mathrm{s}}}}\Phi_{\mathrm{s}} \equiv \sqrt{1 + \delta Z_H}\Phi_{\mathrm{s}},$$
$$\Phi_{\mathrm{h},0} = \sqrt{Z_{\Phi_{\mathrm{h}}}}\Phi_{\mathrm{h}} \equiv \sqrt{1 + \delta Z_\chi}\Phi_{\mathrm{h}}. \tag{5.3.1}$$

Hence, in first-order approximation the renormalized scalar fields H, $\phi^\pm$, φ_{s}, χ and φ_{h} are related to the bare fields by

$$H_0 = \left(1 + \frac{1}{2}\delta Z_H\right)H, \quad \phi_0^\pm = \left(1 + \frac{1}{2}\delta Z_H\right)\phi^\pm, \quad \varphi_{\mathrm{s},0} = \left(1 + \frac{1}{2}\delta Z_H\right)\varphi_{\mathrm{s}},$$
$$\chi_0 = \left(1 + \frac{1}{2}\delta Z_\chi\right)\chi, \quad \varphi_{\mathrm{h},0} = \left(1 + \frac{1}{2}\delta Z_\chi\right)\varphi_{\mathrm{h}}. \tag{5.3.2}$$

Regarding the EHSD model, the last relation in (5.3.2) involving the field φ_{h} has to be dropped.

The renormalized Higgs-potential parameters λ_{s}, λ_{h}, μ_{s}^2, μ_{h}^2 and η are related to the corresponding bare parameters according to

$$\lambda_{\mathrm{s},0} = \lambda_{\mathrm{s}} + \delta\lambda_{\mathrm{s}},$$
$$\lambda_{\mathrm{h},0} = \lambda_{\mathrm{h}} + \delta\lambda_{\mathrm{h}},$$
$$\mu_{\mathrm{s},0}^2 = \mu_{\mathrm{s}}^2 + \delta\mu_{\mathrm{s}}^2, \tag{5.3.3}$$
$$\mu_{\mathrm{h},0}^2 = \mu_{\mathrm{h}}^2 + \delta\mu_{\mathrm{h}}^2,$$
$$\eta_0 = \eta + \delta\eta.$$

The minimum of the potential (3.1.5) is shifted by one-loop corrections. In order to compensate this shift, we introduce the renormalized vevs v_{s} and v_{h} according to

$$v_{\mathrm{s},0} = v_{\mathrm{s}} + \delta v_{\mathrm{s}},$$
$$v_{\mathrm{h},0} = v_{\mathrm{h}} + \delta v_{\mathrm{h}}. \tag{5.3.4}$$

Similarly to (5.3.4) we treat the related one-loop corrections contributing to the tadpole coefficients of the fields H and χ, specified at lowest order in (3.1.16). Corresponding renormalization constants are introduced in order to compensate for these one-loop effects and the renormalized tadpole coefficients t_H and t_χ are related to the respective bare coefficients via

$$t_{H,0} = t_H + \delta t_H, \qquad t_{\chi,0} = t_\chi + \delta t_\chi. \tag{5.3.5}$$

Performing the renormalization transformation in (3.1.16) according to (5.3.3) and (5.3.4) in first-order approximation yields

$$\delta t_H = -\frac{1}{2}v_{\mathrm{s}}v_{\mathrm{h}}^2\delta\eta - \frac{1}{4}v_{\mathrm{s}}^3\delta\lambda_{\mathrm{s}} + v_{\mathrm{s}}\delta\mu_{\mathrm{s}}^2 - v_{\mathrm{s}}v_{\mathrm{h}}\eta\delta v_{\mathrm{h}} - \frac{1}{2}\lambda_{\mathrm{s}}v_{\mathrm{s}}^2\delta v_{\mathrm{s}},$$
$$\delta t_\chi = -\frac{1}{2}v_{\mathrm{h}}v_{\mathrm{s}}^2\delta\eta - \frac{1}{4}v_{\mathrm{h}}^3\delta\lambda_{\mathrm{h}} + v_{\mathrm{h}}\delta\mu_{\mathrm{s}}^2 - v_{\mathrm{s}}v_{\mathrm{h}}\eta\delta v_{\mathrm{s}} - \frac{1}{2}\lambda_{\mathrm{h}}v_{\mathrm{h}}^2\delta v_{\mathrm{h}}. \tag{5.3.6}$$

The renormalized tadpole coefficients t_H and t_χ again vanish due to the renormalized minimum conditions (5.3.4).

Next, we consider the bare squared-mass matrix $\mathcal{M}_0^2$ of the fields H_0 and χ_0 which follows from (3.1.17) after the related renormalization transformation specified by (5.3.3) and (5.3.4). According to

$$\mathcal{M}_0^2 = \mathcal{M}^2 + \delta\mathcal{M}^2, \tag{5.3.7}$$

it is split into the renormalized squared-mass matrix

$$\mathcal{M}^2 = \begin{pmatrix} \frac{1}{2}\lambda_{\mathrm{s}}v_{\mathrm{s}}^2 & \eta v_{\mathrm{s}}v_{\mathrm{h}} \\ \eta v_{\mathrm{s}}v_{\mathrm{h}} & \frac{1}{2}\lambda_{\mathrm{h}}v_{\mathrm{h}}^2 \end{pmatrix} \tag{5.3.8}$$

(simplified by means of the renormalized minimum conditions) and into the corresponding squared-mass counterterm matrix

$$\delta\mathcal{M}^2 = \begin{pmatrix} \delta\mathcal{M}_{11}^2 & \delta\mathcal{M}_{12}^2 \\ \delta\mathcal{M}_{12}^2 & \delta\mathcal{M}_{22}^2 \end{pmatrix}, \tag{5.3.9}$$

with the first-order entries

$$\delta\mathcal{M}_{11}^2 = -\delta\mu_{\mathrm{s}}^2 + \frac{3}{4}v_{\mathrm{s}}^2\delta\lambda_{\mathrm{s}} + \frac{3}{2}v_{\mathrm{s}}\lambda_{\mathrm{s}}\delta v_{\mathrm{s}} + \frac{1}{2}v_{\mathrm{h}}^2\delta\eta + \eta v_{\mathrm{h}}\delta v_{\mathrm{h}},$$
$$\delta\mathcal{M}_{12}^2 = \eta v_{\mathrm{s}}\delta v_{\mathrm{h}} + \eta v_{\mathrm{h}}\delta v_{\mathrm{s}} + v_{\mathrm{s}}v_{\mathrm{h}}\delta\eta, \tag{5.3.10}$$
$$\delta\mathcal{M}_{22}^2 = -\delta\mu_{\mathrm{h}}^2 + \frac{3}{4}v_{\mathrm{h}}^2\delta\lambda_{\mathrm{h}} + \frac{3}{2}v_{\mathrm{h}}\lambda_{\mathrm{h}}\delta v_{\mathrm{h}} + \frac{1}{2}v_{\mathrm{s}}^2\delta\eta + v_{\mathrm{s}}\eta\delta v_{\mathrm{s}}.$$

At this point, we transform the renormalization constants δZ_H, δZ_χ, δt_H, δt_χ, $\delta\mathcal{M}_{11}^2$, $\delta\mathcal{M}_{12}^2$ and $\delta\mathcal{M}_{22}^2$ into the related renormalization constants in the mass-eigenstate basis of the scalar fields. This is simply accomplished with the help of the rotation (3.1.21). After performing the renormalization transformation in (3.1.21) according to (5.3.2) the renormalized mass eigenstates H_1 and H_2 can be separated from the corresponding bare fields as

$$\begin{pmatrix} H_{1,0} \\ H_{2,0} \end{pmatrix} = \begin{pmatrix} 1 + \frac{1}{2}\delta Z_{H_1 H_1} & \frac{1}{2}\delta Z_{H_1 H_2} \\ \frac{1}{2}\delta Z_{H_1 H_2} & 1 + \frac{1}{2}\delta Z_{H_2 H_2} \end{pmatrix} \begin{pmatrix} H_1 \\ H_2 \end{pmatrix}, \tag{5.3.11}$$

with

$$\begin{pmatrix} \delta Z_{H_1 H_1} \\ \delta Z_{H_2 H_2} \end{pmatrix} = \begin{pmatrix} c_\alpha^2 & s_\alpha^2 \\ s_\alpha^2 & c_\alpha^2 \end{pmatrix} \begin{pmatrix} \delta Z_H \\ \delta Z_\chi \end{pmatrix}, \tag{5.3.12}$$

and

$$\delta Z_{H_1 H_2} = -s_\alpha c_\alpha \left(\delta Z_H - \delta Z_\chi \right). \tag{5.3.13}$$

Inversion of (5.3.12) yields

$$\begin{pmatrix} \delta Z_H \\ \delta Z_\chi \end{pmatrix} = \frac{1}{1 - 2s_\alpha^2} \begin{pmatrix} c_\alpha^2 & -s_\alpha^2 \\ -s_\alpha^2 & c_\alpha^2 \end{pmatrix} \begin{pmatrix} \delta Z_{H_1 H_1} \\ \delta Z_{H_2 H_2} \end{pmatrix}, \tag{5.3.14}$$

and hence it is straightforward to replace the original field renormalization constants δZ_H and δZ_χ by the related field renormalization constants $\delta Z_{H_1 H_1}$ and $\delta Z_{H_2 H_2}$ in the mass-eigenstate basis. Equipped with (5.3.13) and (5.3.14) we obtain

$$\delta Z_{H_1 H_2} = \frac{s_\alpha c_\alpha}{c_\alpha^2 - s_\alpha^2} \left(\delta Z_{H_2 H_2} - \delta Z_{H_1 H_1} \right), \tag{5.3.15}$$

i.e. the non-diagonal entries of the matrix-valued field renormalization constant in (5.3.11) are determined by a linear combination of the corresponding diagonal entries. Moreover, it follows that the renormalization constants $\delta t_{H_{1/2}}$ associated with the renormalized tadpole coefficients $t_{H_{1/2}}$ are given by the linear combinations

$$\begin{aligned} \delta t_{H_1} &= c_\alpha \delta t_H + s_\alpha \delta t_\chi, \\ \delta t_{H_2} &= -s_\alpha \delta t_H + c_\alpha \delta t_\chi. \end{aligned} \tag{5.3.16}$$

The squared-mass counterterm matrix $\delta \mathcal{M}_\alpha^2$ in the mass-eigenstate basis is determined by

$$\delta \mathcal{M}_\alpha^2 = \begin{pmatrix} \delta M_{H_1}^2 & \delta M_{H_1 H_2}^2 \\ \delta M_{H_1 H_2}^2 & \delta M_{H_2}^2 \end{pmatrix} \equiv \begin{pmatrix} c_\alpha & s_\alpha \\ -s_\alpha & c_\alpha \end{pmatrix} \delta \mathcal{M}^2 \begin{pmatrix} c_\alpha & -s_\alpha \\ s_\alpha & c_\alpha \end{pmatrix}. \tag{5.3.17}$$

Taking into account (5.3.6), (5.3.10), (5.3.16) and (5.3.17) the original renormalization constants $\delta \lambda_s$, $\delta \lambda_h$, $\delta \mu_s^2$, $\delta \mu_h^2$ and $\delta \eta$ can be translated into the renormalization constants $\delta M_{H_1}^2$, $\delta M_{H_1 H_2}^2$, $\delta M_{H_2}^2$, δt_{H_1} and δt_{H_2} in the mass-eigenstate basis. Note that in this scheme the mixing angle α is not explicitly renormalized because it is introduced after renormalization.

Non-standard gauge sector

Next, we specify the renormalization transformations associated with the non-standard gauge sector of the EHSL model. Analogously to (5.2.5) and (5.3.2), in first-order approximation the renormalized field Z' is related to the corresponding bare field by

$$Z'_{\mu,0} = \left(1 + \frac{1}{2} \delta Z_{Z'Z'} \right) Z'_\mu. \tag{5.3.18}$$

The associated renormalized physical parameters, namely $M_{Z'}$ and g_h, are separated from the related bare parameters as

$$M_{Z',0}^2 = M_{Z'}^2 + \delta M_{Z'}^2, \tag{5.3.19}$$

and

$$g_{h,0} = g_h + \delta g_h. \tag{5.3.20}$$

Performing the renormalization transformation in (3.1.30) according to (5.3.4), (5.3.19) and (5.3.20) in first-order approximation yields

$$\frac{\delta v_{\mathrm{h}}}{v_{\mathrm{h}}} = \frac{1}{2}\frac{\delta M_{Z'}^2}{M_{Z'}^2} - \frac{\delta g_{\mathrm{h}}}{g_{\mathrm{h}}}. \tag{5.3.21}$$

The transition to the global model EHSG is described later.

Gauge-fixing and Faddeev-Popov sector

Finally, we specify the remaining renormalization transformations, namely those of the gauge-fixing parameters in $\mathcal{L}_{\mathrm{EHS}}^{\mathrm{fix}}$ and those of the ghost fields in $\mathcal{L}_{\mathrm{EHS}}^{\mathrm{ghost}}$ (cf. Sect. 3.2). The renormalized gauge-fixing parameters ξ_a ($a = A, Z, W, Z'$) and ξ_a' ($a = Z, W, Z'$) are related to the corresponding bare parameters as follows,

$$\begin{aligned}
\xi_{A,0} &= \xi_A \left(1 + \delta\xi_A\right), \\
\xi_{W,0}^{(\prime)} &= \xi_W^{(\prime)} \left(1 + \delta\xi_W^{(\prime)}\right), \\
\xi_{Z,0}^{(\prime)} &= \xi_Z^{(\prime)} \left(1 + \delta\xi_Z^{(\prime)}\right), \\
\xi_{Z',0}^{(\prime)} &= \xi_{Z'}^{(\prime)} \left(1 + \delta\xi_{Z'}^{(\prime)}\right),
\end{aligned} \tag{5.3.22}$$

and the field renormalization of the Faddeev-Popov ghosts is introduced in first-order approximation by

$$\begin{pmatrix} u_0^Z \\ u_0^A \end{pmatrix} = \begin{pmatrix} 1 + \delta\widetilde{Z}_{ZZ} & \delta\widetilde{Z}_{ZA} \\ \delta\widetilde{Z}_{AZ} & 1 + \delta\widetilde{Z}_{AA} \end{pmatrix} \begin{pmatrix} u^Z \\ u^A \end{pmatrix},$$
$$u_0^\pm = \left(1 + \delta\widetilde{Z}_{WW}\right) u^\pm, \qquad u_0^{Z'} = \left(1 + \delta\widetilde{Z}_{Z'Z'}\right) u^{Z'}. \tag{5.3.23}$$

Due to ghost-number conservation we do not have to renormalize the corresponding anti-ghost fields. The renormalized gauge-fixing parameters are again fixed according to the 't Hooft-Feynman gauge. Regarding the EHSG and EHSD models, the last relation in (5.3.22) and in (5.3.23), involving the non-standard gauge-fixing parameters and the non-standard ghost field, respectively, has to be dropped.

A proper renormalization of the unphysical sector is needed to render all Green functions described by $\mathcal{L}_{\mathrm{EHS}}$ (3.2.5) UV finite and to realize the correct form of renormalized Slavnov-Taylor identities.

5.3.2 Renormalization conditions

As mentioned in the beginning of this chapter, our aim is to establish the renormalization scheme of the EHSL model such that the limit $g_{\mathrm{h}} \to 0$ directly leads us to the renormalized EHSG model. Note that according to $M_{Z'} = g_{\mathrm{h}} v_{\mathrm{h}}$, for fixed v_{h} the
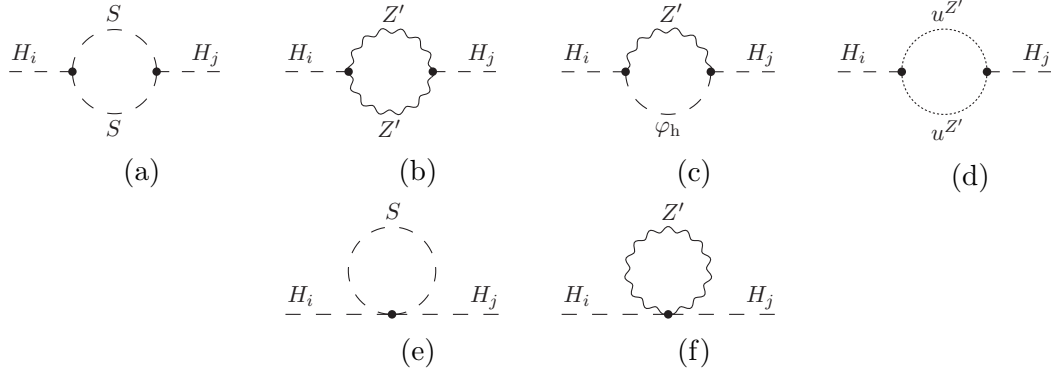
Figure 5.1: One-loop self-energy diagrams in the EHSL model contributing to $\Sigma^{H_i H_j}$, $i, j \in \{1, 2\}$, with non-standard fields only in the internal lines, generic for scalar bosons $S = H_1, H_2, \varphi_{\mathrm{h}}$. The remaining diagrams only contain pure standard-sector fields in the internal lines (analogously to the related SM self-energy Σ^{HH}). In the EHSG (EHSD) model we have to ignore the diagrams involving the fields Z' and $u^{Z'}$ (Z', $u^{Z'}$ and φ_{h}).

limit $M_{Z'} \to 0$ corresponds to the limit $g_{\mathrm{h}} \to 0$.[2] In the following, the renormalization constants introduced above for the three EHS models are fixed by appropriate renormalization conditions.

Extended scalar sector

In order to fix the renormalization constants corresponding to the fields and parameters in $\mathcal{L}_{\mathrm{EHS}}^{\Phi_{\mathrm{s/h}}}$ we define the renormalized OPI two-point functions of the mass eigenstates $H_{1/2}$ by

$$\hat{\Gamma}^{H_i H_j}(k^2) = i \left(k^2 - M_{H_i}^2 \right) \delta_{ij} + i \hat{\Sigma}^{H_i H_j}(k^2), \qquad i, j \in \{1, 2\}, \tag{5.3.24}$$

with the diagonal renormalized self-energies

$$\hat{\Sigma}^{H_i H_i}(k^2) = \Sigma^{H_i H_i}(k^2) + \left(k^2 - M_{H_i}^2 \right) \delta Z_{H_i H_i} - \delta M_{H_i}^2, \tag{5.3.25}$$

and the non-diagonal renormalized self-energy

$$\hat{\Sigma}^{H_1 H_2}(k^2) = \Sigma^{H_1 H_2}(k^2) + \left[k^2 - \frac{M_{H_1}^2 + M_{H_2}^2}{2} \right] \delta Z_{H_1 H_2} - \delta M_{H_1 H_2}^2. \tag{5.3.26}$$

The diagrams contributing to $\Sigma^{H_i H_j}$ are depicted in Fig. 5.1.

The diagonal entries of the squared-mass counterterm matrix $\delta \mathcal{M}_\alpha^2$ (5.3.17) are fixed according to the on-shell scheme, i.e. we require that the squared renormalized masses $M_{H_i}^2$ are equal to the real parts of the poles of the corresponding propagators, which leads us to

$$\delta M_{H_i}^2 = \widetilde{\mathrm{Re}} \Sigma^{H_i H_i}(M_{H_i}^2). \tag{5.3.27}$$

---

[2]A proper replacement of $M_{Z'}$ by means of the parameters g_{h} and v_{h} according to (3.1.30) is implied whenever we take the limit $g_{\mathrm{h}} \to 0$.

Next, we consider the case $i \neq j$ in (5.3.24). In order to fix the non-diagonal entries of $\delta\mathcal{M}_\alpha^2$ we require vanishing mixing for on-shell standard-like Higgs bosons H_1, i.e.

$$\hat{\Gamma}^{H_1 H_2}(M_{H_1}^2) \overset{!}{=} 0, \tag{5.3.28}$$

which according to (5.3.26) implies

$$\delta M_{H_1 H_2}^2 = \Sigma^{H_1 H_2}(M_{H_1}^2) + \frac{M_{H_1}^2 - M_{H_2}^2}{2}\,\delta Z_{H_1 H_2}. \tag{5.3.29}$$

For $k^2 = M_{H_1}^2$ the field renormalization does not drop out in (5.3.26). Thus, we initially have to fix the field renormalization of the extended scalar sector in order to completely determine the squared-mass counterterm matrix $\delta\mathcal{M}_\alpha^2$.

For on-shell renormalized $\delta Z_{H_i H_i}$ threshold effects of H_2 would appear in one-loop matrix elements with external H_1 bosons (and vice versa) due to the underlying mixing. Therefore, it is more convenient to choose the $\overline{\text{MS}}$ scheme for $\delta Z_{H_i H_i}$ which provides us with the renormalization conditions

$$\delta Z_{H_i H_i} = -\left[\widetilde{\text{Re}}\frac{\partial\Sigma^{H_i H_i}(k^2)}{\partial k^2}\bigg|_{k^2 = M_{H_i}^2}\right]^\Delta. \tag{5.3.30}$$

The symbol with the outer bracket $[\ldots]^\Delta$ denotes that only the Δ-dependent part of the expression inside is taken, where Δ is specified in (5.1.2). With (5.3.15), (5.3.27), (5.3.29) and (5.3.30) for each of the three models both the matrix-valued field renormalization constant in (5.3.11) and the squared-mass counterterm matrix $\delta\mathcal{M}_\alpha^2$ in (5.3.17) are determined.

According to (5.3.4), the renormalization of v_{s} and v_{h} generally is treated independently of the associated field renormalization in (5.3.1). As a consequence, in the three models we are free to fix δt_{H_i} by demanding that corresponding one-loop tadpole contributions vanish, i.e. we require

$$\hat{T}_{H_i} = T_{H_i} + \delta t_{H_i} = 0 \tag{5.3.31}$$

for the renormalized one-point amputated Green functions $\hat{T}_{H_i}$.

From the corresponding renormalization conditions above it is straightforward to check that in the limit $g_{\text{h}} \to 0$ the renormalization constants $\delta M_{H_i}^2$, $\delta M_{H_1 H_2}^2$, $\delta Z_{H_i H_i}$, $\delta Z_{H_1 H_2}$ and δt_{H_i} of the EHSL model smoothly turn into the respective ones of the EHSG model. The explicit expressions of these renormalization constants furthermore change when switching to the EHSD model since then related virtual-φ_{h} contributions have to be dropped. However, since $A_0(0) = 0$ the tadpole renormalization constants δt_{H_i} in the EHSG model are identical to those in the EHSD model.

From (5.3.14) and (5.3.30) we obtain (fermion generation index i)

$$\delta Z_H = -\frac{\alpha_{\text{em}}}{8\pi M_W^2 s_W^2}\left[\sum_i \left[3\left(m_{u,i}^2 + m_{d,i}^2\right) + m_{l,i}^2\right] - \left(M_Z^2 + 2M_W^2\right)\right]\Delta, \tag{5.3.32}$$

i.e. in each of the three models δZ_H is just given by the Higgs-field renormalization constant of the SM in the $\overline{\text{MS}}$ scheme. In the EHSL model we furthermore obtain

$$\delta Z_\chi = \frac{g_{\text{h}}^2}{8\pi^2}\,\Delta \tag{5.3.33}$$

in an analogous manner. Hence, we have

$$\lim_{g_{\text{h}}\to 0}\delta Z_\chi = 0, \tag{5.3.34}$$

and we find that the field renormalization constant δZ_χ is not required in the EHSG and EHSD models. This is because in the absence of the non-standard gauge sector no tensor integrals appear in the related χ self-energy which thus has a momentum-independent UV-divergent part. In the EHSG model the corresponding $\text{U}(1)_{Y_\text{h}}$ Ward identities (B.2.2)$-$(B.2.9) specified in Appendix B furthermore show that $\delta Z_\chi = 0$ is implied.

The renormalization constant δv_s is already determined by standard on-shell renormalization constants,

$$\frac{\delta v_\text{s}}{v_\text{s}} = \frac{\delta s_W}{s_W} + \frac{1}{2}\frac{\delta M_W^2}{M_W^2} - \frac{\delta e}{e}, \tag{5.3.35}$$

which follows from the first-order renormalization transformation of (3.1.28) according to (5.2.1) and (5.2.3). Therefore, the explicit expression of δv_s is the same for each of the three models (cf. Sect. 5.2). The renormalization constant δv_h is related to the non-standard gauge sector of the EHSL model discussed next.

Non-standard gauge sector

In order to fix the renormalization constants related to the non-standard gauge sector of the EHSL model, we first specify the renormalized OPI two-point function of the Z' boson by

$$\hat{\Gamma}_{\mu\nu}^{Z'Z'}(k) = -ig_{\mu\nu}\left(k^2 - M_{Z'}^2\right) - ig_{\mu\nu}^{\text{T}}\hat{\Sigma}_{\text{T}}^{Z'Z'}(k^2) - ig_{\mu\nu}^{\text{L}}\hat{\Sigma}_{\text{L}}^{Z'Z'}(k^2), \tag{5.3.36}$$

with the transverse (lower index T) and longitudinal (lower index L) part of the renormalized Z' self-energy,

$$\begin{aligned}\hat{\Sigma}_{\text{T}}^{Z'Z'}(k^2) &= \Sigma_{\text{T}}^{Z'Z'}(k^2) + \left(k^2 - M_{Z'}^2\right)\delta Z_{Z'Z'} - \delta M_{Z'}^2,\\ \hat{\Sigma}_{\text{L}}^{Z'Z'}(k^2) &= \Sigma_{\text{L}}^{Z'Z'}(k^2) + k^2\left(\delta Z_{Z'Z'} - \delta\xi_{Z'}\right) - M_{Z'}^2\delta Z_{Z'Z'} - \delta M_{Z'}^2.\end{aligned} \tag{5.3.37}$$

The one-loop diagrams contributing to $\Sigma_{\text{T}}^{Z'Z'}$ and $\Sigma_{\text{L}}^{Z'Z'}$ are shown in Fig. 5.2.

For the Z' mass renormalization only $\Sigma_{\text{T}}^{Z'Z'}$ is needed. Requiring that the squared renormalized mass $M_{Z'}^2$ is equal to the real part of the pole of the renormalized transverse Z' propagator yields

$$\delta M_{Z'}^2 = \widetilde{\text{Re}}\Sigma_{\text{T}}^{Z'Z'}(M_{Z'}^2). \tag{5.3.38}$$
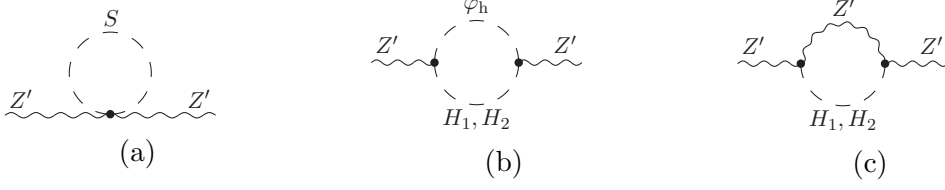
Figure 5.2: Self-energy diagrams contributing to $\Sigma_{\mathrm{T}}^{Z'Z'}$ and $\Sigma_{\mathrm{L}}^{Z'Z'}$ at the one-loop level, with scalar bosons $S = H_1, H_2, \varphi_{\mathrm{h}}$.

Furthermore, requiring that the real part of the residue of the renormalized Z' propagator is equal to unity provides us with

$$\delta Z_{Z'Z'} = -\widetilde{\mathrm{Re}}\frac{\partial \Sigma_{\mathrm{T}}^{Z'Z'}(k^2)}{\partial k^2}\bigg|_{k^2 = M_{Z'}^2}. \tag{5.3.39}$$

From the expressions explicit for $\Sigma_{\mathrm{T}}^{Z'Z'}$ we obtain

$$\left[\frac{\delta M_{Z'}^2}{M_{Z'}^2}\right]^{\Delta} = \frac{13g_{\mathrm{h}}^2}{48\pi^2}\,\Delta, \qquad [\delta Z_{Z'Z'}]^{\Delta} = -\frac{g_{\mathrm{h}}^2}{48\pi^2}\,\Delta, \tag{5.3.40}$$

as well as the limits

$$\lim_{g_{\mathrm{h}} \to 0} \delta Z_{Z'Z'} = 0, \qquad\qquad \lim_{g_{\mathrm{h}} \to 0} \delta M_{Z'}^2 = 0, \tag{5.3.41}$$

and

$$\lim_{g_{\mathrm{h}} \to 0} \frac{\delta M_{Z'}^2}{M_{Z'}^2} = -\frac{s_\alpha^2 M_{H_1}^2 + c_\alpha^2 M_{H_2}^2}{32\pi^2 v_{\mathrm{h}}^2}, \tag{5.3.42}$$

for the transition to the global model EHSG.

Next, we discuss how to fix the renormalization constants δv_{h} and δg_{h}. In compliance with (5.3.4) the renormalization constant δv_{h} also appears in the EHSG and EHSD models. We intend to obtain a proper definition of δv_{h} in the EHSG model just by taking the limit $g_{\mathrm{h}} \to 0$ in (5.3.21). Thus, in the EHSL model it is convenient to fix δv_{h} according to the $\overline{\mathrm{MS}}$ scheme such that the renormalization constant δv_{h} in the EHSG model does not contain the UV-finite remnant of $\delta M_{Z'}^2 / M_{Z'}^2$ in (5.3.42). Accordingly, in the EHSL model we fix δv_{h} via

$$\frac{\delta v_{\mathrm{h}}}{v_{\mathrm{h}}} = \frac{1}{2}\left[\frac{\delta M_{Z'}^2}{M_{Z'}^2}\right]^{\Delta} - \frac{\delta g_{\mathrm{h}}^{\overline{\mathrm{MS}}}}{g_{\mathrm{h}}}, \qquad \frac{\delta g_{\mathrm{h}}^{\overline{\mathrm{MS}}}}{g_{\mathrm{h}}} \equiv \left[\frac{\delta g_{\mathrm{h}}}{g_{\mathrm{h}}}\right]^{\Delta}, \tag{5.3.43}$$

and in order to get $\delta g_{\mathrm{h}}^{\overline{\mathrm{MS}}}$ the UV-divergent part of the three-point vertex $\Gamma_{\mu\nu}^{\chi Z'Z'}$ is calculated at one-loop order from the Feynman diagrams depicted in Fig. 5.3, yielding

$$\left[\Gamma_{\mu\nu}^{\chi Z'Z'}\right]^{\Delta} = -\frac{3M_{Z'}^4}{8\pi^2 v_{\mathrm{h}}^3}\,g_{\mu\nu}\,\Delta. \tag{5.3.44}$$

The Feynman rules specify the counterterm $\delta\Gamma_{\mu\nu}^{\chi Z'Z'}$ of the corresponding renormalized
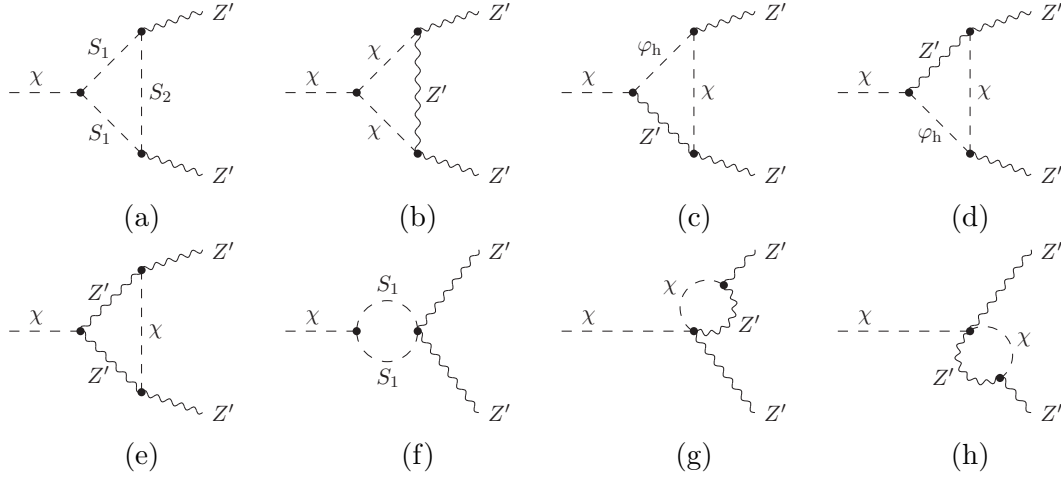
Figure 5.3: One-loop diagrams contributing to the vertex $\Gamma_{\mu\nu}^{\chi Z'Z'}$, generic for scalar bosons $S_1, S_2 \in \{\chi, \varphi_{\mathrm{h}}\}$.

vertex as follows,

$$\hat{\Gamma}_{\mu\nu}^{\chi Z'Z'} = \Gamma_{\mu\nu}^{\chi Z'Z'} + \delta\Gamma_{\mu\nu}^{\chi Z'Z'},$$
$$\delta\Gamma_{\mu\nu}^{\chi Z'Z'} = \frac{2M_{Z'}^2}{v_{\mathrm{h}}} g_{\mu\nu} \left[\frac{\delta M_{Z'}^2}{M_{Z'}^2} - \frac{\delta v_{\mathrm{h}}}{v_{\mathrm{h}}} + \delta Z_{Z'Z'} + \frac{1}{2}\delta Z_{\chi} \right]. \tag{5.3.45}$$

The requirement that $\hat{\Gamma}_{\mu\nu}^{\chi Z'Z'}$ has to be UV finite together with (5.3.33), (5.3.40) and (5.3.43)−(5.3.45) yields

$$\frac{\delta g_{\mathrm{h}}^{\overline{\mathrm{MS}}}}{g_{\mathrm{h}}} = \frac{g_{\mathrm{h}}^2}{96\pi^2} \Delta \tag{5.3.46}$$

and

$$\frac{\delta v_{\mathrm{h}}}{v_{\mathrm{h}}} = \frac{g_{\mathrm{h}}^2}{8\pi^2} \Delta, \qquad \text{(EHSL model)} \tag{5.3.47}$$

such that

$$\lim_{g_{\mathrm{h}} \to 0} \delta v_{\mathrm{h}} = 0. \tag{5.3.48}$$

This result indicates that the renormalization constant δv_{h} is not necessary for the renormalization of the EHSG and EHSD models.

According to the general discussion on vev renormalization in spontaneously broken gauge theories [124] the introduction of the independent renormalization constant δv_{h} is necessary for non-vanishing g_{h} and $\xi'_{Z'} \neq 0$ in the EHSL model, since then the non-standard part of the gauge-fixing Lagrangian (3.2.1) breaks the associated global $\mathrm{U}(1)_{Y_{\mathrm{h}}}$. For vanishing g_{h}, however, the global $\mathrm{U}(1)_{Y_{\mathrm{h}}}$ of the Lagrangian is restored and then, δv_{h} is not required anymore. We confirmed that δv_{h} is not needed to restore the $\mathrm{U}(1)_{Y_{\mathrm{h}}}$ Ward identities specified in Appendix B. Finally, we have checked analytically that with the choice

$$\delta v_{\mathrm{h}} = 0 \qquad \text{(EHSG/EHSD model)} \tag{5.3.49}$$

all the corresponding renormalized one-loop vertex functions are UV finite, both in the EHSG and in the EHSD model. Therefore, we conclude that the renormalization conditions (5.3.47) and (5.3.49) are very convenient allowing a smooth transition from the renormalized EHSL to the renormalized EHSG model.

Gauge-fixing and Faddeev-Popov sector

The bare gauge-fixing part $\mathcal{L}_{\text{EHS},0}^{\text{fix}}$ is obtained from (3.2.1) by introducing the renormalization transformations for the fields and parameters. The bare gauge-fixing operators F_0^a $(a = A, Z, \pm, Z')$ are defined such that these absorb all the corresponding one-loop renormalization constants in $\mathcal{L}_{\text{EHS},0}^{\text{fix}}$ in first-order approximation. Additionally taking into account the renormalization transformations of the ghost fields (5.3.23), the bare Faddeev-Popov part $\mathcal{L}_{\text{EHS},0}^{\text{ghost}}$ is defined analogously to (3.2.4) but with the replacements $\delta F^a(x) \rightarrow \delta F_0^a(x)$, $u^b(y) \rightarrow u_0^b(y)$, $\delta\phi^c(z) \rightarrow \delta\phi_0^c(z)$ and $\delta V_\nu^c(z) \rightarrow \delta V_{\nu,0}^c(z)$. The infinitesimal gauge transformations of the bare fields $\delta V_{\nu,0}^c$ and $\delta\phi_0^c$ are obtained from (2.1.32) and (3.1.32) by introducing the corresponding renormalization transformations. Accordingly, the renormalized vertex functions involving the ghost fields as well as the renormalized ghost-field propagators are determined as listed in Appendix A.

In linear gauges the gauge-fixing operators and parameters are protected from one-loop and higher-order corrections as a consequence of the Slavnov-Taylor identities. Therefore, we do not have to renormalize the gauge-fixing part of the Lagrangian (see e.g. [83]) and it is convenient to require that $\mathcal{L}_{\text{EHS},0}^{\text{fix}}$ is equal to (3.2.1) written in terms of renormalized fields and parameters. This ensures that the usual form of Slavnov-Taylor identities is realized and fixes the renormalization constants of the standard gauge-fixing parameters as follows,

$$\delta\xi_V = \delta Z_{VV}, \qquad\qquad\qquad (V = A, Z, W),$$
$$\delta\xi_V' = \frac{1}{2}\delta Z_{VV} - \frac{1}{2}\frac{\delta M_V^2}{M_V^2} - \frac{1}{2}\delta Z_H, \qquad (V = Z, W), \qquad (5.3.50)$$

and those of the non-standard gauge-fixing parameters as

$$\delta\xi_{Z'} = \delta Z_{Z'Z'}, \qquad \delta\xi_{Z'}' = \frac{1}{2}\delta Z_{Z'Z'} - \frac{1}{2}\frac{\delta M_{Z'}^2}{M_{Z'}^2} - \frac{1}{2}\delta Z_\chi. \qquad (5.3.51)$$

With (5.3.50) and (5.3.51) the poles of the would-be Goldstone-boson propagators coincide with the corresponding ones of the related gauge bosons also at the one-loop level.

It remains to determine the field renormalization of the Faddeev-Popov ghosts as introduced in (5.3.23). According to the on-shell scheme, the related field renormalization constants are fixed such that the ghost fields do not mix at $k^2 = 0$ and $k^2 = M_Z^2$, and such that the real parts of the residues of the corresponding renormalized propagators are equal to one. The counterterm parts of the associated renormalized OPI two-point functions can be obtained from App. A.6. With the respective u^a-u^b self-

energies denoted as $\widetilde{\Sigma}^{ab}$ we hence obtain

$$\delta\widetilde{Z}_{VV} = -\widetilde{\mathrm{Re}}\frac{\partial\widetilde{\Sigma}^{VV}(k^2)}{\partial k^2}\bigg|_{k^2=M_V^2} + \frac{1}{2}\delta Z_{VV}, \qquad (V=A,Z,\pm),$$

$$\delta\widetilde{Z}_{AZ} = -\widetilde{\mathrm{Re}}\frac{\widetilde{\Sigma}^{ZA}(M_Z^2)}{M_Z^2} + \frac{1}{2}\delta Z_{AZ}, \qquad \delta\widetilde{Z}_{ZA} = \frac{\widetilde{\Sigma}^{AZ}(0)}{M_Z^2},$$

$$(5.3.52)$$

and

$$\delta\widetilde{Z}_{Z'Z'} = -\widetilde{\mathrm{Re}}\frac{\partial\widetilde{\Sigma}^{Z'Z'}(k^2)}{\partial k^2}\bigg|_{k^2=M_{Z'}^2} + \frac{1}{2}\delta Z_{Z'Z'}, \tag{5.3.53}$$

where $\delta\widetilde{Z}_{\pm\pm} = \delta\widetilde{Z}_{WW}$ and $\delta Z_{\pm\pm} = \delta Z_{WW}$.

Now that we have introduced and fixed all the one-loop renormalization constants of the EHSL, EHSG and EHSD models, we refer to the associated list of Feynman rules which can be found in Appendix A and includes the entire set of one-loop counterterm vertices.

Chapter 6

Electroweak precision observables

In order to gain further information about the allowed non-standard parameter space we here focus on a distinguished set of precision observables which is affected by non-standard one-loop contributions of the extended Higgs sector. It is commonly known as the set of electroweak precision observables (EWPOs).

EWPOs are given by the $M_W - M_Z$ interdependence via G_{F} and the set of observables at the Z resonance, i.e. line-shape observables like the total Z width Γ_Z and partial widths $\Gamma_f \equiv \Gamma(Z \to f\overline{f})$ as well as various asymmetries which contain the effective electroweak mixing angles. More details on EWPOs can be found e.g. in [81, 125].

Due to associated one-loop contributions of the fields H_1 and H_2 the EWPOs depend on the non-standard parameters α and M_{H_2}. At the one-loop level neither Z'_μ nor φ_{h} contributes to EWPOs and therefore, the remaining non-standard parameters v_{h} and $M_{Z'}$ (or g_{h}) do not appear in this context. The one-loop predictions provided within this chapter thus apply to the EHSL, EHSG and EHSD models which are here referred to as EHS models.

For the Z line-shape observables σ_{had}^0 (hadronic cross section at the peak), Γ_Z, $R_l = \frac{\Gamma_{\mathrm{had}}}{\Gamma_e}$ (hadronic width Γ_{had}) and $R_b = \frac{\Gamma_b}{\Gamma_{\mathrm{had}}}$ it turns out that related non-standard one-loop effects are negligible (considerably smaller than the size of corresponding experimental $\pm 1\sigma$ bounds) in the treated range of α and M_{H_2} (specified in Sect. 6.1). This is why we do not further discuss these insensitive Z line-shape observables.

It appears that the W-boson mass M_W and the effective leptonic mixing angle $\sin^2 \theta_{\mathrm{eff}}^{\mathrm{lep}}$ are the EWPOs which are most sensitive to the non-standard one-loop contributions of the EHS models, and in this chapter we provide the corresponding results. Moreover, we provide the non-standard one-loop prediction for the forward-backward pole asymmetry of the Z-boson decay into a pair of b quarks $A_{\mathrm{FB}}^{0,b}$, for which the SM prediction shows about 2.4σ deviation from the corresponding experimentally measured central value (cf. Tab. 6.2).

Non-standard one-loop contributions to M_W have already been studied in the real-Φ_{h} extension of the SM [52]. Here, we perform a similar analysis but take into account

parameter	experimental central value	reference
$M_H = M_{H_1}$ [GeV]	125.09	[19]
M_Z [GeV]	91.1876	[79]
m_t [GeV]	173.5	[79]
m_b [GeV]	4.93	[79]
G_{F} [GeV^{-2}]	$1.1663787 \cdot 10^{-5}$	[100, 101]
$(\alpha_{\mathrm{em}})^{-1}$	137.035999139	[79]
$\alpha_s (M_Z)$	0.1182	[79]
$\Delta\alpha_{\mathrm{em}}$	0.05907	[126, 127]

Table 6.1: Relevant input parameters we use in our calculations. M_H denotes the mass of the SM Higgs boson. For the quarks the pole masses are listed.

an improved implementation of corresponding higher-order SM contributions.[1] In [53] bounds for the parameters α and M_{H_2} have been derived from the full set of electroweak precision data by taking into account related non-standard one-loop effects in the propagators of the W and Z boson, but with the associated non-standard one-loop effects in the couplings of the Z boson to the fermions neglected. Here, we take into account the complete non-standard one-loop corrections.

At the end of this chapter we present the result for a $\Delta\chi^2$ analysis which takes into account our predicted M_W, $\sin^2\theta_{\mathrm{eff}}^{\mathrm{lep}}$ and $A_{\mathrm{FB}}^{0,b}$ in terms of the model parameters and depicts associated exclusion bounds of 68% and 95% confidence level in the $\alpha - M_{H_2}$ plane.

6.1 Technical aspects and current experimental status

In order to obtain accurate analytical and numerical results for the observables listed above, numerous Feynman diagrams have to be calculated. For the generation and simplification of the corresponding analytical expressions we make use of the `Mathematica` packages `FeynArts` [78] and `FormCalc` [104]. The `Mathematica` output is then converted into a `FORTRAN` code which, together with the `LoopTools` [104] package, allows us to obtain the numerical results in an efficient way.

Up to now, quantum effects of the extended models beyond the one-loop level have not yet been calculated. We therefore combine one-loop standard and non-standard effects with all SM higher-order terms so far known. As there exist no tree-level couplings between the non-standard scalar fields and the massless gauge fields (cf. Chapter 3) corresponding one-loop and higher-order QED and QCD contributions can be directly adopted from the SM.

The important input parameters which are used in our calculations are specified in Tab. 6.1. Here, m_t and m_b denote the pole masses of the t and b quark, G_{F} represents the Fermi constant, α_s the strong coupling constant and $\Delta\alpha_{\mathrm{em}}$ stands for the shift

---

[1]For large α and large M_{H_2} this improved implementation has a non-negligible effect such that the deviation from the related SM prediction for M_W becomes furthermore increased by a few MeV.

observable	SM pred.	Δ_{m_t}	Δ_{M_H}	$\Delta_{\Delta\alpha}$	experiment
M_W [GeV]	80.363	$\pm 6 \cdot 10^{-3}$	$\pm 5 \cdot 10^{-4}$	$\pm 2 \cdot 10^{-3}$	80.385 ± 0.015 [79]
$\sin^2 \theta_{\text{eff}}^{\text{lep}}$	0.23151	$\pm 3 \cdot 10^{-5}$	$\pm 4 \cdot 10^{-6}$	$\pm 4 \cdot 10^{-5}$	0.23153 ± 0.00016 [131]
$A_{\text{FB}}^{0,b}$	0.103	$\pm 2 \cdot 10^{-4}$	$\pm 2 \cdot 10^{-5}$	$\pm 2 \cdot 10^{-4}$	0.0992 ± 0.0016 [132]

Table 6.2: Summary of EWPOs investigated in this work. Current experimental central values and associated $\pm 1\sigma$ bounds are listed as well as corresponding SM predictions. The quantities Δ_{m_t}, Δ_{M_H} and $\Delta_{\Delta\alpha}$ point out the particular change in the predicted observables which stems from a variation of the input parameters m_t and M_H by ± 1 GeV and $\Delta\alpha_{\text{em}}$ by ± 0.0001.

in the electromagnetic fine-structure constant α_{em} induced by QED photon vacuum polarization. The masses of the remaining fermions are taken from [79] and the entries of the quark-mixing matrix are set to the `FormCalc`-8.3 default values.

The current experimental measurements of M_W, $\sin^2 \theta_{\text{eff}}^{\text{lep}}$ and $A_{\text{FB}}^{0,b}$ are summarized in Tab. 6.2 together with the corresponding SM predictions. The latter incorporate the input parameters specified in Tab. 6.1 and include the established one-loop and higher-order contributions. The SM prediction for M_W is taken from [128] whereas the predicted values of $\sin^2 \theta_{\text{eff}}^{\text{lep}}$ and $A_{\text{FB}}^{0,b}$ are obtained by using the program `ZFITTER` [129, 130].

6.1.1 Constraints from Higgs signal strengths

Recent measurements of the various Higgs signal strengths at the LHC can be used to get a quick estimate for the restriction of the mixing angle α to a smaller range than in (3.1.25).

Here, the Higgs signal strength $\hat{\mu}_i$ is defined by the total cross section of the process $pp \to H_1 \to X_i$ (protons p, decay product $X_i \in$ SM) predicted by the EHS models, normalized by the related total cross section predicted by the SM. Hence, we have

$$\hat{\mu}_i = \frac{\sigma(pp \to H_1 \to X_i)}{\sigma(pp \to H \to X_i)_{\text{SM}}} = \frac{\sigma(pp \to H_1)}{\sigma(pp \to H)_{\text{SM}}} \cdot \frac{\text{BR}(H_1 \to X_i)}{\text{BR}(H \to X_i)_{\text{SM}}}, \quad (6.1.1)$$

which in LO approximation simplifies to

$$\hat{\mu}_i = c_\alpha^2 \cdot \frac{\text{BR}(H_1 \to X_i)_{\text{LO}}}{\text{BR}(H \to X_i)_{\text{SM,LO}}}. \quad (6.1.2)$$

From (6.1.2) we can furthermore deduce that

$$\hat{\mu}_i = c_\alpha^2 \cdot \left[1 + \frac{\Gamma(H_1 \to X_{\text{ns}})_{\text{LO}}}{c_\alpha^2 \Gamma_{\text{tot,LO}}^H} \right]^{-1}, \qquad X_{\text{ns}} \notin X_i, \quad (6.1.3)$$

where $\Gamma(H_1 \to X_{ns})$ generically summarizes the potential impact of kinematically allowed non-standard decay modes (cf. Chapter 7) on the total H_1 width

$$\Gamma_{tot}^{H_1} = \sum_i \Gamma(H_1 \to X_i) + \Gamma(H_1 \to X_{ns}), \tag{6.1.4}$$

and Γ_{tot}^{H} denotes the total width of the SM Higgs boson. In the limit $\Gamma(H_1 \to X_{ns}) \to 0$ we have $\mathrm{BR}(H_1 \to X_i)_{LO} = \mathrm{BR}(H \to X_i)_{SM,LO}$ and thus $\hat{\mu}_i = c_\alpha^2$. Here we assume that experimentally measured deviations from $\hat{\mu}_i = 1$ can be related to this factor c_α^2.

Taking into account the combined Higgs signal strength analysis of the ATLAS [133] and CMS [134] collaboration this approach approximately leads us to $\hat{\mu}_i = c_\alpha^2 \gtrsim 0.75$. Therefore, we restrict the angle α to the range

$$-\frac{\pi}{6} \le \alpha \le +\frac{\pi}{6}. \tag{6.1.5}$$

For the second Higgs we assume $M_{H_2} > 70$ GeV in the numerical analysis of EWPOs.[2] Moreover, we do not consider M_{H_2} larger than 1 TeV. Note that according to (6.1.3) the mixing angle α becomes even more constrained by $\hat{\mu}_i$ measurements once non-standard decay modes of H_1 become kinematically allowed.

6.2 W-boson mass and muon decay

6.2.1 Theoretical framework

Originally, the muon lifetime τ_μ has been calculated in the Fermi model. In this context, the corresponding fermions interact directly at one four-fermion vertex and the theoretical result can be written as [81]

$$\frac{1}{\tau_\mu} = \frac{G_F^2 m_\mu^5}{192\pi^3} \left(1 - 8\frac{m_e^2}{m_\mu^2}\right) \cdot K_{QED},$$
$$K_{QED} = 1 + 1.810 \frac{\alpha_{em}(m_\mu)}{\pi} + (6.701 \pm 0.002) \left(\frac{\alpha_{em}(m_\mu)}{\pi}\right)^2, \tag{6.2.1}$$

including the established QED corrections within that model. Here, m_e and m_μ denote the masses of the electron and muon. Nowadays, the Fermi model is considered to describe the effective limit of small momentum transfer in the SM. Still, (6.2.1) serves as the defining equation for the Fermi constant G_F which represents the coupling strength of the effective four-fermion interaction. Including the established QED corrections specified by K_{QED} we obtain the numerical value listed in Tab. 6.1.

Comparing (6.2.1) with the theoretical result for τ_μ calculated in the SM (or in its EHS extensions) and just retaining terms of first order in perturbation theory provides us with the relation

$$\frac{G_F}{\sqrt{2}} = \frac{e^2}{8s_W^2 M_W^2} [1 + \Delta r]. \tag{6.2.2}$$

---

[2]The LEP exclusion limit of $M_H > 114.4$ GeV [135] does not apply to non-standard Higgs bosons with smaller couplings.
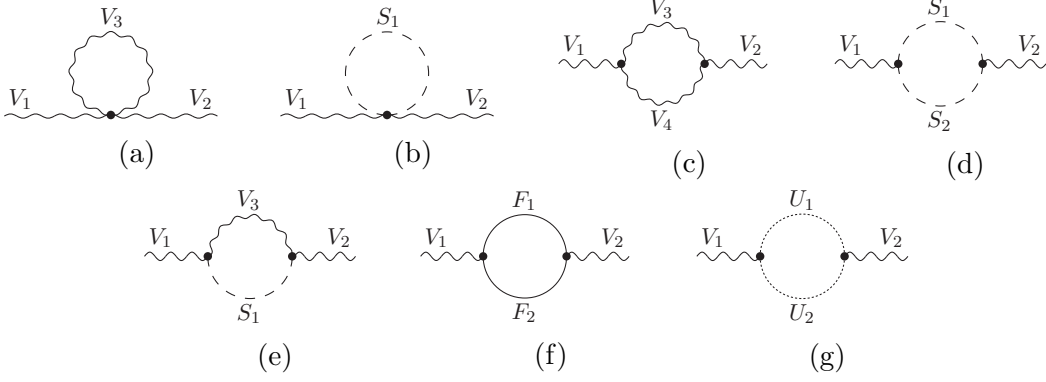
Figure 6.1: Generic gauge-boson self-energy diagrams, with gauge fields $V_1, V_2, V_3, V_4 \in \{A, Z, W^\pm\}$, scalar bosons $S_1, S_2 \in \{H_1, H_2, \varphi_s, \phi^\pm\}$, fermions $F_1, F_2 \in \{\nu_i, l_i, u_i, d_i\}$, and ghost fields $U_1, U_2 \in \{u^A, u^Z, u^\pm\}$.

The finite quantity

$$\Delta r = 2\frac{\delta e}{e} - \frac{c_W^2}{s_W^2}\left(\frac{\delta M_Z^2}{M_Z^2} - \frac{\delta M_W^2}{M_W^2}\right) + \frac{\Sigma_\mathrm{T}^{WW}(0) - \delta M_W^2}{M_W^2} + \delta_\mathrm{vertex+box} \qquad (6.2.3)$$

summarizes the electroweak radiative one-loop corrections which are contributing to the muon decay. The QED corrections are already included in (6.2.1).

In the SM the explicit form of the vertex and box contributions to the muon decay can be written as [81]

$$\delta_\mathrm{vertex+box} = \frac{2}{s_W c_W}\frac{\Sigma_\mathrm{T}^{AZ}(0)}{M_Z^2} + \frac{\alpha_\mathrm{em}}{4\pi s_W^2}\left(6 + \frac{7 - 4s_W^2}{2s_W^2}\log c_W^2\right). \qquad (6.2.4)$$

In the EHS models we can neglect deviations from the expression on the right-hand side of (6.2.4). This is because the corresponding non-standard vertex and box contributions are always proportional to the couplings of H_1 and H_2 to the electron or muon and those couplings always contain a factor $\frac{m_{e/\mu}}{M_W}$, multiplied by c_α and s_α, respectively. Hence, associated virtual contributions are suppressed no matter if we consider the standard ($\alpha = 0$) or the extended scalar sector.

Next, let us have a closer look at the renormalization constants and gauge-boson self-energies which appear in (6.2.3) and (6.2.4). The corresponding renormalization constants are defined in (5.2.9) and (5.2.10). Generally speaking, we have to take into account virtual contributions of the gauge, Higgs, fermion and ghost sector as depicted in Fig. 6.1. Since there exist no direct couplings of H_1 and H_2 to the photon field, the self-energies Σ^{AA} and Σ^{AZ} do not carry any non-standard contributions at the one-loop level and, according to (5.2.10), the same holds for the renormalization constant δe.

It follows that just the self-energy $\Sigma_\mathrm{T}^{WW}(0)$ and the on-shell renormalization constants δM_W^2 and δM_Z^2 defined in (5.2.9) yield non-standard one-loop contributions to Δr. The related transverse gauge-boson self-energies can be written as

$$\Sigma_\mathrm{T}^{WW}(k^2) = \Sigma_\mathrm{SM}^{WW}(k^2) + \Sigma_\mathrm{NS}^{WW}(k^2), \qquad \Sigma_\mathrm{T}^{ZZ}(k^2) = \Sigma_\mathrm{SM}^{ZZ}(k^2) + \Sigma_\mathrm{NS}^{ZZ}(k^2), \qquad (6.2.5)$$
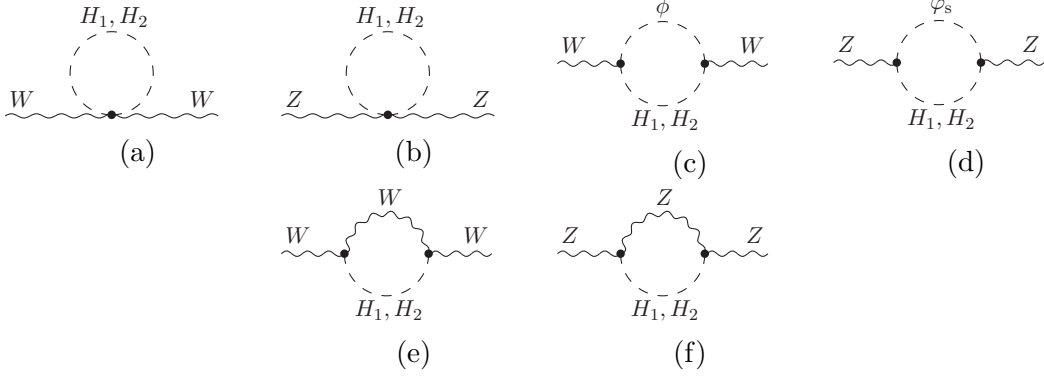
Figure 6.2: Non-standard one-loop contributions to the self-energies of the massive standard gauge bosons, with generic $W = W^\pm$ and $\phi = \phi^\pm$.

with Σ_{SM}^{WW} and Σ_{SM}^{ZZ} comprising the complete SM contributions. The corresponding non-standard contributions are given by

$$
\begin{aligned}
\Sigma_{\text{NS}}^{WW}(k^2) = {} & c_\alpha^2 \frac{\alpha_{\text{em}}}{16\pi s_W^2} \left(A_0(M_{H_1}^2) + 4M_W^2 B_0(k^2, M_{H_1}^2, M_W^2) - 4B_{00}(k^2, M_{H_1}^2, M_W^2) \right) \\
& + s_\alpha^2 \frac{\alpha_{\text{em}}}{16\pi s_W^2} \left(A_0(M_{H_2}^2) + 4M_W^2 B_0(k^2, M_{H_2}^2, M_W^2) - 4B_{00}(k^2, M_{H_2}^2, M_W^2) \right) \\
& - \frac{\alpha_{\text{em}}}{16\pi s_W^2} \left(A_0(M_H^2) + 4M_W^2 B_0(k^2, M_H^2, M_W^2) - 4B_{00}(k^2, M_H^2, M_W^2) \right)
\end{aligned}
$$

$$(6.2.6)$$

and

$$
\begin{aligned}
\Sigma_{\text{NS}}^{ZZ}(k^2) = {} & c_\alpha^2 \frac{\alpha_{\text{em}}}{16\pi s_W^2 c_W^2} \left(A_0(M_{H_1}^2) + 4M_Z^2 B_0(k^2, M_{H_1}^2, M_Z^2) - 4B_{00}(k^2, M_{H_1}^2, M_Z^2) \right) \\
& + s_\alpha^2 \frac{\alpha_{\text{em}}}{16\pi s_W^2 c_W^2} \left(A_0(M_{H_2}^2) + 4M_Z^2 B_0(k^2, M_{H_2}^2, M_Z^2) - 4B_{00}(k^2, M_{H_2}^2, M_Z^2) \right) \\
& - \frac{\alpha_{\text{em}}}{16\pi s_W^2 c_W^2} \left(A_0(M_H^2) + 4M_Z^2 B_0(k^2, M_H^2, M_Z^2) - 4B_{00}(k^2, M_H^2, M_Z^2) \right).
\end{aligned}
$$

$$(6.2.7)$$

The explicit expressions of the scalar one-point integral $A_0(m^2)$, the two-point integral $B_0(k^2, m_1^2, m_2^2)$ and the scalar coefficient function $B_{00}(k^2, m_1^2, m_2^2)$ of the two-point tensor integral $B_{\mu\nu}(k^2, m_1^2, m_2^2) = g_{\mu\nu} B_{00}(k^2, m_1^2, m_2^2) + k_\mu k_\nu B_{11}(k^2, m_1^2, m_2^2)$ can be found in [82]. The last line in (6.2.6) and (6.2.7), respectively, corresponds to the particular SM Higgs contributions which are properly subtracted. The corresponding non-standard diagrams are illustrated in Fig. 6.2.

According to the considerations above Δr can be written as

$$
\Delta r = \Delta r_{\text{SM}}(M_W, M_H, m_t, \dots) + \Delta r_{\text{NS}}(M_W, M_{H_1}, M_{H_2}, \alpha, m_t, \dots), \tag{6.2.8}
$$

such that Δr_{SM} summarizes the corresponding SM contributions and Δr_{NS} takes into account the associated non-standard one-loop contributions. The dots in (6.2.8) indicate that Δr furthermore depends on the remaining SM parameters. The quantity

Δr is sensitive to radiative corrections beyond the one-loop level and as described in Subsect. 6.2.2 we incorporate the established higher-order SM contributions in $\Delta r_{\rm SM}$.

Rearranging (6.2.2) in a way that s_W^2 is expressed in terms of the gauge-boson masses yields

$$M_W^2 = M_Z^2 \left(\frac{1}{2} + \sqrt{\frac{1}{4} - \frac{\alpha_{\rm em}\pi}{\sqrt{2}G_{\rm F}M_Z^2}\left(1 + \Delta r\right)} \right). \tag{6.2.9}$$

Equipped with (6.2.9) the W-boson mass can be predicted in the extended models. Consequently, by taking into account the experimental bounds for M_W we are able to test the EHS models and to obtain constraints for α and M_{H_2}.

As highlighted in (6.2.8) the quantity Δr itself depends on M_W which is why we finally solve (6.2.9) iteratively. Let us now demonstrate how we implement the higher-order SM contributions into our calculation in the improved way.

6.2.2 Implementation of higher-order standard contributions

There exists a simple parametrization [128] for the SM prediction for M_W which incorporates the relevant one-loop and higher-order contributions [136–157]. For $M_H \approx 125$ GeV the resulting numerical value approximates the solution of (6.2.9) to better than 0.2 MeV. The input parameters specified in Tab. 6.1 in combination with this parametrization provide us with the numerical value

$$M_W^{\rm SM} = 80.363 \text{ GeV} \tag{6.2.10}$$

for the predicted SM W-boson mass $M_W^{\rm SM}$ including the established higher orders. Taking into account (6.2.2), it is straightforward to obtain a numerical value for the related quantity $\Delta r_{\rm SM}$ which summarizes the established one-loop and higher-order SM corrections, yielding

$$\Delta r_{\rm SM}(M_W^{\rm SM}, M_H) = \frac{8G_{\rm F}}{\sqrt{2}e^2}\left(M_W^{\rm SM}\right)^2 \left[1 - \left(\frac{M_W^{\rm SM}}{M_Z}\right)^2\right] - 1. \tag{6.2.11}$$

From $\Delta r_{\rm SM}$ we subtract the SM one-loop contributions $\Delta r_{\rm SM}^{\rm 1L}$, calculated according to (6.2.3) and (6.2.4) with the input of the W-boson mass given by (6.2.10). Finally, we add the corresponding one-loop contributions of the EHS models. These are also calculated according to (6.2.3) and (6.2.4) and summarized by the quantity $\Delta r^{\rm 1L}$ which, beside the related standard one-loop contributions, contains the contributions from the non-standard Feynman diagrams listed in Fig. 6.2. Hence, we use

$$\Delta r = \Delta r_{\rm SM}(M_W^{\rm SM}, M_H) - \Delta r_{\rm SM}^{\rm 1L}(M_W^{\rm SM}, M_H) + \Delta r^{\rm 1L}\left(M_W, M_{H_1}, M_{H_2}, \alpha\right) \tag{6.2.12}$$

in order to solve (6.2.9) iteratively. Note that this approach differs from the one in [52] by the input of the W-boson mass in $\Delta r_{\rm SM}^{\rm 1L}$.
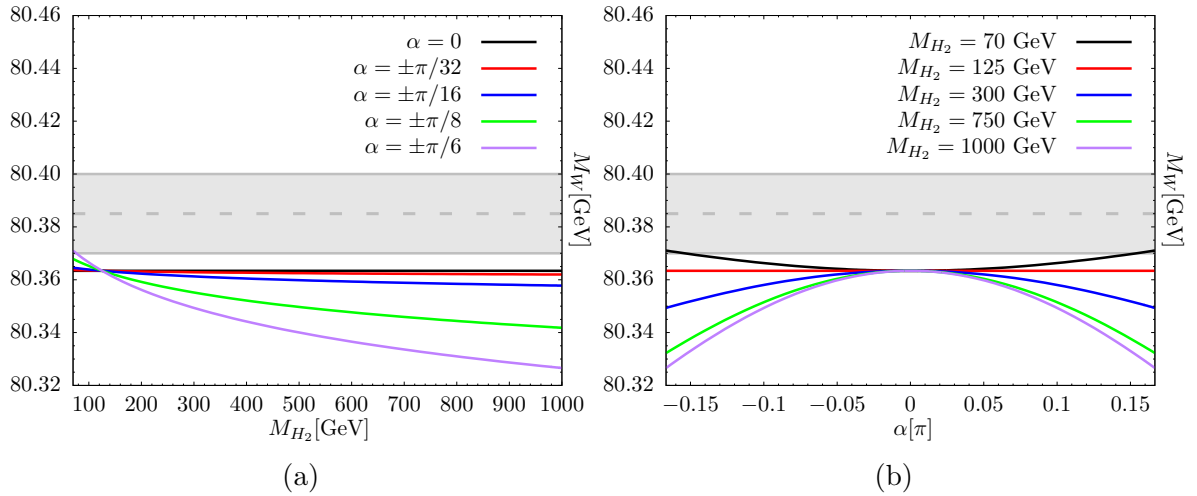
Figure 6.3: Predicted M_W versus M_{H_2} (left side) and α (right side). In either case the dashed grey line stands for the corresponding measured central value and the grey area depicts the associated experimental $\pm 1\sigma$ bounds (cf. Tab. 6.2).

6.2.3 Numerical results

In Fig. 6.3a the predicted M_W is shown as a function of M_{H_2} for different mixing angles α as indicated by the lines of black ($\alpha = 0$), red ($\alpha = \pm\pi/32$), blue ($\alpha = \pm\pi/16$), green ($\alpha = \pm\pi/8$) and purple ($\alpha = \pm\pi/6$) color. Hence, the black horizontal line in Fig. 6.3a represents the corresponding SM prediction. In Fig. 6.3b the predicted M_W is shown as a function of α for different M_{H_2} as indicated by the lines of black ($M_{H_2} = 70$ GeV), red ($M_{H_2} = 125$ GeV), blue ($M_{H_2} = 300$ GeV), green ($M_{H_2} = 750$ GeV) and purple ($M_{H_2} = 1$ TeV) color.

It can be seen that large $|\alpha|$ in combination with the condition $M_{H_2} < M_{H_1}$ provide a shift in the predicted M_W quite close to the experimentally measured $\pm 1\sigma$ band, whereas for large $M_{H_2} > M_{H_1}$ and $\alpha \neq 0$ the gap between the predicted M_W and the measured central value increases. Moreover, we can conclude that in the limit $M_{H_2} \to M_{H_1}$ for any mixing angle α the SM prediction is approached. This is because in this limit we have $\Sigma_{\text{NS}}^{VV}(k^2) = 0$ ($V = W, Z$) as can be directly deduced from (6.2.6) and (6.2.7). Furthermore, Figs. 6.3a,b point out the symmetry of our results under a change of sign in α.

6.3 Z-pole observables

6.3.1 Theoretical framework

Among the Z boson observables, we focus on the predictions for the representative examples $\sin^2\theta_{\text{eff}}^{\text{lep}}$ and $A_{\text{FB}}^{0,b}$ with the best sensitivity on the extended models. These observables are part of the EWPOs associated with the Z resonance in e^+e^- anni-hilations. In this context, the effective vector and axial couplings g_V^f and g_A^f of the Z boson summarize the relevant one-loop and higher-order electroweak effects to the
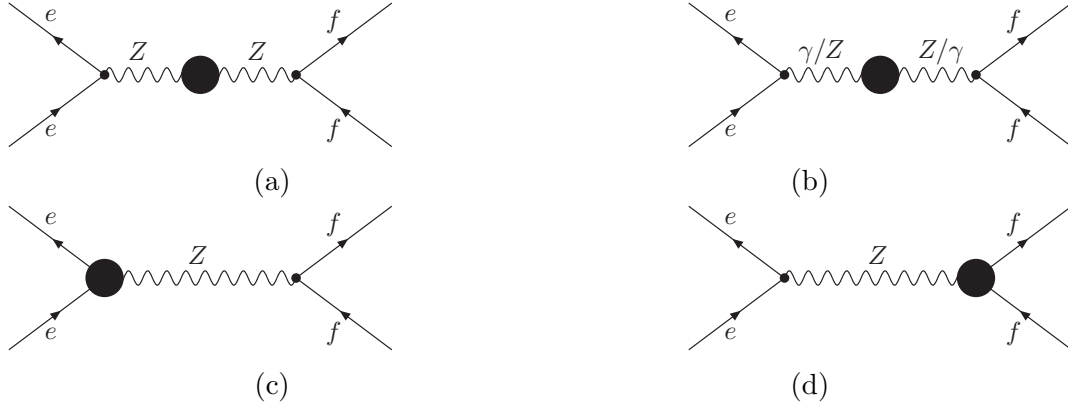
Figure 6.4: Electroweak non-photonic corrections to the process $e^+e^- \longrightarrow f\,\overline{f}$. The large black blobs represent corresponding renormalized two- and three-point functions. Box diagrams are negligible at the Z peak [125].

process $e^+e^- \longrightarrow f\,\overline{f}$. The electroweak non-photonic one-loop and higher-order contributions which have to be considered at the resonance are visualized in Fig. 6.4.[3] We ignore related box-diagram contributions as these are negligible (relative contribution $\sim 10^{-4}$) around the Z peak [125].

As soon as we neglect the external fermion masses, the Lorentz structure of the renormalized one-loop vertex functions in the processes depicted in Figs. 6.4c,d can be reduced to the Lorentz structure of the corresponding tree-level vertices. Since the fermions into which the Z boson can decay are light, this is a reasonable approximation. As a result, the one-loop corrections to the vertices can be absorbed in associated renormalized vector and axial-vector vertex form factors $\hat{F}_V^{Zf}(s)$ and $\hat{F}_A^{Zf}(s)$ which generally depend on the center-of-mass energy $\sqrt{s}$. At the resonance, we set $s = M_Z^2$ in $\hat{F}_V^{Zf}$ and $\hat{F}_A^{Zf}$. By introducing the effective vector and axial-vector couplings [81]

$$
\begin{aligned}
g_V^f &= \left[v_f + 2s_W c_W Q_f \frac{\hat{\Pi}^{AZ}(M_Z^2)}{1 + \hat{\Pi}^A(M_Z^2)} + \hat{F}_V^{Zf} \right] \cdot \left(\frac{1 - \Delta r}{1 + \hat{\Pi}^Z(M_Z^2)} \right)^{1/2}, \\
g_A^f &= \left[a_f + \hat{F}_A^{Zf} \right] \cdot \left(\frac{1 - \Delta r}{1 + \hat{\Pi}^Z(M_Z^2)} \right)^{1/2},
\end{aligned}
\tag{6.3.1}
$$

and the fermionic neutral-current vertices

$$
J_\mu^f = \left[g_V^f \gamma_\mu - g_A^f \gamma_\mu \gamma_5 \right] \cdot \left(\sqrt{2} G_F M_Z^2 \right)^{1/2},
\tag{6.3.2}
$$

the corresponding Z-exchange amplitude A_Z^f can be written as [81]

$$
A_Z^f = \frac{J_\mu^e \otimes J^{f,\mu}}{s - M_Z^2 + is\frac{\Gamma_Z}{M_Z}},
\tag{6.3.3}
$$

---

[3]Related QED corrections form a gauge-invariant subset [81] and thus can be treated separately.
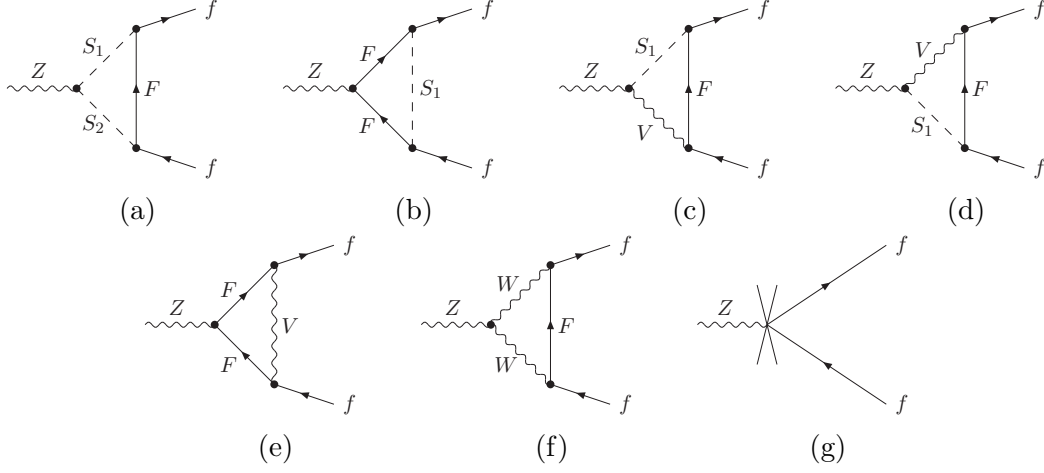
Figure 6.5: Generic one-loop vertex diagrams contributing to $\hat{F}_V^{Zf}$ and $\hat{F}_A^{Zf}$, with scalar bosons $S_1, S_2 \in \{H_1, H_2, \varphi_s, \phi^\pm\}$, fermions $F = l_i, \nu_i, u_i, d_i$, vector bosons $V = W^\pm, Z$, and $W = W^\pm$. The cross in (g) denotes the corresponding vertex counterterm.

with the shorthand notation

$$\gamma_\mu \otimes \gamma^\mu = [\bar{v}_e \gamma_\mu u_e] \times [\bar{u}_f \gamma^\mu v_f] \tag{6.3.4}$$

for the bilinear combinations of the spinors u_f and v_f of the external fermion fields. Furthermore, we introduce the quantities

$$\hat{\Pi}^A(s) = \frac{\hat{\Sigma}_T^{AA}(s)}{s}, \qquad \hat{\Pi}^{AZ}(s) = \frac{\hat{\Sigma}_T^{AZ}(s)}{s}, \qquad \hat{\Pi}^Z(M_Z^2) = \frac{\partial \mathrm{Re}\hat{\Sigma}_T^{ZZ}(s)}{\partial s}\bigg|_{s=M_Z^2}, \quad (6.3.5)$$

and the tree-level vector and axial-vector couplings of the Z boson to fermions f,

$$\begin{aligned} v_f &= I_f^3 - 2s_W^2 Q_f, \\ a_f &= I_f^3. \end{aligned} \tag{6.3.6}$$

In the on-shell renormalization scheme we have (cf. Sect. 5.2)

$$\mathrm{Re}\hat{\Sigma}_T^{AZ}(M_Z^2) = \mathrm{Re}\frac{\partial \hat{\Sigma}_T^{ZZ}(k^2)}{\partial k^2}\bigg|_{k^2=M_Z^2} = 0. \tag{6.3.7}$$

The small imaginary parts of the self-energies and vertex form factors in (6.3.1) can be neglected and thus, the effective vector and axial-vector couplings can be simplified to

$$g_V^f = \left[v_f + \hat{F}_V^{Zf}\right] \cdot (1 - \Delta r)^{1/2}, \qquad g_A^f = \left[a_f + \hat{F}_A^{Zf}\right] \cdot (1 - \Delta r)^{1/2}. \tag{6.3.8}$$

In Figs. 6.5 and 6.6 we illustrate the one-loop $Zf\bar{f}$-vertex diagrams and the fermion self-energy diagrams which contribute to $\hat{F}_V^{Zf}$ and $\hat{F}_A^{Zf}$. The fermion self-energies enter via the field renormalization of the external fermions which is part of the $Zf\bar{f}$-vertex
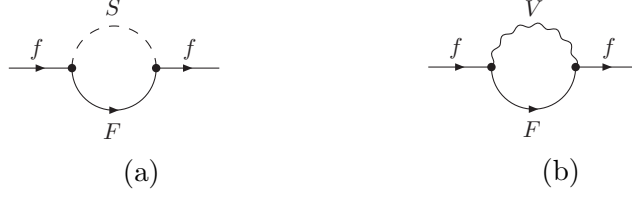
Figure 6.6: Fermion self-energy diagrams contributing to $\hat{F}_V^{Zf}$ and $\hat{F}_A^{Zf}$ via the vertex counterterm depicted in Fig. 6.5g, with scalar bosons $S = H_1, H_2, \varphi_s, \phi^\pm$, fermions $F = l_i, \nu_i, u_i, d_i$, and vector bosons $V = W^\pm, Z$.

counterterm depicted in Fig. 6.5g. The renormalized vector and axial-vector form factors read

$$\hat{F}_V^{Zf} = F_V^{Zf} + \delta F_V^{Zf}, \qquad \hat{F}_A^{Zf} = F_A^{Zf} + \delta F_A^{Zf}, \tag{6.3.9}$$

with the unrenormalized vertex iT_{Zff}^μ,

$$T_{Zff}^\mu = \frac{e}{2 s_W c_W} \left[F_V^{Zf} \gamma^\mu - F_A^{Zf} \gamma^\mu \gamma_5 \right], \tag{6.3.10}$$

which summarizes the one-loop contributions to the $Zf\overline{f}$ coupling induced by the three-point vertex diagrams depicted in Figs. 6.5a−6.5f, and the counterterm

$$
\begin{aligned}
\delta F_V^{Zf} &= v_f \frac{\delta e}{e} + \frac{1}{2} v_f \delta Z_{ZZ} - \frac{v_f(s_W^2 - c_W^2) - 4 s_W^2 c_W^2 Q_f}{2 s_W^2} \left(\frac{\delta M_W^2}{M_W^2} - \frac{\delta M_Z^2}{M_Z^2} \right) \\
&\quad - s_W c_W Q_f \delta Z_{AZ} + \left(I_f^3 - s_W^2 Q_f \right) \delta Z^{f,\mathrm{L}} - s_W^2 Q_f \delta Z^{f,\mathrm{R}}, \\
\delta F_A^{Zf} &= a_f \frac{\delta e}{e} + \frac{1}{2} a_f \delta Z_{ZZ} - \frac{1}{2} a_f \frac{s_W^2 - c_W^2}{s_W^2} \left(\frac{\delta M_W^2}{M_W^2} - \frac{\delta M_Z^2}{M_Z^2} \right) \\
&\quad + \left(I_f^3 - s_W^2 Q_f \right) \delta Z^{f,\mathrm{L}} + s_W^2 Q_f \delta Z^{f,\mathrm{R}},
\end{aligned}
\tag{6.3.11}
$$

according to App. A.15.

The quantities δF_V^{Zf} and δF_A^{Zf} collect the corresponding one-loop renormalization constants associated with the on-shell renormalization scheme. The diagonal field renormalization constants of the fermions $\delta Z^{f,\mathrm{L/R}}$ include the non-photonic electroweak contributions as depicted in Fig. 6.6. Already indicated in Subsect. 6.2.1, δe and δZ_{AZ} have no non-standard contributions at the one-loop level. The important non-standard contributions to $\hat{F}_V^{Zf}$ and $\hat{F}_A^{Zf}$ stem from $\delta M_{W/Z}^2$ and δZ_{ZZ} in (6.3.11). The effects originating from the non-standard vertex and self-energy diagrams illustrated in Figs. 6.5 and 6.6 are small due to the suppressed Yukawa couplings. Only for $f = b$ we obtain some non-negligible non-standard contributions from these diagrams. Note that the effective vector coupling g_V^f furthermore gets non-standard contributions from v_f since the quantity s_W in (6.3.6) depends on M_W.

With the effective vector and axial-vector couplings g_V^f and g_A^f including the non-standard one-loop contributions of the EHS models, we now discuss the related impact on the predictions for $\sin^2 \theta_{\mathrm{eff}}^{\mathrm{lep}}$ and $A_{\mathrm{FB}}^{0,b}$. These two important EWPOs are defined by [125]

$$\sin^2 \theta_{\mathrm{eff}}^{\mathrm{lep}} = \frac{1}{4} \left[1 - \frac{g_V^e}{g_A^e} \right] \tag{6.3.12}$$

and

$$A_{\text{FB}}^{0,b} = \frac{3}{4} A_e A_b, \tag{6.3.13}$$

with

$$A_f = \frac{2 g_{\text{V}}^f g_{\text{A}}^f}{(g_{\text{V}}^f)^2 + (g_{\text{A}}^f)^2}, \qquad f = e, b. \tag{6.3.14}$$

Through the structure of the effective couplings both $\sin^2 \theta_{\text{eff}}^{\text{lep}}$ and $A_{\text{FB}}^{0,b}$ depend on M_W. Consequently, the value of M_W from (6.2.9) with Δr given by (6.2.12) also enters the Z observables.

6.3.2   Implementation of higher-order standard contributions

Our one-loop calculations are combined with the associated higher-order SM contributions for which we apply the program ZFITTER. The latter has the option to use M_W as an input quantity in order to predict the Z-pole observables. From the obtained SM predictions we subtract the corresponding SM one-loop contributions with the input of M_W given by (6.2.10) and finally, we add the respective one-loop contributions of the EHS models.

6.3.3   Numerical results

Our numerical results for $\sin^2 \theta_{\text{eff}}^{\text{lep}}$ and $A_{\text{FB}}^{0,b}$ are illustrated in Figs. 6.7a,b where the observables are plotted as functions of M_{H_2} for different α as indicated by the lines of black ($\alpha = 0$), red ($\alpha = \pm \pi/32$), blue ($\alpha = \pm \pi/16$), green ($\alpha = \pm \pi/8$) and purple ($\alpha = \pm \pi/6$) color. Accordingly, the black horizontal lines in Figs. 6.7a,b represent the corresponding SM predictions. In either case the results are symmetric under a change of sign in α. The α-dependence disappears in the limit $M_{H_2} \to M_{H_1}$ such that the respective SM prediction is approached.

It can be seen that for parameter combinations consisting of large $|\alpha|$ and large M_{H_2}, the predicted $\sin^2 \theta_{\text{eff}}^{\text{lep}}$ can show more than 1σ deviation from the measured value listed in Tab. 6.2. On the other hand, the predicted $\sin^2 \theta_{\text{eff}}^{\text{lep}}$ strongly decreases for large $|\alpha|$ in combination with the condition $M_{H_2} < M_{H_1}$. However, for $M_{H_2} \geq 70$ GeV we do not pass the lower bound of the measured $\pm 1\sigma$ band.

Realizing that the SM prediction for $A_{\text{FB}}^{0,b}$ shows a deviation of more than 2σ from the measured value listed in Tab. 6.2, it is remarkable that parameter combinations consisting of large $|\alpha|$ and large M_{H_2} lead to a predicted $A_{\text{FB}}^{0,b}$ which is considerably more compatible with the experiment. However, this effect is in conflict with the results for M_W and $\sin^2 \theta_{\text{eff}}^{\text{lep}}$ according to which the non-standard parameter region consisting of large $|\alpha|$ and large M_{H_2} clearly leads to a larger deviation from the measured values. The compatibility of the predicted and experimentally measured $A_{\text{FB}}^{0,b}$ becomes worse in the parameter region $M_{H_2} < M_{H_1}$ with $\alpha \neq 0$.

Finally, we perform a $\Delta \chi^2$ analysis combining our non-standard one-loop predictions for M_W, $\sin^2 \theta_{\text{eff}}^{\text{lep}}$ and $A_{\text{FB}}^{0,b}$. The result is depicted in Fig. 6.8. Displayed in the $\alpha - M_{H_2}$ plane are the contours of the yellow ($\Delta \chi^2 \leq 1$) and blue ($\Delta \chi^2 \leq 4$) areas.
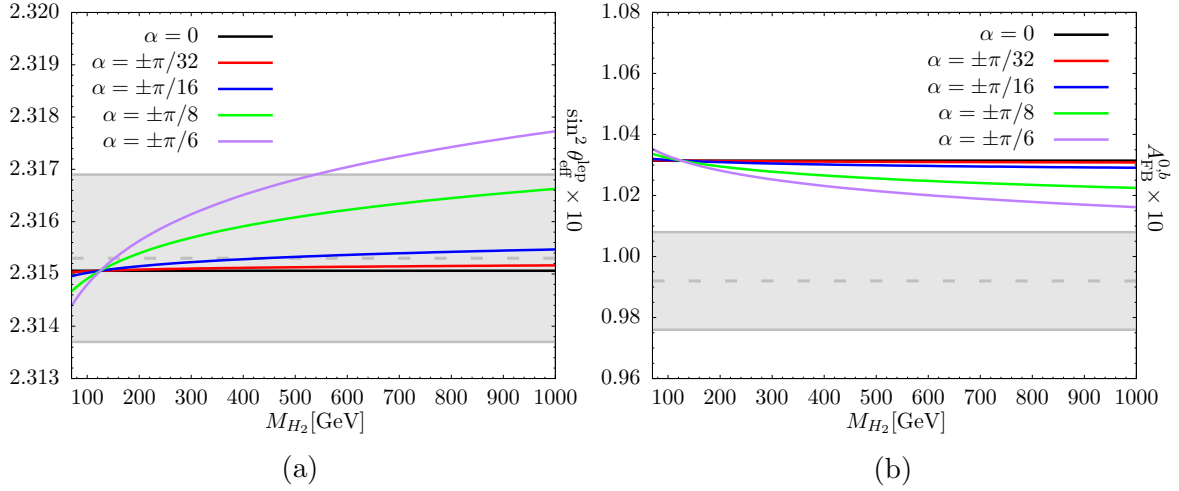
Figure 6.7: Predicted $\sin^2 \theta_{\text{eff}}^{\text{lep}}$ (left side) and $A_{\text{FB}}^{0,b}$ (right side) versus M_{H_2} for various mixing angles α. In either case the dashed grey line stands for the corresponding measured central value and the grey area depicts the associated experimental $\pm 1\sigma$ bounds (cf. Tab. 6.2).

Accordingly, these contours represent exclusion bounds of 68% and 95% confidence level. The solid contours take into account the related parametric uncertainties (approximated by those specified in Tab. 6.2) as well as the theoretical uncertainties from missing higher orders: $\delta M_W|_{\text{h.o.}} \approx 4$ MeV [128], $\delta \sin^2 \theta_{\text{eff}}^{\text{lep}}|_{\text{h.o.}} \approx 5 \cdot 10^{-5}$ [158] and $\delta A_{\text{FB}}^{0,b}|_{\text{h.o.}} \approx 2.7 \cdot 10^{-4}$. Here, $A_{\text{FB}}^{0,b}|_{\text{h.o.}}$ is estimated from $\delta \sin^2 \theta_{\text{eff}}^{\text{lep}}|_{\text{h.o.}}$ by means of Gaussian error propagation in A_e. The dashed contours ignore all these uncertainties. The point of best fit lies outside of the considered α range (6.1.5) and is thus disfavored by Higgs observables.

The overall conclusion is that large M_{H_2} generally constrain $|\alpha|$ to be comparatively small and vice versa. Therefore, Fig. 6.8 underlines the importance of investigating non-standard quantum effects in SM extensions. Together with the constraints from electroweak precision data, a substantial part of non-standard parameter space can be excluded. The exclusion bounds from perturbative unitarity illustrated in Fig. 4.1 provide complementary constraints to the results in Fig. 6.8 from above (for sufficiently small v_{h}).
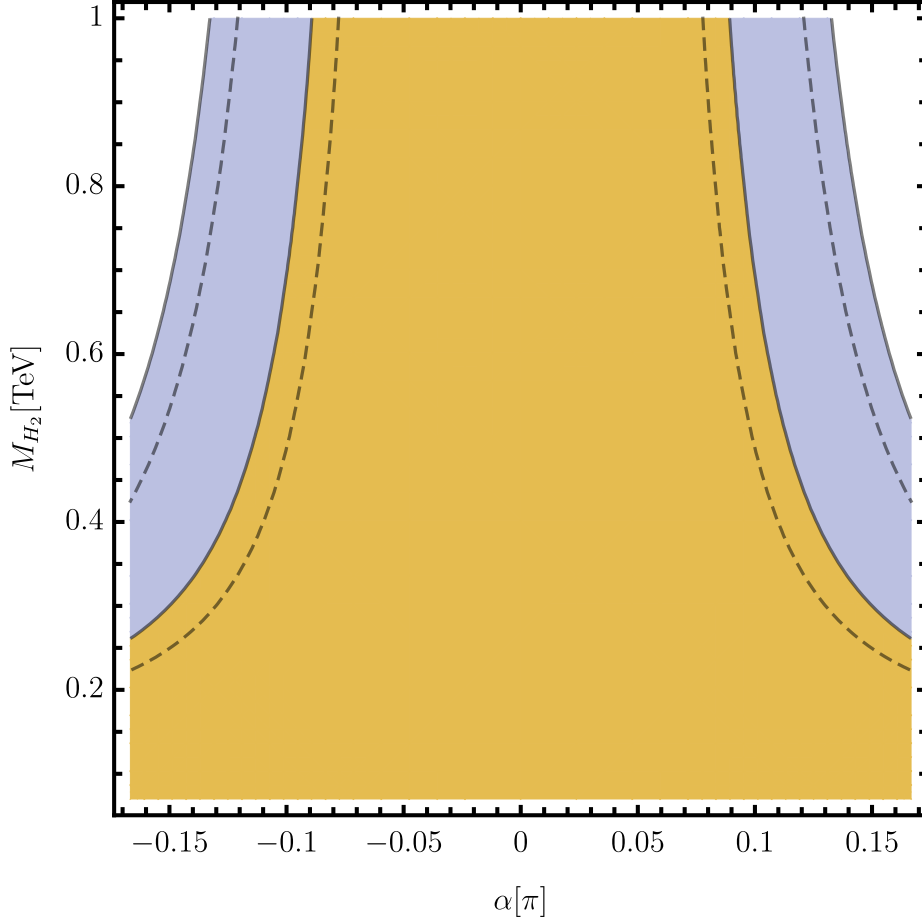
Figure 6.8: Contours of $\Delta\chi^2$ corresponding to our combined NLO analysis of M_W (cf. Fig. 6.3), $\sin^2\theta_{\text{eff}}^{\text{lep}}$ (cf. Fig. 6.7a) and $A_{\text{FB}}^{0,b}$ (cf. Fig. 6.7b) in the EHS models, displayed in the $\alpha - M_{H_2}$ plane. The solid (dashed) contours of the shown yellow ($\Delta\chi^2 \leq 1$) and blue ($\Delta\chi^2 \leq 4$) areas represent exclusion bounds of 68% and 95% confidence level, including (excluding) associated theoretical errors.

Decays of the standard-like Higgs boson

In the SM extensions of the type EHSL, EHSG or EHSD model the predictions for observables related to decays of the standard-like Higgs boson H_1 are in general dependent on the non-standard parameters v_h and $M_{Z'}$ (or g_h), especially once the corresponding non-standard decay channels $H_1 \to Z'Z'$ (EHSL model), $H_1 \to \varphi_h \varphi_h$ (EHSG model) and/or $H_1 \to H_2 H_2$ (EHSL, EHSG and EHSD models) become kinematically allowed. The current experimental uncertainties corresponding to recent measurements of Higgs-decay observables at the LHC experiments [79, 133, 134, 159] are however still comparatively large. In the foreseeable future the total width $\Gamma_{\mathrm{tot}}^{H_1}$ of the standard-like Higgs boson might not become directly observable at the LHC, as well as the corresponding partial widths. However, LHC constraints for the related branching ratios are expected to become more accurate in the years ahead and potential future lepton and hadron collider experiments will further improve the experimental precision [160–165]. Therefore, in models with extended Higgs sectors it is generally worth performing a detailed investigation of the related Higgs-decay observables beyond the LO approximation.

7.1 Concept and technical aspects

In non-standard parameter regions where non-standard decay modes of H_1 are kinematically forbidden (i.e. for $M_{Z'} > M_{H_1}/2$ and $M_{H_2} > M_{H_1}/2$) or sufficiently suppressed, the LO branching ratios of H_1,

$$\mathrm{BR}(H_1 \to \mathrm{X}_i) = \frac{\Gamma(H_1 \to \mathrm{X}_i)}{\Gamma_{\mathrm{tot}}^{H_1}}, \tag{7.1.1}$$

do not differ from those of the SM Higgs boson. This is because a LO partial width $\Gamma(H_1 \to \mathrm{X}_i)_{\mathrm{LO}}$ for the decay of H_1 into the generic SM decay product X_i is just given by the related SM partial width $\Gamma(H \to \mathrm{X}_i)_{\mathrm{LO}}$ multiplied by an additional global factor of c_α^2. This factor stems from the respective H_1 LO coupling due to the mixing (3.1.21), and drops out in the branching ratio. As a consequence, in such regions of non-standard parameters deviations from the SM branching ratios $\mathrm{BR}(H \to \mathrm{X}_i)$

can only be generated by one-loop and higher-order non-standard effects. It is thus important to probe whether non-standard quantum contributions may provide a visible shift in the H_1 branching ratios. Based on our renormalization scheme (cf. Chapter 5) we perform this task at the one-loop level for the first time.[1]

- We take into account the standard and non-standard NLO contributions to the significant fermionic two-body partial widths $\Gamma(H_1 \to b\bar{b})$, $\Gamma(H_1 \to c\bar{c})$ and $\Gamma(H_1 \to \tau\bar{\tau})$.

- We incorporate the dominant non-standard one-loop corrections to the inclusive decays of H_1 into two pairs of on-shell fermions (here denoted as i and j) via the exchange of two virtual standard vector bosons $V = W, Z$. These one-loop corrections are summarized by a proper definition of the corresponding effective renormalized one-loop H_1VV vertices. We provide a new compact analytic formula for the inclusive four-body partial widths $\Gamma(H_1 \to VV) \equiv \sum_{i,j} \Gamma(H_1 \to VV \to ij)$. It enables a convenient (and basically model-independent) implementation of such non-standard one-loop corrections in terms of the above-mentioned effective H_1VV vertices. The latter amongst others depend on the two invariant fermion masses s_i and s_j which are the remaining phase-space integration variables in this formula. In the end we make use of the CUBA [166] library in order to perform the final integration over s_i and s_j numerically.

- The partial widths for the loop-induced decays of H_1, namely $\Gamma(H_1 \to AA)$, $\Gamma(H_1 \to AZ)$ and $\Gamma(H_1 \to gg)$ are approximated by the respective SM expressions [167] multiplied with the factor c_α^2. Thereby, we neglect associated non-standard NLO contributions as two-loop effects which are expected to be small due to the additional suppression by a factor s_α^2. For the numerical evaluation of the SM partial width $\Gamma(H \to gg)$ the FORTRAN package HDECAY [168] (version 6.5) is used. The latter allows us to effectively implement the corresponding substantial QCD corrections which exhibit a rather complicated analytic structure [169].

- In addition to the decays into pure standard particles we provide first NLO results for the partial widths $\Gamma(H_1 \to Z'Z')$, $\Gamma(H_1 \to \varphi_h\varphi_h)$ and $\Gamma(H_1 \to H_2H_2)$ which correspond to the possible non-standard decay modes of H_1. We survey their potential impact on the one-loop corrected $\Gamma_{\text{tot}}^{H_1}$ and $\text{BR}(H_1 \to X_i)$. The heavy-to-light Higgs decay has already been studied at the one-loop level in the EHSD model [51] and in the real-Φ_h extension without the $\mathcal{Z}_2^D$ symmetry [56,60]. Here, the partial width $\Gamma(H_1 \to H_2H_2)$ is investigated in the EHSL, EHSG and EHSD models in order to allow a proper comparison of the related NLO contributions.

- We confirm the validity of the Goldstone-boson equivalence theorem in the non-standard sector at NLO in perturbation theory $-$ a test of consistency of our

---

[1]In [54] the non-standard one-loop contributions to the renormalized Higgs couplings are studied in the real-Φ_h extension of the SM without the $\mathcal{Z}_2^D$ symmetry. Here, we perform a study of the H_1 decay widths and branching ratios in a different and wider class of models.

renormalization schemes. This is achieved by a comparison of the one-loop corrected widths $\Gamma(H_1 \to Z'Z')$ and $\Gamma(H_1 \to \varphi_h\varphi_h)$ in the limit $M_{Z'} \to 0$ (fixed v_h) both analytically and numerically.

The total width $\Gamma_{\text{tot}}^{H_1}$ including the specified non-standard one-loop contributions is obtained by properly adding up the contributions from the various partial widths.[2] Equipped with all the required building blocks a proper one-loop expansion in (7.1.1) finally provides us with the one-loop predictions (henceforth also referred to as NLO predictions) for the branching ratios $\text{BR}(H_1 \to X_i)$, $X_i = AA, ZZ, WW, \tau\bar{\tau}, AZ, gg, b\bar{b}, c\bar{c}$.

7.2 Theoretical framework

In the following the calculations of the partial widths contributing to $\Gamma_{\text{tot}}^{H_1}$ are described, with focus on the non-standard one-loop contributions and their incorporation in the physical observables.

7.2.1 Loop-induced decays

The loop-induced H_1 partial widths into AA, AZ, gg can be expressed in terms of the SM widths $\Gamma(H \to AA)$, $\Gamma(H \to AZ)$ and $\Gamma(H \to gg)$ [167] as follows,

$$
\begin{aligned}
\Gamma(H_1 \to AA) &= c_\alpha^2 \cdot \Gamma(H \to AA), \\
\Gamma(H_1 \to AZ) &= c_\alpha^2 \cdot \Gamma(H \to AZ), \\
\Gamma(H_1 \to gg) &= c_\alpha^2 \cdot \Gamma(H \to gg),
\end{aligned}
\tag{7.2.1}
$$

with the c_α^2 factors originating from the Higgs mixing (3.1.21). The Feynman diagrams corresponding to the related LO processes are depicted in Fig. 7.1. The LO contributions to $\Gamma(H_1 \to AA)$ and $\Gamma(H_1 \to AZ)$ are generated by the diagrams in Figs. 7.1a,b. In Fig. 7.1b only the top quark $F = t$ effectively contributes to the related partial widths. Virtual contributions from the remaining fermions are negligible due to strongly suppressed Yukawa couplings. The dominant LO contribution to $\Gamma(H_1 \to gg)$ stems from the case $Q = t$ in Fig. 7.1c. However, here also the bottom quark $Q = b$ provides a non-negligible virtual contribution. Electroweak non-standard NLO contributions from $\Gamma(H_1 \to AA)$, $\Gamma(H_1 \to AZ)$ and $\Gamma(H_1 \to gg)$ can be neglected as effects at the two-loop level.

The NLO QCD corrections to $\Gamma(H \to AA)$ and $\Gamma(H \to AZ)$ are implemented according to [167]. The established QCD corrections to $\Gamma(H \to gg)$ are incorporated with the help of `HDECAY`. For more details about the standard parts $\Gamma(H \to AA)$, $\Gamma(H \to AZ)$ and $\Gamma(H \to gg)$ we refer to [167] and to references therein.

---

[2]For the sake of completeness, some small contributions from $\Gamma(H_1 \to \mu\bar{\mu})$ and $\Gamma(H_1 \to s\bar{s})$ are incorporated in $\Gamma_{\text{tot}}^{H_1}$, too.
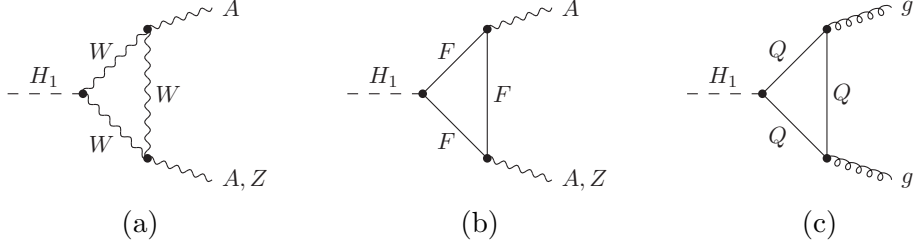
Figure 7.1: Loop-induced decays $H_1 \to AA$, $H_1 \to AZ$ and $H_1 \to gg$ (generic fermions F and quarks Q within the loops) at LO.

7.2.2 Two-body decays into fermions

The fermionic two-body partial widths $\Gamma(H_1 \to f\overline{f})$ are in general given by

$$\Gamma(H_1 \to f\overline{f}) = \frac{1}{2M_{H_1}} N_c^f \left|\mathcal{M}(H_1 \to f\overline{f})\right|^2 \text{LIPS}_2^f, \qquad (7.2.2)$$

with the related matrix element $\mathcal{M}(H_1 \to f\overline{f})$, the color factor N_c^f and the Lorentz-invariant phase-space (LIPS) factor

$$\text{LIPS}_2^f = \frac{1}{8\pi}\sqrt{1 - 4\frac{M_f^2}{M_{H_1}^2}}, \qquad (7.2.3)$$

which depends on the (generic) final-state fermion masses M_f. For $M_{H_1} \approx 125$ GeV only decays into $f = l, q \neq t$ contribute to $\Gamma_{\text{tot}}^{H_1}$. Hence, in good approximation we have $\text{LIPS}_2^f \approx \frac{1}{8\pi}$. At LO the corresponding matrix-element squared reads

$$\left|\mathcal{M}(H_1 \to f\overline{f})_{\text{LO}}\right|^2 = c_\alpha^2 \, 2\sqrt{2} G_F M_{H_1}^2 M_f^2. \qquad (7.2.4)$$

Here, the Fermi constant G_F has been introduced instead of v_s via (3.1.28). Accordingly, in LO approximation the widths (7.2.2) are given by

$$\Gamma(H_1 \to f\overline{f})_{\text{LO}} = c_\alpha^2 \, N_c^f \frac{G_F}{4\sqrt{2}\pi} M_{H_1} M_f^2. \qquad (7.2.5)$$

The fermionic two-body partial widths are influenced by relevant QED and QCD corrections. These are taken into account by multiplying (7.2.5) with the associated correction factor

$$\kappa_f = 1 + \Delta_f^{\text{QED}} + \Delta_f^{\text{QCD}}. \qquad (7.2.6)$$

The quantity Δ_f^{QED} incorporates the $\mathcal{O}(\alpha_{\text{em}})$ corrections from virtual photons and real-photon bremsstrahlung which we adopt from [170]. The quantity Δ_f^{QCD} for final-state quarks $f = q \neq t$ incorporates the QCD corrections up to $\mathcal{O}(\alpha_s^3)$ according to [167]. For decays into quarks the $\overline{\text{MS}}$ scheme is used, and therefore the $\overline{\text{MS}}$ quark masses evaluated at the scale $\mu = M_{H_1}$ have to be taken as input for the partial widths. Therefore, together with (7.2.6) the $\overline{\text{MS}}$ quark masses $M_f = \overline{m}_q(M_{H_1})$ for $f = q$ and
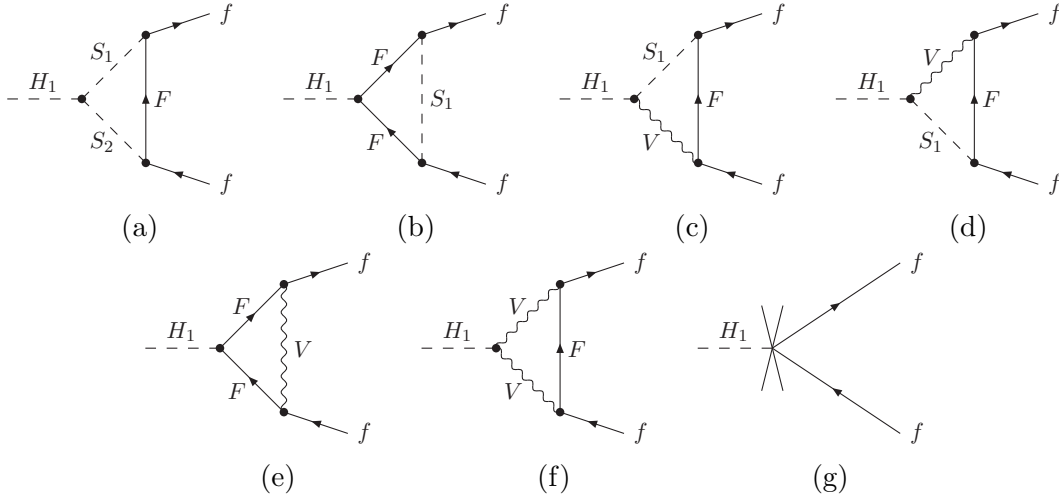
Figure 7.2: Generic weak standard and non-standard one-loop $H_1 f\overline{f}$-vertex corrections in the EHS models, with scalar bosons $S_1, S_2 \in \{H_1, H_2, \varphi_{\mathrm{s}}, \phi^{\pm}\}$, fermions $F = l_i, \nu_i, u_i, d_i$, and vector bosons $V = Z, W$. The cross in (g) denotes the corresponding vertex counterterm.

the on-shell lepton masses $M_f = m_l$ for $f = l = e, \mu, \tau$ have to be used as input in (7.2.5). In practice, contributions from $\Gamma(H_1 \to e\bar{e})$, $\Gamma(H_1 \to u\bar{u})$ and $\Gamma(H_1 \to d\bar{d})$ to $\Gamma_{\mathrm{tot}}^{H_1}$ can be neglected owing to the Yukawa-coupling suppression.

Next, we incorporate the weak (non-QED) standard and non-standard NLO corrections in (7.2.2). Expanded up to the one-loop order the matrix-element squared can be written as follows,

$$
\begin{aligned}
\left|\mathcal{M}(H_1 \to f\overline{f})\right|^2 = {} & (\hat{R}_{H_1} - \Delta r) \left|\mathcal{M}(H_1 \to f\overline{f})_{\mathrm{LO}}\right|^2 \\
& + 2\mathrm{Re}\left[\mathcal{M}(H_1 \to f\overline{f})_{\mathrm{1L}}^{\mathrm{E}}\, \mathcal{M}(H_1 \to f\overline{f})_{\mathrm{LO}}^{\dagger}\right],
\end{aligned}
\tag{7.2.7}
$$

with the wave-function renormalization factor

$$
\hat{R}_{H_1} = 1 - \mathrm{Re}\hat{\Sigma}^{H_1 H_1\,\prime}(M_{H_1}^2)
\tag{7.2.8}
$$

of the $\overline{\mathrm{MS}}$-renormalized field H_1 (cf. Sect. 5.3), where

$$
\hat{\Sigma}^{H_1 H_1\,\prime}(M_{H_1}^2) = \Sigma^{H_1 H_1\,\prime}(M_{H_1}^2) + \delta Z_{H_1 H_1}
\tag{7.2.9}
$$

according to (5.3.25) with the usual notation

$$
\hat{\Sigma}^{S_1 S_2\,\prime}(M_S^2) = \left.\frac{\partial \hat{\Sigma}^{S_1 S_2}(k^2)}{\partial k^2}\right|_{k^2 = M_S^2}.
\tag{7.2.10}
$$

The diagrams with non-standard fields in the internal lines contributing to the H_1 self-energy in the EHS models are depicted in Fig. 5.1. They introduce a dependence on the non-standard parameters M_{H_2}, v_{h} and g_{h} which is absent at LO. In (7.2.7) the quantity Δr appears as NLO correction related to the use of G_{F} in (7.2.4).

The one-loop matrix element $\mathcal{M}(H_1 \to f\overline{f})^{\mathrm{E}}_{\mathrm{1L}}$ contains the remaining weak standard and non-standard one-loop corrections from the vertex diagrams depicted in Fig. 7.2. Analogously to the calculation of $\Gamma(H \to f\overline{f})$ in the SM [170] these corrections can be written in a factorized way,

$$\mathrm{Re}\left[\mathcal{M}(H_1 \to f\overline{f})^{\mathrm{E}}_{\mathrm{1L}}\,\mathcal{M}(H_1 \to f\overline{f})^{\dagger}_{\mathrm{LO}}\right] = \mathrm{Re}\hat{\mathrm{E}}^f\,\left|\mathcal{M}(H_1 \to f\overline{f})_{\mathrm{LO}}\right|^2, \qquad (7.2.11)$$

summarized by the renormalized quantity

$$\hat{\mathrm{E}}^f = \mathrm{E}^f + \delta\mathrm{E}^f, \qquad (7.2.12)$$

which is related to the renormalized $H_1 f\overline{f}$ vertex $i\hat{\mathrm{T}}_{H_1 ff}$ via $\hat{\mathrm{T}}^{\mathrm{1L}}_{H_1 ff} = \hat{\mathrm{E}}^f \cdot \mathrm{T}^{\mathrm{LO}}_{H_1 ff}$, with the vertex counterterm (cf. App. A.16)

$$\begin{aligned}
\delta\mathrm{E}^f &= \frac{\delta M_f}{M_f} + \frac{1}{2}(\delta Z^{f,\mathrm{R}} + \delta Z^{f,\mathrm{L}}) + \frac{\delta e}{e} - \frac{\delta s_W}{s_W} - \frac{1}{2}\frac{\delta M_W^2}{M_W^2} \\
&\quad + \frac{1}{2}\delta Z_{H_1 H_1} - \frac{s_\alpha}{2c_\alpha}\delta Z_{H_1 H_2}.
\end{aligned} \qquad (7.2.13)$$

For $f = l$ the generic fermion-mass renormalization constant δM_f in (7.2.13) is specified by the respective mass renormalization constant in (5.2.8) and thus fixed according to the on-shell scheme. For $f = q$, however, δM_f is defined by the appropriate $\overline{\mathrm{MS}}$ part. The fermion self-energy diagrams contributing to $\hat{\mathrm{E}}^f$ via δM_f and via the diagonal field renormalization constants $\delta Z^{f,\mathrm{L/R}}$ in (7.2.13) are given by those listed in Fig. 6.6 and only involve non-photonic corrections. Note the appearance of the triple Higgs self-coupling in Fig. 7.2a. The latter induces a v_{h}-dependence in $\hat{\mathrm{E}}^f$. However, these effects are suppressed by the associated small Yukawa couplings.

Using the formulas given above, we arrive at the final result

$$\begin{aligned}
\Gamma(H_1 \to f\overline{f}) &= c_\alpha^2\,\mathrm{N}_{\mathrm{c}}^f\,\frac{G_{\mathrm{F}}}{4\sqrt{2}\pi}M_{H_1}M_f^2 \\
&\quad \times \left[\hat{R}_{H_1} - \Delta r + 2\mathrm{Re}\hat{\mathrm{E}}^f + \Delta_f^{\mathrm{QED}} + \Delta_f^{\mathrm{QCD}}\right].
\end{aligned} \qquad (7.2.14)$$

Alongside the established QED and QCD corrections it takes into account the complete set of weak standard and non-standard NLO corrections in the EHS models in terms of the UV-finite quantities $\hat{R}_{H_1}$, Δr and $\hat{\mathrm{E}}^f$, where only $\hat{R}_{H_1}$ may comprise quantum effects related to the non-standard fields Z'_μ and φ_{h}.

7.2.3   Four-body decays into fermions

Next, we focus on the fermionic four-body decay processes illustrated in Fig. 7.3. We consider decays of H_1 into the final-state fermion pairs $\mathtt{i} \equiv f_a f_b$ and $\mathtt{j} \equiv f_c f_d$ via the exchange of two virtual vector bosons $V = Z, W$. The vector bosons are passing on the squared invariant fermion masses which will be the remaining phase-space integration variables in our final formula for the related inclusive partial widths.
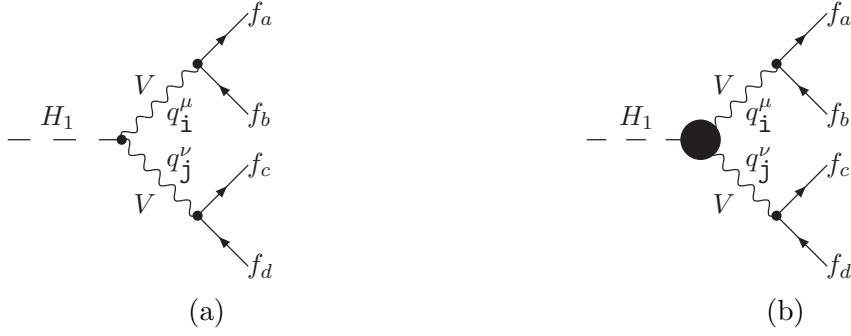
Figure 7.3: Four-body decays of H_1 into pairs of on-shell fermions $\mathtt{i} \equiv f_a f_b$ and $\mathtt{j} \equiv f_c f_d$ via two virtual vector bosons $V = Z, W$.

The corresponding Born processes are depicted in Fig. 7.3a. Here, we are particularly interested in the dominant non-standard one-loop contributions to these processes which stem from the vertex corrections $i\hat{\mathrm{T}}^{\mu\nu}_{H_1 VV}(q_{\mathtt{i}}, q_{\mathtt{j}})$ illustrated by the large black blob in Fig. 7.3b. The related one-loop $H_1 VV$-vertex diagrams are listed in Fig. 7.4. We furthermore take into account the non-standard one-loop effects from the H_1 wave-function renormalization. The residual non-standard one-loop effects associated with the processes $H_1 \to \mathtt{i}\mathtt{j}$ are either suppressed by small Yukawa couplings or by an additional power of one of the illustrated V-boson propagators. Note that for $M_{H_1} \approx 125$ GeV at least one of the two intermediate vector bosons is off its mass shell.

In general, the partial widths can be written as

$$\Gamma(H_1 \to VV \to \mathtt{i}\mathtt{j}) = \frac{1}{2(2\pi)^8 M_{H_1}} \int d\Pi_4 \left|\mathcal{M}_V(H_1 \to \mathtt{i}\mathtt{j})\right|^2, \qquad (7.2.15)$$

with the Lorentz-invariant four-body phase-space integral

$$\int d\Pi_4 = \left(\prod_l \int \frac{d^3 k_l}{2E_l}\right) \delta^{(4)}\left(k_{H_1} - \sum_l k_l\right), \quad l = a, b, c, d, \qquad (7.2.16)$$

and the corresponding matrix-element squared $\left|\mathcal{M}_V(H_1 \to \mathtt{i}\mathtt{j})\right|^2$. The four-momenta k_l with zero-components E_l correspond to the respective final-state fermions f_l. Moreover, the four-momentum of the initial state H_1 is denoted as k_{H_1} with zero-component E_{H_1}. The masses of the final-state fermions can be neglected. Accordingly, we work with $k_l^2 = 0$ in the following.

Introducing the squared invariant fermion masses $s_{\mathtt{i}} = q_{\mathtt{i}}^2 = (k_a + k_b)^2$ and $s_{\mathtt{j}} = q_{\mathtt{j}}^2 = (k_c + k_d)^2$ along with a suitable change of variables in the final-state momenta, repeatedly exploiting Lorentz invariance and summing over all final-state fermion pairs

i and j yields

$$\Gamma(H_1 \to VV) \equiv \sum_{\mathtt{i,j}} \Gamma(H_1 \to VV \to \mathtt{ij}) =$$

$$= \frac{\pi}{128(2\pi)^8 M_{H_1}^2} \sum_{\mathtt{i,j}} \int\limits_0^{s_{\mathtt{i}}^{\max}} ds_{\mathtt{i}} \int\limits_0^{s_{\mathtt{j}}^{\max}} ds_{\mathtt{j}} \tag{7.2.17}$$

$$\times \sqrt{\left(\frac{s_{\mathtt{i}} - s_{\mathtt{j}} + M_{H_1}^2}{2M_{H_1}}\right)^2 - s_{\mathtt{i}}} \int d\hat{\Omega}_{\mathtt{i}} \int d\hat{\Omega}_{\mathtt{j}} \, |\mathcal{M}_V(H_1 \to \mathtt{ij})|^2 \,,$$

with $s_{\mathtt{i}}^{\max} = M_{H_1}^2$, $s_{\mathtt{j}}^{\max} = (M_{H_1} - \sqrt{s_{\mathtt{i}}})^2$ and

$$\int d\hat{\Omega}_{\mathtt{x}} = \int\limits_0^{2\pi} d\hat{\phi}_{\mathtt{x}} \int\limits_0^{\pi} d\hat{\theta}_{\mathtt{x}} \sin\hat{\theta}_{\mathtt{x}}, \quad \mathtt{x} = \mathtt{i}, \mathtt{j}. \tag{7.2.18}$$

The angles $\hat{\phi}_{\mathtt{x}}$ and $\hat{\theta}_{\mathtt{x}}$ are defined in the rest frame of the related fermion pair $\mathtt{x}$. The Lorentz-invariant matrix-element squared $|\mathcal{M}_V(H_1 \to \mathtt{ij})|^2$ is determined by the model parameters and the explicit form of the final-state four-momenta k_l. We choose to calculate $|\mathcal{M}_V(H_1 \to \mathtt{ij})|^2$ in the rest frame of the fermion pair $\mathtt{j}$ where

$$k_{a/b} = \frac{\sqrt{s_{\mathtt{i}}}}{2} \begin{pmatrix} \gamma \mp \gamma\beta \sin\hat{\theta}_{\mathtt{i}} \cos\hat{\phi}_{\mathtt{i}} \\ -\gamma\beta \pm \gamma \sin\hat{\theta}_{\mathtt{i}} \cos\hat{\phi}_{\mathtt{i}} \\ \pm \sin\hat{\theta}_{\mathtt{i}} \sin\hat{\phi}_{\mathtt{i}} \\ \pm \cos\hat{\theta}_{\mathtt{i}} \end{pmatrix}, \quad k_{c/d} = \frac{\sqrt{s_{\mathtt{j}}}}{2} \begin{pmatrix} 1 \\ \pm \sin\hat{\theta}_{\mathtt{j}} \cos\hat{\phi}_{\mathtt{j}} \\ \pm \sin\hat{\theta}_{\mathtt{j}} \sin\hat{\phi}_{\mathtt{j}} \\ \pm \cos\hat{\theta}_{\mathtt{j}} \end{pmatrix}, \tag{7.2.19}$$

with the boost-matrix entries

$$\gamma = \frac{E_{H_1} - \sqrt{s_{\mathtt{j}}}}{\sqrt{s_{\mathtt{i}}}}, \qquad \beta = -\frac{\sqrt{E_{H_1}^2 - M_{H_1}^2}}{E_{H_1} - \sqrt{s_{\mathtt{j}}}} \tag{7.2.20}$$

and

$$E_{H_1} = \frac{M_{H_1} - s_{\mathtt{i}} + s_{\mathtt{j}}}{2\sqrt{s_{\mathtt{j}}}}. \tag{7.2.21}$$

At LO we have

$$|\mathcal{M}_V(H_1 \to \mathtt{ij})_{\mathrm{LO}}|^2 = C_0^V(s_{\mathtt{i}}, s_{\mathtt{j}}) \left[C_{\mathtt{ij}}^{1,V} (k_b \cdot k_d)(k_a \cdot k_c) \right. $$
$$\left. + C_{\mathtt{ij}}^{2,V} (k_b \cdot k_c)(k_a \cdot k_d) \right], \tag{7.2.22}$$

with

$$C_0^V(s_{\mathtt{i}}, s_{\mathtt{j}}) = \frac{16e^6 |C_{H_1 VV}|^2}{[(s_{\mathtt{i}} - M_V^2)^2 + M_V^2 \Gamma_V^2][(s_{\mathtt{j}} - M_V^2)^2 + M_V^2 \Gamma_V^2]} \tag{7.2.23}$$
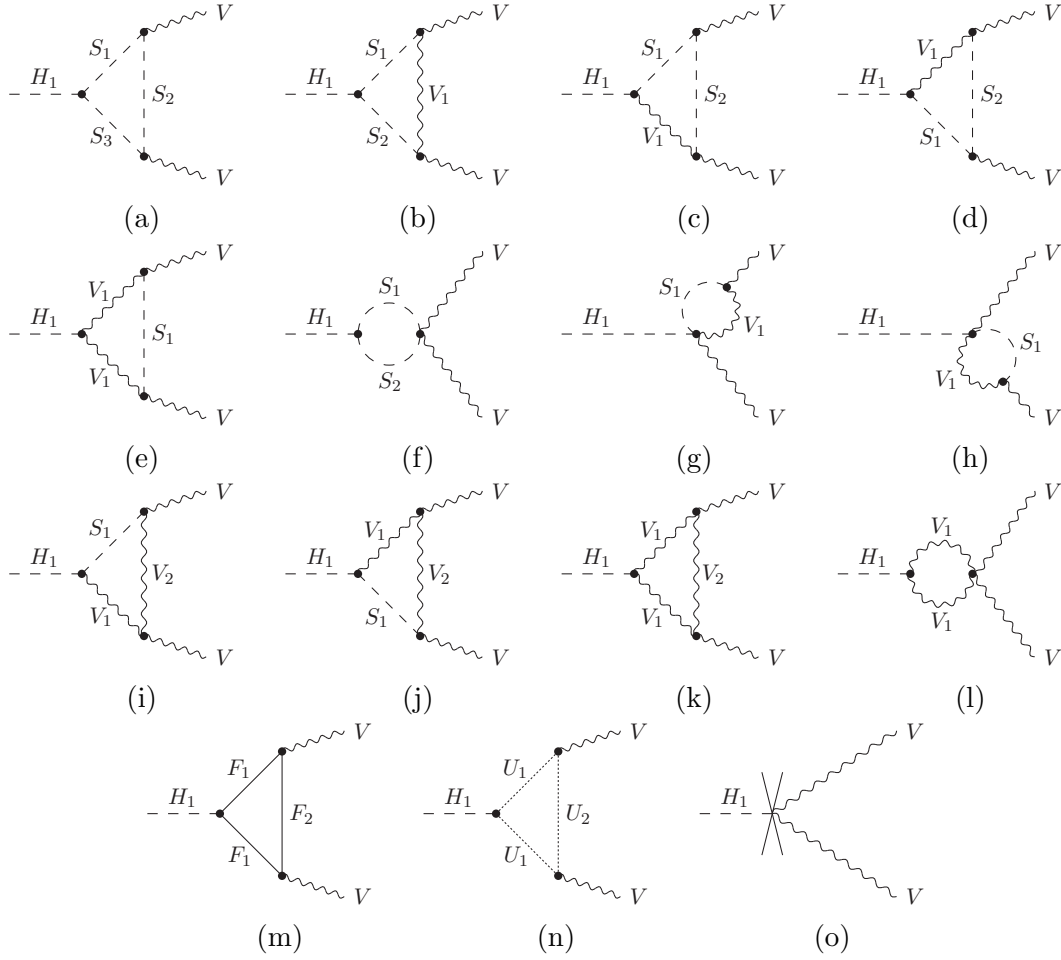
Figure 7.4: Generic H_1VV-vertex diagrams for standard vector bosons $V = Z, W$, with scalar bosons $S_1, S_2, S_3 \in \{H_1, H_2, \varphi_s, \phi^\pm\}$, vector bosons $V_1, V_2 \in \{A, Z, W\}$, fermions $F_1, F_2 \in \{l_i, \nu_i, u_i, d_i\}$, and ghost fields $U_1, U_2 \in \{u^A, u^Z, u^\pm\}$. The cross in (o) denotes the corresponding vertex counterterm.

and

$$
\begin{aligned}
C_{\mathtt{ij}}^{1,V} &= \begin{cases} |C_{\mathtt{i}}^{Z-}|^2|C_{\mathtt{j}}^{Z-}|^2 + |C_{\mathtt{i}}^{Z+}|^2|C_{\mathtt{j}}^{Z+}|^2, & V = Z, \\ |C_{\mathtt{i}}^{W-}|^2|C_{\mathtt{j}}^{W-}|^2, & V = W, \end{cases} \\
C_{\mathtt{ij}}^{2,V} &= \begin{cases} |C_{\mathtt{i}}^{Z-}|^2|C_{\mathtt{j}}^{Z+}|^2 + |C_{\mathtt{i}}^{Z+}|^2|C_{\mathtt{j}}^{Z-}|^2, & V = Z, \\ 0, & V = W. \end{cases}
\end{aligned}
\tag{7.2.24}
$$

Here, the quantity $C_{\mathtt{x}}^{V-}$ ($C_{\mathtt{x}}^{V+}$) denotes the left-handed (right-handed) part of the tree-level coupling between an internal vector boson V and an external fermion pair $\mathtt{x}$, and C_{H_1VV} is the H_1VV tree-level coupling in the vertex $ieC_{H_1VV}g^{\mu\nu}$.[3] The propagators of the internal V bosons incorporate the widths Γ_V as effects of higher order according

---

[3]The explicit form of these couplings can be found in Apps. A.14, A.15.

to the optical theorem, making use of the approximation $\text{Im}\hat{\Sigma}_{\text{T}}^{VV}(s_{\mathtt{x}}) \approx \text{Im}\hat{\Sigma}_{\text{T}}^{VV}(M_V^2)$, which results in a Breit-Wigner form around the mass shell.

The renormalized vertex correction $i\hat{\text{T}}_{H_1VV}^{\mu\nu}(q_{\mathtt{i}}, q_{\mathtt{j}})$ illustrated in Fig. 7.3b can be decomposed as follows,

$$
\begin{aligned}
\hat{\text{T}}_{H_1VV}^{\mu\nu}(q_{\mathtt{i}}, q_{\mathtt{j}}) = eC_{H_1VV} \big[&\text{A}^V(s_{\mathtt{i}}, s_{\mathtt{j}})\, q_{\mathtt{i}}^\mu q_{\mathtt{i}}^\nu + \text{B}^V(s_{\mathtt{i}}, s_{\mathtt{j}})\, q_{\mathtt{j}}^\mu q_{\mathtt{j}}^\nu \\
&+ \text{C}^V(s_{\mathtt{i}}, s_{\mathtt{j}})\, q_{\mathtt{i}}^\mu q_{\mathtt{j}}^\nu + \text{D}^V(s_{\mathtt{i}}, s_{\mathtt{j}})\, q_{\mathtt{j}}^\mu q_{\mathtt{i}}^\nu \\
&+ \hat{\text{E}}^V(s_{\mathtt{i}}, s_{\mathtt{j}})\, g^{\mu\nu} + i\delta_{VW}\text{F}^V(s_{\mathtt{i}}, s_{\mathtt{j}})\, \epsilon^{\mu\nu\rho\sigma} q_{\mathtt{i},\rho} q_{\mathtt{j},\sigma} \big],
\end{aligned}
\tag{7.2.25}
$$

with $\delta_{VW} = 1$ for $V = W$ and $\delta_{VW} = 0$ else, in analogy to the SM [171]. The generic vertex diagrams contributing to (7.2.25) are listed in Fig. 7.4. The quantities $\text{X}^V(s_{\mathtt{i}}, s_{\mathtt{j}})$, $\text{X} = \text{A}, \text{B}, \text{C}, \text{D}, \text{E}, \text{F}$, which summarize the respective (unrenormalized) one-loop contributions are determined by $s_{\mathtt{i}}$, $s_{\mathtt{j}}$ and by the related model parameters. Apart from $\text{E}^V(s_{\mathtt{i}}, s_{\mathtt{j}})$ these quantities are all separately UV finite. Furthermore, each of the quantities introduced in (7.2.25) is infrared finite. This holds even for $V = W$ as a consequence of the fact that at least one of the two gauge-boson legs is always off shell. According to the Dirac equation for massless fermions, the terms which are proportional to $\text{A}^V(s_{\mathtt{i}}, s_{\mathtt{j}})$, $\text{B}^V(s_{\mathtt{i}}, s_{\mathtt{j}})$ and $\text{C}^V(s_{\mathtt{i}}, s_{\mathtt{j}})$ drop out in the one-loop matrix element $\mathcal{M}_V(H_1 \to \mathtt{ij})_{\text{1L}}^{\text{T}}$ with the vertex indicated by the large black blob in Fig. 7.3b. Moreover, the term proportional to the Levi-Civita tensor $\epsilon^{\mu\nu\rho\sigma}$ only appears for $V = W$.[4] The renormalized quantity $\hat{\text{E}}^V(s_{\mathtt{i}}, s_{\mathtt{j}})$ in (7.2.25) can be written as

$$
\hat{\text{E}}^V(s_{\mathtt{i}}, s_{\mathtt{j}}) = \text{E}^V(s_{\mathtt{i}}, s_{\mathtt{j}}) + \delta\text{E}^V,
\tag{7.2.26}
$$

with the vertex counterterm (Fig. 7.4o)

$$
\delta\text{E}^V = \begin{cases}
\dfrac{\delta e}{e} + \dfrac{2s_W^2 - c_W^2}{c_W^2}\dfrac{\delta s_W}{s_W} + \dfrac{1}{2}\dfrac{\delta M_W^2}{M_W^2} + \delta Z_{ZZ} + \dfrac{1}{2}\delta Z_{H_1 H_1} - \dfrac{s_\alpha}{2c_\alpha}\delta Z_{H_1 H_2}, & V = Z, \\[2ex]
\dfrac{\delta e}{e} - \dfrac{\delta s_W}{s_W} + \dfrac{1}{2}\dfrac{\delta M_W^2}{M_W^2} + \delta Z_{WW} + \dfrac{1}{2}\delta Z_{H_1 H_1} - \dfrac{s_\alpha}{2c_\alpha}\delta Z_{H_1 H_2}, & V = W,
\end{cases}
\tag{7.2.27}
$$

which renders $\hat{\text{E}}^V(s_{\mathtt{i}}, s_{\mathtt{j}})$ UV finite.

Expanded up to one-loop order the matrix-element squared in (7.2.17) reads

$$
\begin{aligned}
|\mathcal{M}_V(H_1 \to \mathtt{ij})|^2 = &\hat{R}_{H_1}\, |\mathcal{M}_V(H_1 \to \mathtt{ij})_{\text{LO}}|^2 \\
&+ 2\text{Re}\left[\mathcal{M}_V(H_1 \to \mathtt{ij})_{\text{1L}}^{\text{T}}\, \mathcal{M}_V(H_1 \to \mathtt{ij})_{\text{LO}}^\dagger \right],
\end{aligned}
\tag{7.2.28}
$$

where

$$
\begin{aligned}
\mathcal{M}_V(H_1 \to \mathtt{ij})_{\text{1L}}^{\text{T}} = &\mathcal{M}_V(H_1 \to \mathtt{ij})_{\text{1L}}^{\text{D}} + \mathcal{M}_V(H_1 \to \mathtt{ij})_{\text{1L}}^{\text{E}} \\
&+ \delta_{VW}\mathcal{M}_V(H_1 \to \mathtt{ij})_{\text{1L}}^{\text{F}}
\end{aligned}
\tag{7.2.29}
$$

takes into account the relevant one-loop contributions summarized by the quantities D^V, $\hat{\text{E}}^V$ and F^V. According to (7.2.25), the $\hat{\text{E}}^V$ contributions are proportional to the

---

[4]It originates from the fermion triangle depicted in Fig. 7.4m with two different types of fermions inside the loop.

tensor structure of the corresponding H_1VV tree-level vertex such that

$$\text{Re}\left[\mathcal{M}_V(H_1 \to \text{ij})^{\text{E}}_{\text{1L}}\,\mathcal{M}_V(H_1 \to \text{ij})^{\dagger}_{\text{LO}}\right] = \text{Re}\hat{\text{E}}^V\,|\mathcal{M}_V(H_1 \to \text{ij})_{\text{LO}}|^2, \qquad (7.2.30)$$

with $|\mathcal{M}_V(H_1 \to \text{ij})_{\text{LO}}|^2$ specified in (7.2.22). We obtain

$$\text{Re}\left[\mathcal{M}_V(H_1 \to \text{ij})^{\text{D}}_{\text{1L}}\,\mathcal{M}_V(H_1 \to \text{ij})^{\dagger}_{\text{LO}}\right] = \frac{1}{16}C^V_0\,\text{Re}\left[\text{Tr}^{\text{D},V}_{\text{ij}}\text{D}^V\right], \qquad (7.2.31)$$

and

$$\text{Re}\left[\mathcal{M}_W(H_1 \to \text{ij})^{\text{F}}_{\text{1L}}\,\mathcal{M}_W(H_1 \to \text{ij})^{\dagger}_{\text{LO}}\right] = \frac{1}{16}C^W_0\,\text{Re}\left[\text{Tr}^{\text{F},W}_{\text{ij}}\text{F}^W\right], \qquad (7.2.32)$$

with the products of traces (Feynman slash notation)

$$\begin{aligned}
\text{Tr}^{\text{D},Z}_{\text{ij}} = {}& \text{Tr}\left[\slashed{k}_a\slashed{q}_{\text{j}}\left(C^{Z-}_{\text{i}}\omega_- + C^{Z+}_{\text{i}}\omega_+\right)\slashed{k}_b\gamma^\lambda\left(C^{Z-}_{\text{i}}\omega_- + C^{Z+}_{\text{i}}\omega_+\right)^{\dagger}\right] \\
&\times \text{Tr}\left[\slashed{k}_c\slashed{q}_{\text{i}}\left(C^{Z-}_{\text{j}}\omega_- + C^{Z+}_{\text{j}}\omega_+\right)\slashed{k}_d\gamma_\lambda\left(C^{Z-}_{\text{j}}\omega_- + C^{Z+}_{\text{j}}\omega_+\right)^{\dagger}\right], \qquad (7.2.33) \\
\text{Tr}^{\text{D},W}_{\text{ij}} = {}& \text{Tr}\left[\slashed{k}_a\slashed{q}_{\text{j}}C^{W-}_{\text{i}}\omega_-\slashed{k}_b\gamma^\lambda C^{W-\dagger}_{\text{i}}\right]\times\text{Tr}\left[\slashed{k}_c\slashed{q}_{\text{i}}C^{W-}_{\text{j}}\omega_-\slashed{k}_d\gamma_\lambda C^{W-\dagger}_{\text{j}}\right],
\end{aligned}$$

and

$$\begin{aligned}
\text{Tr}^{\text{F},W}_{\text{ij}} = {}& i\epsilon^{\mu\nu\rho\sigma}q_{\text{j},\rho}q_{\text{i},\sigma}\text{Tr}\left[\slashed{k}_a\gamma_\nu C^{W-}_{\text{i}}\omega_-\slashed{k}_b\gamma^\lambda C^{W-\dagger}_{\text{i}}\right] \\
&\times \text{Tr}\left[\slashed{k}_c\gamma_\mu C^{W-}_{\text{j}}\omega_-\slashed{k}_d\gamma_\lambda C^{W-\dagger}_{\text{j}}\right]. \qquad (7.2.34)
\end{aligned}$$

These products of traces depend on the phase-space angles $\hat{\phi}_{\text{i/j}}$ and $\hat{\theta}_{\text{i/j}}$ according to (7.2.19). In contrast, the quantities D^V, $\hat{\text{E}}^V$ and F^V only depend on the invariants s_{i} and s_{j}.[5] With (7.2.19)−(7.2.34) we are able to analytically perform the four-dimensional angular integration in (7.2.17) over the matrix-element squared specified in (7.2.28). We obtain

$$\int d\hat{\Omega}_{\text{i}}\int d\hat{\Omega}_{\text{j}}\,\text{Im}\text{Tr}^{\text{D},V}_{\text{ij}} = 0, \qquad (7.2.35)$$

and

$$\int d\hat{\Omega}_{\text{i}}\int d\hat{\Omega}_{\text{j}}\,\text{Re}\text{Tr}^{\text{F},W}_{\text{ij}} = \int d\hat{\Omega}_{\text{i}}\int d\hat{\Omega}_{\text{j}}\,\text{Im}\text{Tr}^{\text{F},W}_{\text{ij}} = 0, \qquad (7.2.36)$$

due to the asymmetry of the integrands. Together with (7.2.31) and (7.2.32) we conclude that the quantity F^V as well as the imaginary part of D^V do not contribute to $\Gamma(H_1 \to VV)$. Thus, we arrive at

$$\begin{aligned}
\int d\hat{\Omega}_{\text{i}}\int d\hat{\Omega}_{\text{j}}\,|\mathcal{M}_V(H_1 \to \text{ij})|^2 = {}& \\
= \int d\hat{\Omega}_{\text{i}}\int d\hat{\Omega}_{\text{j}}\,\Bigg[&\left(\hat{R}_{H_1} + 2\text{Re}\hat{\text{E}}^V\right)|\mathcal{M}_V(H_1 \to \text{ij})_{\text{LO}}|^2 \\
&+ \frac{1}{8}C^V_0\,\text{Re}\text{D}^V\,\text{Re}\text{Tr}^{\text{D},V}_{\text{ij}}\Bigg] \\
= \frac{1}{9}\pi^2 M^6_{H_1}C^V_0\left(C^{1,V}_{\text{ij}} + C^{2,V}_{\text{ij}}\right)&\left[\text{I}_{\text{E}}\left(\hat{R}_{H_1} + 2\text{Re}\hat{\text{E}}^V\right) + \text{I}_{\text{D}}\,\text{Re}\text{D}^V\right],
\end{aligned} \qquad (7.2.37)$$

---

[5]We have $(q_{\text{i}} + q_{\text{j}})^2 = M^2_{H_1}$ and hence $(q_{\text{i}}\cdot q_{\text{j}}) = [M^2_{H_1} - s_{\text{i}} - s_{\text{j}}]/2$.

with

$$I_E = \frac{1}{M_{H_1}^2} \left[1 - 2\frac{s_i}{M_{H_1}^2} - 2\frac{s_j}{M_{H_1}^2} + \frac{s_i^2}{M_{H_1}^4} + \frac{s_j^2}{M_{H_1}^4} + 10\frac{s_i s_j}{M_{H_1}^4} \right] \tag{7.2.38}$$

and

$$\begin{aligned}
I_D = 1 &- 3\frac{s_i}{M_{H_1}^2} - 3\frac{s_j}{M_{H_1}^2} + 3\frac{s_i^2}{M_{H_1}^4} + 3\frac{s_j^2}{M_{H_1}^4} + 2\frac{s_i s_j}{M_{H_1}^4} \\
&- \frac{s_i^3}{M_{H_1}^6} - \frac{s_j^3}{M_{H_1}^6} + \frac{s_i^2 s_j}{M_{H_1}^6} + \frac{s_i s_j^2}{M_{H_1}^6}.
\end{aligned} \tag{7.2.39}$$

According to (7.2.24) the factor $(C_{ij}^{1,V} + C_{ij}^{2,V})$ in the last line of (7.2.37) is independent of the remaining integration variables s_i and s_j and hence can be placed in front of the corresponding integrals in (7.2.17). The residual integrals over the invariant masses are the same for all i and j. Therefore, we can explicitly perform the sum over the accessible final-state fermion pairs which yields

$$\sum_{i,j} \left(C_{ij}^{1,V} + C_{ij}^{2,V} \right) = \frac{36}{\alpha_{em}^2} \left(\frac{\Gamma_V}{M_V} \right)^2, \tag{7.2.40}$$

with (quark-mixing matrix $\mathbf{V} = \mathbb{1}_{3\times3}$ approximation)

$$\Gamma_W = \frac{3\alpha_{em} M_W}{4 s_W^2}, \qquad \Gamma_Z = \frac{\alpha_{em} M_Z}{72 s_W^2 c_W^2} [103 - 200 c_W^2 + 160 c_W^4]. \tag{7.2.41}$$

For the SM Higgs boson the NLO results for the partial widths into four fermions are available e.g. via the code PROPHECY4F [172–174]. Therefore, we explicitly calculate here the additional non-standard one-loop contributions in the EHS models. Hence, we have to subtract the related standard one-loop effects. Putting all these steps together, we obtain ($s_i^{max} = M_{H_1}^2$, $s_j^{max} = (M_{H_1} - \sqrt{s_i})^2$)

$$\begin{aligned}
\Gamma(H_1 \to VV) = \frac{1}{\pi^2} \int_0^{s_i^{max}} &\frac{ds_i M_V \Gamma_V}{[(s_i - M_V^2)^2 + M_V^2 \Gamma_V^2]} \int_0^{s_j^{max}} \frac{ds_j M_V \Gamma_V}{[(s_j - M_V^2)^2 + M_V^2 \Gamma_V^2]} \\
&\times \left[\Gamma_E^V \left(c_\alpha^2 + \mathrm{Re}\Delta_E^V \right) + \Gamma_D^V \, \mathrm{Re}\Delta_D^V \right],
\end{aligned} \tag{7.2.42}$$

with the subtracted non-standard form factors

$$\Delta_E^V = 2[c_\alpha^2 \hat{E}^V - \hat{E}_{SM}^V] - [c_\alpha^2 \hat{\Sigma}^{H_1 H_1 \prime}(M_{H_1}^2) - \hat{\Sigma}^{HH \prime}(M_H^2)] - [c_\alpha^2 \Delta r - \Delta r_{SM}] \tag{7.2.43}$$

and

$$\Delta_D^V = 2[c_\alpha^2 \mathrm{D}^V - \mathrm{D}_{SM}^V], \tag{7.2.44}$$

which summarize the relevant non-standard one-loop contributions of the EHS models, and with

$$\Gamma_E^V = \frac{1}{16\sqrt{2}\pi} G_F \delta^V M_{H_1}^5 I_E \sqrt{\lambda(s_i, s_j, M_{H_1}^2)}, \tag{7.2.45}$$

and

$$\Gamma_{\mathrm{D}}^V = \frac{1}{32\sqrt{2}\pi} G_{\mathrm{F}} \delta^V M_{H_1}^5 I_{\mathrm{D}} \sqrt{\lambda(s_{\mathrm{i}}, s_{\mathrm{j}}, M_{H_1}^2)}. \tag{7.2.46}$$

Here, we introduce the kinematic function

$$\lambda(s_{\mathrm{i}}, s_{\mathrm{j}}, M_{H_1}^2) = (1 - s_{\mathrm{i}}/M_{H_1}^2 - s_{\mathrm{j}}/M_{H_1}^2)^2 - 4 s_{\mathrm{i}} s_{\mathrm{j}}/M_{H_1}^4 \tag{7.2.47}$$

and the symmetry factor

$$\delta^V = \begin{cases} 2, & V = W, \\ 1, & V = Z. \end{cases} \tag{7.2.48}$$

The Fermi constant G_{F} has been introduced according to (6.2.2), which is why the related quantities Δr and Δr_{SM} (cf. Sect. 6.2) appear in (7.2.43) at the given order. The quantity Δ_{E}^V incorporates the non-standard one-loop contributions which multiply from the LO integrand in (7.2.42) whereas the quantity Δ_{D}^V comprises the corresponding effects which originate from the term proportional to $q_{\mathrm{j}}^\mu q_{\mathrm{i}}^\nu$ in the vertex correction (7.2.25). Accordingly, the related inclusive LO partial widths $\Gamma(H_1 \to VV)_{\mathrm{LO}}$ are contained in (7.2.42) for $\Delta_{\mathrm{E}}^V = \Delta_{\mathrm{D}}^V = 0$, and for $\alpha = 0$ we recover the result for the SM Higgs decays in [167].

The final integration over s_{i} and s_{j} in (7.2.42) is performed numerically with the help of the `CUBA` [166] library and will be done for the numerical analysis in Sect. 7.3. Note that it is straightforward to adjust our (basically model-independent) formula (7.2.42) such that it applies to other models with extended sectors (like e.g. the two-Higgs-doublet model). All one has to do is to appropriately replace the factors $\left(c_\alpha^2 + \mathrm{Re}\Delta_{\mathrm{E}}^V\right)$ and $\mathrm{Re}\Delta_{\mathrm{D}}^V$ in (7.2.42). Therefore, non-standard quantum effects corresponding to different models can be explored in the same way.

7.2.4   Two-body decays into massive non-standard scalars

In all considered models, for $\alpha \neq 0$ and $M_{H_2} < M_{H_1}/2$ the non-standard decay mode $H_1 \to H_2 H_2$ affects the total width and branching ratios of H_1. In each of the three models we have the same $H_1 H_2 H_2$ tree-level vertex $iC_{H_1 H_2 H_2}$, with (cf. App. A.10)

$$C_{H_1 H_2 H_2} = -s_\alpha c_\alpha \left(M_{H_1}^2 + 2 M_{H_2}^2\right) \left[\frac{s_\alpha}{v_{\mathrm{s}}} + \frac{c_\alpha}{v_{\mathrm{h}}}\right]. \tag{7.2.49}$$

Therefore, the LO partial widths for this channel are the same in the three models. Here, the related NLO contributions are of particular interest. These are generally different in the three models due to the different field contents entering at the one-loop level.

In general, the partial width can be written as

$$\Gamma(H_1 \to H_2 H_2) = \frac{1}{2} \frac{1}{2 M_{H_1}} |\mathcal{M}(H_1 \to H_2 H_2)|^2 \, \mathrm{LIPS}_2^{H_2}, \tag{7.2.50}$$

including the symmetry factor $1/2$, the matrix-element squared $|\mathcal{M}(H_1 \to H_2 H_2)|^2$ and the phase-space factor

$$\mathrm{LIPS}_2^{H_2} = \frac{1}{8\pi} \sqrt{1 - 4\frac{M_{H_2}^2}{M_{H_1}^2}}. \tag{7.2.51}$$

With the LO coupling (7.2.49) one obtains

$$\Gamma(H_1 \to H_2 H_2)_{\mathrm{LO}} = s_\alpha^2 c_\alpha^2 \left(\frac{s_\alpha}{v_{\mathrm{s}}} + \frac{c_\alpha}{v_{\mathrm{h}}}\right)^2 \frac{(M_{H_1}^2 + 2M_{H_2}^2)^2}{32\pi M_{H_1}} \sqrt{1 - 4\frac{M_{H_2}^2}{M_{H_1}^2}}. \tag{7.2.52}$$

At NLO we have

$$|\mathcal{M}(H_1 \to H_2 H_2)|^2 =$$
$$= |\mathcal{M}(H_1 \to H_2 H_2)_{\mathrm{LO}}|^2 \left[1 - \mathrm{Re}\hat{\Sigma}^{H_1 H_1\prime}(M_{H_1}^2) - 2\mathrm{Re}\hat{\Sigma}^{H_2 H_2\prime}(M_{H_2}^2)\right.$$
$$\left. + 2\mathrm{Re}\hat{\mathrm{E}}^{H_2} + \frac{s_\alpha v_{\mathrm{s}} - c_\alpha v_{\mathrm{h}}}{c_\alpha v_{\mathrm{s}} + s_\alpha v_{\mathrm{h}}} \frac{8M_{H_1}^2 + 4M_{H_2}^2}{M_{H_1}^4 + M_{H_1}^2 M_{H_2}^2 - 2M_{H_2}^4} \mathrm{Re}\hat{\Sigma}^{H_1 H_2}(M_{H_2}^2)\right]. \tag{7.2.53}$$

Here, the derivatives of the renormalized diagonal scalar self-energies correspond to the factors $\hat{R}_{H_1}$ and $\hat{R}_{H_2}$ for the wave-function renormalization, with $\hat{R}_{H_1}$ already specified in (7.2.8). Analogously, we have

$$\hat{R}_{H_2} = 1 - \mathrm{Re}\hat{\Sigma}^{H_2 H_2\prime}(M_{H_2}^2), \tag{7.2.54}$$

with

$$\hat{\Sigma}^{H_2 H_2\prime}(M_{H_2}^2) = \Sigma^{H_2 H_2\prime}(M_{H_2}^2) + \delta Z_{H_2 H_2} \tag{7.2.55}$$

according to (5.3.25), and the self-energy diagrams in Fig. 5.1. The renormalized quantity $\hat{\mathrm{E}}^{H_2}$ belongs to the renormalized one-loop $H_1 H_2 H_2$ vertex $i\hat{\mathrm{T}}_{H_1 H_2 H_2}$,

$$\hat{\mathrm{T}}_{H_1 H_2 H_2} = \hat{\mathrm{E}}^{H_2} \cdot C_{H_1 H_2 H_2},$$
$$\hat{\mathrm{E}}^{H_2} = \mathrm{E}^{H_2} + \delta\mathrm{E}^{H_2}, \tag{7.2.56}$$

and takes into account the contributions from the vertex diagrams in Fig. 7.5. The counterterm part $\delta\mathrm{E}^{H_2}$ stems from the diagram in Fig. 7.5q. We have $\delta\mathrm{E}^{H_2} = \delta C_{H_1 H_2 H_2}$ with the rather lengthy $\delta C_{H_1 H_2 H_2}$ specified in App. A.19. Accordingly, $\delta\mathrm{E}^{H_2}$ depends on the renormalization constants δt_{H_1}, δt_{H_2}, δv_{s}, δv_{h}, $\delta M_{H_1}^2$, $\delta M_{H_1 H_2}^2$, $\delta M_{H_2}^2$, $\delta Z_{H_1 H_1}$, $\delta Z_{H_1 H_2}$ and $\delta Z_{H_2 H_2}$. The term in (7.2.53) with the non-diagonal scalar self-energy originates from $H_1 - H_2$ mixing and the tree-level coupling

$$C_{H_1 H_1 H_2} = \frac{s_\alpha v_{\mathrm{s}} - c_\alpha v_{\mathrm{h}}}{c_\alpha v_{\mathrm{s}} + s_\alpha v_{\mathrm{h}}} \frac{2M_{H_1}^2 + M_{H_2}^2}{2M_{H_2}^2 + M_{H_1}^2} \cdot C_{H_1 H_2 H_2}. \tag{7.2.57}$$

We have $\hat{\Sigma}^{H_1 H_2}(M_{H_2}^2) \neq 0$ in our renormalization scheme (cf. Sect. 5.3) and corresponding effects are not included in the diagonal LSZ factors of H_1 and H_2. The counterterm
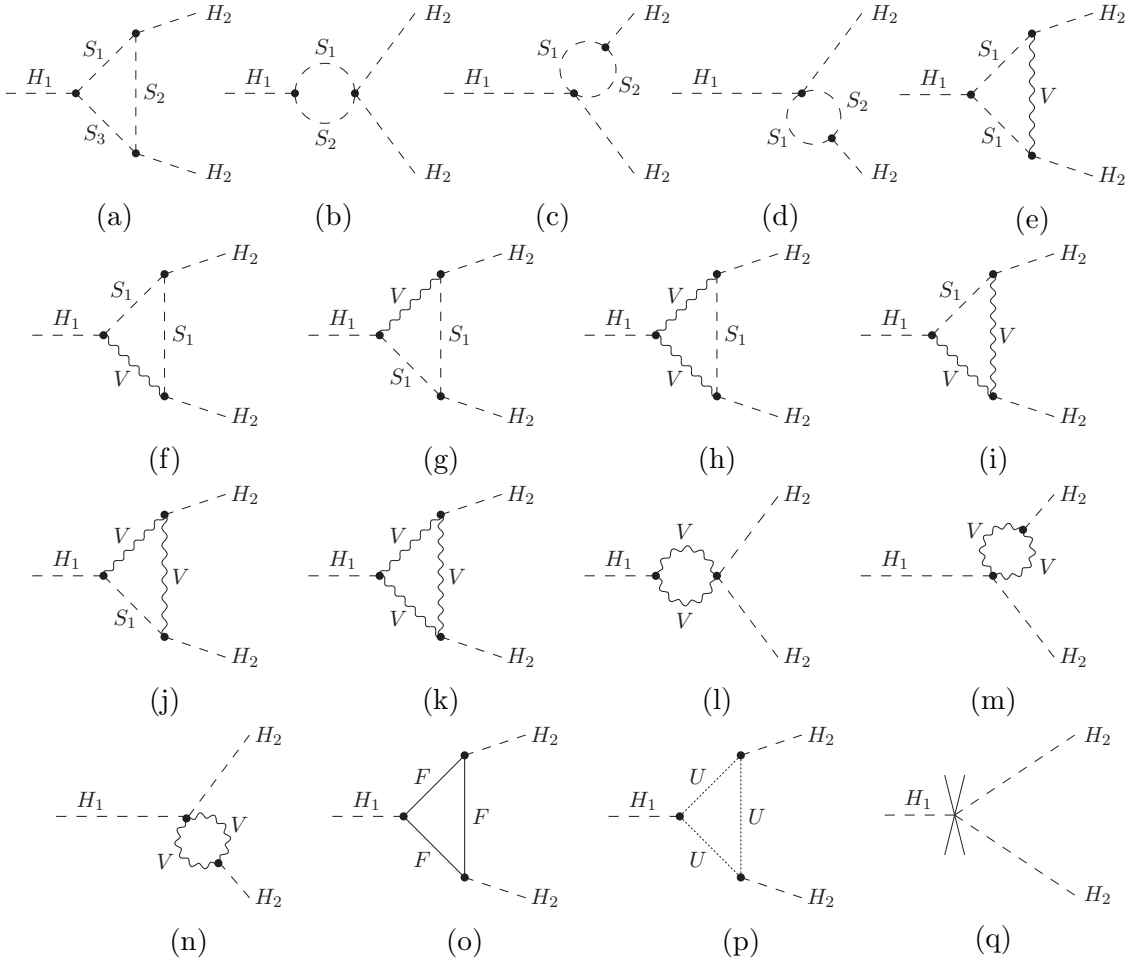
Figure 7.5: Generic $H_1 H_2 H_2$-vertex diagrams, with scalar bosons $S_1, S_2, S_3 \in \{H_1, H_2, \varphi_{\mathrm{s}}, \phi^{\pm}, \varphi_{\mathrm{h}}\}$, fermions $F = l_i, u_i, d_i$, vector bosons $V = Z, W, Z'$, and ghost fields $U = u^Z, u^{\pm}, u^{Z'}$. In the EHSG (EHSD) model without the fields Z' and $u^{Z'}$ (Z', $u^{Z'}$ and φ_{h}). The cross in (q) denotes the corresponding vertex counterterm.

structure of $\hat{\Sigma}^{H_1 H_2}(k^2)$ is already specified in (5.3.26). With $\hat{\Sigma}^{H_1 H_2}(M_{H_1}^2) = 0$ (5.3.28) and (7.2.50)$-$(7.2.53) we obtain

$$
\begin{aligned}
\Gamma\left(H_1 \to H_2 H_2\right) = {} & \Gamma\left(H_1 \to H_2 H_2\right)_{\mathrm{LO}} \\
& \times \left[1 - \mathrm{Re}\hat{\Sigma}^{H_1 H_1 \prime}(M_{H_1}^2) - 2\mathrm{Re}\hat{\Sigma}^{H_2 H_2 \prime}(M_{H_2}^2) + 2\mathrm{Re}\hat{\mathrm{E}}^{H_2} \right. \\
& \left. + \frac{s_\alpha v_{\mathrm{s}} - c_\alpha v_{\mathrm{h}}}{c_\alpha v_{\mathrm{s}} + s_\alpha v_{\mathrm{h}}} \frac{8M_{H_1}^2 + 4M_{H_2}^2}{M_{H_1}^4 + M_{H_1}^2 M_{H_2}^2 - 2M_{H_2}^4} \mathrm{Re}\hat{\Sigma}^{H_1 H_2}(M_{H_2}^2) \right]
\end{aligned}
\tag{7.2.58}
$$

at the one-loop level.

7.2.5 Two-body decays into non-standard gauge bosons

In the EHSL model with the local $U(1)_{Y_h}$ gauge symmetry and the related Z' boson, once we consider the case $M_{Z'} < M_{H_1}/2$, we have to take into account the extra contributions from the non-standard decay channel $H_1 \rightarrow Z'Z'$ to the total width and branching ratios of H_1. The related non-standard partial width is in general given by

$$\Gamma\left(H_1 \rightarrow Z'Z'\right) = \frac{1}{2}\frac{1}{2M_{H_1}}\left|\mathcal{M}(H_1 \rightarrow Z'Z')\right|^2 \mathrm{LIPS}_2^{Z'}, \qquad (7.2.59)$$

with the phase-space factor for the final-state Z' bosons,

$$\mathrm{LIPS}_2^{Z'} = \frac{1}{8\pi}\sqrt{1 - 4\frac{M_{Z'}^2}{M_{H_1}^2}}, \qquad (7.2.60)$$

and the corresponding matrix-element squared $\left|\mathcal{M}(H_1 \rightarrow Z'Z')\right|^2$. With the $H_1 Z'Z'$ tree-level vertex $iC_{H_1 Z'Z'}g^{\mu\nu}$ specified by $C_{H_1 Z'Z'} = 2s_\alpha M_{Z'}^2/v_h$ (cf. App. A.14) one obtains at LO

$$\left|\mathcal{M}(H_1 \rightarrow Z'Z')_{\mathrm{LO}}\right|^2 = s_\alpha^2 \frac{M_{H_1}^4}{v_h^2}\left[1 - 4\frac{M_{Z'}^2}{M_{H_1}^2} + 12\frac{M_{Z'}^4}{M_{H_1}^4}\right], \qquad (7.2.61)$$

and thus the partial width

$$\Gamma\left(H_1 \rightarrow Z'Z'\right)_{\mathrm{LO}} = s_\alpha^2 \frac{M_{H_1}^3}{32\pi v_h^2}\left[1 - 4\frac{M_{Z'}^2}{M_{H_1}^2} + 12\frac{M_{Z'}^4}{M_{H_1}^4}\right]\sqrt{1 - 4\frac{M_{Z'}^2}{M_{H_1}^2}}. \qquad (7.2.62)$$

Consequently, also the non-standard decay channel $H_1 \rightarrow Z'Z'$ can provide a sizable contribution for large $|\alpha|$ and small v_h.

Next, we investigate the corresponding NLO effects. In our renormalization scheme these can be summarized by the factor $\hat{R}_{H_1}$ from wave-function renormalization and by the renormalized one-loop $H_1 Z'Z'$ vertex $i\hat{\mathrm{T}}_{H_1 Z'Z'}^{\mu\nu}$ which, analogously to (7.2.25), can be decomposed as $(q_1^2 = q_2^2 = M_{Z'}^2)$

$$\begin{aligned}
\hat{\mathrm{T}}_{H_1 Z'Z'}^{\mu\nu}(q_1, q_2) = C_{H_1 Z'Z'}[&\mathrm{A}^{Z'}q_1^\mu q_1^\nu + \mathrm{B}^{Z'}q_2^\mu q_2^\nu \\
&+\mathrm{C}^{Z'}q_1^\mu q_2^\nu + \mathrm{D}^{Z'}q_2^\mu q_1^\nu + \hat{\mathrm{E}}^{Z'}g^{\mu\nu}],
\end{aligned} \qquad (7.2.63)$$

and takes into account the one-loop corrections originating from the vertex diagrams in Fig. 7.6. The vertex counterterm depicted in Fig. 7.6i affects only the form factor

$$\begin{aligned}
\hat{\mathrm{E}}^{Z'} &= \mathrm{E}^{Z'} + \delta\mathrm{E}^{Z'}, \\
\delta\mathrm{E}^{Z'} &= \frac{\delta M_{Z'}^2}{M_{Z'}^2} - \frac{\delta v_h}{v_h} + \delta Z_{Z'Z'} + \frac{1}{2}\delta Z_{H_1 H_1} + \frac{c_\alpha}{2s_\alpha}\delta Z_{H_1 H_2}.
\end{aligned} \qquad (7.2.64)$$

The terms with $\mathrm{A}^{Z'}$, $\mathrm{B}^{Z'}$ and $\mathrm{C}^{Z'}$ drop out in the corresponding matrix element when contracted with the polarization vectors. Therefore, in (7.2.63) only the terms $\mathrm{D}^{Z'}$ and
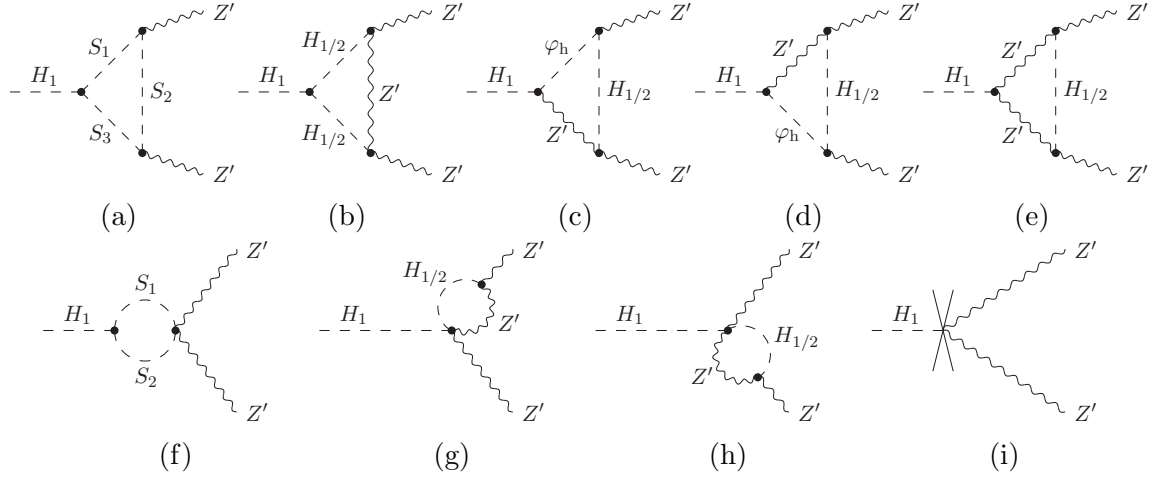
Figure 7.6: One-loop $H_1 Z' Z'$-vertex diagrams, generic for scalar bosons $S_1, S_2, S_3 \in \{H_1, H_2, \varphi_{\text{h}}\}$. The cross in (i) denotes the corresponding vertex counterterm.

$\hat{\text{E}}^{Z'}$ have to be considered and the NLO expansion of the matrix-element squared in (7.2.59) yields

$$
\begin{aligned}
|\mathcal{M}(H_1 \to Z'Z')|^2 &= \hat{R}_{H_1} \, |\mathcal{M}(H_1 \to Z'Z')_{\text{LO}}|^2 \\
&\quad + 2\text{Re}\left[\mathcal{M}(H_1 \to Z'Z')_{\text{1L}}^{\text{T}} \, \mathcal{M}(H_1 \to Z'Z')_{\text{LO}}^{\dagger}\right],
\end{aligned}
\tag{7.2.65}
$$

with

$$
\mathcal{M}(H_1 \to Z'Z')_{\text{1L}}^{\text{T}} = \mathcal{M}(H_1 \to Z'Z')_{\text{1L}}^{\text{D}} + \mathcal{M}(H_1 \to Z'Z')_{\text{1L}}^{\text{E}},
\tag{7.2.66}
$$

where

$$
\begin{aligned}
\text{Re}\left[\mathcal{M}(H_1 \to Z'Z')_{\text{1L}}^{\text{D}} \, \mathcal{M}(H_1 \to Z'Z')_{\text{LO}}^{\dagger}\right] &= \\
&= \frac{4 s_\alpha^2 M_{Z'}^4}{v_{\text{h}}^2}\left[M_{H_1}^2 + \frac{M_{H_1}^6}{8 M_{Z'}^4} - \frac{3 M_{H_1}^4}{M_{Z'}^2}\right] \text{ReD}^{Z'}
\end{aligned}
\tag{7.2.67}
$$

and

$$
\text{Re}\left[\mathcal{M}(H_1 \to Z'Z')_{\text{1L}}^{\text{E}} \mathcal{M}(H_1 \to Z'Z')_{\text{LO}}^{\dagger}\right] = |\mathcal{M}(H_1 \to Z'Z')_{\text{LO}}|^2 \, \text{Re}\hat{\text{E}}^{Z'}.
\tag{7.2.68}
$$

The LSZ factors of the external Z' bosons are unity according to the on-shell renormalization (5.3.39). Hence, at one-loop order the width $\Gamma(H_1 \to Z'Z')$ can be written as

$$
\begin{aligned}
\Gamma(H_1 \to Z'Z') &= \Gamma(H_1 \to Z'Z')_{\text{LO}} \\
&\quad \times \left[\hat{R}_{H_1} + 2\text{Re}\hat{\text{E}}^{Z'} + \frac{M_{H_1}^6 - 6 M_{H_1}^4 M_{Z'}^2 + 8 M_{H_1}^2 M_{Z'}^4}{M_{H_1}^4 - 4 M_{H_1}^2 M_{Z'}^2 + 12 M_{Z'}^4} \text{ReD}^{Z'}\right].
\end{aligned}
\tag{7.2.69}
$$

7.2.6   Two-body decays into hidden Goldstone bosons

In the EHSG model the hidden Goldstone bosons φ_{h} represent physical massless scalar particles. Consequently, for $\alpha \neq 0$ the total width of H_1 inevitably receives contributions from the corresponding non-standard decay mode $H_1 \to \varphi_{\mathrm{h}}\varphi_{\mathrm{h}}$ and, accordingly, the H_1 branching ratios are affected likewise. In generic form, the partial width associated with this process can be written as

$$\Gamma\left(H_1 \to \varphi_{\mathrm{h}}\varphi_{\mathrm{h}}\right) = \frac{1}{2}\frac{1}{2M_{H_1}} \left|\mathcal{M}(H_1 \to \varphi_{\mathrm{h}}\varphi_{\mathrm{h}})\right|^2 \mathrm{LIPS}_2^{\varphi_{\mathrm{h}}}, \tag{7.2.70}$$

with $\mathrm{LIPS}_2^{\varphi_{\mathrm{h}}} = (8\pi)^{-1}$ and the related matrix-element squared $\left|\mathcal{M}(H_1 \to \varphi_{\mathrm{h}}\varphi_{\mathrm{h}})\right|^2$. With the $H_1\varphi_{\mathrm{h}}\varphi_{\mathrm{h}}$ tree-level vertex $iC_{H_1\varphi_{\mathrm{h}}\varphi_{\mathrm{h}}}$ from App. A.10 we have

$$\left|\mathcal{M}(H_1 \to \varphi_{\mathrm{h}}\varphi_{\mathrm{h}})_{\mathrm{LO}}\right|^2 = s_\alpha^2 M_{H_1}^4 / v_{\mathrm{h}}^2 \tag{7.2.71}$$

and

$$\Gamma\left(H_1 \to \varphi_{\mathrm{h}}\varphi_{\mathrm{h}}\right)_{\mathrm{LO}} = s_\alpha^2 \frac{M_{H_1}^3}{32\pi v_{\mathrm{h}}^2} \tag{7.2.72}$$

in LO approximation. We conclude that $\Gamma\left(H_1 \to \varphi_{\mathrm{h}}\varphi_{\mathrm{h}}\right)$ provides major contributions to $\Gamma_{\mathrm{tot}}^{H_1}$ for large $|\alpha|$ and small v_{h}.

At the one-loop level the matrix-element squared in (7.2.70) can be written as

$$\begin{aligned}
\left|\mathcal{M}(H_1 \to \varphi_{\mathrm{h}}\varphi_{\mathrm{h}})\right|^2 &= \left|\mathcal{M}(H_1 \to \varphi_{\mathrm{h}}\varphi_{\mathrm{h}})_{\mathrm{LO}}\right|^2 \\
&\times \left[1 - \mathrm{Re}\hat{\Sigma}^{H_1 H_1\prime}(M_{H_1}^2) - 2\mathrm{Re}\hat{\Sigma}^{\varphi_{\mathrm{h}}\varphi_{\mathrm{h}}\prime}(0) + 2\mathrm{Re}\hat{\mathrm{E}}^{\varphi_{\mathrm{h}}}\right].
\end{aligned} \tag{7.2.73}$$

Here, the renormalized quantity $\hat{\mathrm{E}}^{\varphi_{\mathrm{h}}}$ is introduced along with the renormalized one-loop $H_1\varphi_{\mathrm{h}}\varphi_{\mathrm{h}}$ vertex $i\hat{\mathrm{T}}_{H_1\varphi_{\mathrm{h}}\varphi_{\mathrm{h}}}$,

$$\begin{aligned}
\hat{\mathrm{T}}_{H_1\varphi_{\mathrm{h}}\varphi_{\mathrm{h}}} &= \hat{\mathrm{E}}^{\varphi_{\mathrm{h}}} \cdot C_{H_1\varphi_{\mathrm{h}}\varphi_{\mathrm{h}}}, \\
\hat{\mathrm{E}}^{\varphi_{\mathrm{h}}} &= \mathrm{E}^{\varphi_{\mathrm{h}}} + \delta\mathrm{E}^{\varphi_{\mathrm{h}}},
\end{aligned} \tag{7.2.74}$$

and summarizes the one-loop contributions originating from the vertex diagrams depicted in Fig. 7.7. It is rendered UV finite by the corresponding vertex counterterm,

$$\begin{aligned}
\delta\mathrm{E}^{\varphi_{\mathrm{h}}} &= \frac{s_\alpha}{v_{\mathrm{h}}M_{H_1}^2}\delta t_{H_1} + \frac{c_\alpha}{v_{\mathrm{h}}M_{H_1}^2}\delta t_{H_2} + \frac{\delta M_{H_1}^2}{M_{H_1}^2} + \frac{c_\alpha}{s_\alpha M_{H_1}^2}\delta M_{H_1 H_2}^2 \\
&+ \frac{1}{2}\delta Z_{H_1 H_1} + \frac{c_\alpha M_{H_2}^2}{2s_\alpha M_{H_1}^2}\delta Z_{H_1 H_2},
\end{aligned} \tag{7.2.75}$$

listed in App. A.10 with the renormalization constants δZ_χ and δv_{h} set to zero. The remaining one-loop contributions in (7.2.73) arise from the wave-function renormalization factors $\hat{R}_{H_1}$ and

$$\hat{R}_{\varphi_{\mathrm{h}}} = 1 - \mathrm{Re}\hat{\Sigma}^{\varphi_{\mathrm{h}}\varphi_{\mathrm{h}}\prime}(0). \tag{7.2.76}$$

With the renormalized φ_{h} self-energy (cf. App. A.5)

$$\hat{\Sigma}^{\varphi_{\mathrm{h}}\varphi_{\mathrm{h}}}(k^2) = \Sigma^{\varphi_{\mathrm{h}}\varphi_{\mathrm{h}}}(k^2) + s_\alpha\frac{\delta t_{H_1}}{v_{\mathrm{h}}} + c_\alpha\frac{\delta t_{H_2}}{v_{\mathrm{h}}} \tag{7.2.77}$$
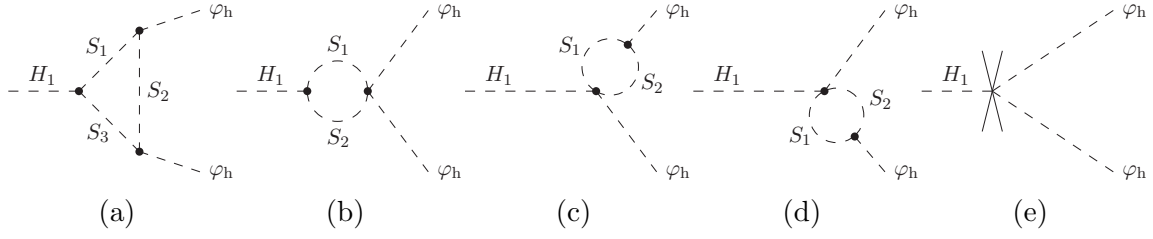
Figure 7.7: Generic $H_1\varphi_\mathrm{h}\varphi_\mathrm{h}$-vertex diagrams in the EHSG model, with scalar bosons $S_1, S_2, S_3 \in \{H_1, H_2, \varphi_\mathrm{s}, \phi^\pm, \varphi_\mathrm{h}\}$. The cross in (e) denotes the corresponding vertex counterterm.

Figure 7.8: Self-energy diagrams of the non-standard Goldstone boson φ_h in the EHSG model, with scalar bosons $S = H_1, H_2, \varphi_\mathrm{s}, \phi^\pm, \varphi_\mathrm{h}$.

we obtain from the diagrams in Fig. 7.8b

$$\hat{\Sigma}^{\varphi_\mathrm{h}\varphi_\mathrm{h}\prime}(0) = \Sigma^{\varphi_\mathrm{h}\varphi_\mathrm{h}\prime}(0) = \frac{1}{16\pi^2 v_\mathrm{h}^2}\left(s_\alpha^2 M_{H_1}^4 B_0'[0,0,M_{H_1}^2] + c_\alpha^2 M_{H_2}^4 B_0'[0,0,M_{H_2}^2]\right)$$
$$= \frac{s_\alpha^2 M_{H_1}^2 + c_\alpha^2 M_{H_2}^2}{32\pi^2 v_\mathrm{h}^2} + \mathcal{O}(\epsilon), \tag{7.2.78}$$

with the notation

$$B_0'[M^2, M_1^2, M_2^2] = \left.\frac{\partial B_0[k^2, M_1^2, M_2^2]}{\partial k^2}\right|_{k^2 = M^2}. \tag{7.2.79}$$

The NLO-corrected $H_1 \to \varphi_\mathrm{h}\varphi_\mathrm{h}$ partial width is then given by

$$\Gamma\left(H_1 \to \varphi_\mathrm{h}\varphi_\mathrm{h}\right) = \Gamma\left(H_1 \to \varphi_\mathrm{h}\varphi_\mathrm{h}\right)_\mathrm{LO}$$
$$\times \left[1 - \mathrm{Re}\hat{\Sigma}^{H_1 H_1\prime}(M_{H_1}^2) - 2\mathrm{Re}\hat{\Sigma}^{\varphi_\mathrm{h}\varphi_\mathrm{h}\prime}(0) + 2\mathrm{Re}\hat{\mathrm{E}}^{\varphi_\mathrm{h}}\right]. \tag{7.2.80}$$

7.2.7 Non-standard gauge bosons in the high-energy limit

As already mentioned in Chapter 4, the Goldstone-boson equivalence theorem (GBET) provides high-energy relations between amplitudes involving external longitudinally-polarized vector bosons V_L and the corresponding amplitudes with the V_L replaced by the related would-be Goldstone bosons. The GBET arises from BRS symmetry (cf. Sects. 2.3 and 3.3) and, beyond the LO, receives loop corrections which are likewise

dictated by BRS invariance (see e.g. [83]). In the EHSL model, for $v_{\rm h} \neq 0$ the high-energy limit $M_{Z'}/k^0 \to 0$ (four-momentum k of the Z' boson) corresponds to the limit of a vanishing hidden gauge-coupling constant $g_{\rm h} \to 0$ since $M_{Z'} = g_{\rm h} v_{\rm h}$ according to (3.1.30). Hence, for $M_{Z'} \to 0$ the Z' boson decouples from the theory and the hidden Goldstone boson $\varphi_{\rm h}$ (which originally constituted the longitudinal polarization mode of the Z' boson) becomes physical. Recall that in the limit of a decoupled hidden gauge sector our one-loop renormalized quantized Lagrangian (3.2.5) of the EHSL model smoothly converges to the one of the EHSG model (cf. Chapters 3 and 5). Consequently, at the one-loop level we expect to observe

$$\lim_{M_{Z'} \to 0} \Gamma\left(H_1 \to Z'Z'\right) = \Gamma\left(H_1 \to \varphi_{\rm h}\varphi_{\rm h}\right), \qquad (7.2.81)$$

with the non-standard partial widths $\Gamma\left(H_1 \to Z'Z'\right)$ and $\Gamma\left(H_1 \to \varphi_{\rm h}\varphi_{\rm h}\right)$ specified in (7.2.69) and (7.2.80) up to one-loop order. Verification at the one-loop level yields a test of consistency, in particular of gauge invariance of our renormalization scheme. The crucial step in order to verify (7.2.81) analytically is to explicitly derive the above-mentioned one-loop GBET-correction factor for the partial width $\Gamma\left(H_1 \to Z'Z'\right)$. We follow the discussion of the GBET-correction factors for the W and Z bosons in the SM in [83].

Starting point are the Slavnov-Taylor identities

$$\left\langle T F^{Z'}(z) F^{Z'}(y) H_1^{\rm phys}(x) \right\rangle_{\rm c} = 0 \qquad (7.2.82)$$

and

$$\left\langle T F^{Z'}(z) Z'^{,\rm phys}(y) H_1^{\rm phys}(x) \right\rangle_{\rm c} = 0, \qquad (7.2.83)$$

obtained analogously to [83] from the BRS invariance of the bare EHSL Lagrangian (3.2.5). The lower index c denotes that the Green functions are connected and the physical fields $H_1^{\rm phys}$ and $Z'^{,\rm phys}$ have vanishing BRS variations according to (3.3.7). The identities (7.2.82) and (7.2.83) can be derived from (3.3.6) with the generic-field products $\prod_l \Psi_{I_l}$ replaced by $\bar{u}^{Z'} F^{Z'} H_1^{\rm phys}$ and $\bar{u}^{Z'} Z'^{,\rm phys} H_1^{\rm phys}$, respectively.[6] In that regard, we have to take into account the BRS transformation of $\bar{u}^{Z'}$ (3.3.3), the vanishing BRS variation of the physical fields (3.3.7), and the equation of motion

$$i \left\langle T \frac{\delta}{\delta \bar{u}^{Z'}(x)} \prod_l \Psi_{I_l} \right\rangle = - \left\langle T \left(\boldsymbol{s} F^{Z'}(x) \right) \prod_l \Psi_{I_l} \right\rangle \qquad (7.2.84)$$

of the non-standard anti-ghost. By definition, the physical fields already include the corresponding (properly normalized) wave functions.

The renormalization of the gauge-fixing operators in (7.2.82) and (7.2.83) is irrelevant according to (5.3.51). Therefore, it is convenient to directly write $F^{Z'}$ in terms of

---

[6]We refer to [175] for an inductive proof relating to BRS invariance of Green functions involving arbitrarily many gauge-fixing terms and physical fields.

Figure 7.9: One-loop diagrams contributing to the self-energy $\Sigma^{Z'\varphi_{\mathrm{h}}}$.

renormalized fields and parameters. Hence, in momentum space (7.2.82) and (7.2.83) can be written as (the index c is omitted in the following)

$$\left\langle T[k_3^\mu Z'_\mu(k_3) + iM_{Z'}\varphi_{\mathrm{h}}(k_3)][k_2^\nu Z'_\nu(k_2) + iM_{Z'}\varphi_{\mathrm{h}}(k_2)]H_1^{\mathrm{phys}}(k_1)\right\rangle = 0 \qquad (7.2.85)$$

and

$$\left\langle T[k_3^\mu Z'_\mu(k_3) + iM_{Z'}\varphi_{\mathrm{h}}(k_3)]Z'^{,\mathrm{phys}}(k_2)H_1^{\mathrm{phys}}(k_1)\right\rangle = 0, \qquad (7.2.86)$$

with the renormalized gauge-fixing parameters set to unity ('t Hooft-Feynman gauge) and the incoming momenta k_j, $j = 1, 2, 3$.

Next, the fields in the gauge fixing will be truncated. For this, we need the propagator matrix

$$G_{\mu\nu}^{Z'\varphi_{\mathrm{h}}}(k) = \begin{pmatrix} g_{\mu\nu}^{\mathrm{T}}G_{\mathrm{T}}^{Z'Z'}(k^2) + g_{\mu\nu}^{\mathrm{L}}G_{\mathrm{L}}^{Z'Z'}(k^2) & k_\mu G^{Z'\varphi_{\mathrm{h}}}(k^2) \\ -k_\nu G^{Z'\varphi_{\mathrm{h}}}(k^2) & G^{\varphi_{\mathrm{h}}\varphi_{\mathrm{h}}}(k^2) \end{pmatrix}, \qquad (7.2.87)$$

which includes mixing between Z' and φ_{h} (cf. Fig. 7.9). The tensors $g_{\mu\nu}^{\mathrm{T}}$ (2.2.4) and $g_{\mu\nu}^{\mathrm{L}}$ (2.2.5) denote the transverse and longitudinal part of the diagonal Z' propagator. In the entries of (7.2.87) the incoming momentum k belongs to the boson associated with the first field index of the corresponding propagator. These propagators are introduced by explicitly writing out the ones of the fields in the gauge fixing, and after some calculation, the identities (7.2.85) and (7.2.86) lead to (underlined fields are truncated)

$$\begin{aligned} \Big\langle T[k_3^\sigma \underline{Z}'_\sigma(k_3) - iM_{Z'}A^{Z'}(k_3^2)\,\underline{\varphi}_{\mathrm{h}}(k_3)] \\ \times [k_2^\rho \underline{Z}'_\rho(k_2) - iM_{Z'}A^{Z'}(k_2^2)\,\underline{\varphi}_{\mathrm{h}}(k_2)]H_1^{\mathrm{phys}}(k_1)\Big\rangle = 0 \end{aligned} \qquad (7.2.88)$$

and

$$\begin{aligned} k_3^\sigma \left\langle T\underline{Z}'_\sigma(k_3)Z'^{,\mathrm{phys}}(k_2)H_1^{\mathrm{phys}}(k_1)\right\rangle \\ - iM_{Z'}A^{Z'}(k_3^2)\left\langle T\underline{\varphi}_{\mathrm{h}}(k_3)Z'^{,\mathrm{phys}}(k_2)H_1^{\mathrm{phys}}(k_1)\right\rangle = 0, \end{aligned} \qquad (7.2.89)$$

where

$$A^{Z'}(k^2) = \frac{ik^2 G^{Z'\varphi_{\mathrm{h}}}(k^2) - M_{Z'}G^{\varphi_{\mathrm{h}}\varphi_{\mathrm{h}}}(k^2)}{M_{Z'}[G_{\mathrm{L}}^{Z'Z'}(k^2) - iM_{Z'}G^{Z'\varphi_{\mathrm{h}}}(k^2)]}. \qquad (7.2.90)$$

The correction factor $A^{Z'}$ can be rewritten in terms of two-point vertex functions. In order to do so, one more Slavnov-Taylor identity is required, namely

$$\left\langle TF^{Z'}(x)F^{Z'}(y)\right\rangle = -i\delta^{(4)}(x - y), \qquad (7.2.91)$$

which follows from the original Slavnov-Taylor identities (3.3.6) with the generic-field products $\prod_l \Psi_{I_l}$ replaced by $\bar{u}^{Z'} F^{Z'}$. In momentum space, (7.2.91) reads

$$k^2 G_{\mathrm{L}}^{Z'Z'}(k^2) - 2iM_{Z'}k^2 G^{Z'\varphi_{\mathrm{h}}}(k^2) + M_{Z'}^2 G^{\varphi_{\mathrm{h}}\varphi_{\mathrm{h}}}(k^2) = -i. \tag{7.2.92}$$

The adequate matrix of two-point vertex functions

$$\Gamma_{\mu\nu}^{Z'\varphi_{\mathrm{h}}}(k) = \begin{pmatrix} g_{\mu\nu}^{\mathrm{T}}\Gamma_{\mathrm{T}}^{Z'Z'}(k^2) + g_{\mu\nu}^{\mathrm{L}}\Gamma_{\mathrm{L}}^{Z'Z'}(k^2) & k_\mu\Gamma^{Z'\varphi_{\mathrm{h}}}(k^2) \\ -k_\nu\Gamma^{Z'\varphi_{\mathrm{h}}}(k^2) & \Gamma^{\varphi_{\mathrm{h}}\varphi_{\mathrm{h}}}(k^2) \end{pmatrix} \tag{7.2.93}$$

is related to (7.2.87) via

$$G_{\mu\lambda}^{Z'\varphi_{\mathrm{h}}}(k)\,\Gamma^{Z'\varphi_{\mathrm{h}},\lambda\nu}(k) = i\begin{pmatrix} \delta_\mu^\nu & 0 \\ 0 & 1 \end{pmatrix}. \tag{7.2.94}$$

The identities (7.2.92) and (7.2.94) together form a system of equations which allows to express the correction factor $A^{Z'}$ as

$$A^{Z'}(k^2) = \frac{k^2 + \Gamma_{\mathrm{L}}^{Z'Z'}(k^2)}{M_{Z'}[M_{Z'} - i\Gamma^{Z'\varphi_{\mathrm{h}}}(k^2)]}. \tag{7.2.95}$$

With $\Gamma_{\mathrm{L}}^{Z'Z'}(k^2) = -(k^2 - M_{Z'}^2) - \Sigma_{\mathrm{L}}^{Z'Z'}(k^2)$ and $\Gamma^{Z'\varphi_{\mathrm{h}}}(k^2) = \Sigma^{Z'\varphi_{\mathrm{h}}}(k^2)$ we hence obtain

$$A^{Z'}(k^2) = 1 + \delta A^{Z'}(k^2), \qquad \delta A^{Z'}(k^2) = -\frac{\Sigma_{\mathrm{L}}^{Z'Z'}(k^2)}{M_{Z'}^2} + i\frac{\Sigma^{Z'\varphi_{\mathrm{h}}}(k^2)}{M_{Z'}}, \tag{7.2.96}$$

in one-loop approximation. The self-energy diagrams contributing to $\Sigma_{\mathrm{L}}^{Z'Z'}$ and $\Sigma^{Z'\varphi_{\mathrm{h}}}$ are illustrated in Figs. 5.2 and 7.9.

Next, we restrict ourselves to the above-mentioned high-energy limit in which the longitudinal polarization vectors of the Z' bosons can be written as

$$\epsilon_{\mathrm{L}}^\mu(k) = \frac{k^\mu}{M_{Z'}} + \mathcal{O}\left(\frac{M_{Z'}}{k^0}\right) \tag{7.2.97}$$

and thus become proportional to the associated four momentum. Consequently, in (7.2.88) and (7.2.89) we are allowed to replace the momenta k_2^ρ and k_3^σ (which are related to the unphysical vector bosons in the gauge fixing) by $\epsilon_{\mathrm{L}}^\rho(k_2)\,M_{Z'}$ and $\epsilon_{\mathrm{L}}^\sigma(k_3)\,M_{Z'}$. Additionally performing the truncation of the physical fields and putting the external legs on mass shell yields (with $\hat{R}_{Z'} = 1$)

$$\hat{R}_{H_1}^{1/2}\Big\langle T[\epsilon_{\mathrm{L}}^\sigma(k_3)\underline{Z}'_\sigma(k_3) - iA^{Z'}(M_{Z'}^2)\,\underline{\varphi}_{\mathrm{h}}(k_3)] \\ \times[\epsilon_{\mathrm{L}}^\rho(k_2)\underline{Z}'_\rho(k_2) - iA^{Z'}(M_{Z'}^2)\,\underline{\varphi}_{\mathrm{h}}(k_2)]\underline{H_1}(k_1)\Big\rangle = 0 \tag{7.2.98}$$

and

$$\epsilon_{\mathrm{L}}^\sigma(k_3)\epsilon_{\mathrm{L}}^\rho(k_2)\left\langle T\underline{Z}'_\sigma(k_3)\underline{Z}'_\rho(k_2)\underline{H_1}(k_1)\right\rangle = \\ = iA^{Z'}(M_{Z'}^2)\epsilon_{\mathrm{L}}^\rho(k_2)\left\langle T\underline{\varphi}_{\mathrm{h}}(k_3)\underline{Z}'_\rho(k_2)\underline{H_1}(k_1)\right\rangle, \tag{7.2.99}$$

up to terms of order $\mathcal{O}\left(M_{Z'}/k_l^0\right)$, $l = 2, 3$. Combined, this leads to the important relation

$$-\epsilon_{\mathrm{L}}^{\sigma}(k_3)\epsilon_{\mathrm{L}}^{\rho}(k_2)\left\langle T\underline{Z}'_{\sigma}(k_3)\underline{Z}'_{\rho}(k_2)\underline{H_1}(k_1)\right\rangle = \\ = \left[A^{Z'}(M_{Z'}^2)\right]^2\left\langle T\underline{\varphi_{\mathrm{h}}}(k_3)\underline{\varphi_{\mathrm{h}}}(k_2)\underline{H_1}(k_1)\right\rangle,$$
(7.2.100)

which is exact in the limit $M_{Z'} \to 0$ where φ_{h} becomes physical. Here, the physical fields have already been rewritten in terms of corresponding renormalized mass eigenstates. Since $\hat{\Sigma}^{H_1 H_2}(M_{H_1}^2) = 0$ (cf. Sect. 5.3) Green functions involving external H_2 are not involved in this context.

At the one-loop level we have

$$\lim_{M_{Z'}\to 0}\left[\frac{\Sigma_{\mathrm{L}}^{Z'Z'}(M_{Z'}^2)}{M_{Z'}^2}\right] = \lim_{M_{Z'}\to 0}\left[i\frac{\Sigma^{Z'\varphi_{\mathrm{h}}}(M_{Z'}^2)}{M_{Z'}}\right] = -\frac{s_\alpha^2 M_{H_1}^2 + c_\alpha^2 M_{H_2}^2}{32\pi^2 v_{\mathrm{h}}^2}.$$
(7.2.101)

Together with (7.2.96) we hence obtain

$$\lim_{M_{Z'}\to 0}\left[A^{Z'}(M_{Z'}^2)\right] = 1,$$
(7.2.102)

and therefore

$$\lim_{M_{Z'}\to 0}\left[\epsilon_{\mathrm{L}}^{\sigma}(k_3)\epsilon_{\mathrm{L}}^{\rho}(k_2)\left\langle T\underline{Z}'_{\sigma}(k_3)\underline{Z}'_{\rho}(k_2)\underline{H_1}(k_1)\right\rangle^{\mathrm{EHSL}}\right] = \\ = -\left\langle T\underline{\varphi_{\mathrm{h}}^{\mathrm{phys}}}(k_3)\underline{\varphi_{\mathrm{h}}^{\mathrm{phys}}}(k_2)\underline{H_1}(k_1)\right\rangle^{\mathrm{EHSG}} = \\ = -\hat{R}_{\varphi_{\mathrm{h}}}\left\langle T\underline{\varphi_{\mathrm{h}}}(k_3)\underline{\varphi_{\mathrm{h}}}(k_2)\underline{H_1}(k_1)\right\rangle^{\mathrm{EHSG}}.$$
(7.2.103)

In the last line we made the wave-function renormalization $\hat{R}_{\varphi_{\mathrm{h}}} = 1 - \mathrm{Re}\hat{\Sigma}^{\varphi_{\mathrm{h}}\varphi_{\mathrm{h}}\prime}(0)$ for the physical hidden Goldstone bosons explicit according to the conventions above. For the related LO and NLO matrix elements (7.2.103) yields

$$\lim_{M_{Z'}\to 0}\mathcal{M}(H_1 \to Z'Z')^{\mathrm{EHSL}} = \mathcal{M}(H_1 \to \varphi_{\mathrm{h}}\varphi_{\mathrm{h}})^{\mathrm{EHSG}},$$
(7.2.104)

and together with (7.2.59) and (7.2.70) we finally obtain the limit (7.2.81) for the corresponding partial widths. The validity of (7.2.81) at NLO is confirmed by our numerical results (cf. Fig. 7.14) provided in the following section.

7.2.8 Total width and branching ratios

According to (6.1.4) the model-dependent total width $\Gamma_{\mathrm{tot}}^{H_1}$ of the H_1 boson is defined by the sum over the various partial widths. Thereby, the two-body decays of H_1 into very light fermions $f = u, d, e$ can be neglected.[7] We include small contributions from $\Gamma(H_1 \to \mu\bar{\mu})$ and $\Gamma(H_1 \to s\bar{s})$ (corresponding QCD corrections included by means of HDECAY) without the associated minuscule NLO corrections from the electroweak sector.

---

[7]Corresponding branching ratios are generally smaller than 10^{-4}.

For $f = b, c, \tau$, however, the partial widths $\Gamma(H_1 \to f\bar{f})$ are incorporated as specified in (7.2.14) and thus take into account the electroweak standard and non-standard NLO effects.

For a one-loop discussion each partial width is decomposed as follows,

$$\Gamma(H_1 \to X_j) = \Gamma(H_1 \to X_j)_{\text{LO}} + \Delta\Gamma(H_1 \to X_j). \tag{7.2.105}$$

$\Gamma(H_1 \to X_j)_{\text{LO}}$ takes into account the corresponding LO contributions together with the established QED and QCD corrections (if required); $\Delta\Gamma(H_1 \to X_j)$ summarizes the related weak standard and non-standard one-loop corrections in case. Accordingly, the total width is written as

$$\Gamma_{\text{tot}}^{H_1} = \sum_j \Gamma(H_1 \to X_j) = \Gamma_{\text{tot,LO}}^{H_1} + \Delta\Gamma_{\text{tot}}^{H_1}, \tag{7.2.106}$$

with

$$\Delta\Gamma_{\text{tot}}^{H_1} = \sum_j \Delta\Gamma(H_1 \to X_j). \tag{7.2.107}$$

For the H_1 branching ratios ($X_i = AA, ZZ, WW, \tau\bar{\tau}, AZ, gg, b\bar{b}, c\bar{c}$)

$$\text{BR}(H_1 \to X_i) = \frac{\Gamma(H_1 \to X_i)}{\Gamma_{\text{tot}}^{H_1}}, \tag{7.2.108}$$

the appropriate one-loop expansion is given by

$$\text{BR}(H_1 \to X_i) = \frac{\Gamma(H_1 \to X_i)_{\text{LO}}}{\Gamma_{\text{tot,LO}}^{H_1}} \left(1 - \frac{\Delta\Gamma_{\text{tot}}^{H_1}}{\Gamma_{\text{tot,LO}}^{H_1}}\right) + \frac{\Delta\Gamma(H_1 \to X_i)}{\Gamma_{\text{tot,LO}}^{H_1}}. \tag{7.2.109}$$

7.3   Numerical results

The following predictions result from the calculations in Sect. 7.2 and take into account the input parameters specified in Sect. 6.1. The $\overline{\text{MS}}$ quark masses at the scale $\mu = M_{H_1}$ (for the two-body decays into quarks) are taken from the `Mathematica` package `RunDec` [176], just like the strong coupling constant at $\mu = M_{H_1}$ (for the loop-induced decays). `RunDec` incorporates the established QCD corrections [177–183] for the running and provides us with

$$\begin{aligned}
\alpha_s(M_{H_1}) &= 0.1128, \\
\overline{m}_b(M_{H_1}) &= 2.78 \text{ GeV}, \\
\overline{m}_c(M_{H_1}) &= 0.61 \text{ GeV},
\end{aligned} \tag{7.3.1}$$

for the given setting of input parameters.

In Tab. 7.1 we summarize the numerical results for the total width and branching ratios of the standard scalar H, which constitute the important Higgs observables in the SM. These are the results obtained in the limit $\alpha \to 0$. Before we show the corresponding results for $\alpha \neq 0$ in the EHSL, EHSG and EHSD models, we explore the

observable	SM prediction
$\mathrm{BR}(H \to AA)$	$23.55 \cdot 10^{-4}$
$\mathrm{BR}(H \to AZ)$	$15.92 \cdot 10^{-4}$
$\mathrm{BR}(H \to gg)$	$80.90 \cdot 10^{-3}$
$\mathrm{BR}(H \to b\bar{b})$	$59.25 \cdot 10^{-2}$
$\mathrm{BR}(H \to c\bar{c})$	$28.99 \cdot 10^{-3}$
$\mathrm{BR}(H \to \tau\bar{\tau})$	$64.33 \cdot 10^{-3}$
$\mathrm{BR}(H \to WW)$	$20.28 \cdot 10^{-2}$
$\mathrm{BR}(H \to ZZ)$	$26.15 \cdot 10^{-3}$
$\Gamma_{\mathrm{tot}}^{H}$ [MeV]	3.958

Table 7.1: Summary of the H_1 branching ratios in the SM limit $\alpha \to 0$ (where $H_1 = H$). Moreover, the corresponding total width $\Gamma_{\mathrm{tot}}^{H}$ is listed. The predictions include the weak one-loop and the established QED and QCD corrections according to Sect. 7.2. Due to off-shell effects, the branching ratios for the decays into W and Z bosons are quite sensitive to the Higgs mass $M_{H_1} = M_H$.

underlying predictions for the individual H_1 partial widths. Afterwards, non-standard effects to $\Gamma_{\mathrm{tot}}^{H_1}$ and $\mathrm{BR}(H_1 \to \mathrm{X}_i)$ will be discussed.

For the numerical analysis we select two scenarios with representative small and large v_{h}: $v_{\mathrm{h}} = 280$ GeV and $v_{\mathrm{h}} = 10$ TeV. Within the considered range $|\alpha| \leq \pi/6$ (6.1.5) in each of these two scenarios H_2 masses $M_{H_2} \lesssim 1$ TeV are compatible with (tree-level) perturbative unitarity (cf. Chapter 4).[8] For even smaller $v_{\mathrm{h}} \lesssim 280$ GeV this would not anymore be the case. Still, we are particularly interested in the potential enhancement of associated non-standard contributions for small v_{h} because the hidden vev only appears in the denominators of the corresponding non-standard couplings (cf. Sect. 4.3). For $v_{\mathrm{h}} \gtrsim 10$ TeV the partial widths into SM particles do not change anymore since then associated one-loop effects are sufficiently suppressed.

First, we examine the EHSL predictions for the widths $\Gamma(H_1 \to \mathrm{X}_j)$ corresponding to the decays into SM final states $\mathrm{X}_j = b\bar{b}, c\bar{c}, \tau\bar{\tau}, WW, ZZ$, with $M_{Z'} > M_{H_1}/2$. Hence, the following results apply to the scenario where $\Gamma(H_1 \to Z'Z') = 0$. Accordingly, the potential impact of the non-standard one-loop effects in $\Gamma(H_1 \to \mathrm{X}_j)$ on $\Gamma_{\mathrm{tot}}^{H_1}$ and $\mathrm{BR}(H_1 \to \mathrm{X}_i)$ can be evaluated in the absence of any non-standard decay modes (at least for $M_{H_2} > M_{H_1}/2$).

It turns out that the respective (same-v_{h}) one-loop EHSG and EHSD predictions for $\Gamma(H_1 \to \mathrm{X}_j)$, $\mathrm{X}_j = b\bar{b}, c\bar{c}, \tau\bar{\tau}, WW, ZZ$, do not differ in a noteworthy manner from the EHSL predictions. Maximal relative deviations from the shown EHSL predictions are smaller than 0.02% and thus hardly visible in the plots. The lowest-order predictions for these partial widths do not depend on the choice of the specific EHS model. Due to the absence of tree-level couplings between Z', φ_{h} and the SM particles X_j, the same holds for the corresponding $H_1\mathrm{X}_j$-vertex corrections (cf. Figs. 7.2 and 7.4). At the one-loop level the model dependence in these partial widths only appears in the wave-

---

[8]In the EHSL model this holds at least for sufficiently small $M_{Z'}$.

function renormalization $\hat{R}_{H_1}$, but it turns out that these model-dependent effects are negligible within the considered regions of non-standard parameters. As a consequence, our EHSL one-loop predictions presented in Subsects. 7.3.1 and 7.3.2 are very similar to the corresponding predictions of the EHSG and EHSD models.

7.3.1 Two-body decays into fermions

The $v_\mathrm{h} = 280$ GeV and $v_\mathrm{h} = 10$ TeV EHSL predictions for $\Gamma(H_1 \to b\bar{b})$, $\Gamma(H_1 \to \tau\bar{\tau})$ and $\Gamma(H_1 \to c\bar{c})$ are depicted in Fig. 7.10 and Fig. C.1 (Appendix C). The partial widths are shown for 1 GeV $\leq M_{H_2} \leq 1$ TeV and $\alpha = \pm\pi/6$ for an estimate of the potential size of the non-standard NLO contributions.

The black-dashed lines (labeled as $\alpha = \pm\frac{\pi}{6}, \mathrm{LO}$) represent the weak LO predictions involving the QCD and QED corrections specified by Δ_f^{QCD} and Δ_f^{QED} in (7.2.14). The black-solid lines (labeled as $\alpha = \pm\frac{\pi}{6}, \mathrm{NLO_{SM}}$) represent the respective predictions which additionally comprise the associated weak-standard one-loop contributions, derived from (7.2.14) for $\alpha = 0$ and incorporated by rescaling with the global factor c_α^2. These lines are included for comparison with the blue- and red-solid lines in Fig. 7.10 and Fig. C.1 (Appendix C), which represent the full predictions according to (7.2.14) for $\alpha = -\pi/6$ and $\alpha = +\pi/6$, respectively, and thus take into account the corresponding non-standard one-loop effects.

Regarding the blue- and red-solid lines, the particle thresholds in the vicinity of $M_{H_2} = M_{H_1}/2$ are clearly visible. It is shown that in contrast to the small-v_h region for large $v_\mathrm{h} = 10$ TeV the NLO predictions are symmetric under a sign flip in α. From the triple Higgs self-couplings (cf. App. A.10) involved in the corresponding NLO terms (cf. Figs. 5.1 and 7.2) it follows that the v_h-dependent parts can provide contributions which are asymmetric in the sign of α. These contributions are suppressed for large v_h. One-loop diagrams without the triple Higgs self-couplings are symmetric in α.

As an overall result, the non-standard NLO contributions only provide mild corrections of at most -1% on top of the corresponding predictions which only include the weak-standard NLO contributions (black-solid lines, $\alpha = \pm\frac{\pi}{6}, \mathrm{NLO_{SM}}$). In all cases, for $v_\mathrm{h} \geq 10$ TeV and large $M_{H_2} \approx 1$ TeV the $\alpha = \pm\frac{\pi}{6}, \mathrm{NLO_{SM}}$ results provide a good approximation of the corresponding NLO predictions.

7.3.2 Four-body decays into fermions

In the same way we present in Fig. 7.11 our numerical results for the (fermionic four-body) partial widths $\Gamma(H_1 \to WW)$ and $\Gamma(H_1 \to ZZ)$, calculated in the EHSL model according to the approach presented in Subsect. 7.2.3.

Here, the black-dashed lines indicate the LO results obtained from (7.2.42) with the input of M_W given by (6.2.10). Complementarily, we show the solid-yellow lines which indicate deviations from these LO results due to the one-loop shift in M_W with α and M_{H_2} (cf. Sect. 6.2) in the LO expressions of the partial widths. Note that the solution of (6.2.9) is used throughout as input for M_W in our one-loop calculations. The blue- and red-solid lines in Fig. 7.11 (denoted as $\mathrm{NLO_{NS}}$) represent our full predictions for
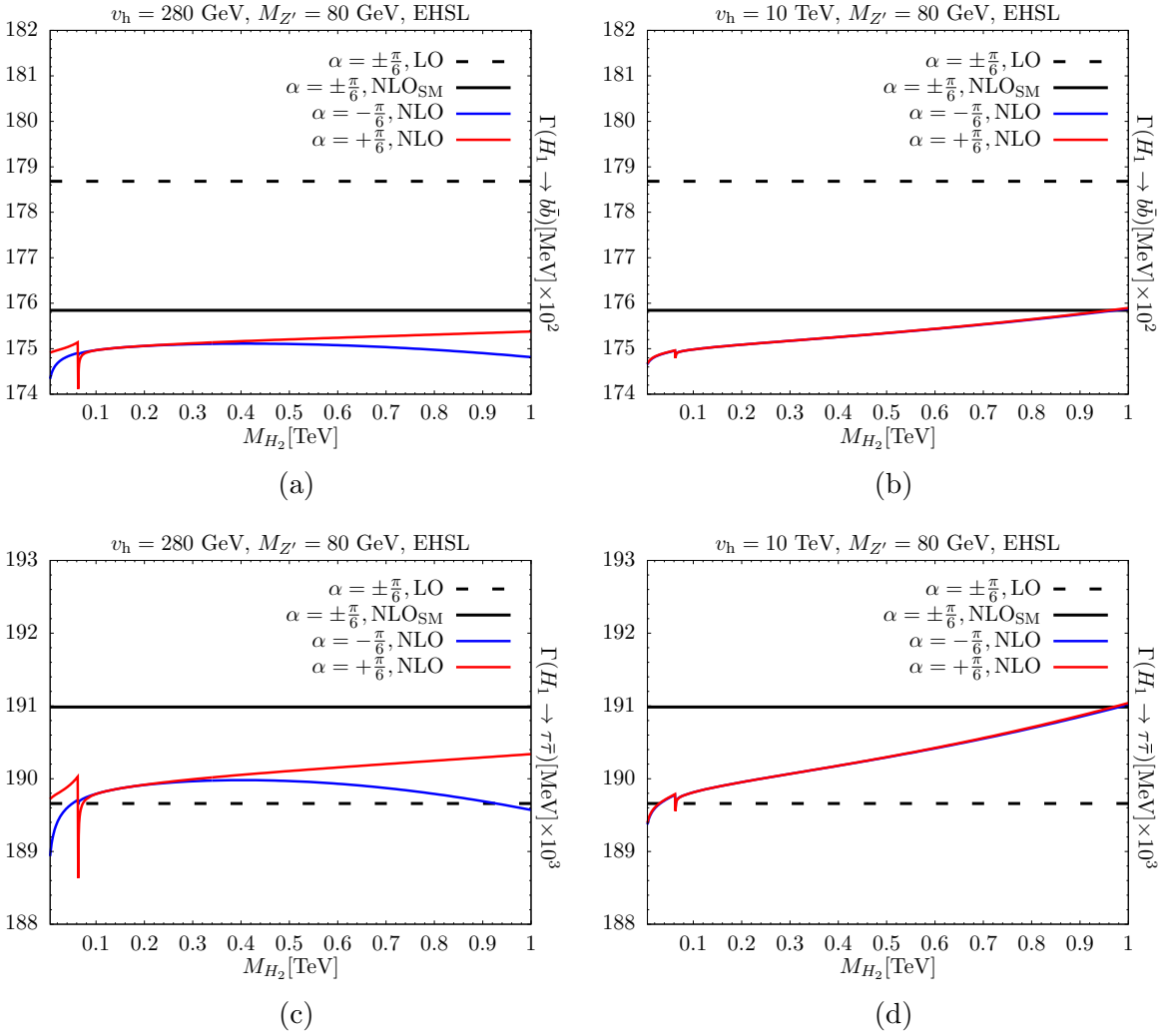
Figure 7.10: EHSL predictions for the partial widths $\Gamma(H_1 \to b\bar{b})$ (upper row) and $\Gamma(H_1 \to \tau\bar{\tau})$ (lower row) for $v_\mathrm{h} = 280$ GeV (left side) and $v_\mathrm{h} = 10$ TeV (right side), with $M_{Z'} = 80$ GeV and $\alpha = \pm\pi/6$.

$\alpha = -\pi/6$ and $\alpha = +\pi/6$ and thus take into account the non-standard one-loop effects according to (7.2.42).

In principle, these results can be explained analogously to those of $\Gamma(H_1 \to f\bar{f})$. Again, the symmetry (asymmetry) with respect to the sign of α for large v_h (small v_h) becomes apparent and the thresholds near $M_{H_2} = M_{H_1}/2$ are clearly visible. From the $\alpha = \pm\frac{\pi}{6}$, LO prediction for $\Gamma(H_1 \to VV)$ we obtain maximal relative deviations of about -0.6% ($V = W$) or -0.8% ($V = Z$) for $v_\mathrm{h} = 280$ GeV, large $M_{H_2} = 1$ TeV and $\alpha = -\pi/6$. For $v_\mathrm{h} = 10$ TeV these maximal relative deviations amount to about -0.6% for $M_{H_2} \approx 140$ GeV ($V = W$) or $M_{H_2} \approx 200$ GeV ($V = Z$). Without the Δ_D^V terms in (7.2.42) the blue- and red-solid lines in Fig. 7.11 receive a global downwards shift of approximately 0.2% (0.1%) for $V = W$ ($V = Z$).

In summary, for $X_j = b\bar{b}, c\bar{c}, \tau\bar{\tau}, WW, ZZ$ the non-standard one-loop corrections to
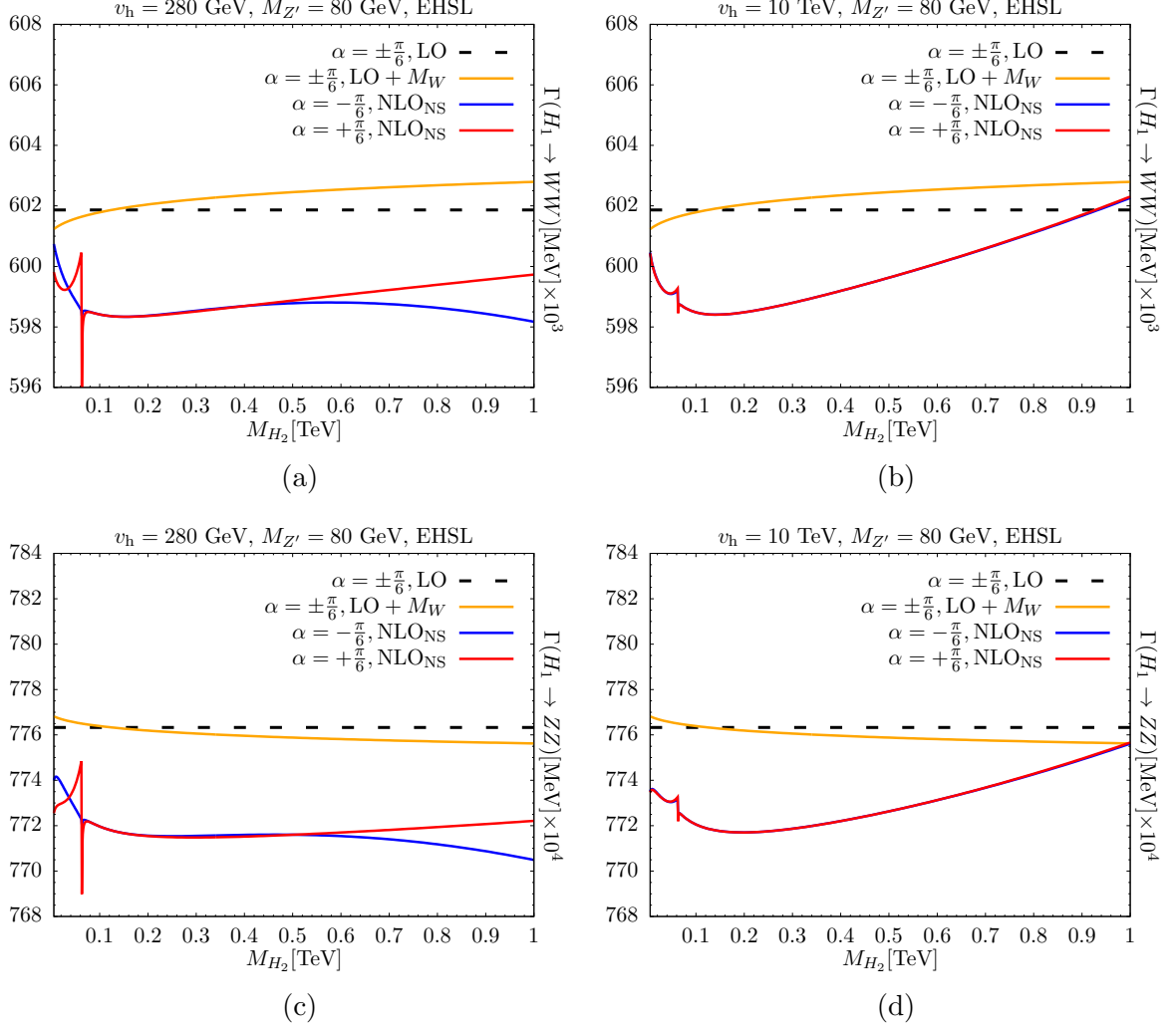
Figure 7.11: EHSL predictions for the partial widths $\Gamma(H_1 \to WW)$ (upper row) and $\Gamma(H_1 \to ZZ)$ (lower row) for $v_\mathrm{h} = 280$ GeV (left side) and $v_\mathrm{h} = 10$ TeV (right side), with $M_{Z'} = 80$ GeV and $\alpha = \pm\pi/6$.

$\Gamma(H_1 \to X_j)$ just provide small contributions at the level of at most -1% relative to the results obtained by simply rescaling the corresponding SM Higgs partial widths by the global factor c_α^2. In the following three subsections, we survey the numerical results for the remaining partial widths associated with the non-standard decay modes of H_1.

7.3.3   Two-body decays into massive non-standard scalars

In Fig. 7.12 we present our results for the partial width $\Gamma(H_1 \to H_2 H_2)$ predicted according to (7.2.58) in the EHSL, EHSG and EHSD models. The yellow- and black-solid lines in Figs. 7.12a,b illustrate the LO results for $\alpha = -\pi/6$ and $\alpha = +\pi/6$. The blue and red finely-dashed lines in Figs. 7.12a,b represent the $\alpha = -\pi/6$ and $\alpha = +\pi/6$ NLO predictions for both the EHSG and EHSD models since the maximal
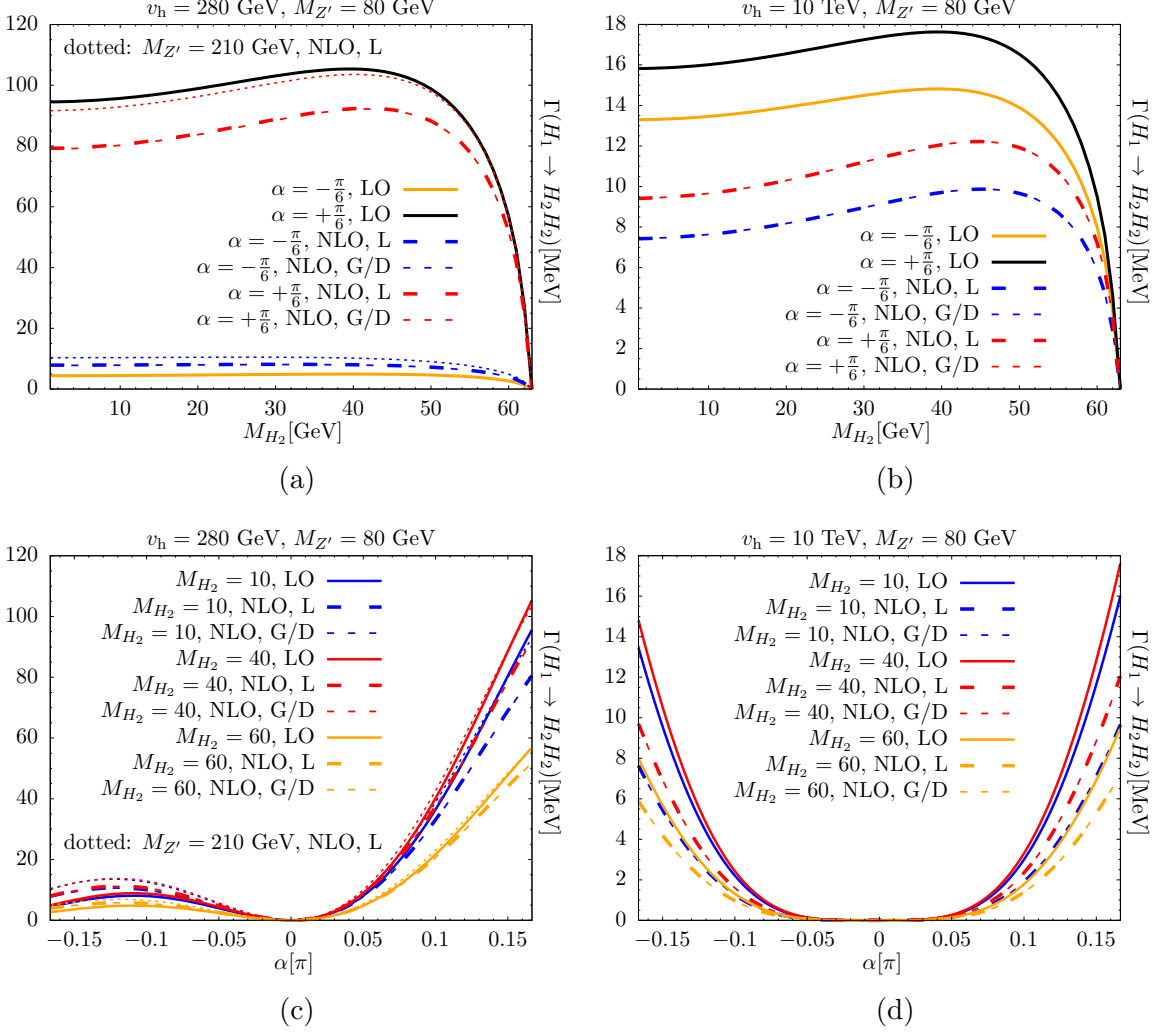
Figure 7.12: Predictions for $\Gamma\left(H_1 \to H_2 H_2\right)$ in the EHSL (L), EHSG (G) and EHSD (D) models for $v_\mathrm{h} = 280$ GeV (left side) and $v_\mathrm{h} = 10$ TeV (right side) versus M_{H_2} (upper row) and α (lower row).

relative deviations are tiny and invisible in the given plots (below the per-mille level). The corresponding one-loop EHSL predictions for $M_{Z'} = 80$ GeV are given by the blue- and red-dashed lines.

The same dash-type coding is used in Figs. 7.12c,d in which the blue, red and yellow lines represent the predictions obtained for $M_{H_2} = 10$ GeV, $M_{H_2} = 40$ GeV and $M_{H_2} = 60$ GeV. The additional solid lines (same color coding) in Figs. 7.12c,d display the associated LO predictions.

In Figs. 7.12a,c we additionally provide the dotted lines which indicate the $v_\mathrm{h} = 280$ GeV EHSL one-loop predictions for larger $M_{Z'} = 210$ GeV. These show the potential enhancement of the relative deviations from the corresponding EHSG/EHSD predictions for larger $g_\mathrm{h} = 0.75$ (up to almost 25% for $\alpha = -\pi/6$ and small M_{H_2}). We do not show such results for $v_\mathrm{h} = 10$ TeV where we would have to consider extremely

heavy $M_{Z'}$ in order reach sufficiently large g_h according to $M_{Z'} = g_h v_h$ (3.1.30). For $M_{Z'} = 80$ GeV, the maximal relative deviations from the corresponding EHSG/EHSD predictions are insignificant for $v_h = 10$ TeV but lie in the range of $+1\%$ for $v_h = 280$ GeV. Accordingly, these effects would be even smaller for $M_{Z'} < 80$ GeV in Fig. 7.12.

Basically, the specific shapes of the lines in Fig. 7.12 are a consequence of the interplay between the related phase-space factor $\text{LIPS}_2^{H_2}$ (7.2.51) and the absolute value of the significant LO coupling $C_{H_1 H_2 H_2}$ (7.2.49). While $\text{LIPS}_2^{H_2}$ increases for smaller M_{H_2} the absolute value of $C_{H_1 H_2 H_2}$ decreases. It is remarkable that the asymmetry in the prediction for $\Gamma(H_1 \to H_2 H_2)$ with respect to the sign in α is more pronounced for $v_h = 280$ GeV. For the most part this is due to the respective asymmetry in the LO coupling $C_{H_1 H_2 H_2}$ which, for sufficiently large v_h, is zero not only for $\alpha = 0$ but also for another negative α within the considered range $|\alpha| \leq \pi/6$. The latter is the case for $v_h = 10$ TeV where the related second zero in $\Gamma(H_1 \to H_2 H_2)$ lies comparatively close to $\alpha = 0$ (cf. Fig. 7.12d). For $v_h = 280$ GeV, however, this second zero is obtained for $\alpha < -\pi/6$ (cf. Fig. 7.12c) which explains the relatively large suppression of $\Gamma(H_1 \to H_2 H_2)$ in the range of negative α.

Fig. 7.12 demonstrates that the associated non-standard NLO effects in the partial width $\Gamma(H_1 \to H_2 H_2)$ play an important role. The relative differences between the LO and NLO predictions are larger for $v_h = 10$ TeV in comparison to the case of $v_h = 280$ GeV, but generally of importance.

7.3.4 Two-body decays into non-standard gauge bosons

In the EHSL model, with the local $\text{U}(1)_{Y_h}$ symmetry and the related Z' boson, the partial width $\Gamma(H_1 \to Z'Z')$ is non-zero for $M_{Z'} < M_{H_1}/2$ and $\alpha \neq 0$. In Fig. 7.13 we present the NLO predictions for $\Gamma(H_1 \to Z'Z')$ calculated according to (7.2.69). The brown-, yellow-, red- and blue-dashed lines represent the results obtained for $M_{Z'} = 0.1$ GeV, $M_{Z'} = 10$ GeV, $M_{Z'} = 40$ GeV and $M_{Z'} = 60$ GeV. Depending on whether we have $M_{H_2} = 70$ GeV or $M_{H_2} = 1$ TeV as corresponding input these lines are dashed or fine-dashed.

According to (7.2.69) the width $\Gamma(H_1 \to Z'Z')$ is directly proportional to the factor s_α^2 which stems from the $H_1 Z'Z'$ tree-level coupling and explains the strong suppression of this non-standard decay mode in the small-$|\alpha|$ range. Furthermore, the overall $1/v_h^2$ suppression in (7.2.69) explains the different orders of magnitude in the predicted $\Gamma(H_1 \to Z'Z')$ for $v_h = 280$ GeV (several 10 MeV) and $v_h = 10$ TeV (several 10 keV). Accordingly, for small v_h close to the electroweak scale the EHSL model is indeed strongly constrained by the measured Higgs signal strengths (cf. Sect. 6.1). At the given scales in the plots the M_{H_2}-dependence of the corresponding NLO results is hardly visible. Here, the parameter M_{H_2} first enters at the one-loop level.

Relative to the corresponding LO prediction, with the input $v_h = 10$ TeV our NLO predicted width $\Gamma(H_1 \to Z'Z')$ yields maximal deviations of about $+1.7\%$ ($+0.9\%$) for $\alpha = \pm\pi/6$ and $M_{H_2} = 70$ GeV ($M_{H_2} = 1$ TeV). This holds for all the considered values of $M_{Z'}$. On the contrary, for $v_h = 280$ GeV these maximal deviations more strongly depend on the parameter $M_{Z'}$ and have a size of about $+2.4\%$ ($+0.4\%$) for $\alpha = \pm\pi/6$,
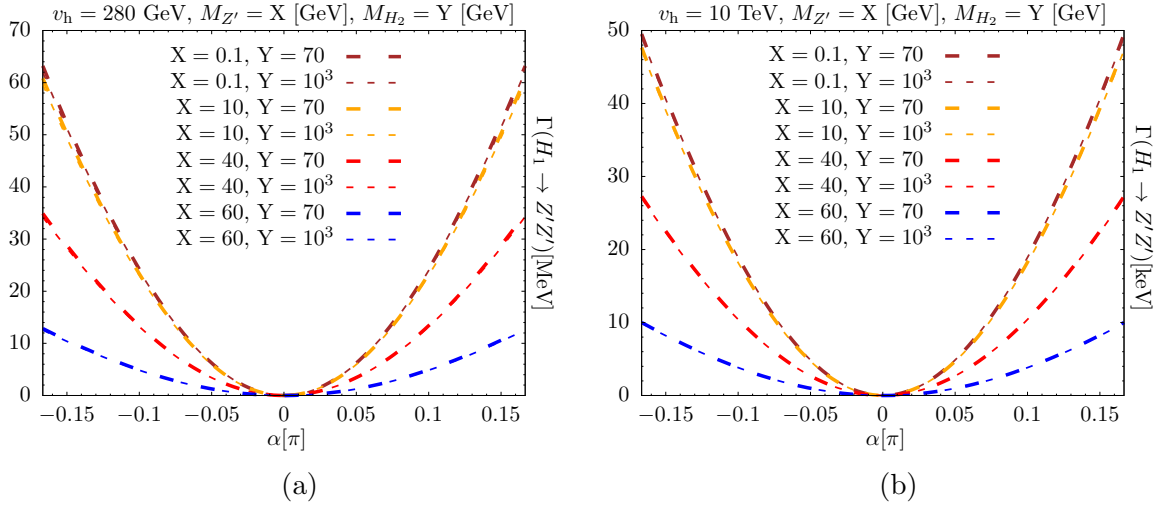
Figure 7.13: NLO predictions for $\Gamma(H_1 \to Z'Z')$ versus α for $v_\mathrm{h} = 280$ GeV (left side) and $v_\mathrm{h} = 10$ TeV (right side).

$M_{Z'} = 60$ GeV and $M_{H_2} = 70$ GeV ($M_{H_2} = 1$ TeV). Both for $v_\mathrm{h} = 280$ GeV and $v_\mathrm{h} = 10$ TeV we hence obtain the largest NLO contributions for small $M_{H_2} = 70$ GeV. For larger M_{H_2} the NLO contributions to $\Gamma(H_1 \to Z'Z')$ generally become smaller. The one-loop contributions from the $\mathrm{D}^{Z'}$ term in (7.2.69) at most yield $+0.1\%$ and are thus negligible.

7.3.5   Two-body decays into hidden Goldstone bosons

In Fig. 7.14 both the EHSL predictions for $\Gamma(H_1 \to Z'Z')$ for Z' bosons with a very small mass $M_{Z'} = 0.1$ GeV and the related EHSG predictions for $\Gamma(H_1 \to \varphi_\mathrm{h}\varphi_\mathrm{h})$ are depicted as functions of M_{H_2} for comparison. The black-dashed lines indicate the corresponding LO predictions. The blue- and red-solid lines represent the $\alpha = -\pi/6$ and $\alpha = +\pi/6$ one-loop predictions, calculated according to (7.2.69) and (7.2.80).

A comparison between the upper and lower row in Fig. 7.14 clearly demonstrates that our LO and NLO predictions obey the Goldstone-boson equivalence theorem (cf. Subsect. 7.2.7), i.e. that the limit (7.2.81) is fulfilled by our numerical results, too. Even in the $M_{H_2} = M_{H_1}/2$ threshold region deviations from (7.2.81) are not visible. Thus, for $M_{H_1} = M_H^\mathrm{exp}$ the chosen $M_{Z'} = 0.1$ GeV is small enough such that the high-energy limit as defined in Subsect. 7.2.7 is a very good approximation. We conclude that the brown-dashed lines in Figs. 7.13a,b can be also interpreted as the one-loop predictions for $\Gamma(H_1 \to \varphi_\mathrm{h}\varphi_\mathrm{h})$ versus α. Accordingly, for small v_h also the EHSG model is strongly constrained by the measured Higgs signal strengths. Analogously to $\Gamma(H_1 \to Z'Z')$ we have a strong suppression of $\Gamma(H_1 \to \varphi_\mathrm{h}\varphi_\mathrm{h})$ for small $|\alpha|$ and large v_h due to the global factor $s_\alpha^2/v_\mathrm{h}^2$ in (7.2.80). For $v_\mathrm{h} = 10$ TeV the decay mode $H_1 \to \varphi_\mathrm{h}\varphi_\mathrm{h}$ may just provide a shift of a few extra keV to the total H_1 width $\Gamma_\mathrm{tot}^{H_1}$.
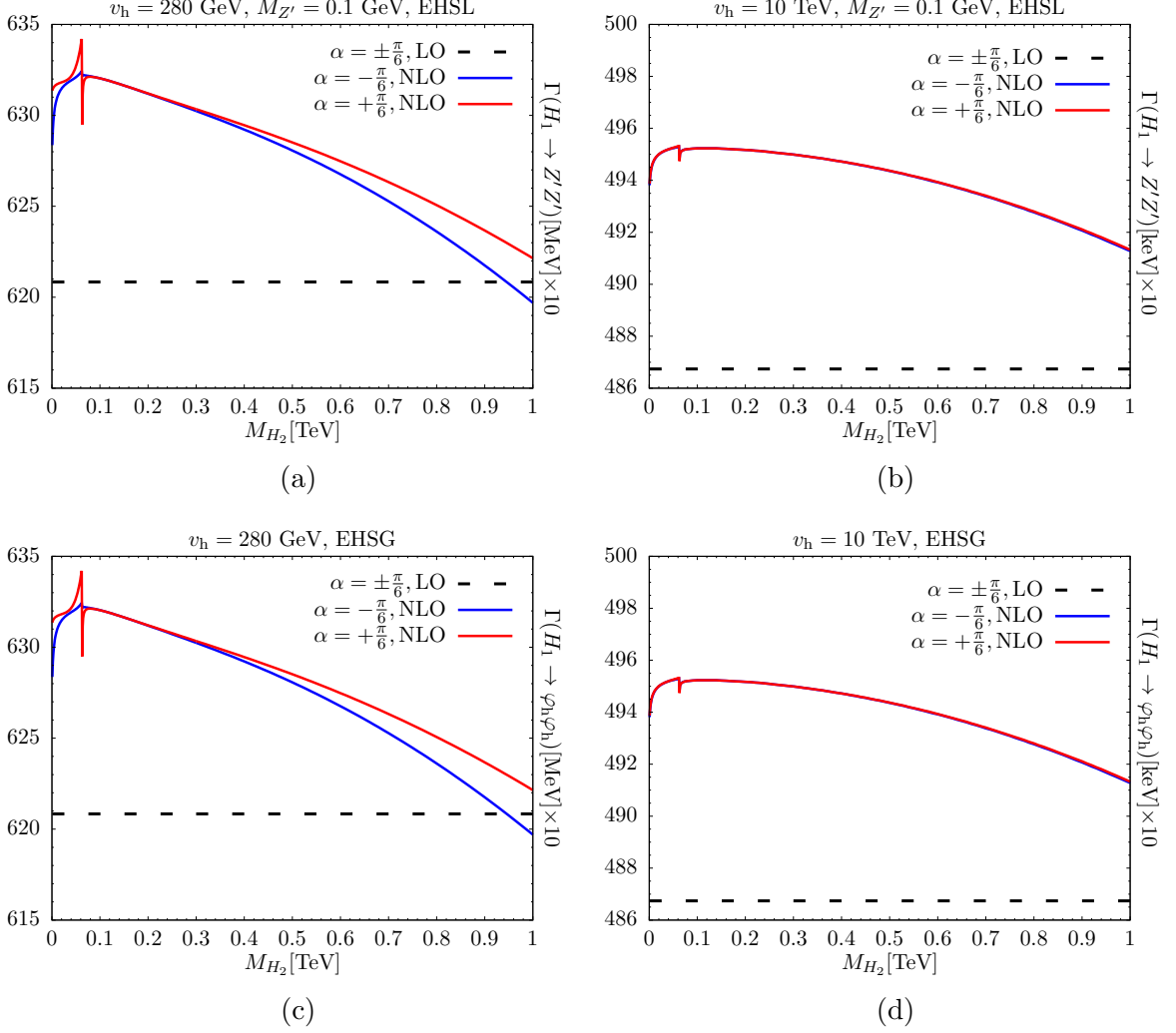
Figure 7.14: EHSL predictions ($\alpha = \pm\pi/6$ and $M_{Z'} = 0.1$ GeV) for $\Gamma(H_1 \to Z'Z')$ versus M_{H_2} (upper row) and the corresponding EHSG predictions for $\Gamma(H_1 \to \varphi_{\mathrm{h}}\varphi_{\mathrm{h}})$ (lower row) for $v_{\mathrm{h}} = 280$ GeV (left side) and $v_{\mathrm{h}} = 10$ TeV (right side).

7.3.6 Total width

Now that we have numerically explored the significant partial widths of H_1 let us examine their combined effect in the total H_1 width $\Gamma_{\mathrm{tot}}^{H_1}$. Numerical results are illustrated in Fig. 7.15. In the shapes of the depicted lines one discovers the features of the individual decay channels.

In Figs. 7.15a,b the EHSL predictions are shown for $M_{Z'} = 80$ GeV, $\alpha = \pm\pi/6$ and $M_{H_2} \geq 70$ GeV. These two plots primarily illustrate the potential impact of the non-standard one-loop corrections in the absence of any non-standard decay modes. The black-dashed lines illustrate the weak LO predictions, including the specific QCD and QED corrections in $\Gamma(H_1 \to X_i)$, $X_i = AA, AZ, gg, f_j\bar{f}_j$. The solid-yellow lines indicate deviations from the black-dashed lines due to the one-loop shift in M_W with α and M_{H_2} in the LO expressions of $\Gamma(H_1 \to X_i)$, $X_i = AA, AZ, WW, ZZ$. The black-solid lines
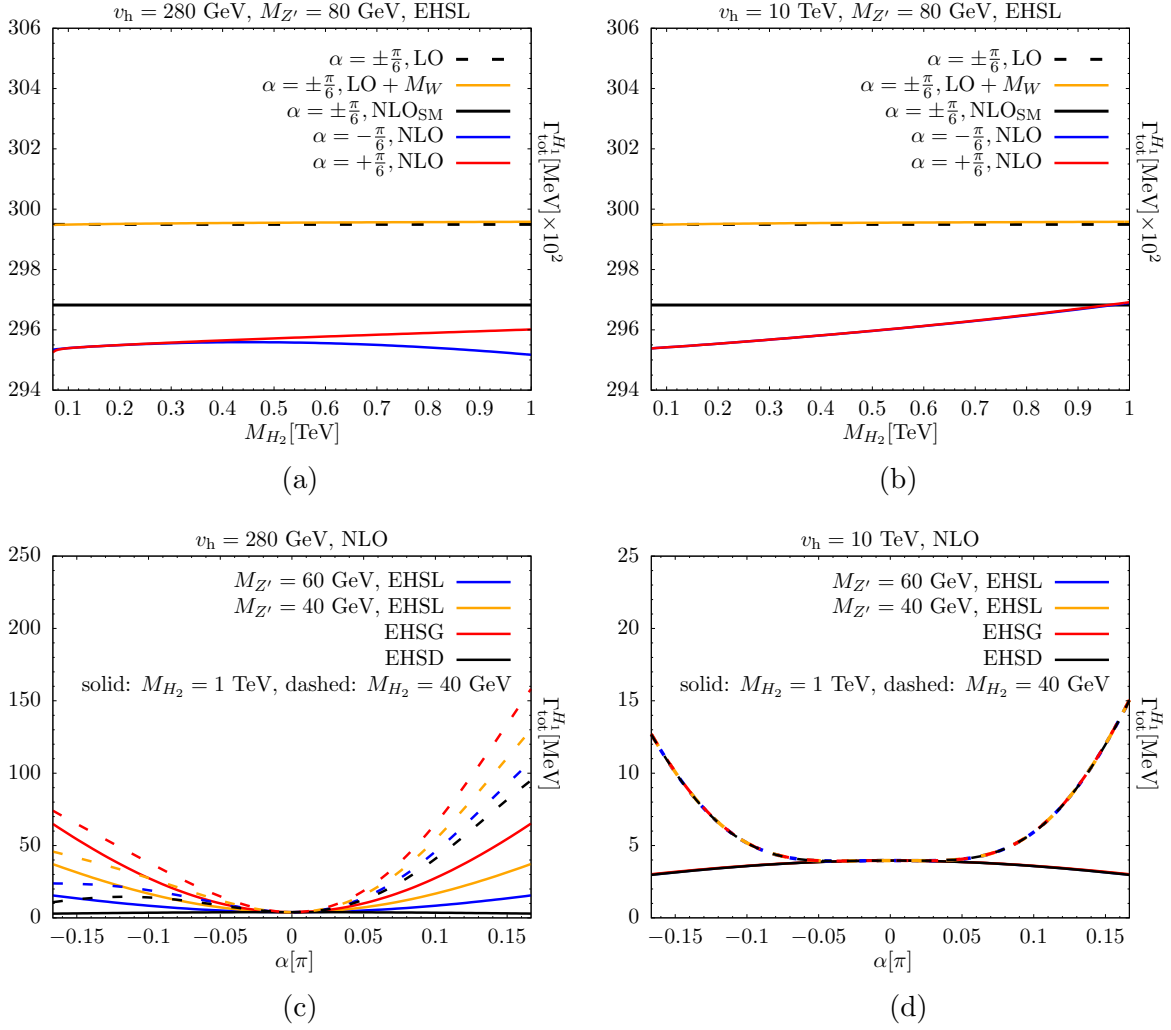
Figure 7.15: Predictions for $\Gamma_{\text{tot}}^{H_1}$ for $v_{\text{h}} = 280$ GeV (left side) and $v_{\text{h}} = 10$ TeV (right side) versus M_{H_2} (upper row) and α (lower row).

additionally include the weak-standard one-loop contributions derived for $\alpha = 0$ in $\Gamma(H_1 \to f\bar{f})$, $f = b, c, \tau$. The blue- and red-solid lines represent our full predictions for $\alpha = -\pi/6$ and $\alpha = +\pi/6$ and thus incorporate all the discussed non-standard one-loop effects.

In Figs. 7.15c,d our full one-loop predictions for $\Gamma_{\text{tot}}^{H_1}$, including the various contributions from the decays into non-standard particles of the EHS models, are shown as functions of α. The solid (dashed) lines correspond to the input $M_{H_2} = 1$ TeV ($M_{H_2} = 40$ GeV) with the dedicated colors blue, yellow, red and black indicating the EHSL ($M_{Z'} = 60$ GeV), EHSL ($M_{Z'} = 40$ GeV), EHSG and EHSD results. The solid (dashed) lines thus represent the case of zero (non-zero) $H_1 \to H_2 H_2$ contributions. The latter are maximized for $M_{H_2} \approx 40$ GeV according to Fig. 7.12. Only the black-solid lines go together with the one-loop predictions in Figs. 7.15a,b where only decay modes into SM particles provide non-vanishing contributions.

With zero contributions from decays into non-standard particles (Figs. 7.15a,b), the one-loop predictions for $\Gamma_{\text{tot}}^{H_1}$ are likewise symmetric (asymmetric) under a sign flip in α for $v_{\text{h}} = 10$ TeV ($v_{\text{h}} = 280$ GeV). Then, we overall obtain maximal relative deviations of about -1.4% (-0.5%) from the respective $\alpha = \pm\frac{\pi}{6}$, LO ($\alpha = \pm\frac{\pi}{6}$, NLO_{SM}) predictions. In good approximations, the blue- and red-solid lines in Figs. 7.15a,b furthermore represent the corresponding EHSD results, and the predictions in Fig. 7.15b also apply to the respective $v_{\text{h}} > 10$ TeV results.

The different predictions for $M_{H_2} = 1$ TeV in Fig. 7.15c are well separated due to the various large contributions from $\Gamma(H_1 \to Z'Z')$ and $\Gamma(H_1 \to \varphi_{\text{h}}\varphi_{\text{h}})$ in the small-v_{h} region. By contrast, the different predictions for $M_{H_2} = 1$ TeV in Fig. 7.15d approximately lie on top of each other. This is because for $v_{\text{h}} = 10$ TeV the related contributions from $\Gamma(H_1 \to Z'Z')$ and $\Gamma(H_1 \to \varphi_{\text{h}}\varphi_{\text{h}})$ are negligible. Moreover, according to the discussion of Fig. 7.12, the model-dependent deviations in the NLO contributions from $\Gamma(H_1 \to H_2H_2)$ are negligible. Therefore, also the different predictions for $M_{H_2} = 40$ GeV in Fig. 7.15d share the same curve, and the EHSG predictions in Figs. 7.15c,d also represent the corresponding $M_{Z'} \to 0$ EHSL predictions in good approximation.

In particular the results in Figs. 7.15c,d clarify that in the EHSL, EHSG and EHSD models quite some regions of non-standard parameters might be excluded by recent indirect ATLAS and CMS constraints for the Higgs total width, which are typically of order $(5 - 10) \times \Gamma_{\text{tot}}^{H}$ [184–186], with Γ_{tot}^{H} specified in Tab. 7.1.

7.3.7 Branching ratios

Finally, we investigate the impact of all the discussed effects on the H_1 branching ratios, providing first NLO predictions for the relevant H_1 branching ratios into SM particles $\text{BR}(H_1 \to \text{X}_i)$, $\text{X}_i = AA, ZZ, WW, \tau\bar{\tau}, AZ, gg, b\bar{b}, c\bar{c}$. The corresponding numerical results can be found as listed below:

$\text{BR}(H_1 \to AA)$:	Fig. 7.16,	$\text{BR}(H_1 \to AZ)$:	Fig. C.2 (Appendix C),
$\text{BR}(H_1 \to ZZ)$:	Fig. 7.17,	$\text{BR}(H_1 \to gg)$:	Fig. C.3 (Appendix C),
$\text{BR}(H_1 \to WW)$:	Fig. 7.18,	$\text{BR}(H_1 \to b\bar{b})$:	Fig. C.4 (Appendix C),
$\text{BR}(H_1 \to \tau\bar{\tau})$:	Fig. 7.19,	$\text{BR}(H_1 \to c\bar{c})$:	Fig. C.5 (Appendix C).

The branching ratios for decays with priority relevance for precise experimental analyses are depicted in Figs. 7.16−7.19, further branching ratios are to be found in Appendix C, Figs. C.2−C.5. These figures are arranged as explained in the following.

The left (right) columns illustrate the results for $v_{\text{h}} = 280$ GeV ($v_{\text{h}} = 10$ TeV) versus M_{H_2} and α. The plots in the upper rows show the EHSL predictions for $M_{H_2} \geq 70$ GeV and $M_{Z'} = 80$ GeV and therefore represent the scenario in which decays into

non-standard particles do not contribute via $\Gamma_{\text{tot}}^{H_1}$. The plots in the middle rows depict the results for the same scenario versus α, and in addition show the respective EHSG results with the non-vanishing contributions from the decay $H_1 \to \varphi_{\text{h}}\varphi_{\text{h}}$ for comparison. Finally, the plots in the lower rows illustrate the results (versus α) for the EHSL, EHSG and EHSD scenarios with non-vanishing contributions from the various decays into non-standard particles $H_1 \to Z'Z'$, $H_1 \to \varphi_{\text{h}}\varphi_{\text{h}}$ and $H_1 \to H_2H_2$.

Here, we go through the results for the branching ratio $\text{BR}(H_1 \to AA)$, which only obtains non-standard one-loop contributions from the total width in the denominator. The results for the other branching ratios are presented in a uniform manner and their explanation basically proceeds in the same way. However, note that in contrast to the branching ratios for the loop-induced decays into $X_i = AA, AZ, gg$, the branching ratios for the decays into $X_i = ZZ, WW, \tau\bar{\tau}, b\bar{b}, c\bar{c}$ receive further non-standard one-loop contributions from the respective partial widths in the corresponding numerators. These additional corrections are just visible on the scales of the plots in the upper and middle rows and generally compensate for the non-standard one-loop contributions from $\Gamma_{\text{tot}}^{H_1}$ in the corresponding denominators.

The black-solid (black-dashed) lines in Figs. 7.16a,b illustrate the weak NLO (LO) predictions for $\alpha = 0$ (i.e. the respective SM predictions), which incorporate the associated QCD and QED corrections. The solid-yellow lines are the related $\alpha = \pm\pi/6$ LO predictions which furthermore include the one-loop shift in M_W with α and M_{H_2}. Recall that the global factors c_α^2 in the numerators and denominators of the H_1 branching ratios drop out in the absence of any non-standard decay modes. Therefore, in Figs. 7.16a,b we could just as well designate the black-dashed and black-solid lines as $\alpha = \pm\pi/6, \text{LO}$ and $\alpha = \pm\pi/6, \text{NLO}_{\text{SM}}$ in order to indicate the correspondence with the results for $\Gamma_{\text{tot}}^{H_1}$ in Figs. 7.15a,b. The blue- and red-solid lines in Figs. 7.16a,b illustrate our full predictions for $\alpha = -\pi/6$ and $\alpha = +\pi/6$ and hence incorporate all the discussed non-standard one-loop effects. In the absence of any non-standard decay modes we obtain maximal deviations from the corresponding $\alpha = 0$ NLO predictions of about $+0.6\%$ ($+0.5\%$) for $v_{\text{h}} = 280$ GeV ($v_{\text{h}} = 10$ TeV). Analogously to the previous results for the decays of H_1 into SM particles, the blue- and red-solid lines in Figs. 7.16a,b also represent the corresponding EHSD results in good approximation.

In Figs. 7.16c,d the one-loop predictions for the same scenario are shown as functions of α for $M_{H_2} = 70$ GeV (yellow-solid lines), $M_{H_2} = 500$ GeV (blue-solid lines) and $M_{H_2} = 1$ TeV (red-solid lines). One more time these colored-solid lines point out the symmetry (asymmetry) of the one-loop contributions under a sign flip in α for $v_{\text{h}} = 10$ TeV ($v_{\text{h}} = 280$ GeV) in the absence of non-standard decay modes. The black-solid lines in Figs. 7.16c,d represent the corresponding SM ($\alpha = 0$) NLO predictions and thus correspond to the black-solid lines in Figs. 7.16a,b. Let us re-emphasize that according to the previous considerations, the so far discussed EHSL predictions for $\text{BR}(H_1 \to AA)$ also apply to the respective predictions of the EHSD model in good approximation.

Complementary to the colored-solid lines in Figs. 7.16c,d we provide the dashed lines which represent the corresponding one-loop EHSG results (same color coding with respect to the M_{H_2} input). According to Subsect. 7.2.7, these dashed lines furthermore

represent the respective EHSL one-loop predictions for very small $M_{Z'}$ (e.g. $M_{Z'} = 0.1$ GeV as in Fig. 7.14). Either way, the differences between the same-colored solid and dashed lines in Figs. 7.16c,d arise due to the extra contributions from one related non-standard decay mode ($H_1 \to \varphi_\mathrm{h}\varphi_\mathrm{h}$ or $H_1 \to Z'Z'$). For large $v_\mathrm{h} = 10$ TeV these extra contributions are comparatively small (maximal relative deviations of about -1.6% from the corresponding solid lines). This is different for $v_\mathrm{h} = 280$ GeV where $\mathrm{BR}(H_1 \to AA)$ receives a drastic suppression even for small $|\alpha|$. Note that in line with the results in Figs. 7.13a,b contributions from $\Gamma(H_1 \to Z'Z')$ are largest for vanishing $M_{Z'}$. Hence, for larger $M_{Z'} < M_{H_1}/2$ the corresponding predictions would lie somewhere in between the respective solid and dashed lines in Figs. 7.16c,d.

In Figs. 7.16e,f we present our one-loop EHSL, EHSG and EHSD predictions for $\mathrm{BR}(H_1 \to AA)$ analogously to those for $\Gamma_\mathrm{tot}^{H_1}$ in Figs. 7.15c,d. The solid (dashed) lines belong to the input $M_{H_2} = 1$ TeV ($M_{H_2} = 40$ GeV) with the blue, yellow, red and black color coding denoting the EHSL ($M_{Z'} = 60$ GeV), EHSL ($M_{Z'} = 40$ GeV), EHSG and EHSD results. Here, the differences between the same-colored solid and dashed lines are basically generated by the additional decay mode $H_1 \to H_2 H_2$ which is kinematically allowed for $M_{H_2} = 40$ GeV. Only the EHSD predictions for $M_{H_2} = 1$ TeV in Figs. 7.16e,f represent results without any contributions from decays into non-standard particles.

In contrast to the respective results in Fig. 7.16e, the different $M_{H_2} = 1$ TeV predictions in Fig. 7.16f can hardly be distinguished on the given plot scale. For $v_\mathrm{h} = 10$ TeV the extra suppression of the branching ratio due to the non-standard decay modes $H_1 \to Z'Z'$ or $H_1 \to \varphi_\mathrm{h}\varphi_\mathrm{h}$ only plays a minor role. Moreover, the deviations due to the distinct (model-dependent) one-loop contributions in $\Gamma(H_1 \to H_2 H_2)$ are negligible in that regard. Consequently, also the different predictions for $M_{H_2} = 40$ GeV in Fig. 7.16f approximately lie on top of each other.

Recent prospects for future collider experiments estimate the measurement accuracies of the branching ratios for the significant decay modes of a standard-like Higgs boson to be somewhere in the region of $5 - 10\%$ (future LHC versions) [160, 161] and $1 - 2\%$ (future e^+e^- colliders TLEP, CLIC and ILC) [162–164]. Therefore, it might very well be possible that our one-loop predictions for the H_1 branching ratios will some day lead to stringent bounds for the EHSL, EHSG and EHSD models. But also by taking into account the current signal-strength measurement accuracies (about $10-20\%$ [159]) for the individual Higgs decay channels, considerable constraints for the free parameters of the three EHS models are obtained by means of our results for the H_1 branching ratios. In particular the EHSG model is almost excluded for $v_\mathrm{h} = 280$ GeV, such that only small α are still allowed. According to (6.1.3), the measured Higgs signal strengths already put strong constraints on the non-standard parameters once the H_1 partial widths into non-standard particles provide contributions of the size of Γ_tot^H — and for small v_h the contributions from $\Gamma(H_1 \to H_2 H_2)$, $\Gamma(H_1 \to Z'Z')$ or $\Gamma(H_1 \to \varphi_\mathrm{h}\varphi_\mathrm{h})$ can be significantly larger (cf. Figs. 7.12−7.14). In the absence of any of these non-standard decay modes, however, it will be extremely difficult to constrain the three EHS models via future measurements of the branching ratios of the standard-like Higgs boson.
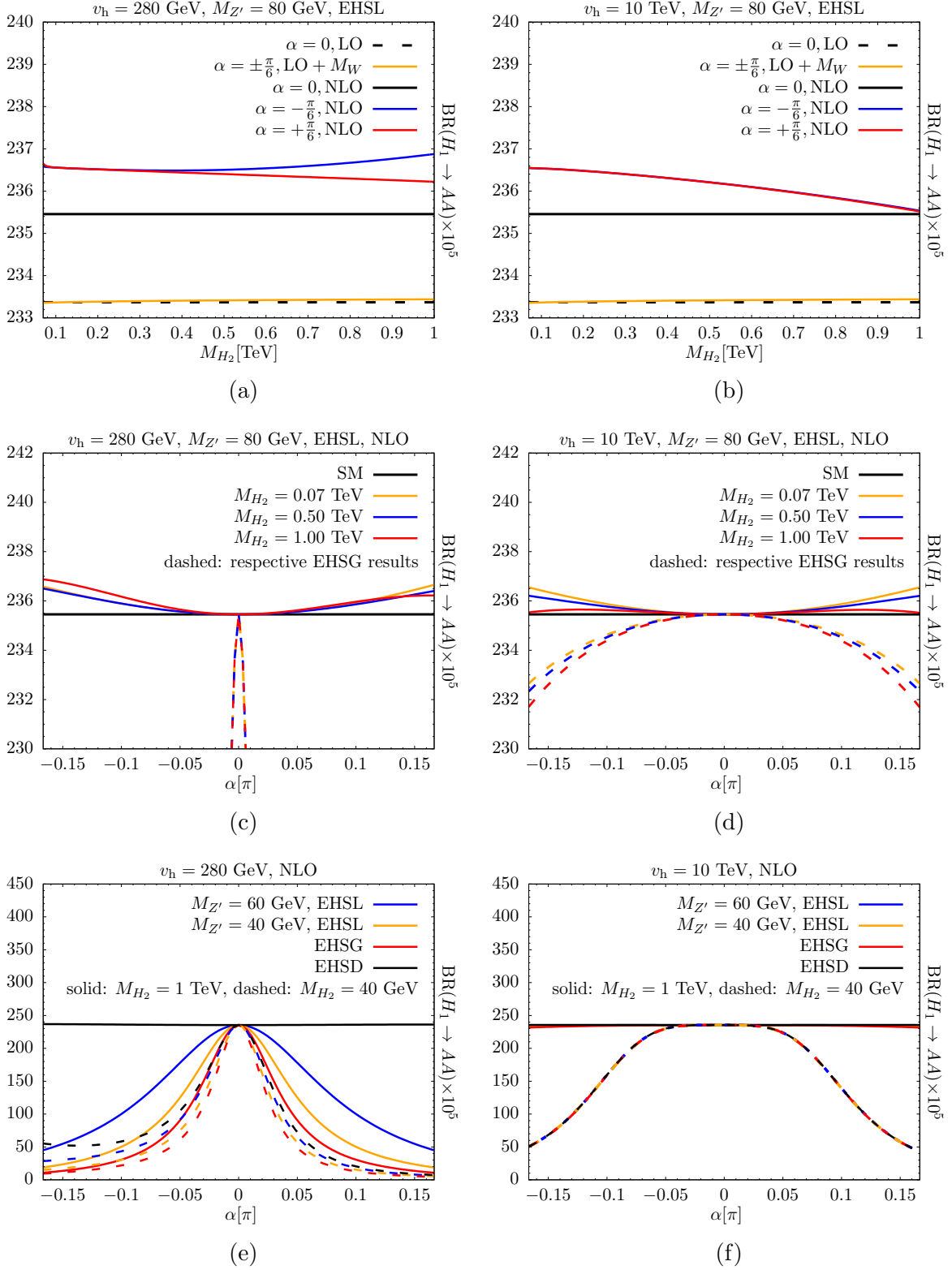
Figure 7.16: Predictions for $BR(H_1 \to AA)$ in the EHSL, EHSG and EHSD models.
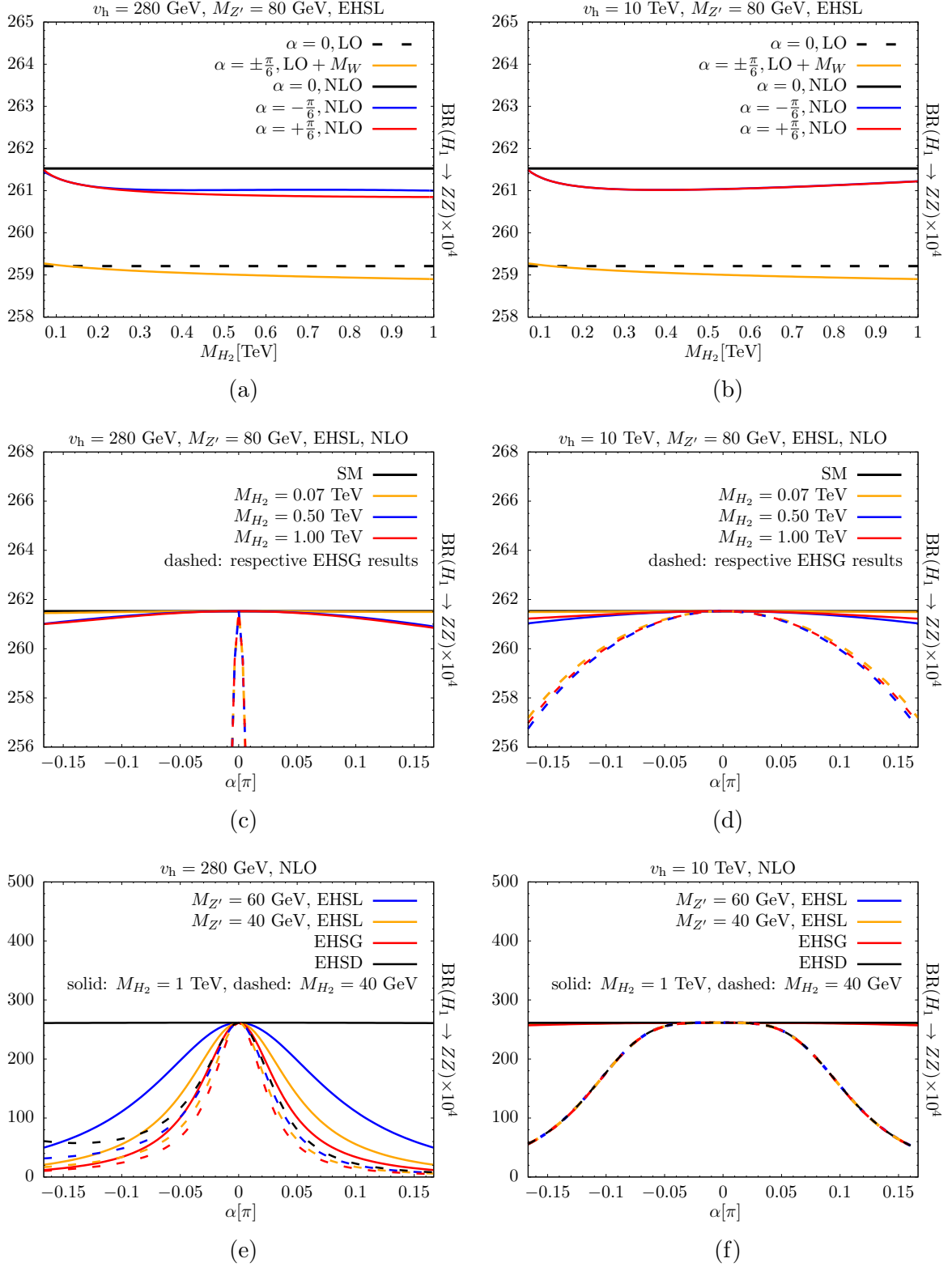
Figure 7.17: Predictions for $\mathrm{BR}(H_1 \to ZZ)$ in the EHSL, EHSG and EHSD models.
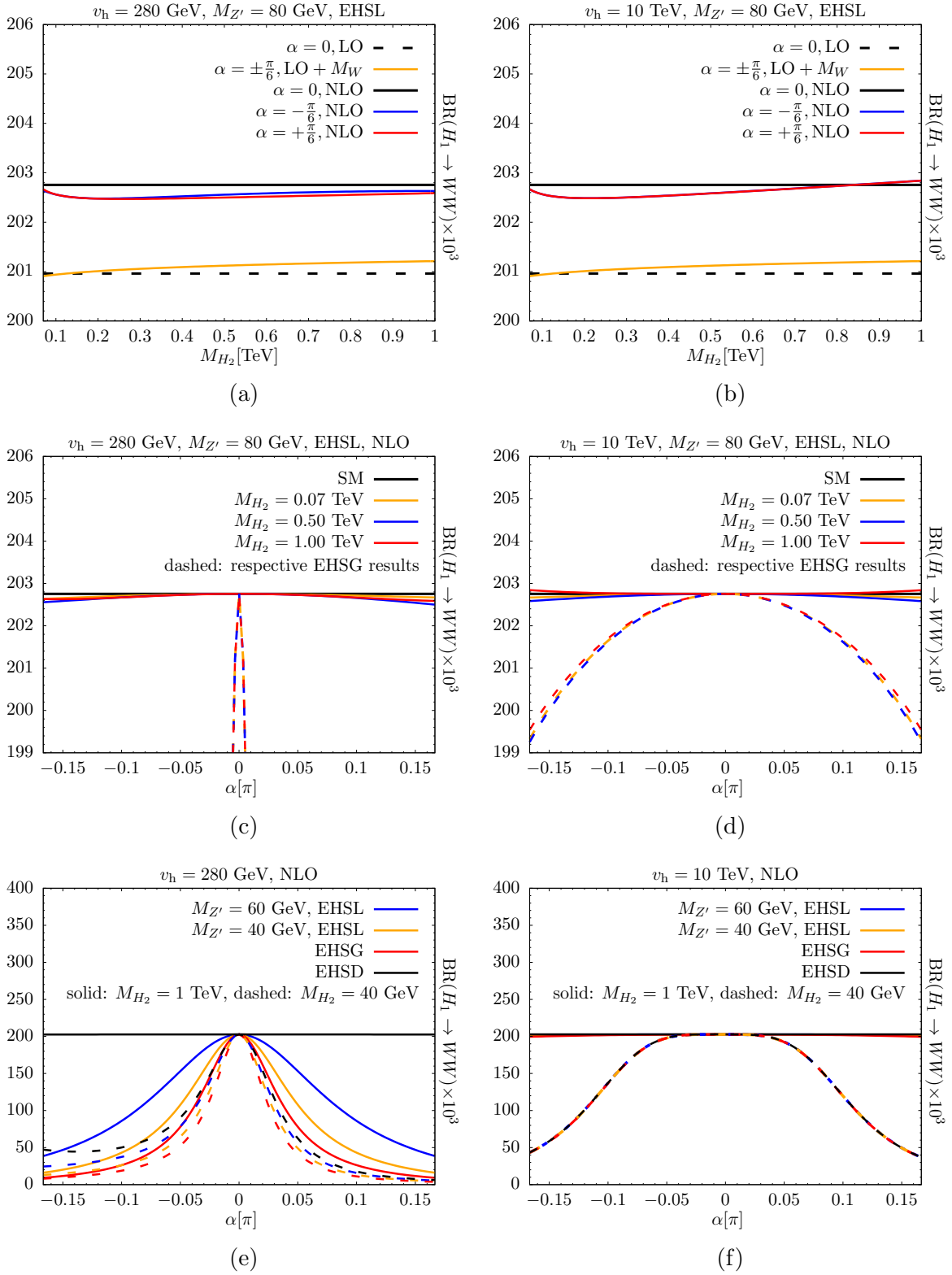
Figure 7.18: Predictions for $\mathrm{BR}(H_1 \to WW)$ in the EHSL, EHSG and EHSD models.
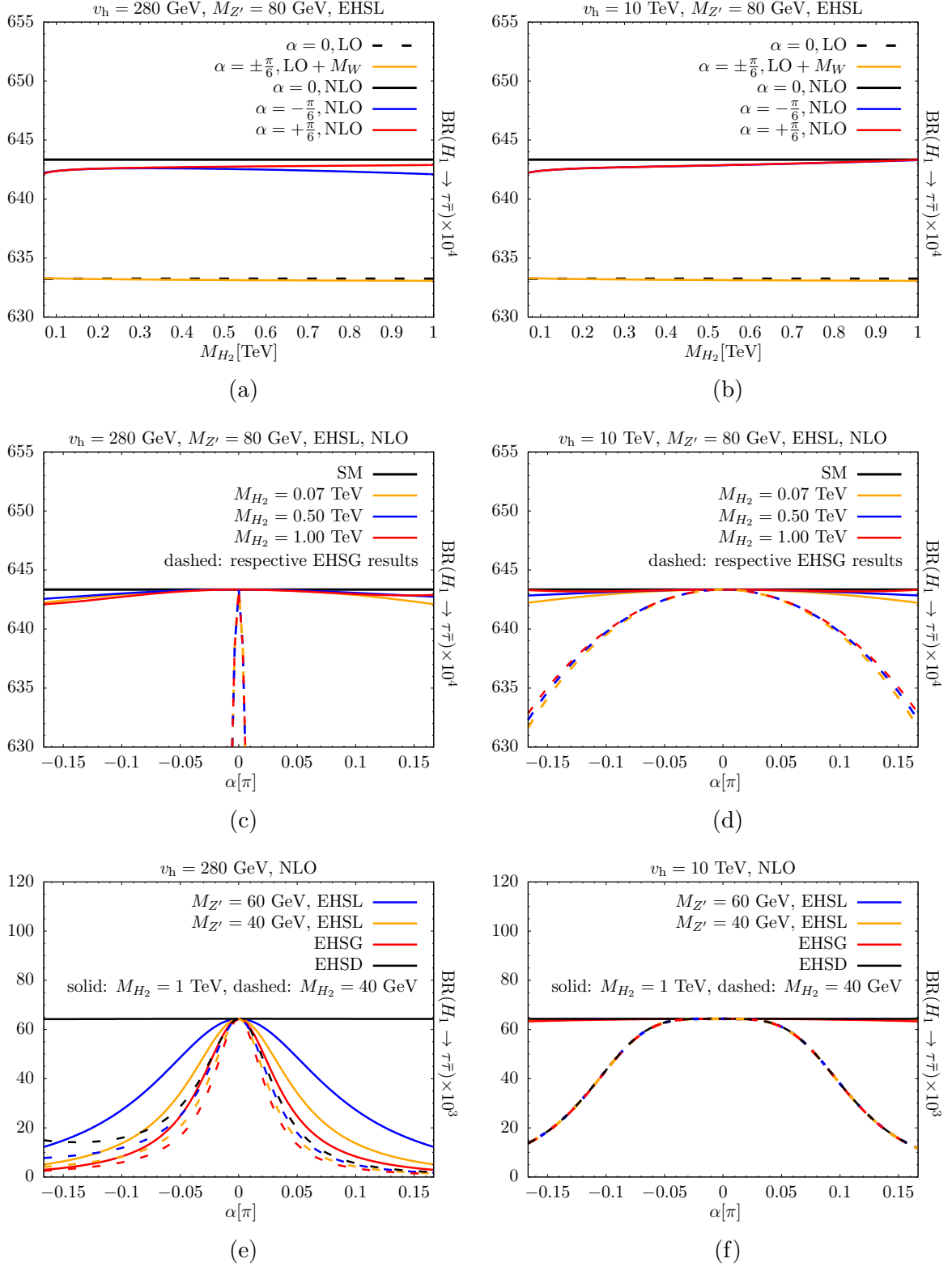
Figure 7.19: Predictions for $\text{BR}(H_1 \to \tau\bar{\tau})$ in the EHSL, EHSG and EHSD models.

Chapter 8

Conclusions

After the discovery of a Higgs-like particle by the LHC experiments it is important to work out if the observed state is exactly the particle predicted by the Standard Model (SM) Higgs mechanism or if it belongs to a more involved Higgs sector. An extended Higgs sector might very well play a key role in solving some major open issues in elementary particle physics.

In this thesis, the extension of the SM Higgs sector by an extra Higgs singlet (EHS) described by the additional scalar field Φ_h is investigated. The singlet exclusively couples to the standard sector via a renormalizable quartic interaction term of the form $(\Phi_s^\dagger \Phi_s)(\Phi_h^\dagger \Phi_h)$, the Higgs portal, with the standard Higgs doublet Φ_s in the extended Higgs potential. Three minimal scenarios are considered in terms of the hidden (non-standard) symmetry group under which Φ_h transforms − a local U(1) symmetry with a complex Φ_h (EHSL model), a global U(1) symmetry with a complex Φ_h (EHSG model), and a discrete $\mathcal{Z}_2$ symmetry with a real Φ_h (EHSD model). In each model the underlying non-standard symmetry is spontaneously broken by the non-vanishing vacuum expectation value v_h of Φ_h.

The Z' boson is the massive gauge field associated with the spontaneously broken local hidden U(1) symmetry of the EHSL Lagrangian. It does not mix with the standard sector owing to an additionally imposed $\mathcal{Z}_2$ symmetry. Its mass $M_{Z'}$ is treated as a free parameter. In the limit of a vanishing hidden U(1) gauge-coupling constant the imaginary part of the field Φ_h (here denoted as φ_h) turns into a physical Goldstone boson and the Lagrangian of the EHSG model is obtained. The Lagrangian of the EHSD model then follows just by erasing the hidden Goldstone boson φ_h.

In each of the considered models a mixing between the real part of Φ_h and the real part of the neutral component of Φ_s is generated by the Higgs-portal coupling in combination with the non-vanishing v_h. This mixing is parametrized by the angle α. Consequently, the associated scalar mass eigenstates H_1 and H_2 (corresponding masses M_{H_1} and M_{H_2}) have a standard and a non-standard field component. It is assumed that H_1 is the standard-like 125.09 GeV Higgs boson and its mass is fixed accordingly. The non-standard parameters α, M_{H_2} and v_h are treated as free parameters and the decoupling limit $\alpha \to 0$ always brings us back to the phenomenology of the SM.

The extended Lagrangians are surveyed in detail with special emphasis on gauge invariance and quantization. Bounds for the common parameters α, M_{H_2} and $v_{\rm h}$ are derived by an analysis of tree-level perturbative unitarity. A comparison of the different models shows that stronger bounds are obtained for the models with a complex $\Phi_{\rm h}$ field.

For the calculation of quantum effects in the three models suitable one-loop renormalization schemes are developed including also the unphysical sector. These are constructed such that the above-mentioned transition from the EHSL Lagrangian to the EHSD Lagrangian via the EHSG Lagrangian also holds for the corresponding renormalized Lagrangians. This feature allows a convenient comparison of associated one-loop contributions in the three models. The complete list of Feynman rules is derived as well as a corresponding `FeynArts` modelfile for automatic one-loop calculations. The Feynman rules are presented in the appendix of this work. Ward identities from the hidden U(1) are derived and also listed in the appendix for checks of consistency of the renormalization schemes.

In order to test and further constrain the three EHS models precise predictions for relevant observables accessible in collider experiments are made. One-loop contributions are combined with known higher-order SM terms where possible.

Considerable indirect constraints for the parameters α and M_{H_2} are obtained from the non-standard one-loop predictions for electroweak precision observables (EWPOs) when compared to experimental data. At the one-loop level only the fields H_1 and H_2 appear and consequently the three models make the same predictions. Explicit results are provided for the most sensitive EWPOs, the W-boson mass M_W, the effective leptonic mixing angle $\sin^2 \theta_{\rm eff}^{\rm lep}$ and the forward-backward pole asymmetry $A_{\rm FB}^{0,b}$ of the Z-boson decay into a pair of b quarks. The outcome of a $\Delta\chi^2$ analysis illustrates the corresponding exclusion bounds of 68% and 95% confidence level. In order to get additional sensitivity to $M_{Z'}$ and $v_{\rm h}$ a non-standard two-loop calculation would be required.

With the by now measured Higgs signal strengths and the indirect constraints for the Higgs total width, precise predictions for observables associated with the decays of the standard-like Higgs boson H_1 become important. At the tree-level and at the one-loop level the entire spectrum of non-standard parameters in the EHSL, EHSG and EHSD models enter the predictions for the H_1 total width $\Gamma_{\rm tot}^{H_1}$ and branching ratios $\mathrm{BR}(H_1 \to \mathrm{X}_i) = \Gamma(H_1 \to \mathrm{X}_i)/\Gamma_{\rm tot}^{H_1}$ into SM final states X_i. Two representative settings of the $v_{\rm h}$ parameter are numerically explored at the one-loop level: small $v_{\rm h} = 280$ GeV and large $v_{\rm h} = 10$ TeV.

First weak NLO predictions involving associated non-standard one-loop contributions are made for the fermionic two-body partial widths into b quarks $\Gamma(H_1 \to b\bar{b})$, c quarks $\Gamma(H_1 \to c\bar{c})$ and τ leptons $\Gamma(H_1 \to \tau\bar{\tau})$. Moreover, new predictions for the inclusive four-body partial widths $\Gamma(H_1 \to VV)$ into fermion pairs via the exchange of two standard gauge bosons $V = W, Z$ are provided. According to a new formula (which can be easily adjusted in order to apply to other SM extensions) the predictions for $\Gamma(H_1 \to VV)$ incorporate the dominant non-standard one-loop corrections which arise from the corresponding H_1VV vertices.

The non-standard one-loop contributions to $\Gamma(H_1 \to b\bar{b})$, $\Gamma(H_1 \to c\bar{c})$, $\Gamma(H_1 \to \tau\bar{\tau})$

and $\Gamma(H_1 \to VV)$ are mild, at most -1% on top of the results obtained by simply rescaling the respective SM Higgs widths by the global factor c_α^2 from the mixing. This is valid in good approximation in the three considered models and the effects can become a bit enhanced for $v_{\rm h}$ smaller than 280 GeV.

In the absence of any non-standard decay modes, the LO branching ratios of H_1 are not different from the respective SM Higgs branching ratios. Deviations can only be generated by non-standard quantum effects − but, as pointed out above, these effects are relatively small.

In addition to the decays into SM particles, non-standard decay channels can occur when kinematically allowed: $H_1 \to H_2 H_2$, $H_1 \to Z'Z'$ and $H_1 \to \varphi_{\rm h}\varphi_{\rm h}$. New one-loop results for the partial widths $\Gamma(H_1 \to H_2 H_2)$, $\Gamma(H_1 \to Z'Z')$ and $\Gamma(H_1 \to \varphi_{\rm h}\varphi_{\rm h})$ are provided.

In the considered non-standard parameter regions the one-loop effects in the partial widths $\Gamma(H_1 \to Z'Z')$ and $\Gamma(H_1 \to \varphi_{\rm h}\varphi_{\rm h})$ provide maximal contributions of about 2% relative to the corresponding LO predictions. In the limit $M_{Z'} \to 0$ the NLO-corrected $\Gamma(H_1 \to Z'Z')$ converges into the NLO-corrected $\Gamma(H_1 \to \varphi_{\rm h}\varphi_{\rm h})$ in compliance with the Goldstone-boson equivalence theorem. Due to the overall factor $s_\alpha^2/v_{\rm h}^2$ in $\Gamma(H_1 \to Z'Z')$ and $\Gamma(H_1 \to \varphi_{\rm h}\varphi_{\rm h})$ these decay modes are strongly suppressed for large $v_{\rm h}$ or small $|\alpha|$. For small $v_{\rm h}$, however, the decay modes $H_1 \to Z'Z'$ and $H_1 \to \varphi_{\rm h}\varphi_{\rm h}$ can provide significant invisible contributions to the total width $\Gamma_{\rm tot}^{H_1}$. In these cases, the dependence on M_{H_2} is not very pronounced. This changes as soon as the decay mode $H_1 \to H_2 H_2$ becomes kinematically allowed.

The contributions to $\Gamma_{\rm tot}^{H_1}$ from $\Gamma(H_1 \to H_2 H_2)$ are likewise larger for smaller $v_{\rm h}$, but in contrast to those from $\Gamma(H_1 \to Z'Z')$ and $\Gamma(H_1 \to \varphi_{\rm h}\varphi_{\rm h})$ they do not vanish in the limit of large $v_{\rm h}$. The partial width $\Gamma(H_1 \to H_2 H_2)$ receives substantial one-loop contributions which are generally model dependent. For an increasing gauge coupling in the non-standard gauge sector of the EHSL model, specific one-loop effects become non-negligible in $\Gamma(H_1 \to H_2 H_2)$.

Explicit numerical results incorporating all the stated non-standard effects are provided for $\Gamma_{\rm tot}^{H_1}$ and $\mathrm{BR}(H_1 \to \mathrm{X}_i)$, $\mathrm{X}_i = AA, ZZ, WW, \tau\bar\tau, AZ, gg, b\bar b, c\bar c$ (photons A and gluons g). Together with recent experimental bounds from the Higgs measurements these can be used to considerably constrain the non-standard parameter ranges in the EHSL, EHSG and EHSD models.

List of Feynman rules

In the following we list the Feynman rules of the renormalized EHSL model. From the latter the Feynman rules of the renormalized EHSG model can be derived in a simple way, by properly taking the limit $g_\mathrm{h} \to 0$ after a consistent reintroduction of the parameter g_h according to $M_{Z'} = g_\mathrm{h} v_\mathrm{h}$. In this limit the corresponding counterterms behave as explained in Subsect. 5.3.2. A subsequent drop of all rules involving the hidden Goldstone boson φ_h finally yields the Feynman rules of the renormalized EHSD model.

According to the procedures specified in Chapter 3 and Chapter 5 the Feynman rules take into account the renormalization of the unphysical sector. We use the 't Hooft-Feynman gauge for the renormalized gauge-fixing parameters. The Feynman rules are specified in the physical basis. Field renormalization of the Goldstone bosons φ_s, $\phi^\pm$ and φ_h is denoted by the field-renormalization constants for the SM and non-SM Higgs multiplets δZ_H and δZ_χ. All momenta in the vertices are defined as incoming. For the standard fields and parameters we adopt the conventions of [82].

A.1 Propagators

Gauge bosons $V = A$, Z, $W^\pm$, Z':

$$V_\mu \mathord{\sim\!\!\!\sim\!\!\!\sim}^{k} V_\nu = \frac{-i g_{\mu\nu}}{k^2 - M_V^2}.$$

Faddeev-Popov ghosts $U = u^A$, u^Z, $u^\pm$, $u^{Z'}$:

$$U \mathrel{\cdots\!\!\!\cdots}^{k} \overline{U} = \frac{i}{k^2 - M_U^2}.$$

Scalar fields $S = H_1$, H_2, φ_s, $\phi^\pm$, φ_h:

$$S \mathrel{-\,-\,-}^{k} S = \frac{i}{k^2 - M_S^2}.$$

Fermion fields $F = f_i$:

$$F \bullet \xrightarrow{\quad k \quad} \bullet \overline{F} \;=\; \frac{i(\slashed{k} + m_F)}{k^2 - m_F^2}.$$

Corresponding masses:

$$\begin{aligned}
M_{u^A} &= M_A = 0, \\
M_{u^Z} &= M_{\varphi_{\mathrm s}} = M_Z, \\
M_{u^\pm} &= M_{\phi^\pm} = M_{W^\pm} = M_W, \\
M_{u^{Z'}} &= M_{\varphi_{\mathrm h}} = M_{Z'}, \\
m_{f_i} &= m_{f,i}.
\end{aligned} \tag{A.1.1}$$

A.2   Tadpoles

$$\xcancel{} \text{-}\,\text{-}\,\text{-}\,\text{-}\,\underset{S}{\text{-}}\,\text{-} \;=\; iC,$$

with respective values of S and C

$$\begin{aligned}
H_1 &: C = \delta t_{H_1}, \\
H_2 &: C = \delta t_{H_2}.
\end{aligned} \tag{A.2.1}$$

A.3 VV counterterms

$$V_{1,\mu}, k \;\;\wwbar\;\; V_{2,\nu} \;=\; -ig_{\mu\nu}[C_1 k^2 - C_2] + ik_\mu k_\nu C_3,$$

with respective values of V_1, V_2, C_1, C_2 and C_3

$$\begin{aligned}
W^+W^- &: & C_1 &= \delta Z_{WW}, & C_2 &= M_W^2 \delta Z_{WW} + \delta M_W^2, & C_3 &= \delta Z_{WW}, \\
ZZ &: & C_1 &= \delta Z_{ZZ}, & C_2 &= M_Z^2 \delta Z_{ZZ} + \delta M_Z^2, & C_3 &= \delta Z_{ZZ}, \\
AZ &: & C_1 &= \frac{\delta Z_{AZ} + \delta Z_{ZA}}{2}, & C_2 &= \frac{M_Z^2}{2} \delta Z_{ZA}, & C_3 &= \frac{\delta Z_{AZ} + \delta Z_{ZA}}{2}, \\
AA &: & C_1 &= \delta Z_{AA}, & C_2 &= 0, & C_3 &= \delta Z_{AA}, \\
Z'Z' &: & C_1 &= \delta Z_{Z'Z'}, & C_2 &= M_{Z'}^2 \delta Z_{Z'Z'} + \delta M_{Z'}^2, & C_3 &= \delta Z_{Z'Z'}.
\end{aligned}$$

$$\tag{A.3.1}$$

A.4 SV counterterms

$$S, k \; ---\!\!\!\bigtimes\!\!\!\wedge\!\!\wedge\!\!\wedge\!\!\wedge^{V_\mu} = \; ik_\mu C,$$

with respective values of S, V and C

$$
\begin{aligned}
\phi^\pm W^\mp: \quad & C = \pm \frac{M_W}{2} \left(\delta Z_{WW} + \delta Z_H + \frac{\delta M_W^2}{M_W^2} \right), \\
\varphi_s Z: \quad & C = -i \frac{M_Z}{2} \left(\delta Z_{ZZ} + \delta Z_H + \frac{\delta M_Z^2}{M_Z^2} \right), \\
\varphi_s A: \quad & C = -i \frac{M_Z}{2} \delta Z_{ZA}, \\
\varphi_h Z': \quad & C = -i \frac{M_{Z'}}{2} \left(\delta Z_{Z'Z'} + \delta Z_\chi + \frac{\delta M_{Z'}^2}{M_{Z'}^2} \right).
\end{aligned}
\tag{A.4.1}
$$

A.5 SS counterterms

$$S_1, k \; ---\!\!\!\bigtimes\!\!\!---^{S_2} = \; i[C_1 k^2 - C_2],$$

with respective values of S_1, S_2, C_1 and C_2

$$
\begin{aligned}
H_1 H_1: \quad & C_1 = \delta Z_{H_1 H_1}, \quad & C_2 = \delta M_{H_1}^2 + M_{H_1}^2 \delta Z_{H_1 H_1}, \\
H_1 H_2: \quad & C_1 = \delta Z_{H_1 H_2}, \quad & C_2 = \frac{1}{2} M_{H_1}^2 \delta Z_{H_1 H_2} + \frac{1}{2} M_{H_2}^2 \delta Z_{H_1 H_2} + \delta M_{H_1 H_2}^2, \\
H_2 H_2: \quad & C_1 = \delta Z_{H_2 H_2}, \quad & C_2 = \delta M_{H_2}^2 + M_{H_2}^2 \delta Z_{H_2 H_2}, \\
\varphi_s \varphi_s: \quad & C_1 = \delta Z_H, \quad & C_2 = -\frac{c_\alpha \delta t_{H_1}}{v_s} + \frac{s_\alpha \delta t_{H_2}}{v_s}, \\
\varphi_h \varphi_h: \quad & C_1 = \delta Z_\chi, \quad & C_2 = -\frac{c_\alpha \delta t_{H_2}}{v_h} - \frac{s_\alpha \delta t_{H_1}}{v_h}, \\
\phi^+ \phi^-: \quad & C_1 = \delta Z_H, \quad & C_2 = -\frac{c_\alpha \delta t_{H_1}}{v_s} + \frac{s_\alpha \delta t_{H_2}}{v_s}.
\end{aligned}
\tag{A.5.1}
$$

A.6 UU **counterterms**

$$U_1, k \quad \cdots\!\!\!\longrightarrow\!\!\!\times\!\!\!\longrightarrow\!\!\!\cdots \quad \overline{U}_2 \quad = \quad i[C_1 k^2 - C_2],$$

with respective values of U_1, $\overline{U}_2$, C_1 and C_2

$$
\begin{aligned}
u^A \bar{u}^A : \quad & C_1 = \delta\widetilde{Z}_{AA} - \frac{1}{2}\delta Z_{AA}, & C_2 &= 0, \\[2mm]
u^Z \bar{u}^Z : \quad & C_1 = \delta\widetilde{Z}_{ZZ} - \frac{1}{2}\delta Z_{ZZ}, & C_2 &= M_Z^2\left(\delta\widetilde{Z}_{ZZ} - \frac{1}{2}\delta Z_H\right) + \frac{1}{2}\delta M_Z^2, \\[2mm]
u^Z \bar{u}^A : \quad & C_1 = \delta\widetilde{Z}_{AZ} - \frac{1}{2}\delta Z_{AZ}, & C_2 &= 0, \\[2mm]
u^A \bar{u}^Z : \quad & C_1 = \delta\widetilde{Z}_{ZA} - \frac{1}{2}\delta Z_{ZA}, & C_2 &= M_Z^2\delta\widetilde{Z}_{ZA}, \\[2mm]
u^\pm \bar{u}^\pm : \quad & C_1 = \delta\widetilde{Z}_{WW} - \frac{1}{2}\delta Z_{WW}, & C_2 &= M_W^2\left(\delta\widetilde{Z}_{WW} - \frac{1}{2}\delta Z_H\right) + \frac{1}{2}\delta M_W^2, \\[2mm]
u^{Z'} \bar{u}^{Z'} : \quad & C_1 = \delta\widetilde{Z}_{Z'Z'} - \frac{1}{2}\delta Z_{Z'Z'}, & C_2 &= M_{Z'}^2\left(\delta\widetilde{Z}_{Z'Z'} - \frac{1}{2}\delta Z_\chi\right) + \frac{1}{2}\delta M_{Z'}^2.
\end{aligned}
$$

$$(A.6.1)$$
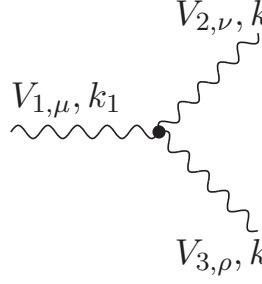
A.7 FF **counterterms**

$$F_1, k \quad \longrightarrow\!\!\!\times\!\!\!\longrightarrow \quad \overline{F}_2 \quad = \quad i[C_\mathrm{L}\slashed{k}\omega_- + C_\mathrm{R}\slashed{k}\omega_+ - C_\mathrm{S}^-\omega_- - C_\mathrm{S}^+\omega_+],$$

with respective values for F_1, $\overline{F}_2$, C_L, C_R, C_S^- and C_S^+

$$
f_j \bar{f}_i : \quad
\begin{cases}
C_\mathrm{L} = \dfrac{1}{2}(\delta Z_{ij}^{f,\mathrm{L}} + \delta Z_{ij}^{f,\mathrm{L}\dagger}), \\[3mm]
C_\mathrm{R} = \dfrac{1}{2}(\delta Z_{ij}^{f,\mathrm{R}} + \delta Z_{ij}^{f,\mathrm{R}\dagger}), \\[3mm]
C_\mathrm{S}^- = \dfrac{1}{2}m_{f,i}\delta Z_{ij}^{f,\mathrm{L}} + \dfrac{1}{2}m_{f,j}\delta Z_{ij}^{f,\mathrm{R}\dagger} + \delta_{ij}\delta m_{f,i}, \\[3mm]
C_\mathrm{S}^+ = \dfrac{1}{2}m_{f,i}\delta Z_{ij}^{f,\mathrm{R}} + \dfrac{1}{2}m_{f,j}\delta Z_{ij}^{f,\mathrm{L}\dagger} + \delta_{ij}\delta m_{f,i}.
\end{cases}
\qquad (A.7.1)
$$

A.8 VVV couplings
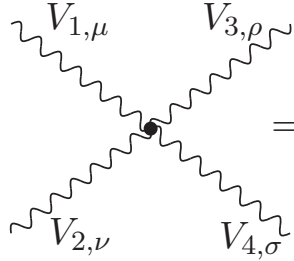
$$= -ieC[g_{\mu\nu}(k_2-k_1)_\rho + g_{\nu\rho}(k_3-k_2)_\mu + g_{\rho\mu}(k_1-k_3)_\nu],$$

with respective values for V_1, V_2, V_3 and C

$$AW^+W^- \quad : \quad C = 1 + \frac{\delta e}{e} + \delta Z_{WW} + \frac{1}{2}\delta Z_{AA} - \frac{1}{2}\frac{c_W}{s_W}\delta Z_{ZA},$$

$$ZW^+W^- \quad : \quad C = -\frac{c_W}{s_W} \times \left[1 + \frac{\delta e}{e} - \frac{1}{c_W^2}\frac{\delta s_W}{s_W} + \delta Z_{WW} + \frac{1}{2}\delta Z_{ZZ}\right] + \frac{1}{2}\delta Z_{AZ}.$$

$$(\text{A.8.1})$$

A.9 $VVVV$ couplings

$$= ie^2 C[2g_{\mu\nu}g_{\sigma\rho} - g_{\nu\rho}g_{\mu\sigma} - g_{\rho\mu}g_{\nu\sigma}],$$

with respective values for V_1, V_2, V_3, V_4 and C

$$W^+W^+W^-W^- : \quad C = \frac{1}{s_W^2} \times \left[1 + 2\frac{\delta e}{e} - 2\frac{\delta s_W}{s_W} + 2\delta Z_{WW}\right],$$

$$W^+W^-ZZ \quad : \quad C = -\frac{c_W^2}{s_W^2} \times \left[1 + 2\frac{\delta e}{e} - 2\frac{1}{c_W^2}\frac{\delta s_W}{s_W} + \delta Z_{WW} + \delta Z_{ZZ}\right] + \frac{c_W}{s_W}\delta Z_{AZ},$$

$$W^+W^-AZ \quad : \quad C = \frac{c_W}{s_W} \times \left[1 + 2\frac{\delta e}{e} - \frac{1}{c_W^2}\frac{\delta s_W}{s_W} + \delta Z_{WW} + \frac{1}{2}\delta Z_{ZZ} + \frac{1}{2}\delta Z_{AA}\right]$$

$$- \frac{1}{2}\delta Z_{AZ} - \frac{1}{2}\frac{c_W^2}{s_W^2}\delta Z_{ZA},$$

$$W^+W^-AA \quad : \quad C = -\left[1 + 2\frac{\delta e}{e} + \delta Z_{WW} + \delta Z_{AA}\right] + \frac{c_W}{s_W}\delta Z_{ZA}.$$

$$(\text{A.9.1})$$

A.10 SSS **couplings**

$$ieC,$$

with respective values for S_1, S_2, S_3 and C (explicit expressions of the corresponding counterterms $\delta C_{H_1 H_1 H_1}$, $\delta C_{H_1 H_1 H_2}$, $\delta C_{H_1 H_2 H_2}$ and $\delta C_{H_2 H_2 H_2}$ are specified in App. A.19)

$$H_1 H_1 H_1 : \quad C = -\frac{3 M_{H_1}^2 \left(\frac{e c_\alpha^3}{2 s_W M_W} + \frac{s_\alpha^3}{v_{\rm h}} \right)}{e} \times \left[1 + \delta C_{H_1 H_1 H_1} \right],$$

$$H_1 H_1 H_2 : \quad C = -\frac{c_\alpha \left(2 M_{H_1}^2 + M_{H_2}^2 \right) s_\alpha \left(\frac{s_\alpha}{v_{\rm h}} - \frac{e c_\alpha}{2 s_W M_W} \right)}{e} \times \left[1 + \delta C_{H_1 H_1 H_2} \right],$$

$$H_1 H_2 H_2 : \quad C = -\frac{c_\alpha \left(M_{H_1}^2 + 2 M_{H_2}^2 \right) s_\alpha \left(\frac{c_\alpha}{v_{\rm h}} + \frac{e s_\alpha}{2 s_W M_W} \right)}{e} \times \left[1 + \delta C_{H_1 H_2 H_2} \right],$$

$$H_2 H_2 H_2 : \quad C = \frac{3}{2} M_{H_2}^2 \left(\frac{s_\alpha^3}{s_W M_W} - \frac{2 c_\alpha^3}{e v_{\rm h}} \right) \times \left[1 + \delta C_{H_2 H_2 H_2} \right],$$

$$H_1 \varphi_{\rm s} \varphi_{\rm s} : \quad C = -\frac{c_\alpha M_{H_1}^2}{2 s_W M_W} \times \Bigg[1 - \frac{\delta v_{\rm s}}{v_{\rm s}} + \frac{c_\alpha}{v_{\rm s} M_{H_1}^2} \delta t_{H_1} - \frac{s_\alpha}{v_{\rm s} M_{H_1}^2} \delta t_{H_2} + \frac{\delta M_{H_1}^2}{M_{H_1}^2}$$
$$- \frac{s_\alpha}{c_\alpha} \frac{\delta M_{H_1 H_2}^2}{M_{H_1}^2} + \frac{1}{2} \delta Z_{H_1 H_1} - \frac{s_\alpha M_{H_2}^2}{2 c_\alpha M_{H_1}^2} \delta Z_{H_1 H_2} + \delta Z_H \Bigg],$$

$$H_2 \varphi_{\rm s} \varphi_{\rm s} : \quad C = \frac{s_\alpha M_{H_2}^2}{2 s_W M_W} \times \Bigg[1 - \frac{\delta v_{\rm s}}{v_{\rm s}} + \frac{c_\alpha}{v_{\rm s} M_{H_2}^2} \delta t_{H_1} - \frac{s_\alpha}{v_{\rm s} M_{H_2}^2} \delta t_{H_2} + \frac{\delta M_{H_2}^2}{M_{H_2}^2}$$
$$- \frac{c_\alpha}{s_\alpha} \frac{\delta M_{H_1 H_2}^2}{M_{H_2}^2} + \frac{1}{2} \delta Z_{H_2 H_2} - \frac{c_\alpha M_{H_1}^2}{2 s_\alpha M_{H_2}^2} \delta Z_{H_1 H_2} + \delta Z_H \Bigg],$$

$$H_1 \varphi_{\rm h} \varphi_{\rm h} : \quad C = -\frac{s_\alpha M_{H_1}^2}{e v_{\rm h}} \times \Bigg[1 - \frac{\delta v_{\rm h}}{v_{\rm h}} + \frac{s_\alpha}{v_{\rm h} M_{H_1}^2} \delta t_{H_1} + \frac{c_\alpha}{v_{\rm h} M_{H_1}^2} \delta t_{H_2} + \frac{\delta M_{H_1}^2}{M_{H_1}^2}$$
$$+ \frac{c_\alpha}{s_\alpha} \frac{\delta M_{H_1 H_2}^2}{M_{H_1}^2} + \frac{1}{2} \delta Z_{H_1 H_1} + \frac{c_\alpha M_{H_2}^2}{2 s_\alpha M_{H_1}^2} \delta Z_{H_1 H_2} + \delta Z_\chi \Bigg],$$

$$(A.10.1)$$

$$H_2 \varphi_{\mathrm{h}} \varphi_{\mathrm{h}} : \quad C = -\frac{c_\alpha M_{H_2}^2}{e v_{\mathrm{h}}} \times \left[1 - \frac{\delta v_{\mathrm{h}}}{v_{\mathrm{h}}} + \frac{s_\alpha}{v_{\mathrm{h}} M_{H_2}^2} \delta t_{H_1} + \frac{c_\alpha}{v_{\mathrm{h}} M_{H_2}^2} \delta t_{H_2} + \frac{\delta M_{H_2}^2}{M_{H_2}^2} \right.$$
$$\left. + \frac{s_\alpha}{c_\alpha} \frac{\delta M_{H_1 H_2}^2}{M_{H_2}^2} + \frac{1}{2} \delta Z_{H_2 H_2} + \frac{s_\alpha M_{H_1}^2}{2 c_\alpha M_{H_2}^2} \delta Z_{H_1 H_2} + \delta Z_\chi \right] ,$$

$$H_1 \phi^+ \phi^- : \quad C = -\frac{c_\alpha M_{H_1}^2}{2 s_W M_W} \times \left[1 - \frac{\delta v_{\mathrm{s}}}{v_{\mathrm{s}}} + \frac{c_\alpha}{v_{\mathrm{s}} M_{H_1}^2} \delta t_{H_1} - \frac{s_\alpha}{v_{\mathrm{s}} M_{H_1}^2} \delta t_{H_2} + \frac{\delta M_{H_1}^2}{M_{H_1}^2} \right.$$
$$\left. - \frac{s_\alpha}{c_\alpha} \frac{\delta M_{H_1 H_2}^2}{M_{H_1}^2} + \frac{1}{2} \delta Z_{H_1 H_1} - \frac{s_\alpha M_{H_2}^2}{2 c_\alpha M_{H_1}^2} \delta Z_{H_1 H_2} + \delta Z_H \right] ,$$

$$H_2 \phi^+ \phi^- : \quad C = \frac{s_\alpha M_{H_2}^2}{2 s_W M_W} \times \left[1 - \frac{\delta v_{\mathrm{s}}}{v_{\mathrm{s}}} + \frac{c_\alpha}{v_{\mathrm{s}} M_{H_2}^2} \delta t_{H_1} - \frac{s_\alpha}{v_{\mathrm{s}} M_{H_2}^2} \delta t_{H_2} + \frac{\delta M_{H_2}^2}{M_{H_2}^2} \right.$$
$$\left. - \frac{c_\alpha}{s_\alpha} \frac{\delta M_{H_1 H_2}^2}{M_{H_2}^2} + \frac{1}{2} \delta Z_{H_2 H_2} - \frac{c_\alpha M_{H_1}^2}{2 s_\alpha M_{H_2}^2} \delta Z_{H_1 H_2} + \delta Z_H \right] .$$

$$(A.10.2)$$

A.11   *SSSS* **couplings**

$$= \ i e^2 C,$$

with respective values for S_1, S_2, S_3, S_4 and C (explicit expressions of the corresponding counterterms $\delta C_{S_1 S_2 S_3 S_4}$ are specified in App. A.20)

$$H_1 H_1 H_1 H_1 : \quad C = \left(\frac{3 s_\alpha^4 \left((c_\alpha^2 - 1) M_{H_1}^2 - c_\alpha^2 M_{H_2}^2 \right)}{e^2 v_{\mathrm{h}}^2} \right.$$
$$- \frac{3 c_\alpha^3 \left(M_{H_1}^2 - M_{H_2}^2 \right) s_\alpha^3}{e s_W v_{\mathrm{h}} M_W}$$
$$\left. - \frac{3 c_\alpha^4 \left(c_\alpha^2 \left(M_{H_1}^2 - M_{H_2}^2 \right) + M_{H_2}^2 \right)}{4 s_W^2 M_W^2} \right) \times [1 + \delta C_{H_1 H_1 H_1 H_1}],$$

$$(A.11.1)$$

$$H_1 H_1 H_1 H_2: \quad C = \left(\frac{3 c_\alpha s_\alpha^3 \left(\left(c_\alpha^2 - 1 \right) M_{H_1}^2 - c_\alpha^2 M_{H_2}^2 \right)}{e^2 v_{\mathrm{h}}^2} \right.$$

$$- \frac{3 \left(2 c_\alpha^2 - 1 \right) c_\alpha^2 \left(M_{H_1}^2 - M_{H_2}^2 \right) s_\alpha^2}{2 e s_W v_{\mathrm{h}} M_W}$$

$$\left. + \frac{3 c_\alpha^3 s_\alpha \left(c_\alpha^2 \left(M_{H_1}^2 - M_{H_2}^2 \right) + M_{H_2}^2 \right)}{4 s_W^2 M_W^2} \right) \times [1 + \delta C_{H_1 H_1 H_1 H_2}],$$

$$H_1 H_1 H_2 H_2: \quad C = \left(\frac{3 c_\alpha^2 s_\alpha^2 \left(\left(c_\alpha^2 - 1 \right) M_{H_1}^2 - c_\alpha^2 M_{H_2}^2 \right)}{e^2 v_{\mathrm{h}}^2} \right.$$

$$- \frac{c_\alpha \left(6 c_\alpha^4 - 6 c_\alpha^2 + 1 \right) \left(M_{H_1}^2 - M_{H_2}^2 \right) s_\alpha}{2 e s_W v_{\mathrm{h}} M_W}$$

$$\left. - \frac{3 c_\alpha^2 s_\alpha^2 \left(c_\alpha^2 \left(M_{H_1}^2 - M_{H_2}^2 \right) + M_{H_2}^2 \right)}{4 s_W^2 M_W^2} \right) \times [1 + \delta C_{H_1 H_1 H_2 H_2}],$$

$$H_1 H_2 H_2 H_2: \quad C = \left(\frac{3 c_\alpha^3 s_\alpha \left(\left(c_\alpha^2 - 1 \right) M_{H_1}^2 - c_\alpha^2 M_{H_2}^2 \right)}{e^2 v_{\mathrm{h}}^2} \right.$$

$$+ \frac{3 \left(2 c_\alpha^2 - 1 \right) c_\alpha^2 \left(M_{H_1}^2 - M_{H_2}^2 \right) s_\alpha^2}{2 e s_W v_{\mathrm{h}} M_W}$$

$$\left. + \frac{3 c_\alpha s_\alpha^3 \left(c_\alpha^2 \left(M_{H_1}^2 - M_{H_2}^2 \right) + M_{H_2}^2 \right)}{4 s_W^2 M_W^2} \right) \times [1 + \delta C_{H_1 H_2 H_2 H_2}],$$

$$H_2 H_2 H_2 H_2: \quad C = \left(- \frac{3 c_\alpha^4 \left(\left(1 - c_\alpha^2 \right) M_{H_1}^2 + c_\alpha^2 M_{H_2}^2 \right)}{e^2 v_{\mathrm{h}}^2} \right.$$

$$- \frac{3 c_\alpha^3 \left(M_{H_1}^2 - M_{H_2}^2 \right) s_\alpha^3}{e s_W v_{\mathrm{h}} M_W}$$

$$\left. - \frac{3 s_\alpha^4 \left(c_\alpha^2 \left(M_{H_1}^2 - M_{H_2}^2 \right) + M_{H_2}^2 \right)}{4 s_W^2 M_W^2} \right) \times [1 + \delta C_{H_2 H_2 H_2 H_2}],$$

$$H_1 H_1 \varphi_{\mathrm{s}} \varphi_{\mathrm{s}}: \quad C = \left(- \frac{c_\alpha \left(M_{H_1}^2 - M_{H_2}^2 \right) s_\alpha^3}{2 e s_W v_{\mathrm{h}} M_W} \right.$$

$$\left. - \frac{c_\alpha^2 \left(\left(2 c_\alpha^2 - 1 \right) \left(M_{H_1}^2 - M_{H_2}^2 \right) + M_{H_1}^2 + M_{H_2}^2 \right)}{8 s_W^2 M_W^2} \right)$$

$$\times [1 + \delta C_{H_1 H_1 \varphi_{\mathrm{s}} \varphi_{\mathrm{s}}}],$$

$$(A.11.2)$$

$$H_1 H_1 \varphi_{\mathrm{h}} \varphi_{\mathrm{h}} : \quad C = \left(-\frac{s_\alpha^2 \left((2c_\alpha^2 - 1) \left(M_{H_2}^2 - M_{H_1}^2 \right) + M_{H_1}^2 + M_{H_2}^2 \right)}{2 e^2 v_{\mathrm{h}}^2} \right.$$

$$\left. -\frac{c_\alpha^3 \left(M_{H_1}^2 - M_{H_2}^2 \right) s_\alpha}{2 e s_W v_{\mathrm{h}} M_W} \right)$$

$$\times [1 + \delta C_{H_1 H_1 \varphi_{\mathrm{h}} \varphi_{\mathrm{h}}}],$$

$$H_2 H_2 \varphi_{\mathrm{s}} \varphi_{\mathrm{s}} : \quad C = \left(-\frac{c_\alpha^3 \left(M_{H_1}^2 - M_{H_2}^2 \right) s_\alpha}{2 e s_W v_{\mathrm{h}} M_W} \right.$$

$$\left. -\frac{s_\alpha^2 \left((2c_\alpha^2 - 1) \left(M_{H_1}^2 - M_{H_2}^2 \right) + M_{H_1}^2 + M_{H_2}^2 \right)}{8 s_W^2 M_W^2} \right)$$

$$\times [1 + \delta C_{H_2 H_2 \varphi_{\mathrm{s}} \varphi_{\mathrm{s}}}],$$

$$H_2 H_2 \varphi_{\mathrm{h}} \varphi_{\mathrm{h}} : \quad C = \left(-\frac{c_\alpha^2 \left((2c_\alpha^2 - 1) \left(M_{H_2}^2 - M_{H_1}^2 \right) + M_{H_1}^2 + M_{H_2}^2 \right)}{2 e^2 v_{\mathrm{h}}^2} \right.$$

$$\left. -\frac{c_\alpha \left(M_{H_1}^2 - M_{H_2}^2 \right) s_\alpha^3}{2 e s_W v_{\mathrm{h}} M_W} \right)$$

$$\times [1 + \delta C_{H_2 H_2 \varphi_{\mathrm{h}} \varphi_{\mathrm{h}}}],$$

$$H_1 H_2 \varphi_{\mathrm{s}} \varphi_{\mathrm{s}} : \quad C = \left(\frac{c_\alpha s_\alpha \left(c_\alpha \left(M_{H_1}^2 - M_{H_2}^2 \right) \left(e c_\alpha v_{\mathrm{h}} - 2 s_W M_W s_\alpha \right) + e v_{\mathrm{h}} M_{H_2}^2 \right)}{4 e s_W^2 v_{\mathrm{h}} M_W^2} \right)$$

$$\times [1 + \delta C_{H_1 H_2 \varphi_{\mathrm{s}} \varphi_{\mathrm{s}}}],$$

$$H_1 H_2 \varphi_{\mathrm{h}} \varphi_{\mathrm{h}} : \quad C = \left(\frac{c_\alpha s_\alpha \left((c_\alpha^2 - 1) M_{H_1}^2 - c_\alpha^2 M_{H_2}^2 \right)}{e^2 v_{\mathrm{h}}^2} + \frac{c_\alpha^2 \left(M_{H_1}^2 - M_{H_2}^2 \right) s_\alpha^2}{2 e s_W v_{\mathrm{h}} M_W} \right)$$

$$\times [1 + \delta C_{H_1 H_2 \varphi_{\mathrm{h}} \varphi_{\mathrm{h}}}],$$

$$\varphi_{\mathrm{s}} \varphi_{\mathrm{s}} \varphi_{\mathrm{s}} \varphi_{\mathrm{s}} : \quad C = \frac{3 \left(c_\alpha^2 \left(M_{H_2}^2 - M_{H_1}^2 \right) - M_{H_2}^2 \right)}{4 s_W^2 M_W^2} \times [1 + \delta C_{\varphi_{\mathrm{s}} \varphi_{\mathrm{s}} \varphi_{\mathrm{s}} \varphi_{\mathrm{s}}}],$$

$$\varphi_{\mathrm{h}} \varphi_{\mathrm{h}} \varphi_{\mathrm{h}} \varphi_{\mathrm{h}} : \quad C = -\frac{3 \left(c_\alpha^2 \left(M_{H_2}^2 - M_{H_1}^2 \right) + M_{H_1}^2 \right)}{e^2 v_{\mathrm{h}}^2} \times [1 + \delta C_{\varphi_{\mathrm{h}} \varphi_{\mathrm{h}} \varphi_{\mathrm{h}} \varphi_{\mathrm{h}}}],$$

$$\varphi_{\mathrm{s}} \varphi_{\mathrm{s}} \varphi_{\mathrm{h}} \varphi_{\mathrm{h}} : \quad C = -\frac{c_\alpha \left(M_{H_1}^2 - M_{H_2}^2 \right) s_\alpha}{2 e s_W v_{\mathrm{h}} M_W} \times [1 + \delta C_{\varphi_{\mathrm{s}} \varphi_{\mathrm{s}} \varphi_{\mathrm{h}} \varphi_{\mathrm{h}}}],$$

$$\phi^+ \phi^- \phi^+ \phi^- : \quad C = \frac{c_\alpha^2 \left(M_{H_2}^2 - M_{H_1}^2 \right) - M_{H_2}^2}{2 s_W^2 M_W^2} \times [1 + \delta C_{\phi^+ \phi^- \phi^+ \phi^-}],$$

$$\varphi_{\mathrm{s}} \varphi_{\mathrm{s}} \phi^+ \phi^- : \quad C = \frac{c_\alpha^2 \left(M_{H_2}^2 - M_{H_1}^2 \right) - M_{H_2}^2}{4 s_W^2 M_W^2} \times [1 + \delta C_{\varphi_{\mathrm{s}} \varphi_{\mathrm{s}} \phi^+ \phi^-}],$$

$$\varphi_{\mathrm{h}} \varphi_{\mathrm{h}} \phi^+ \phi^- : \quad C = -\frac{c_\alpha \left(M_{H_1}^2 - M_{H_2}^2 \right) s_\alpha}{2 e s_W v_{\mathrm{h}} M_W} \times [1 + \delta C_{\varphi_{\mathrm{h}} \varphi_{\mathrm{h}} \phi^+ \phi^-}],$$

$$(\text{A.11.3})$$

$$H_1H_1\phi^+\phi^- : \quad C = \left(-\frac{c_\alpha \left(M_{H_1}^2 - M_{H_2}^2\right) s_\alpha^3}{2es_W v_{\rm h} M_W}\right.$$

$$\left. -\frac{c_\alpha^2 \left((2c_\alpha^2 - 1)\left(M_{H_1}^2 - M_{H_2}^2\right) + M_{H_1}^2 + M_{H_2}^2\right)}{8s_W^2 M_W^2}\right)$$

$$\times \left[1 + \delta C_{H_1H_1\phi^+\phi^-}\right],$$

$$H_1H_2\phi^+\phi^- : \quad C = \left(\frac{c_\alpha^2 \left(M_{H_1}^2 - M_{H_2}^2\right) s_\alpha \left(ec_\alpha v_{\rm h} - 2s_W M_W s_\alpha\right)}{4es_W^2 v_{\rm h} M_W^2} + \frac{c_\alpha M_{H_2}^2 s_\alpha}{4s_W^2 M_W^2}\right)$$

$$\times \left[1 + \delta C_{H_1H_2\phi^+\phi^-}\right],$$

$$H_2H_2\phi^+\phi^- : \quad C = \left(\frac{s_\alpha^2 \left(-(2c_\alpha^2 - 1)\left(M_{H_1}^2 - M_{H_2}^2\right) - M_{H_1}^2 - M_{H_2}^2\right)}{8s_W^2 M_W^2}\right.$$

$$\left. -\frac{c_\alpha^3 \left(M_{H_1}^2 - M_{H_2}^2\right) s_\alpha}{2es_W v_{\rm h} M_W}\right)$$

$$\times \left[1 + \delta C_{H_2H_2\phi^+\phi^-}\right].$$

$$(\text{A.11.4})$$

A.12 $VVSS$ **couplings**

$$= ie^2 g_{\mu\nu} C,$$

with respective values for V_1, V_2, S_1, S_2 and C

$$W^+W^-H_1H_1 : \quad C = \frac{c_\alpha^2}{2s_W^2} \times \left[1 + 2\frac{\delta e}{e} - 2\frac{\delta s_W}{s_W} + \delta Z_{WW} + \delta Z_{H_1H_1} - \frac{s_\alpha}{c_\alpha}\delta Z_{H_1H_2}\right],$$

$$W^+W^-H_2H_2 : \quad C = \frac{s_\alpha^2}{2s_W^2} \times \left[1 + 2\frac{\delta e}{e} - 2\frac{\delta s_W}{s_W} + \delta Z_{WW} + \delta Z_{H_2H_2} - \frac{c_\alpha}{s_\alpha}\delta Z_{H_1H_2}\right],$$

$$W^+W^-H_1H_2 : \quad C = -\frac{s_\alpha c_\alpha}{2s_W^2} \times \left[1 + 2\frac{\delta e}{e} - 2\frac{\delta s_W}{s_W} + \delta Z_{WW} + \frac{1}{2}\delta Z_{H_1H_1}+\right.$$

$$\left. +\frac{1}{2}\delta Z_{H_2H_2} - \frac{s_\alpha}{2c_\alpha}\delta Z_{H_1H_2} - \frac{c_\alpha}{2s_\alpha}\delta Z_{H_1H_2}\right],$$

$$(\text{A.12.1})$$

$$W^+W^-\varphi_s\varphi_s: \quad C = \frac{1}{2s_W^2} \times \left[1 + 2\frac{\delta e}{e} - 2\frac{\delta s_W}{s_W} + \delta Z_{WW} + \delta Z_H\right],$$

$$W^+W^-\phi^+\phi^-: \quad C = \frac{1}{2s_W^2} \times \left[1 + 2\frac{\delta e}{e} - 2\frac{\delta s_W}{s_W} + \delta Z_{WW} + \delta Z_H\right],$$

$$ZZ\phi^+\phi^-: \quad C = \frac{(s_W^2 - c_W^2)^2}{2c_W^2 s_W^2} \times \left[1 + 2\frac{\delta e}{e} + \frac{2}{c_W^2(s_W^2 - c_W^2)}\frac{\delta s_W}{s_W}\right.$$
$$\left. + \delta Z_{ZZ} + \delta Z_H + \frac{2s_W c_W}{s_W^2 - c_W^2}\delta Z_{AZ}\right],$$

$$AZ\phi^+\phi^-: \quad C = \frac{s_W^2 - c_W^2}{s_W c_W} \times \left[1 + 2\frac{\delta e}{e} + \frac{1}{c_W^2(s_W^2 - c_W^2)}\frac{\delta s_W}{s_W}\right.$$
$$+ \frac{1}{2}\delta Z_{ZZ} + \frac{1}{2}\delta Z_{AA} + \frac{s_W^2 - c_W^2}{4s_W c_W}\delta Z_{ZA}$$
$$\left. + \frac{s_W c_W}{s_W^2 - c_W^2}\delta Z_{AZ} + \delta Z_H\right],$$

$$AA\phi^+\phi^-: \quad C = 2 \times \left[1 + 2\frac{\delta e}{e} + \delta Z_{AA} + \delta Z_H\right] + \frac{s_W^2 - c_W^2}{s_W c_W}\delta Z_{ZA},$$

$$ZZH_1H_1: \quad C = \frac{c_\alpha^2}{2c_W^2 s_W^2} \times \left[1 + 2\frac{\delta e}{e} + 2\frac{s_W^2 - c_W^2}{c_W^2}\frac{\delta s_W}{s_W}\right.$$
$$\left. + \delta Z_{ZZ} + \delta Z_{H_1 H_1} - \frac{s_\alpha}{c_\alpha}\delta Z_{H_1 H_2}\right],$$

$$ZZH_2H_2: \quad C = \frac{s_\alpha^2}{2c_W^2 s_W^2} \times \left[1 + 2\frac{\delta e}{e} + 2\frac{s_W^2 - c_W^2}{c_W^2}\frac{\delta s_W}{s_W}\right.$$
$$\left. + \delta Z_{ZZ} + \delta Z_{H_2 H_2} - \frac{c_\alpha}{s_\alpha}\delta Z_{H_1 H_2}\right],$$

$$ZZH_1H_2: \quad C = -\frac{s_\alpha c_\alpha}{2c_W^2 s_W^2} \times \left[1 + 2\frac{\delta e}{e} + 2\frac{s_W^2 - c_W^2}{c_W^2}\frac{\delta s_W}{s_W} + \delta Z_{ZZ} + \frac{1}{2}\delta Z_{H_1 H_1}\right.$$
$$\left. + \frac{1}{2}\delta Z_{H_2 H_2} - \frac{s_\alpha}{2c_\alpha}\delta Z_{H_1 H_2} - \frac{c_\alpha}{2s_\alpha}\delta Z_{H_1 H_2}\right],$$

$$ZZ\varphi_s\varphi_s: \quad C = \frac{1}{2c_W^2 s_W^2} \times \left[1 + 2\frac{\delta e}{e} + 2\frac{s_W^2 - c_W^2}{c_W^2}\frac{\delta s_W}{s_W} + \delta Z_{ZZ} + \delta Z_H\right],$$

$$AZH_1H_1: \quad C = \frac{c_\alpha^2}{2c_W^2 s_W^2}\frac{1}{2}\delta Z_{ZA},$$

$$AZH_2H_2: \quad C = \frac{s_\alpha^2}{2c_W^2 s_W^2}\frac{1}{2}\delta Z_{ZA},$$

$$AZH_1H_2: \quad C = -\frac{s_\alpha c_\alpha}{2c_W^2 s_W^2}\frac{1}{2}\delta Z_{ZA},$$

$$(A.12.2)$$

$$AZ\varphi_\mathrm{s}\varphi_\mathrm{s}: \quad C = \frac{1}{2c_W^2 s_W^2}\frac{1}{2}\delta Z_{ZA},$$

$$W^\pm Z\phi^\mp H_1: \quad C = -\frac{c_\alpha}{2c_W} \times \left[1 + 2\frac{\delta e}{e} - \frac{\delta c_W}{c_W} + \frac{\delta Z_{WW}}{2} + \frac{\delta Z_{H_1 H_1}}{2} + \frac{\delta Z_{ZZ}}{2} \right. $$
$$\left. -\frac{s_\alpha}{2c_\alpha}\delta Z_{H_1 H_2} + \frac{c_W}{s_W}\frac{\delta Z_{AZ}}{2} + \frac{1}{2}\delta Z_H \right],$$

$$W^\pm Z\phi^\mp H_2: \quad C = \frac{s_\alpha}{2c_W} \times \left[1 + 2\frac{\delta e}{e} - \frac{\delta c_W}{c_W} + \frac{\delta Z_{WW}}{2} + \frac{\delta Z_{H_2 H_2}}{2} + \frac{\delta Z_{ZZ}}{2} \right. $$
$$\left. -\frac{c_\alpha}{2s_\alpha}\delta Z_{H_1 H_2} + \frac{c_W}{s_W}\frac{\delta Z_{AZ}}{2} + \frac{1}{2}\delta Z_H \right],$$

$$W^\pm A\phi^\mp H_1: \quad C = -\frac{c_\alpha}{2s_W} \times \left[1 + 2\frac{\delta e}{e} - \frac{\delta s_W}{s_W} + \frac{\delta Z_{WW}}{2} + \frac{\delta Z_{H_1 H_1}}{2} + \frac{\delta Z_{AA}}{2} \right. $$
$$\left. -\frac{s_\alpha}{2c_\alpha}\delta Z_{H_1 H_2} + \frac{s_W}{c_W}\frac{\delta Z_{ZA}}{2} + \frac{1}{2}\delta Z_H \right],$$

$$W^\pm A\phi^\mp H_2: \quad C = \frac{s_\alpha}{2s_W} \times \left[1 + 2\frac{\delta e}{e} - \frac{\delta s_W}{s_W} + \frac{\delta Z_{WW}}{2} + \frac{\delta Z_{H_2 H_2}}{2} + \frac{\delta Z_{AA}}{2} \right. $$
$$\left. -\frac{c_\alpha}{2s_\alpha}\delta Z_{H_1 H_2} + \frac{s_W}{c_W}\frac{\delta Z_{ZA}}{2} + \frac{1}{2}\delta Z_H \right],$$

$$W^\pm Z\phi^\mp\varphi_\mathrm{s}: \quad C = \mp\frac{i}{2c_W} \times \left[1 + 2\frac{\delta e}{e} - \frac{\delta c_W}{c_W} + \frac{\delta Z_{WW}}{2} + \frac{\delta Z_{ZZ}}{2} \right. $$
$$\left. +\frac{c_W}{s_W}\frac{\delta Z_{AZ}}{2} + \delta Z_H \right],$$

$$W^\pm A\phi^\mp\varphi_\mathrm{s}: \quad C = \mp\frac{i}{2s_W} \times \left[1 + 2\frac{\delta e}{e} - \frac{\delta s_W}{s_W} + \frac{\delta Z_{WW}}{2} + \frac{\delta Z_{AA}}{2} \right. $$
$$\left. +\frac{s_W}{c_W}\frac{\delta Z_{ZA}}{2} + \delta Z_H \right],$$

$$Z'Z'H_1 H_1: \quad C = 2\left(\frac{M_{Z'}s_\alpha}{ev_\mathrm{h}}\right)^2 \times \left[1 + \delta Z_{Z'Z'} + \frac{\delta M_{Z'}^2}{M_{Z'}^2} \right. $$
$$\left. -2\frac{\delta v_\mathrm{h}}{v_\mathrm{h}} + \delta Z_{H_1 H_1} + \frac{c_\alpha}{s_\alpha}\delta Z_{H_1 H_2} \right],$$

$$Z'Z'H_2 H_2: \quad C = 2\left(\frac{M_{Z'}c_\alpha}{ev_\mathrm{h}}\right)^2 \times \left[1 + \delta Z_{Z'Z'} + \frac{\delta M_{Z'}^2}{M_{Z'}^2} \right. $$
$$\left. -2\frac{\delta v_\mathrm{h}}{v_\mathrm{h}} + \delta Z_{H_2 H_2} + \frac{s_\alpha}{c_\alpha}\delta Z_{H_1 H_2} \right],$$

$$(\text{A.12.3})$$

$$Z'Z'H_1H_2: \quad C = 2s_\alpha c_\alpha \left(\frac{M_{Z'}}{ev_h}\right)^2 \times \left[1 + \delta Z_{Z'Z'} + \frac{\delta M_{Z'}^2}{M_{Z'}^2} - 2\frac{\delta v_h}{v_h} \right.$$

$$\left. + \frac{1}{2}\delta Z_{H_1H_1} + \frac{1}{2}\delta Z_{H_2H_2} + \frac{1}{2s_\alpha c_\alpha}\delta Z_{H_1H_2}\right],$$

$$Z'Z'\varphi_h\varphi_h: \quad C = 2\left(\frac{M_{Z'}}{ev_h}\right)^2 \times \left[1 + \delta Z_{Z'Z'} + \frac{\delta M_{Z'}^2}{M_{Z'}^2} - 2\frac{\delta v_h}{v_h} + \delta Z_\chi\right].$$

$$(\text{A.12.4})$$

A.13 VSS **couplings**

$$= \; ieC(k_1-k_2)_\mu,$$
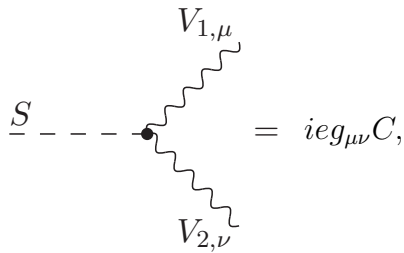
with respective values for V, S_1, S_2 and C

$$A\varphi_s H_1: \quad C = -\frac{ic_\alpha}{2c_W s_W}\frac{1}{2}\delta Z_{ZA},$$

$$A\varphi_s H_2: \quad C = \frac{is_\alpha}{2c_W s_W}\frac{1}{2}\delta Z_{ZA},$$

$$Z\varphi_s H_1: \quad C = -\frac{ic_\alpha}{2c_W s_W} \times \left[1 + \frac{\delta e}{e} + \frac{s_W^2 - c_W^2}{c_W^2}\frac{\delta s_W}{s_W} + \frac{1}{2}\delta Z_{H_1H_1}\right.$$

$$\left. + \frac{1}{2}\delta Z_{ZZ} - \frac{s_\alpha}{2c_\alpha}\delta Z_{H_1H_2} + \frac{1}{2}\delta Z_H\right],$$

$$Z\varphi_s H_2: \quad C = \frac{is_\alpha}{2c_W s_W} \times \left[1 + \frac{\delta e}{e} + \frac{s_W^2 - c_W^2}{c_W^2}\frac{\delta s_W}{s_W} + \frac{1}{2}\delta Z_{H_2H_2}\right. \qquad (\text{A.13.1})$$

$$\left. + \frac{1}{2}\delta Z_{ZZ} - \frac{c_\alpha}{2s_\alpha}\delta Z_{H_1H_2} + \frac{1}{2}\delta Z_H\right],$$

$$A\phi^+\phi^-: \quad C = -\left[1 + \frac{\delta e}{e} + \frac{1}{2}\delta Z_{AA} + \frac{s_W^2 - c_W^2}{2s_W c_W}\frac{1}{2}\delta Z_{ZA} + \delta Z_H\right],$$

$$Z\phi^+\phi^-: \quad C = -\frac{s_W^2 - c_W^2}{2c_W s_W} \times \left[1 + \frac{\delta e}{e} + \frac{1}{c_W^2(s_W^2 - c_W^2)}\frac{\delta s_W}{s_W}\right.$$

$$\left. + \frac{1}{2}\delta Z_{ZZ} + \frac{2s_W c_W}{s_W^2 - c_W^2}\frac{1}{2}\delta Z_{AZ} + \delta Z_H\right],$$

$$W^\pm \phi^\mp H_1: \quad C = \mp \frac{c_\alpha}{2s_W} \times \left[1 + \frac{\delta e}{e} - \frac{\delta s_W}{s_W} + \frac{1}{2}\delta Z_{WW} \right.$$

$$\left. + \frac{1}{2}\delta Z_{H_1 H_1} - \frac{s_\alpha}{2c_\alpha}\delta Z_{H_1 H_2} + \frac{1}{2}\delta Z_H \right],$$

$$W^\pm \phi^\mp H_2: \quad C = \pm \frac{s_\alpha}{2s_W} \times \left[1 + \frac{\delta e}{e} - \frac{\delta s_W}{s_W} + \frac{1}{2}\delta Z_{WW} \right.$$

$$\left. + \frac{1}{2}\delta Z_{H_2 H_2} - \frac{c_\alpha}{2s_\alpha}\delta Z_{H_1 H_2} + \frac{1}{2}\delta Z_H \right],$$

$$W^\pm \phi^\mp \varphi_s: \quad C = -\frac{i}{2s_W} \times \left[1 + \frac{\delta e}{e} - \frac{\delta s_W}{s_W} + \frac{1}{2}\delta Z_{WW} + \delta Z_H \right], \tag{A.13.2}$$

$$Z'\varphi_h H_1: \quad C = -i\frac{s_\alpha M_{Z'}}{e v_h} \times \left[1 + \frac{1}{2}\delta Z_{Z'Z'} + \frac{1}{2}\frac{\delta M_{Z'}^2}{M_{Z'}^2} - \frac{\delta v_h}{v_h} \right.$$

$$\left. + \frac{1}{2}\delta Z_{H_1 H_1} + \frac{c_\alpha}{2s_\alpha}\delta Z_{H_1 H_2} + \frac{1}{2}\delta Z_\chi \right],$$

$$Z'\varphi_h H_2: \quad C = -i\frac{c_\alpha M_{Z'}}{e v_h} \times \left[1 + \frac{1}{2}\delta Z_{Z'Z'} + \frac{1}{2}\frac{\delta M_{Z'}^2}{M_{Z'}^2} - \frac{\delta v_h}{v_h} \right.$$

$$\left. + \frac{1}{2}\delta Z_{H_2 H_2} + \frac{s_\alpha}{2c_\alpha}\delta Z_{H_1 H_2} + \frac{1}{2}\delta Z_\chi \right].$$

A.14 SVV couplings

$$S \!-\!-\!-\!-\!\bullet\!\!\!\!\!\begin{matrix} V_{1,\mu} \\ \\ V_{2,\nu} \end{matrix} \quad = \quad ieg_{\mu\nu}C,$$

with respective values for S, V_1, V_2 and C

$$H_1 W^+ W^-: \quad C = \frac{M_W c_\alpha}{s_W} \times \left[1 + \frac{\delta e}{e} - \frac{\delta s_W}{s_W} + \frac{1}{2}\frac{\delta M_W^2}{M_W^2} + \frac{1}{2}\delta Z_{H_1 H_1} \right.$$

$$\left. + \delta Z_{WW} - \frac{s_\alpha}{2c_\alpha}\delta Z_{H_1 H_2} \right], \tag{A.14.1}$$

$$H_2W^+W^- : \quad C = -\frac{M_W s_\alpha}{s_W} \times \left[1 + \frac{\delta e}{e} - \frac{\delta s_W}{s_W} + \frac{1}{2}\frac{\delta M_W^2}{M_W^2} + \frac{1}{2}\delta Z_{H_2H_2} \right.$$
$$\left. + \delta Z_{WW} - \frac{c_\alpha}{2s_\alpha}\delta Z_{H_1H_2} \right],$$

$$H_1ZZ : \quad C = \frac{M_W c_\alpha}{s_W c_W^2} \times \left[1 + \frac{\delta e}{e} + \frac{2s_W^2 - c_W^2}{c_W^2}\frac{\delta s_W}{s_W} + \frac{1}{2}\frac{\delta M_W^2}{M_W^2} + \frac{1}{2}\delta Z_{H_1H_1} \right.$$
$$\left. + \delta Z_{ZZ} - \frac{s_\alpha}{2c_\alpha}\delta Z_{H_1H_2} \right],$$

$$H_2ZZ : \quad C = -\frac{M_W s_\alpha}{s_W c_W^2} \times \left[1 + \frac{\delta e}{e} + \frac{2s_W^2 - c_W^2}{c_W^2}\frac{\delta s_W}{s_W} + \frac{1}{2}\frac{\delta M_W^2}{M_W^2} \right.$$
$$\left. + \frac{1}{2}\delta Z_{H_2H_2} + \delta Z_{ZZ} - \frac{c_\alpha}{2s_\alpha}\delta Z_{H_1H_2} \right],$$

$$H_1ZA : \quad C = \frac{M_W c_\alpha}{s_W c_W^2}\frac{1}{2}\delta Z_{ZA},$$

$$H_2ZA : \quad C = -\frac{M_W s_\alpha}{s_W c_W^2}\frac{1}{2}\delta Z_{ZA},$$

$$\phi^\pm W^\mp Z : \quad C = -M_W\frac{s_W}{c_W} \times \left[1 + \frac{\delta e}{e} + \frac{1}{c_W^2}\frac{\delta s_W}{s_W} + \frac{1}{2}\frac{\delta M_W^2}{M_W^2} + \frac{1}{2}\delta Z_{WW} \right.$$
$$\left. + \frac{1}{2}\delta Z_{ZZ} + \frac{c_W}{s_W}\frac{1}{2}\delta Z_{AZ} + \frac{1}{2}\delta Z_H \right],$$

$$\phi^\pm W^\mp A : \quad C = -M_W \times \left[1 + \frac{\delta e}{e} + \frac{1}{2}\frac{\delta M_W^2}{M_W^2} + \frac{1}{2}\delta Z_{WW} \right.$$
$$\left. + \frac{1}{2}\delta Z_{AA} + \frac{s_W}{c_W}\frac{1}{2}\delta Z_{ZA} + \frac{1}{2}\delta Z_H \right],$$

$$H_1Z'Z' : \quad C = \frac{2s_\alpha M_{Z'}^2}{ev_{\rm h}} \times \left[1 + \delta Z_{Z'Z'} + \frac{\delta M_{Z'}^2}{M_{Z'}^2} - \frac{\delta v_{\rm h}}{v_{\rm h}} + \frac{1}{2}\delta Z_{H_1H_1} + \frac{c_\alpha}{2s_\alpha}\delta Z_{H_1H_2} \right],$$

$$H_2Z'Z' : \quad C = \frac{2c_\alpha M_{Z'}^2}{ev_{\rm h}} \times \left[1 + \delta Z_{Z'Z'} + \frac{\delta M_{Z'}^2}{M_{Z'}^2} - \frac{\delta v_{\rm h}}{v_{\rm h}} + \frac{1}{2}\delta Z_{H_2H_2} + \frac{s_\alpha}{2c_\alpha}\delta Z_{H_1H_2} \right].$$

$$(\text{A.14.2})$$

A.15 VFF **couplings**

$$= ie\gamma_\mu(C^-\omega_- + C^+\omega_+),$$

with respective values for V, $\overline{F}_1$, F_2, C^+ and C^-

$$\gamma\overline{f}_if_j: \begin{cases} C^+ = -Q_f \times \left[\delta_{ij}\left(1 + \dfrac{\delta e}{e} + \dfrac{1}{2}\delta Z_{AA}\right) + \dfrac{1}{2}\left(\delta Z_{ij}^{f,\mathrm{R}} + \delta Z_{ij}^{f,\mathrm{R}\dagger}\right)\right] \\ \hspace{6cm} + \delta_{ij}g_f^+ \dfrac{1}{2}\delta Z_{ZA}, \\[2mm] C^- = -Q_f \times \left[\delta_{ij}\left(1 + \dfrac{\delta e}{e} + \dfrac{1}{2}\delta Z_{AA}\right) + \dfrac{1}{2}\left(\delta Z_{ij}^{f,\mathrm{L}} + \delta Z_{ij}^{f,\mathrm{L}\dagger}\right)\right] \\ \hspace{6cm} + \delta_{ij}g_f^- \dfrac{1}{2}\delta Z_{ZA}, \end{cases} \tag{A.15.1}$$

$$Z\overline{f}_if_j: \begin{cases} C^+ = g_f^+ \times \left[\delta_{ij}\left(1 + \dfrac{\delta g_f^+}{g_f^+} + \dfrac{1}{2}\delta Z_{ZZ}\right) + \dfrac{1}{2}\left(\delta Z_{ij}^{f,\mathrm{R}} + \delta Z_{ij}^{f,\mathrm{R}\dagger}\right)\right] \\ \hspace{6cm} - \delta_{ij}Q_f \dfrac{1}{2}\delta Z_{AZ}, \\[2mm] C^- = g_f^- \times \left[\delta_{ij}\left(1 + \dfrac{\delta g_f^-}{g_f^-} + \dfrac{1}{2}\delta Z_{ZZ}\right) + \dfrac{1}{2}\left(\delta Z_{ij}^{f,\mathrm{L}} + \delta Z_{ij}^{f,\mathrm{L}\dagger}\right)\right] \\ \hspace{6cm} - \delta_{ij}Q_f \dfrac{1}{2}\delta Z_{AZ}, \end{cases} \tag{A.15.2}$$

$$W^+\overline{u}_id_j: \begin{cases} C^+ = 0, \\ C^- = \dfrac{1}{\sqrt{2}s_W} \times \left[\mathbf{V}_{ij}\left(1 + \dfrac{\delta e}{e} - \dfrac{\delta s_W}{s_W} + \dfrac{1}{2}\delta Z_{WW}\right) + \delta\mathbf{V}_{ij}\right. \\ \hspace{4cm} \left. + \dfrac{1}{2}\sum_k\left(\delta Z_{ik}^{u,\mathrm{L}\dagger}\mathbf{V}_{kj} + \mathbf{V}_{ik}\delta Z_{kj}^{d,\mathrm{L}}\right)\right], \end{cases}$$
$$W^-\overline{d}_ju_i: \begin{cases} C^+ = 0, \\ C^- = \dfrac{1}{\sqrt{2}s_W} \times \left[\mathbf{V}_{ji}^\dagger\left(1 + \dfrac{\delta e}{e} - \dfrac{\delta s_W}{s_W} + \dfrac{1}{2}\delta Z_{WW}\right) + \delta\mathbf{V}_{ji}^\dagger\right. \\ \hspace{4cm} \left. + \dfrac{1}{2}\sum_k\left(\delta Z_{jk}^{d,\mathrm{L}\dagger}\mathbf{V}_{kj}^\dagger + \mathbf{V}_{jk}^\dagger\delta Z_{ki}^{u,\mathrm{L}}\right)\right], \end{cases} \tag{A.15.3}$$

$$W^+ \bar{\nu}_i l_j : \begin{cases} C^+ = 0, \\ C^- = \dfrac{1}{\sqrt{2}s_W}\delta_{ij} \times \left[1 + \dfrac{\delta e}{e} - \dfrac{\delta s_W}{s_W} + \dfrac{1}{2}\delta Z_{WW} + \dfrac{1}{2}\left(\delta Z_{ii}^{\nu,\mathrm{L}\dagger} + \delta Z_{ii}^{l,\mathrm{L}}\right)\right], \end{cases}$$

$$W^- \bar{l}_j \nu_i : \begin{cases} C^+ = 0, \\ C^- = \dfrac{1}{\sqrt{2}s_W}\delta_{ij} \times \left[1 + \dfrac{\delta e}{e} - \dfrac{\delta s_W}{s_W} + \dfrac{1}{2}\delta Z_{WW} + \dfrac{1}{2}\left(\delta Z_{ii}^{l,\mathrm{L}\dagger} + \delta Z_{ii}^{\nu,\mathrm{L}}\right)\right]. \end{cases}$$

$$(\mathrm{A.15.4})$$

Here, $g_f^\pm$ and $\delta g_f^\pm$ are given by

$$g_f^+ = -\frac{s_W}{c_W}Q_f, \qquad \delta g_f^+ = -\frac{s_W}{c_W}Q_f\left[\frac{\delta e}{e} + \frac{1}{c_W^2}\frac{\delta s_W}{s_W}\right],$$

$$g_f^- = \frac{I_f^3 - s_W^2 Q_f}{s_W c_W}, \qquad \delta g_f^- = \frac{I_f^3}{s_W c_W}\left[\frac{\delta e}{e} + \frac{s_W^2 - c_W^2}{c_W^2}\frac{\delta s_W}{s_W}\right] + \delta g_f^+,$$

$$(\mathrm{A.15.5})$$

and the vector- and axial-vector couplings of the Z boson can be written as follows,

$$v_f^Z = \frac{1}{2}\left(g_f^- + g_f^+\right) = \frac{I_f^3 - 2s_W^2 Q_f}{2s_W c_W} \qquad (\mathrm{A.15.6})$$

and

$$a_f^Z = \frac{1}{2}\left(g_f^- - g_f^+\right) = \frac{I_f^3}{2s_W c_W}. \qquad (\mathrm{A.15.7})$$

A.16 SFF **couplings**

$$= \ ie(C^- \omega_- + C^+ \omega_+),$$

with respective values for S, $\overline{F}_1$, F_2, C^+ and C^-

$$H_1 \overline{f}_i f_j : \begin{cases} C^+ = -\dfrac{c_\alpha}{2s_W M_W} \times \left[\delta_{ij} m_{f,i} \left(1 + \dfrac{\delta e}{e} - \dfrac{\delta s_W}{s_W} + \dfrac{\delta m_{f,i}}{m_{f,i}} \right. \right. \\ \qquad\qquad \left. -\dfrac{1}{2}\dfrac{\delta M_W^2}{M_W^2} + \dfrac{1}{2}\delta Z_{H_1 H_1} - \dfrac{s_\alpha}{c_\alpha}\dfrac{1}{2}\delta Z_{H_1 H_2} \right) \\ \qquad\qquad\qquad \left. +\dfrac{1}{2}\left(m_{f,i}\delta Z_{ij}^{f,\mathrm{R}} + \delta Z_{ij}^{f,\mathrm{L}\dagger} m_{f,j} \right) \right], \\[2em] C^- = -\dfrac{c_\alpha}{2s_W M_W} \times \left[\delta_{ij} m_{f,i} \left(1 + \dfrac{\delta e}{e} - \dfrac{\delta s_W}{s_W} + \dfrac{\delta m_{f,i}}{m_{f,i}} \right. \right. \\ \qquad\qquad \left. -\dfrac{1}{2}\dfrac{\delta M_W^2}{M_W^2} + \dfrac{1}{2}\delta Z_{H_1 H_1} - \dfrac{s_\alpha}{c_\alpha}\dfrac{1}{2}\delta Z_{H_1 H_2} \right) \\ \qquad\qquad\qquad \left. +\dfrac{1}{2}\left(m_{f,i}\delta Z_{ij}^{f,\mathrm{L}} + \delta Z_{ij}^{f,\mathrm{R}\dagger} m_{f,j} \right) \right], \end{cases}$$

$$(A.16.1)$$

$$H_2 \overline{f}_i f_j : \begin{cases} C^+ = \dfrac{s_\alpha}{2s_W M_W} \times \left[\delta_{ij} m_{f,i} \left(1 + \dfrac{\delta e}{e} - \dfrac{\delta s_W}{s_W} + \dfrac{\delta m_{f,i}}{m_{f,i}} \right. \right. \\ \qquad\qquad \left. -\dfrac{1}{2}\dfrac{\delta M_W^2}{M_W^2} + \dfrac{1}{2}\delta Z_{H_2 H_2} - \dfrac{c_\alpha}{s_\alpha}\dfrac{1}{2}\delta Z_{H_1 H_2} \right) \\ \qquad\qquad\qquad \left. +\dfrac{1}{2}\left(m_{f,i}\delta Z_{ij}^{f,\mathrm{R}} + \delta Z_{ij}^{f,\mathrm{L}\dagger} m_{f,j} \right) \right], \\[2em] C^- = \dfrac{s_\alpha}{2s_W M_W} \times \left[\delta_{ij} m_{f,i} \left(1 + \dfrac{\delta e}{e} - \dfrac{\delta s_W}{s_W} + \dfrac{\delta m_{f,i}}{m_{f,i}} \right. \right. \\ \qquad\qquad \left. -\dfrac{1}{2}\dfrac{\delta M_W^2}{M_W^2} + \dfrac{1}{2}\delta Z_{H_2 H_2} - \dfrac{c_\alpha}{s_\alpha}\dfrac{1}{2}\delta Z_{H_1 H_2} \right) \\ \qquad\qquad\qquad \left. +\dfrac{1}{2}\left(m_{f,i}\delta Z_{ij}^{f,\mathrm{L}} + \delta Z_{ij}^{f,\mathrm{R}\dagger} m_{f,j} \right) \right], \end{cases}$$

$$(A.16.2)$$

$$
\varphi_s \overline{f}_i f_j : \begin{cases} C^+ = i\dfrac{1}{2s_W M_W} 2I_f^3 \times \left[\delta_{ij} m_{f,i} \left(1 + \dfrac{\delta e}{e} - \dfrac{\delta s_W}{s_W} + \dfrac{\delta m_{f,i}}{m_{f,i}}\right.\right. \\[2mm] \hspace{6cm} \left.\left. -\dfrac{1}{2}\dfrac{\delta M_W^2}{M_W^2} + \dfrac{1}{2}\delta Z_H\right)\right. \\[2mm] \hspace{4.5cm} \left. +\dfrac{1}{2}\left(m_{f,i}\delta Z_{ij}^{f,\mathrm{R}} + \delta Z_{ij}^{f,\mathrm{L}\dagger} m_{f,j}\right)\right], \\[6mm] C^- = -i\dfrac{1}{2s_W M_W} 2I_f^3 \times \left[\delta_{ij} m_{f,i} \left(1 + \dfrac{\delta e}{e} - \dfrac{\delta s_W}{s_W} + \dfrac{\delta m_{f,i}}{m_{f,i}}\right.\right. \\[2mm] \hspace{6cm} \left.\left. -\dfrac{1}{2}\dfrac{\delta M_W^2}{M_W^2} + \dfrac{1}{2}\delta Z_H\right)\right. \\[2mm] \hspace{4.5cm} \left. +\dfrac{1}{2}\left(m_{f,i}\delta Z_{ij}^{f,\mathrm{L}} + \delta Z_{ij}^{f,\mathrm{R}\dagger} m_{f,j}\right)\right], \end{cases}
$$

$$(\mathrm{A.16.3})$$

$$
\phi^+ \overline{u}_i d_j : \begin{cases} C^+ = -\dfrac{1}{\sqrt{2}s_W M_W} \times \left[\mathbf{V}_{ij} m_{d,j} \left(1 + \dfrac{\delta e}{e} - \dfrac{\delta s_W}{s_W} + \dfrac{\delta m_{d,j}}{m_{d,j}}\right.\right. \\[2mm] \hspace{6cm} \left.\left. -\dfrac{1}{2}\dfrac{\delta M_W^2}{M_W^2} + \dfrac{1}{2}\delta Z_H\right)\right. \\[2mm] \hspace{2.8cm} \left. +\delta\mathbf{V}_{ij} m_{d,j} + \dfrac{1}{2}\sum_k \left(\delta Z_{ik}^{u,\mathrm{L}\dagger}\mathbf{V}_{kj} m_{d,j} + \mathbf{V}_{ik} m_{d,k}\delta Z_{kj}^{d,\mathrm{R}}\right)\right], \\[6mm] C^- = \dfrac{1}{\sqrt{2}s_W M_W} \times \left[m_{u,i}\mathbf{V}_{ij} \left(1 + \dfrac{\delta e}{e} - \dfrac{\delta s_W}{s_W} + \dfrac{\delta m_{u,i}}{m_{u,i}}\right.\right. \\[2mm] \hspace{6cm} \left.\left. -\dfrac{1}{2}\dfrac{\delta M_W^2}{M_W^2} + \dfrac{1}{2}\delta Z_H\right)\right. \\[2mm] \hspace{2.8cm} \left. +m_{u,i}\delta\mathbf{V}_{ij} + \dfrac{1}{2}\sum_k \left(\delta Z_{ik}^{u,\mathrm{R}\dagger} m_{u,k}\mathbf{V}_{kj} + m_{u,i}\mathbf{V}_{ik}\delta Z_{kj}^{d,\mathrm{L}}\right)\right], \end{cases}
$$

$$(\mathrm{A.16.4})$$

$$\phi^- \overline{d}_j u_i : \begin{cases} C^+ = \dfrac{1}{\sqrt{2}s_W M_W} \times \left[\mathbf{V}_{ji}^\dagger m_{u,i} \left(1 + \dfrac{\delta e}{e} - \dfrac{\delta s_W}{s_W} + \dfrac{\delta m_{u,i}}{m_{u,i}} \right. \right. \\ \left. \left. \qquad\qquad\qquad\qquad -\dfrac{1}{2}\dfrac{\delta M_W^2}{M_W^2} + \dfrac{1}{2}\delta Z_H \right) \right. \\ \left. \qquad\qquad +\delta\mathbf{V}_{ji}^\dagger m_{u,i} + \dfrac{1}{2}\sum_k \left(\delta Z_{jk}^{d,\mathrm{L}\dagger}\mathbf{V}_{ki}^\dagger m_{u,i} + \mathbf{V}_{jk}^\dagger m_{u,k}\delta Z_{ki}^{u,\mathrm{R}} \right) \right], \\[2ex] C^- = -\dfrac{1}{\sqrt{2}s_W M_W} \times \left[m_{d,j}\mathbf{V}_{ji}^\dagger \left(1 + \dfrac{\delta e}{e} - \dfrac{\delta s_W}{s_W} + \dfrac{\delta m_{d,j}}{m_{d,j}} \right. \right. \\ \left. \left. \qquad\qquad\qquad\qquad -\dfrac{1}{2}\dfrac{\delta M_W^2}{M_W^2} + \dfrac{1}{2}\delta Z_H \right) \right. \\ \left. \qquad\qquad +m_{d,j}\delta\mathbf{V}_{ji}^\dagger + \dfrac{1}{2}\sum_k \left(\delta Z_{jk}^{d,\mathrm{R}\dagger} m_{d,k}\mathbf{V}_{ki}^\dagger + m_{d,j}\mathbf{V}_{jk}^\dagger \delta Z_{ki}^{u,\mathrm{L}} \right) \right], \end{cases}$$

$$(\mathrm{A.16.5})$$

$$\phi^+ \overline{\nu}_i l_j : \begin{cases} C^+ = -\dfrac{m_{l,i}}{\sqrt{2}s_W M_W}\delta_{ij} \times \left[1 + \dfrac{\delta e}{e} - \dfrac{\delta s_W}{s_W} + \dfrac{\delta m_{l,i}}{m_{l,i}} + \dfrac{1}{2}\delta Z_H \right. \\ \left. \qquad\qquad\qquad\qquad -\dfrac{1}{2}\dfrac{\delta M_W^2}{M_W^2} + \dfrac{1}{2}\left(\delta Z_{ii}^{\nu,\mathrm{L}\dagger} + \delta Z_{ii}^{l,\mathrm{R}} \right) \right], \\[2ex] C^- = 0, \end{cases} \qquad (\mathrm{A.16.6})$$

$$\phi^- \overline{l}_j \nu_i : \begin{cases} C^+ = 0, \\[1ex] C^- = -\dfrac{m_{l,i}}{\sqrt{2}s_W M_W}\delta_{ij} \times \left[1 + \dfrac{\delta e}{e} - \dfrac{\delta s_W}{s_W} + \dfrac{\delta m_{l,i}}{m_{l,i}} + \dfrac{1}{2}\delta Z_H \right. \\ \left. \qquad\qquad\qquad\qquad -\dfrac{1}{2}\dfrac{\delta M_W^2}{M_W^2} + \dfrac{1}{2}\left(\delta Z_{ii}^{l,\mathrm{R}\dagger} + \delta Z_{ii}^{\nu,\mathrm{L}} \right) \right]. \end{cases} \qquad (\mathrm{A.16.7})$$

A.17 VUU **couplings**

$$= iek_{1,\mu}C,$$

with respective values for V, $\overline{U}_1$, U_2 and C

$$A\bar{u}^\pm u^\pm: \quad C = \pm\left[1 + \frac{\delta e}{e} + \frac{1}{2}\delta Z_{AA} - \frac{1}{2}\delta Z_{WW} + \delta\widetilde{Z}_{WW} - \frac{c_W}{2s_W}\delta Z_{ZA}\right],$$

$$Z\bar{u}^\pm u^\pm: \quad C = \mp\frac{c_W}{s_W} \times \left[1 + \frac{\delta e}{e} - \frac{1}{c_W^2}\frac{\delta s_W}{s_W} + \frac{1}{2}\delta Z_{ZZ}\right.$$
$$\left. -\frac{1}{2}\delta Z_{WW} + \delta\widetilde{Z}_{WW} - \frac{s_W}{2c_W}\delta Z_{AZ}\right],$$

$$W^\pm\bar{u}^\pm u^Z: \quad C = \pm\frac{c_W}{s_W} \times \left[1 + \frac{\delta e}{e} - \frac{1}{c_W^2}\frac{\delta s_W}{s_W} + \delta\widetilde{Z}_{ZZ} - \frac{s_W}{c_W}\delta\widetilde{Z}_{AZ}\right],$$

$$W^\pm\bar{u}^Z u^\mp: \quad C = \mp\frac{c_W}{s_W} \times \left[1 + \frac{\delta e}{e} - \frac{1}{c_W^2}\frac{\delta s_W}{s_W} + \frac{1}{2}\delta Z_{WW}\right.$$
$$\left. -\frac{1}{2}\delta Z_{ZZ} + \delta\widetilde{Z}_{WW} + \frac{s_W}{2c_W}\delta Z_{ZA}\right],$$

$$W^\pm\bar{u}^\pm u^A: \quad C = \mp\left[1 + \frac{\delta e}{e} + \delta\widetilde{Z}_{AA} - \frac{c_W}{s_W}\delta\widetilde{Z}_{ZA}\right],$$

$$W^\pm\bar{u}^A u^\mp: \quad C = \pm\left[1 + \frac{\delta e}{e} + \frac{1}{2}\delta Z_{WW} - \frac{1}{2}\delta Z_{AA} + \delta\widetilde{Z}_{WW} + \frac{c_W}{2s_W}\delta Z_{AZ}\right].$$

$$(A.17.1)$$

A.18 SUU **couplings**

$$= ieC,$$

with respective values for S, $\overline{U}_1$, U_2 and C

$$H_1\bar{u}^Z u^Z: \quad C = -\frac{c_\alpha M_Z}{2s_W c_W} \times \left[1 + \frac{\delta e}{e} + \frac{s_W^2 - c_W^2}{c_W^2}\frac{\delta s_W}{s_W} + \frac{1}{2}\delta Z_{H_1 H_1}\right.$$
$$\left. -\frac{1}{2}\delta Z_H + \delta\widetilde{Z}_{ZZ} - \frac{s_\alpha}{2c_\alpha}\delta Z_{H_1 H_2}\right],$$

$$(A.18.1)$$

$$H_2\bar{u}^Z u^Z: \quad C = \frac{s_\alpha M_Z}{2 s_W c_W} \times \left[1 + \frac{\delta e}{e} + \frac{s_W^2 - c_W^2}{c_W^2} \frac{\delta s_W}{s_W} + \frac{1}{2}\delta Z_{H_2 H_2} \right.$$

$$\left. - \frac{1}{2}\delta Z_H + \delta\widetilde{Z}_{ZZ} - \frac{c_\alpha}{2 s_\alpha}\delta Z_{H_1 H_2} \right],$$

$$H_1\bar{u}^Z u^A: \quad C = -\frac{c_\alpha M_Z}{2 s_W c_W}\delta\widetilde{Z}_{ZA},$$

$$H_2\bar{u}^Z u^A: \quad C = \frac{s_\alpha M_Z}{2 s_W c_W}\delta\widetilde{Z}_{ZA},$$

$$H_1\bar{u}^\pm u^\pm: \quad C = -\frac{c_\alpha M_W}{2 s_W} \times \left[1 + \frac{\delta e}{e} - \frac{\delta s_W}{s_W} + \frac{1}{2}\delta Z_{H_1 H_1} \right.$$

$$\left. - \frac{s_\alpha}{2 c_\alpha}\delta Z_{H_1 H_2} + \delta\widetilde{Z}_{WW} - \frac{1}{2}\delta Z_H \right],$$

$$H_2\bar{u}^\pm u^\pm: \quad C = \frac{s_\alpha M_W}{2 s_W} \times \left[1 + \frac{\delta e}{e} - \frac{\delta s_W}{s_W} + \frac{1}{2}\delta Z_{H_2 H_2} \right.$$

$$\left. - \frac{c_\alpha}{2 s_\alpha}\delta Z_{H_1 H_2} + \delta\widetilde{Z}_{WW} - \frac{1}{2}\delta Z_H \right],$$

$$\text{(A.18.2)}$$

$$\varphi_{\mathrm{s}}\bar{u}^\pm u^\pm: \quad C = \mp i\frac{M_W}{2 s_W} \times \left[1 + \frac{\delta e}{e} - \frac{\delta s_W}{s_W} + \delta\widetilde{Z}_{WW} \right],$$

$$\phi^\pm\bar{u}^Z u^\mp: \quad C = \frac{M_Z}{2 s_W} \times \left[1 + \frac{\delta e}{e} - \frac{\delta s_W}{s_W} + \delta\widetilde{Z}_{WW} \right],$$

$$\phi^\pm\bar{u}^\pm u^Z: \quad C = \frac{s_W^2 - c_W^2}{2 s_W c_W}M_W \times \left[1 + \frac{\delta e}{e} + \frac{1}{(s_W^2 - c_W^2)c_W^2}\frac{\delta s_W}{s_W} \right.$$

$$\left. + \delta\widetilde{Z}_{ZZ} + \frac{2 s_W c_W}{s_W^2 - c_W^2}\delta\widetilde{Z}_{AZ} \right],$$

$$\phi^\pm\bar{u}^\pm u^A: \quad C = M_W \times \left[1 + \frac{\delta e}{e} + \delta\widetilde{Z}_{AA} + \frac{s_W^2 - c_W^2}{2 s_W c_W}\delta\widetilde{Z}_{ZA} \right],$$

$$H_1\bar{u}^{Z'} u^{Z'}: \quad C = -\frac{s_\alpha M_{Z'}^2}{e v_{\mathrm{h}}} \times \left[1 + \delta\widetilde{Z}_{Z'Z'} + \frac{1}{2}\delta Z_{H_1 H_1} + \frac{1}{2}\frac{\delta M_{Z'}^2}{M_{Z'}^2} \right.$$

$$\left. - \frac{\delta v_{\mathrm{h}}}{v_{\mathrm{h}}} - \frac{1}{2}\delta Z_\chi + \frac{c_\alpha}{2 s_\alpha}\delta Z_{H_1 H_2} \right],$$

$$H_2\bar{u}^{Z'} u^{Z'}: \quad C = -\frac{c_\alpha M_{Z'}^2}{e v_{\mathrm{h}}} \times \left[1 + \delta\widetilde{Z}_{Z'Z'} + \frac{1}{2}\delta Z_{H_2 H_2} + \frac{1}{2}\frac{\delta M_{Z'}^2}{M_{Z'}^2} \right.$$

$$\left. - \frac{\delta v_{\mathrm{h}}}{v_{\mathrm{h}}} - \frac{1}{2}\delta Z_\chi + \frac{s_\alpha}{2 c_\alpha}\delta Z_{H_1 H_2} \right].$$

A.19 SSS counterterms

$$
\begin{aligned}
\delta C_{H_1H_1H_1} = {}& \delta t_{H_1} \times \frac{4\left(c_\alpha^4 v_h^2 + s_\alpha^4 v_s^2\right)}{M_{H_1}^2 v_s v_h \left(c_\alpha^3 v_h - 3c_\alpha(s_\alpha^2-1)v_h + 4s_\alpha^3 v_s\right)} + \delta t_{H_2} \times \frac{4c_\alpha^3 s_\alpha v_s^2 - 4c_\alpha^3 s_\alpha v_h^2}{M_{H_2}^2 v_s v_h \left(c_\alpha^3 v_h - 3c_\alpha(s_\alpha^2-1)v_h + 4s_\alpha^3 v_s\right)} \\
& - \delta v_s \times \frac{4c_\alpha^3 v_h}{v_s \left(c_\alpha^3 v_h - 3c_\alpha(s_\alpha^2-1)v_h + 4s_\alpha^3 v_s\right)} - \delta v_h \times \frac{4s_\alpha^3 v_s}{v_h \left(c_\alpha^3 v_h - 3c_\alpha(s_\alpha^2-1)v_h + 4s_\alpha^3 v_s\right)} \\
& + \delta M_{H_1}^2 \times \frac{1}{M_{H_1}^2} - \delta M_{H_1 H_2}^2 \times \frac{4c_\alpha s_\alpha(c_\alpha v_h - s_\alpha v_s)}{M_{H_1}^2 \left(c_\alpha^3 v_h - 3c_\alpha(s_\alpha^2-1)v_h + 4s_\alpha^3 v_s\right)} - \delta Z_{H_1 H_2} \times \frac{2c_\alpha s_\alpha\left(2M_{H_1}^2 + M_{H_2}^2\right)(c_\alpha v_h - s_\alpha v_s)}{M_{H_1}^2 \left(c_\alpha^3 v_h - 3c_\alpha(s_\alpha^2-1)v_h + 4s_\alpha^3 v_s\right)} + \delta Z_{H_1 H_1} \times \frac{3}{2}, \\[2ex]
\delta C_{H_1H_1H_2} = {}& \delta t_{H_1} \times \frac{3c_\alpha v_h + 3s_\alpha v_s}{2M_{H_1}^2 v_s v_h + M_{H_2}^2 v_s v_h} + \delta t_{H_2} \times \frac{3c_\alpha s_\alpha\left(v_s^2 + v_h^2\right)}{v_s v_h\left(2M_{H_1}^2 + M_{H_2}^2\right)(s_\alpha v_s - c_\alpha v_h)} + \delta v_s \times \frac{c_\alpha v_h}{s_\alpha v_s^2 - c_\alpha v_s v_h} + \delta v_h \times \frac{s_\alpha v_s}{c_\alpha v_h^2 - s_\alpha v_s v_h} \\
& + \delta M_{H_1}^2 \times \frac{2}{2M_{H_1}^2 + M_{H_2}^2} + \delta M_{H_2}^2 \times \frac{1}{2M_{H_1}^2 + M_{H_2}^2} - \delta M_{H_1 H_2}^2 \times \frac{\left(\left(c_\alpha + \frac{1}{c_\alpha}\right)v_s + \left(s_\alpha + \frac{1}{s_\alpha}\right)v_h\right)}{\left(2M_{H_1}^2 + M_{H_2}^2\right)(c_\alpha v_h - s_\alpha v_s)} \\
& + \delta Z_{H_1 H_2} \times \frac{\left(c_\alpha v_s\left(M_{H_1}^2 - 4M_{H_2}^2\right) - 3M_{H_1}^2\left(\frac{v_s}{c_\alpha} + \frac{v_h}{s_\alpha}\right) + s_\alpha v_h\left(M_{H_1}^2 - 4M_{H_2}^2\right)\right)}{2\left(2M_{H_1}^2 + M_{H_2}^2\right)(c_\alpha v_h - s_\alpha v_s)} + \delta Z_{H_1 H_1} + \delta Z_{H_2 H_2} \times \frac{1}{2}, \\[2ex]
\delta C_{H_1H_2H_2} = {}& \delta t_{H_1} \times \frac{3c_\alpha s_\alpha\left(v_s^2 + v_h^2\right)}{v_s v_h\left(M_{H_1}^2 + 2M_{H_2}^2\right)(c_\alpha v_s + s_\alpha v_h)} + \delta t_{H_2} \times \frac{24c_\alpha^3 s_\alpha v_s^2 - 24c_\alpha^3 s_\alpha v_h^2}{8c_\alpha s_\alpha v_s v_h\left(M_{H_1}^2 + 2M_{H_2}^2\right)(c_\alpha v_s + s_\alpha v_h)} - \delta v_s \times \frac{s_\alpha v_h}{v_s(c_\alpha v_s + s_\alpha v_h)} - \delta v_h \times \frac{c_\alpha v_s}{v_h(c_\alpha v_s + s_\alpha v_h)} \\
& + \delta M_{H_1}^2 \times \frac{8c_\alpha s_\alpha v_s^2 v_h + 8c_\alpha s_\alpha^2 v_s v_h^2}{8c_\alpha s_\alpha v_s v_h\left(M_{H_1}^2 + 2M_{H_2}^2\right)(c_\alpha v_s + s_\alpha v_h)} + \delta M_{H_2}^2 \times \frac{16c_\alpha^2 s_\alpha v_s^2 v_h + 16c_\alpha s_\alpha^2 v_s^2 v_h}{8c_\alpha s_\alpha v_s v_h\left(M_{H_1}^2 + 2M_{H_2}^2\right)(c_\alpha v_s + s_\alpha v_h)} + \delta M_{H_1 H_2}^2 \times \frac{\left(-2c_\alpha v_s^2 v_h(c_\alpha^2 - 3s_\alpha^2 - 5) - 2s_\alpha v_s v_h^2(3c_\alpha^2 - s_\alpha^2 + 5)\right)}{8c_\alpha s_\alpha v_s v_h\left(M_{H_1}^2 + 2M_{H_2}^2\right)(c_\alpha v_s + s_\alpha v_h)} \\
& + \delta Z_{H_1 H_2} \times \frac{\left(c_\alpha v_s^2 v_h\left(M_{H_2}^2(c_\alpha^2 - 3s_\alpha^2 + 11) - 4M_{H_1}^2(c_\alpha^2 - s_\alpha^2)\right) - 2s_\alpha v_s v_h^2\left(4M_{H_1}^2 - M_{H_2}^2\right) - 2s_\alpha v_s^3\left(4M_{H_1}^2 + 5M_{H_2}^2\right)\right)}{8c_\alpha s_\alpha v_s v_h\left(M_{H_1}^2 + 2M_{H_2}^2\right)(c_\alpha v_s + s_\alpha v_h)} \\
& + \delta Z_{H_1 H_1} \times \frac{\left(4c_\alpha^2 s_\alpha v_s^2 v_h\left(M_{H_1}^2 + 2M_{H_2}^2\right) + 4c_\alpha s_\alpha^2 v_s v_h^2\left(M_{H_1}^2 + 2M_{H_2}^2\right)\right)}{8c_\alpha s_\alpha v_s v_h\left(M_{H_1}^2 + 2M_{H_2}^2\right)(c_\alpha v_s + s_\alpha v_h)} + \delta Z_{H_2 H_2} \times \frac{\left(8c_\alpha^2 s_\alpha v_s^2 v_h\left(M_{H_1}^2 + 2M_{H_2}^2\right) + 8c_\alpha s_\alpha^2 v_s v_h^2\left(M_{H_1}^2 + 2M_{H_2}^2\right)\right)}{8c_\alpha s_\alpha v_s v_h\left(M_{H_1}^2 + 2M_{H_2}^2\right)(c_\alpha v_s + s_\alpha v_h)}, \\[2ex]
\delta C_{H_2H_2H_2} = {}& \delta t_{H_1} \times \frac{4\left(c_\alpha s_\alpha^3 v_h - c_\alpha^3 s_\alpha v_s\right)}{M_{H_1}^2 v_s v_h\left(4s_\alpha^3 v_h - c_\alpha v_s(c_\alpha^2 - 3s_\alpha^2 + 3)\right)} - \delta t_{H_2} \times \frac{4\left(c_\alpha^4 v_s^2 + s_\alpha^4 v_h^2\right)}{M_{H_2}^2 v_s v_h\left(4s_\alpha^3 v_h - c_\alpha v_s(c_\alpha^2 - 3s_\alpha^2 + 3)\right)} \\
& + \delta v_s \times \frac{4c_\alpha^3 v_h}{v_s\left(c_\alpha v_s(c_\alpha^2 - 3s_\alpha^2 + 3) - 4s_\alpha^3 v_h\right)} + \delta v_h \times \frac{4s_\alpha^3 v_h}{v_h\left(4s_\alpha^3 v_h - c_\alpha v_s(c_\alpha^2 - 3s_\alpha^2 + 3)\right)} \\
& + \delta M_{H_2}^2 \times \frac{1}{M_{H_2}^2} - \delta M_{H_1 H_2}^2 \times \frac{4c_\alpha s_\alpha(c_\alpha v_s + s_\alpha v_h)}{M_{H_2}^2\left(4s_\alpha^3 v_h - c_\alpha v_s(c_\alpha^2 - 3s_\alpha^2 + 3)\right)} - \delta Z_{H_1 H_2} \times \frac{2c_\alpha s_\alpha\left(M_{H_1}^2 + 2M_{H_2}^2\right)(c_\alpha v_s + s_\alpha v_h)}{M_{H_2}^2\left(4s_\alpha^3 v_h - c_\alpha v_s(c_\alpha^2 - 3s_\alpha^2 + 3)\right)} + \delta Z_{H_2 H_2} \times \frac{3}{2}.
\end{aligned}
\tag{A.19.1}
$$

A.20 SSSS counterterms

$$
\begin{aligned}
\delta C_{H_1H_1H_1H_1} = \ & \delta t_{H_1} \times \frac{\left(\left(M_{H_1}^2 - M_{H_2}^2\right) v_h^2 c_\alpha^6 + M_{H_2}^2 v_h^2 c_\alpha^4 - \left(M_{H_1}^2 - M_{H_2}^2\right) s_\alpha^3 v_s (s_\alpha v_s - 2c_\alpha v_h) c_\alpha^2 + M_{H_1}^2 s_\alpha^4 v_s^2\right)\left(v_h^3 c_\alpha^5 + s_\alpha^5 v_s^3\right)}{v_s v_h} \\[4pt]
& + \delta t_{H_2} \times \frac{\left(\left(M_{H_1}^2 - M_{H_2}^2\right) v_h^2 c_\alpha^6 + M_{H_2}^2 v_h^2 c_\alpha^4 - \left(M_{H_1}^2 - M_{H_2}^2\right) s_\alpha^3 v_s (s_\alpha v_s - 2c_\alpha v_h) c_\alpha^2 + M_{H_1}^2 s_\alpha^4 v_s^2\right)\left(2c_\alpha s_\alpha v_s^3 - 2c_\alpha^4 s_\alpha v_h^3\right)}{2 v_s v_h} \\[4pt]
& - \delta v_s \times \frac{\left(\left(M_{H_1}^2 - M_{H_2}^2\right) v_h^2 c_\alpha^6 + M_{H_2}^2 v_h^2 c_\alpha^4 - \left(M_{H_1}^2 - M_{H_2}^2\right) s_\alpha^3 v_s + c_\alpha^3 \left(M_{H_1}^2 - M_{H_2}^2\right) v_h\right) 2c_\alpha^3 v_h \left(c_\alpha v_h M_{H_2}^2 + \left(M_{H_1}^2 - M_{H_2}^2\right) s_\alpha v_s c_\alpha^2 + 2c_\alpha^3 \left(M_{H_1}^2 - M_{H_2}^2\right) s_\alpha^3 v_s v_h + M_{H_1}^2 s_\alpha^4 v_s^2\right)}{v_s} \\[4pt]
& - \delta v_h \times \frac{\left(-\left(M_{H_1}^2 - M_{H_2}^2\right) s_\alpha v_s c_\alpha^2 + c_\alpha^3 \left(M_{H_1}^2 - M_{H_2}^2\right) v_h + M_{H_1}^2 s_\alpha v_s\right) 2 s_\alpha^3 v_s \left(\left(M_{H_1}^2 - M_{H_2}^2\right) v_h^2 c_\alpha^6 + M_{H_2}^2 v_h^2 c_\alpha^4 - \left(M_{H_1}^2 - M_{H_2}^2\right) s_\alpha^4 v_s^2 c_\alpha^2 + 2c_\alpha^3 \left(M_{H_1}^2 - M_{H_2}^2\right) s_\alpha^3 v_s v_h + M_{H_1}^2 s_\alpha^4 v_s^2\right)}{v_h} \\[4pt]
& + \delta M_{H_1}^2 \times 16 \frac{\left(\left(M_{H_1}^2 - M_{H_2}^2\right) v_h^2 c_\alpha^6 + M_{H_2}^2 v_h^2 c_\alpha^4 - \left(M_{H_1}^2 - M_{H_2}^2\right) s_\alpha^4 v_s^2 c_\alpha^2 + 2c_\alpha^3 \left(M_{H_1}^2 - M_{H_2}^2\right) s_\alpha^3 v_s v_h + M_{H_1}^2 s_\alpha^4 v_s^2\right)}{\left(4 s_\alpha^3 v_s + 3 c_\alpha v_h + \left(c_\alpha^3 - 3c_\alpha s_\alpha^2 v_h\right)\right)^2} \\[4pt]
& + \delta M_{H_2}^2 \times \frac{\left(\left(M_{H_1}^2 - M_{H_2}^2\right) v_h^2 c_\alpha^6 + M_{H_2}^2 v_h^2 c_\alpha^4 - \left(M_{H_1}^2 - M_{H_2}^2\right) s_\alpha^4 v_s^2 c_\alpha^2 + 2c_\alpha^3 \left(M_{H_1}^2 - M_{H_2}^2\right) s_\alpha^3 v_s v_h + M_{H_1}^2 s_\alpha^4 v_s^2\right)}{c_\alpha^2 s_\alpha^2 \left(c_\alpha v_h - s_\alpha v_s\right)^2} \\[4pt]
& - \delta M_{H_1H_2}^2 \times \frac{\left(\left(M_{H_1}^2 - M_{H_2}^2\right) v_h^2 c_\alpha^6 + M_{H_2}^2 v_h^2 c_\alpha^4 - \left(M_{H_1}^2 - M_{H_2}^2\right) s_\alpha^4 v_s^2 c_\alpha^2 + 2c_\alpha^3 \left(M_{H_1}^2 - M_{H_2}^2\right) s_\alpha^3 v_s v_h + M_{H_1}^2 s_\alpha^4 v_s^2\right) 2 c_\alpha s_\alpha \left(v_h^2 c_\alpha^4 - 2c_\alpha^3 s_\alpha v_s v_h + s_\alpha v_s v_h c_\alpha - s_\alpha^4 v_s^2\right)}{\left(M_{H_1}^2 - M_{H_2}^2\right)} \\[4pt]
& - \delta Z_{H_1H_2} \times \frac{s_\alpha c_\alpha \left(\left(\left(3 M_{H_1}^2 + M_{H_2}^2\right) s_\alpha + \left(M_{H_1}^2 - M_{H_2}^2\right) \left(3c_\alpha^2 s_\alpha - s_\alpha^3\right)\right) v_s + c_\alpha \left(3 M_{H_1}^2 + M_{H_2}^2\right) v_h + \left(M_{H_1}^2 - M_{H_2}^2\right) \left(c_\alpha^3 - 3c_\alpha s_\alpha^2\right) v_h\right)\left(c_\alpha v_h - s_\alpha v_s\right)}{2 \left(\left(M_{H_1}^2 - M_{H_2}^2\right) v_h^2 c_\alpha^6 + M_{H_2}^2 v_h^2 c_\alpha^4 - \left(M_{H_1}^2 - M_{H_2}^2\right) s_\alpha^4 v_s^2 c_\alpha^2 + 2c_\alpha^3 \left(M_{H_1}^2 - M_{H_2}^2\right) s_\alpha^3 v_s v_h + M_{H_1}^2 s_\alpha^4 v_s^2\right)} \\[4pt]
& + \delta Z_{H_1H_1} \times 2,
\end{aligned}
$$

(A.20.1)

$$
\begin{aligned}
\delta C_{H_1H_1H_1H_2} = \;& \delta t_{H_1} \times \frac{4\left(s_\alpha^2 v_{\rm s}^2 + c_\alpha s_\alpha v_{\rm h} v_{\rm s} + c_\alpha^2 v_{\rm h}^2\right)}{v_{\rm s} v_{\rm h}\left(\left(3M_{H_1}^2+M_{H_2}^2\right)s_\alpha v_{\rm s} + \left(M_{H_2}^2-M_{H_1}^2\right)\left(3c_\alpha^2 s_\alpha - s_\alpha^3\right)v_{\rm s} + c_\alpha\left(3M_{H_1}^2+M_{H_2}^2\right)v_{\rm h} + \left(M_{H_1}^2-M_{H_2}^2\right)\left(c_\alpha^3 - 3c_\alpha s_\alpha^2\right)v_{\rm h}\right)} \\[4pt]
& - \delta t_{H_2} \times \frac{v_{\rm s} v_{\rm h}(c_\alpha v_{\rm h} - s_\alpha v_{\rm s})\left(\left(3M_{H_1}^2+M_{H_2}^2\right)s_\alpha v_{\rm s} + \left(M_{H_2}^2-M_{H_1}^2\right)\left(3c_\alpha^2 s_\alpha - s_\alpha^3\right)v_{\rm s} + c_\alpha\left(3M_{H_1}^2+M_{H_2}^2\right)v_{\rm h} + \left(M_{H_1}^2-M_{H_2}^2\right)\left(c_\alpha^3 - 3c_\alpha s_\alpha^2\right)v_{\rm h}\right)}{4c_\alpha s_\alpha\left(s_\alpha v_{\rm s}^3 + c_\alpha v_{\rm h}^3\right)} \\[4pt]
& + \delta v_{\rm s} \times \frac{v_{\rm h}\left(4(c_\alpha^2 - s_\alpha^2)v_{\rm h} M_{H_1}^2 + \left(3M_{H_1}^2+M_{H_2}^2\right)s_\alpha v_{\rm s} + \left(M_{H_2}^2-M_{H_1}^2\right)\left(3c_\alpha^2 s_\alpha - s_\alpha^3\right)v_{\rm s} + c_\alpha\left(3M_{H_1}^2+M_{H_2}^2\right)v_{\rm h} + \left(M_{H_1}^2-M_{H_2}^2\right)\left(c_\alpha^4 - 6s_\alpha^2 c_\alpha^2 + s_\alpha^4\right)v_{\rm h} - \left(4c_\alpha^3 s_\alpha - 4c_\alpha s_\alpha^3\right)v_{\rm s}\right)\right)}{v_{\rm s}(s_\alpha v_{\rm s} - c_\alpha v_{\rm h})\left(\left(3M_{H_1}^2+M_{H_2}^2\right)s_\alpha v_{\rm s} + \left(M_{H_2}^2-M_{H_1}^2\right)\left(3c_\alpha^2 s_\alpha - s_\alpha^3\right)v_{\rm s} + c_\alpha\left(3M_{H_1}^2+M_{H_2}^2\right)v_{\rm h} + \left(M_{H_1}^2-M_{H_2}^2\right)\left(c_\alpha^3 - 3c_\alpha s_\alpha^2\right)v_{\rm h}\right)} \\[4pt]
& + \delta v_{\rm h} \times \frac{v_{\rm s}\left(-4(c_\alpha^2 - s_\alpha^2)v_{\rm s} M_{H_1}^2 + \left(3M_{H_1}^2+M_{H_2}^2\right)s_\alpha v_{\rm s} + \left(M_{H_2}^2-M_{H_1}^2\right)\left(3c_\alpha^2 s_\alpha - s_\alpha^3\right)v_{\rm s} + c_\alpha\left(3M_{H_1}^2+M_{H_2}^2\right)v_{\rm h} + \left(M_{H_1}^2-M_{H_2}^2\right)\left(c_\alpha^4 - 6s_\alpha^2 c_\alpha^2 + s_\alpha^4\right)v_{\rm h} + \left(4c_\alpha^3 s_\alpha - 4c_\alpha s_\alpha^3\right)v_{\rm s}\right)\right)}{v_{\rm h}(c_\alpha v_{\rm h} - s_\alpha v_{\rm s})\left(\left(3M_{H_1}^2+M_{H_2}^2\right)s_\alpha v_{\rm s} + \left(M_{H_2}^2-M_{H_1}^2\right)\left(3c_\alpha^2 s_\alpha - s_\alpha^3\right)v_{\rm s} + c_\alpha\left(3M_{H_1}^2+M_{H_2}^2\right)v_{\rm h} + \left(M_{H_1}^2-M_{H_2}^2\right)\left(c_\alpha^3 - 3c_\alpha s_\alpha^2\right)v_{\rm h}\right)} \\[4pt]
& + \delta M_{H_1}^2 \times \frac{\left(3M_{H_1}^2+M_{H_2}^2\right)s_\alpha v_{\rm s} + \left(M_{H_2}^2-M_{H_1}^2\right)\left(3c_\alpha^2 s_\alpha - s_\alpha^3\right)v_{\rm s} + c_\alpha\left(3M_{H_1}^2+M_{H_2}^2\right)v_{\rm h} + \left(M_{H_1}^2-M_{H_2}^2\right)\left(c_\alpha^3 - 3c_\alpha s_\alpha^2\right)v_{\rm h}}{4\left(s_\alpha^3 v_{\rm s} + c_\alpha^3 v_{\rm h}\right)} \\[4pt]
& + \delta M_{H_2}^2 \times \frac{\left(3M_{H_1}^2+M_{H_2}^2\right)s_\alpha v_{\rm s} + \left(M_{H_2}^2-M_{H_1}^2\right)\left(3c_\alpha^2 s_\alpha - s_\alpha^3\right)v_{\rm s} + c_\alpha\left(3M_{H_1}^2+M_{H_2}^2\right)v_{\rm h} + \left(M_{H_1}^2-M_{H_2}^2\right)\left(c_\alpha^3 - 3c_\alpha s_\alpha^2\right)v_{\rm h}}{4c_\alpha s_\alpha\left(c_\alpha v_{\rm s} + s_\alpha v_{\rm h}\right)} \\[4pt]
& + \delta M_{H_1 H_2}^2 \times \frac{(c_\alpha v_{\rm h} - s_\alpha v_{\rm s})\left(\left(3M_{H_1}^2+M_{H_2}^2\right)s_\alpha v_{\rm s} + \left(M_{H_2}^2-M_{H_1}^2\right)\left(3c_\alpha^2 s_\alpha - s_\alpha^3\right)v_{\rm s} + c_\alpha\left(3M_{H_1}^2+M_{H_2}^2\right)v_{\rm h} + \left(M_{H_1}^2-M_{H_2}^2\right)\left(c_\alpha^3 - 3c_\alpha s_\alpha^2\right)v_{\rm h}\right)}{\left(-4v_{\rm s} v_{\rm h}(c_\alpha^2 - s_\alpha^2)^2 - 4c_\alpha s_\alpha\left(v_{\rm s}^2 + v_{\rm h}^2 + (c_\alpha^2 - s_\alpha^2)(v_{\rm h}^2 - v_{\rm s}^2)\right)\right)} \\[4pt]
& + \delta Z_{H_1 H_2} \times \frac{-\dfrac{4M_{H_1}^2 s_\alpha v_{\rm s}^2}{c_\alpha} + 2v_{\rm s} v_{\rm h}\left(c_\alpha^4 - 6c_\alpha^2 s_\alpha^2 + s_\alpha^4\right)\left(M_{H_1}^2-M_{H_2}^2\right) + 2v_{\rm s} v_{\rm h}\left(M_{H_2}^2 - M_{H_1}^2\right)}{-8c_\alpha s_\alpha v_{\rm s} v_{\rm h}(c_\alpha^2 - s_\alpha^2)\left(M_{H_1}^2-M_{H_2}^2\right) + (v_{\rm h}^2 - v_{\rm s}^2)\left(\left(c_\alpha^4 - 6c_\alpha^2 s_\alpha^2 + s_\alpha^4\right)\left(M_{H_1}^2-M_{H_2}^2\right) + 4M_{H_1}^2(c_\alpha^2 - s_\alpha^2)\right)\left(v_{\rm s}^2 + v_{\rm h}^2\right)} \\[4pt]
& + \delta Z_{H_1 H_1} \times \frac{\left(4c_\alpha s_\alpha(c_\alpha^2 - s_\alpha^2)\left(M_{H_1}^2-M_{H_2}^2\right) + (v_{\rm h}^2 - v_{\rm s}^2)\left(\left(c_\alpha^4 - 6c_\alpha^2 s_\alpha^2 + s_\alpha^4\right)(v_{\rm s}^2 - v_{\rm h}^2) - \dfrac{4c_\alpha M_{H_1}^2 v_{\rm h}^2}{s_\alpha} - 8c_\alpha M_{H_2}^2 s_\alpha\left(v_{\rm s}^2 + v_{\rm h}^2\right)\right)\right)}{-8c_\alpha s_\alpha v_{\rm s} v_{\rm h}(c_\alpha^2 - s_\alpha^2)\left(M_{H_1}^2-M_{H_2}^2\right) + \left(c_\alpha^4 - 6c_\alpha^2 s_\alpha^2 + s_\alpha^4\right)\left(M_{H_1}^2-M_{H_2}^2\right) + 3M_{H_1}^2 + M_{H_2}^2 + 4M_{H_1}^2(c_\alpha^2 - s_\alpha^2)\left(v_{\rm s}^2 + v_{\rm h}^2\right)} \\[4pt]
& + \delta Z_{H_1 H_1} \times \frac{3}{2} + \delta Z_{H_2 H_2} \times \frac{1}{2},
\end{aligned}
$$

$$\tag{A.20.2}$$

$$
\begin{aligned}
\delta C_{H_1 H_1 H_2 H_2} = {}& \delta t_{H_1} \times \frac{24 c_\alpha s_\alpha \left(s_\alpha v_s^3 + c_\alpha v_h^3\right)}{v_s v_h} \times \Big(6\left(M_{H_1}^2 - M_{H_2}^2\right)\left(c_\alpha^4 - 6 s_\alpha^2 c_\alpha^2 + s_\alpha^4\right) v_s v_h + 12 c_\alpha \left(M_{H_1}^2 + M_{H_2}^2\right) s_\alpha \left(v_s^2 + v_h^2\right) + \left(M_{H_1}^2 - M_{H_2}^2\right)\left(2 v_s v_h + 3(4 c_\alpha^3 s_\alpha - 4 c_\alpha s_\alpha^3)\left(v_h^2 - v_s^2\right)\right)\Big) \\[4pt]
& + \delta t_{H_2} \times \frac{24 c_\alpha s_\alpha \left(c_\alpha v_s^3 - s_\alpha v_h^3\right)}{v_s v_h} \times \Big(6\left(M_{H_1}^2 - M_{H_2}^2\right)\left(c_\alpha^4 - 6 s_\alpha^2 c_\alpha^2 + s_\alpha^4\right) v_s v_h + 12 c_\alpha \left(M_{H_1}^2 + M_{H_2}^2\right) s_\alpha \left(v_s^2 + v_h^2\right) + \left(M_{H_1}^2 + M_{H_2}^2\right) s_\alpha v_h + \left(M_{H_1}^2 - M_{H_2}^2\right)\left(2 v_s v_h + 3(4 c_\alpha^3 s_\alpha - 4 c_\alpha s_\alpha^3)\left(v_h^2 - v_s^2\right)\right)\Big) \\[4pt]
& - \delta v_s \times \frac{2 v_h \left(3\left(M_{H_1}^2 - M_{H_2}^2\right)\left(c_\alpha^4 - 6 s_\alpha^2 c_\alpha^2 + s_\alpha^4\right) v_s v_h + 12 c_\alpha \left(M_{H_1}^2 + M_{H_2}^2\right) s_\alpha \left(v_s^2 + v_h^2\right) + \left(M_{H_1}^2 - M_{H_2}^2\right)\left(v_s + 3(4 c_\alpha^3 s_\alpha - 4 c_\alpha s_\alpha^3) v_h\right)\right)}{v_s} \\[4pt]
& - \delta v_h \times \frac{2 v_s \left(12 c_\alpha \left(M_{H_1}^2 + M_{H_2}^2\right) s_\alpha v_s + 3\left(M_{H_1}^2 - M_{H_2}^2\right)\left(c_\alpha^4 - 6 s_\alpha^2 c_\alpha^2 + s_\alpha^4\right) v_s v_h + \left(M_{H_1}^2 - M_{H_2}^2\right)\left(v_h - 3(4 c_\alpha^3 s_\alpha - 4 c_\alpha s_\alpha^3) v_s\right)\right)}{v_h} \\[4pt]
& + \delta M_{H_1}^2 \times \frac{6 \left(M_{H_1}^2 - M_{H_2}^2\right)\left(c_\alpha^4 - 6 s_\alpha^2 c_\alpha^2 + s_\alpha^4\right) v_s v_h + 12 c_\alpha \left(M_{H_1}^2 + M_{H_2}^2\right) s_\alpha \left(v_s^2 + v_h^2\right) + \left(M_{H_1}^2 - M_{H_2}^2\right)\left(2 v_s v_h + 3(4 c_\alpha^3 s_\alpha - 4 c_\alpha s_\alpha^3)\left(v_h^2 - v_s^2\right)\right)}{-3(4 c_\alpha^3 s_\alpha - 4 c_\alpha s_\alpha^3) v_s^2 + 6 \left(c_\alpha^4 - 6 s_\alpha^2 c_\alpha^2 + s_\alpha^4\right) v_s v_h + 12 c_\alpha \left(M_{H_1}^2 + M_{H_2}^2\right) s_\alpha} \\[4pt]
& + \delta M_{H_2}^2 \times \frac{6 \left(M_{H_1}^2 - M_{H_2}^2\right)\left(c_\alpha^4 - 6 s_\alpha^2 c_\alpha^2 + s_\alpha^4\right) v_s v_h + 12 c_\alpha \left(M_{H_1}^2 + M_{H_2}^2\right) s_\alpha \left(v_s^2 + v_h^2\right) + \left(M_{H_1}^2 - M_{H_2}^2\right)\left(2 v_s v_h + 3(4 c_\alpha^3 s_\alpha - 4 c_\alpha s_\alpha^3)\left(v_h^2 - v_s^2\right)\right)}{3(4 c_\alpha^3 s_\alpha - 4 c_\alpha s_\alpha^3) v_s^2 - 6 \left(c_\alpha^4 - 6 s_\alpha^2 c_\alpha^2 + s_\alpha^4\right) v_h v_s - 2 v_h v_s + 12 c_\alpha s_\alpha v_h^2} \\[4pt]
& + \delta M_{H_1 H_2}^2 \times \frac{6 \left(M_{H_1}^2 - M_{H_2}^2\right)\left(c_\alpha^4 - 6 s_\alpha^2 c_\alpha^2 + s_\alpha^4\right) v_s v_h + 12 c_\alpha \left(M_{H_1}^2 + M_{H_2}^2\right) s_\alpha \left(v_s^2 + v_h^2\right) + \left(M_{H_1}^2 - M_{H_2}^2\right)\left(2 v_s v_h + 3(4 c_\alpha^3 s_\alpha - 4 c_\alpha s_\alpha^3)\left(v_h^2 - v_s^2\right)\right)}{2 c_\alpha s_\alpha \left(96 c_\alpha^3 \left(v_s^2 - v_h^2\right) s_\alpha^3 + 10 \left(c_\alpha^2 - s_\alpha^2\right) v_s v_h + 6\left(c_\alpha^6 - 15 s_\alpha^2 c_\alpha^4 + 15 s_\alpha^4 c_\alpha^2 - s_\alpha^6\right) v_s v_h\right)} \\[4pt]
& + \delta Z_{H_1 H_2} \times \frac{6 \left(M_{H_1}^2 - M_{H_2}^2\right)\left(c_\alpha^4 - 6 s_\alpha^2 c_\alpha^2 + s_\alpha^4\right) v_s v_h + 12 c_\alpha \left(M_{H_1}^2 + M_{H_2}^2\right) s_\alpha \left(v_s^2 + v_h^2\right) + \left(M_{H_1}^2 - M_{H_2}^2\right)\left(2 v_s v_h + 3(4 c_\alpha^3 s_\alpha - 4 c_\alpha s_\alpha^3)\left(v_h^2 - v_s^2\right)\right)}{24 \left(M_{H_1}^2 v_s^2 - M_{H_2}^2 v_h^2 - c_\alpha^2 \left(M_{H_1}^2 + M_{H_2}^2\right) s_\alpha \left(v_s^2 + v_h^2\right)\right)} \\[4pt]
& + \delta Z_{H_1 H_1} + \delta Z_{H_2 H_2},
\end{aligned}
$$

$$(A.20.3)$$

$$
\begin{aligned}
\delta C_{H_1 H_2 H_2 H_2} = {} & \delta t_{H_1} \times \frac{4c_\alpha s_\alpha\left(s_\alpha v_{\mathrm h}^3 - c_\alpha v_{\mathrm s}^3\right)}{v_{\mathrm s} v_{\mathrm h}(c_\alpha v_{\mathrm s} + s_\alpha v_{\mathrm h})} \\[4pt]
& + \delta t_{H_2} \times \frac{\left(-c_\alpha\left(M_{H_1}^2 + 3M_{H_2}^2\right)v_{\mathrm s} + \left(M_{H_1}^2 - M_{H_2}^2\right)\left(c_\alpha^3 - 3c_\alpha s_\alpha^2\right)v_{\mathrm s} + 2s_\alpha\left(M_{H_1}^2 + M_{H_2}^2 + \left(M_{H_1}^2 - M_{H_2}^2\right)\left(c_\alpha^2 - s_\alpha^2\right)\right)v_{\mathrm h}\right)}{v_{\mathrm s} v_{\mathrm h}(c_\alpha v_{\mathrm s} + s_\alpha v_{\mathrm h})} \\
& \qquad \left(3c_\alpha v_{\mathrm s}^3 + (c_\alpha^3 - 3c_\alpha s_\alpha^2)v_{\mathrm s}^3 + 4s_\alpha^3 v_{\mathrm h}^3\right) \\[4pt]
& + \delta v_{\mathrm s} \times \frac{2s_\alpha v_{\mathrm h}\left(c_\alpha\left(M_{H_1}^2 - M_{H_2}^2\right)v_{\mathrm s} - \left(M_{H_1}^2 - M_{H_2}^2\right)\left(c_\alpha^3 - 3c_\alpha s_\alpha^2\right)v_{\mathrm s} + 2s_\alpha\left(M_{H_1}^2 + M_{H_2}^2 + \left(M_{H_1}^2 - M_{H_2}^2\right)\left(c_\alpha^2 - s_\alpha^2\right)\right)v_{\mathrm h}\right)}{v_{\mathrm s}(c_\alpha v_{\mathrm s} + s_\alpha v_{\mathrm h})} \\[4pt]
& + \delta v_{\mathrm h} \times \frac{2c_\alpha v_{\mathrm s}\left(c_\alpha\left(M_{H_1}^2 + 3M_{H_2}^2\right)v_{\mathrm s} - \left(M_{H_1}^2 - M_{H_2}^2\right)v_{\mathrm s} - \left(M_{H_1}^2 - M_{H_2}^2\right)\left(c_\alpha^3 - 3c_\alpha s_\alpha^2\right)v_{\mathrm s} + 2s_\alpha\left(M_{H_1}^2 + M_{H_2}^2 + \left(M_{H_1}^2 - M_{H_2}^2\right)\left((c_\alpha^3 - 3c_\alpha s_\alpha^2)v_{\mathrm s} + (3c_\alpha^2 s_\alpha - s_\alpha^3)v_{\mathrm h}\right)\right)\right)}{v_{\mathrm h}(c_\alpha v_{\mathrm s} + s_\alpha v_{\mathrm h})} \\[4pt]
& + \delta M_{H_1}^2 \times \frac{-c_\alpha\left(M_{H_1}^2 + 3M_{H_2}^2\right)v_{\mathrm s} + \left(M_{H_1}^2 - M_{H_2}^2\right)\left(c_\alpha^3 - 3c_\alpha s_\alpha^2\right)v_{\mathrm s} + 2s_\alpha\left(M_{H_1}^2 + M_{H_2}^2 + \left(M_{H_1}^2 - M_{H_2}^2\right)\left(c_\alpha^2 - s_\alpha^2\right)\right)v_{\mathrm h}}{4c_\alpha s_\alpha(c_\alpha v_{\mathrm h} - s_\alpha v_{\mathrm s})} \\[4pt]
& + \delta M_{H_2}^2 \times \frac{c_\alpha\left(M_{H_1}^2 + 3M_{H_2}^2\right)v_{\mathrm s} - \left(M_{H_1}^2 - M_{H_2}^2\right)\left(c_\alpha^3 - 3c_\alpha s_\alpha^2\right)v_{\mathrm s} - 2s_\alpha\left(M_{H_1}^2 + M_{H_2}^2 + \left(M_{H_1}^2 - M_{H_2}^2\right)\left(c_\alpha^2 - s_\alpha^2\right)\right)v_{\mathrm h}}{\left(-4v_{\mathrm h}s_\alpha^3 + 3c_\alpha v_{\mathrm s}^3 + 3c_\alpha s_\alpha^2 v_{\mathrm s} + (c_\alpha^3 - 3c_\alpha s_\alpha^2)v_{\mathrm s}\right)} \\[4pt]
& + \delta M_{H_1 H_2}^2 \times \frac{\left(-c_\alpha\left(M_{H_1}^2 + 3M_{H_2}^2\right)v_{\mathrm s} + \left(M_{H_1}^2 - M_{H_2}^2\right)\left(c_\alpha^3 - 3c_\alpha s_\alpha^2\right)v_{\mathrm s} - 2s_\alpha\left(M_{H_1}^2 + M_{H_2}^2 + \left(M_{H_1}^2 - M_{H_2}^2\right)\left(c_\alpha^2 - s_\alpha^2\right)\right)v_{\mathrm h}\right)}{\left(\left(4c_\alpha^3 s_\alpha - 4c_\alpha s_\alpha^3\right)v_{\mathrm s}^2 - 2\left(c_\alpha^4 - 6s_\alpha^2 c_\alpha^2 + s_\alpha^4\right)v_{\mathrm s} v_{\mathrm h} - 2v_{\mathrm h} v_{\mathrm s} - (4c_\alpha^3 s_\alpha - 4c_\alpha s_\alpha^3)v_{\mathrm h}^2 + 4c_\alpha s_\alpha\left(v_{\mathrm s}^2 + v_{\mathrm h}^2\right)\right)} \\[4pt]
& - \delta Z_{H_1 H_2} \times \frac{4c_\alpha s_\alpha v_{\mathrm s} v_{\mathrm h} M_{H_1}^2 + 2\left(6s_\alpha c_\alpha^5 - 20s_\alpha^3 c_\alpha^3 + 6c_\alpha s_\alpha^5\right)v_{\mathrm s} v_{\mathrm h} M_{H_1}^2 - 4c_\alpha M_{H_2}^2 s_\alpha v_{\mathrm s} v_{\mathrm h}}{8c_\alpha s_\alpha(c_\alpha v_{\mathrm s} + s_\alpha v_{\mathrm h})}\left(-c_\alpha\left(M_{H_1}^2 + 3M_{H_2}^2\right)v_{\mathrm s} + \left(M_{H_1}^2 - M_{H_2}^2\right)\left(c_\alpha^3 - 3c_\alpha s_\alpha^2\right)v_{\mathrm s} + 2s_\alpha\left(M_{H_1}^2 + M_{H_2}^2 + \left(M_{H_1}^2 - M_{H_2}^2\right)\left(c_\alpha^2 - s_\alpha^2\right)\right)v_{\mathrm h}\right) \\[4pt]
& - \delta Z_{H_1 H_2} \times \frac{\left(8v_{\mathrm h}^2 M_{H_2}^2 - 2\left(6s_\alpha c_\alpha^5 - 20s_\alpha^3 c_\alpha^3 + 6c_\alpha s_\alpha^5\right)v_{\mathrm s} v_{\mathrm h} M_{H_2}^2 + 4M_{H_1}^2 v_{\mathrm h}^2 - M_{H_2}^2\left(c_\alpha^6 - 15s_\alpha^2 c_\alpha^4 + 15s_\alpha^4 c_\alpha^2 - s_\alpha^6\right)v_{\mathrm h}^2\right)}{8c_\alpha s_\alpha(c_\alpha v_{\mathrm s} + s_\alpha v_{\mathrm h})}\left(-c_\alpha\left(M_{H_1}^2 + 3M_{H_2}^2\right)v_{\mathrm s} + \left(M_{H_1}^2 - M_{H_2}^2\right)\left(c_\alpha^3 - 3c_\alpha s_\alpha^2\right)v_{\mathrm s} + 2s_\alpha\left(M_{H_1}^2 + M_{H_2}^2 + \left(M_{H_1}^2 - M_{H_2}^2\right)\left(c_\alpha^2 - s_\alpha^2\right)\right)v_{\mathrm h}\right) \\[4pt]
& - \delta Z_{H_1 H_2} \times \frac{\left(-4\left(c_\alpha^4 - 6s_\alpha^2 c_\alpha^2 + s_\alpha^4\right)\left(v_{\mathrm s}^2 + v_{\mathrm h}^2\right)M_{H_1}^2 + \left(M_{H_1}^2 - 9M_{H_2}^2\right)\left(c_\alpha^2 - s_\alpha^2\right)\left(v_{\mathrm h}^2 - v_{\mathrm s}^2\right)\right)}{8c_\alpha s_\alpha(c_\alpha v_{\mathrm s} + s_\alpha v_{\mathrm h})}\left(-c_\alpha\left(M_{H_1}^2 + 3M_{H_2}^2\right)v_{\mathrm s} + \left(M_{H_1}^2 - M_{H_2}^2\right)\left(c_\alpha^6 - 15s_\alpha^2 c_\alpha^4 + 15s_\alpha^4 c_\alpha^2 - s_\alpha^6\right)v_{\mathrm s} + 2s_\alpha\left(M_{H_1}^2 + M_{H_2}^2 + \left(M_{H_1}^2 - M_{H_2}^2\right)\left(c_\alpha^2 - s_\alpha^2\right)\right)v_{\mathrm h}\right) \\[4pt]
& - \delta Z_{H_1 H_1} \times \frac{\left(4M_{H_1}^2 v_{\mathrm s}^2 + 8M_{H_2}^2 v_{\mathrm s}^2 + M_{H_1}^2\left(c_\alpha^6 - 15s_\alpha^2 c_\alpha^4 + 15s_\alpha^4 c_\alpha^2 - s_\alpha^6\right)v_{\mathrm s}^2\right)}{8c_\alpha s_\alpha(c_\alpha v_{\mathrm s} + s_\alpha v_{\mathrm h})}\left(-c_\alpha\left(M_{H_1}^2 + 3M_{H_2}^2\right)v_{\mathrm s} + \left(M_{H_1}^2 - M_{H_2}^2\right)\left(c_\alpha^3 - 3c_\alpha s_\alpha^2\right)v_{\mathrm s} + 2s_\alpha\left(M_{H_1}^2 + M_{H_2}^2 + \left(M_{H_1}^2 - M_{H_2}^2\right)\left(c_\alpha^2 - s_\alpha^2\right)\right)v_{\mathrm h}\right) \\[4pt]
& + \delta Z_{H_1 H_1} \times \frac{1}{2} + \delta Z_{H_2 H_2} \times \frac{3}{2},
\end{aligned}
$$

$$\text{(A.20.4)}$$

$$
\begin{aligned}
\delta C_{H_2 H_2 H_2} = {} & \delta t_{H_1} \times \frac{c_\alpha s_\alpha \left(c_\alpha^3 v_s^3 + s_\alpha^3 v_h^3\right)}{v_s v_h \left(\left(M_{H_2}^2 - M_{H_1}^2\right) v_s^2 c_\alpha^6 + M_{H_1}^2 v_s^2 c_\alpha^4 + \left(M_{H_1}^2 - M_{H_2}^2\right) s_\alpha^3 v_h (2c_\alpha v_s + s_\alpha v_h) c_\alpha^2 + M_{H_2}^2 s_\alpha^4 v_h^2\right)} \\[4pt]
& + \delta t_{H_2} \times \frac{\left(2c_\alpha^5 v_s^3 - 2s_\alpha^5 v_h^3\right)}{2 v_s v_h \left(\left(M_{H_2}^2 - M_{H_1}^2\right) v_s^2 c_\alpha^6 + M_{H_1}^2 v_s^2 c_\alpha^4 + \left(M_{H_1}^2 - M_{H_2}^2\right) s_\alpha^3 v_h (2c_\alpha v_s + s_\alpha v_h) c_\alpha^2 + M_{H_2}^2 s_\alpha^4 v_h^2\right)} \\[4pt]
& - \delta v_s \times \frac{2 s_\alpha^3 v_h \left(s_\alpha v_h M_{H_2}^2 + c_\alpha^3 \left(M_{H_1}^2 - M_{H_2}^2\right) v_s + c_\alpha^2 \left(M_{H_1}^2 - M_{H_2}^2\right) s_\alpha v_h\right)}{v_s \left(-\left(M_{H_1}^2 - M_{H_2}^2\right) v_s^2 c_\alpha^6 + M_{H_1}^2 v_s^2 c_\alpha^4 + \left(M_{H_1}^2 - M_{H_2}^2\right) s_\alpha^4 v_h c_\alpha^2 + 2 \left(M_{H_1}^2 - M_{H_2}^2\right) s_\alpha^3 v_s v_h c_\alpha^3 + M_{H_2}^2 s_\alpha^4 v_h^2\right)} \\[4pt]
& - \delta v_h \times \frac{2 c_\alpha^3 v_s \left(c_\alpha v_s M_{H_1}^2 - c_\alpha^3 \left(M_{H_1}^2 - M_{H_2}^2\right) v_s + \left(M_{H_1}^2 - M_{H_2}^2\right) s_\alpha^3 v_h\right)}{v_h \left(-\left(M_{H_1}^2 - M_{H_2}^2\right) v_s^2 c_\alpha^6 + M_{H_1}^2 v_s^2 c_\alpha^4 + \left(M_{H_1}^2 - M_{H_2}^2\right) s_\alpha^4 v_h c_\alpha^2 + 2 \left(M_{H_1}^2 - M_{H_2}^2\right) s_\alpha^3 v_s v_h c_\alpha^3 + M_{H_2}^2 s_\alpha^4 v_h^2\right)} \\[4pt]
& + \delta M_{H_1}^2 \times \frac{c_\alpha^2 s_\alpha^2 (c_\alpha v_s + s_\alpha v_h)^2}{-\left(M_{H_1}^2 - M_{H_2}^2\right) v_s^2 c_\alpha^6 + M_{H_1}^2 v_s^2 c_\alpha^4 + \left(M_{H_1}^2 - M_{H_2}^2\right) s_\alpha^4 v_h c_\alpha^2 + 2 \left(M_{H_1}^2 - M_{H_2}^2\right) s_\alpha^3 v_s v_h c_\alpha^3 + M_{H_2}^2 s_\alpha^4 v_h^2} \\[4pt]
& + \delta M_{H_2}^2 \times \frac{\left(3c_\alpha v_s + (c_\alpha^3 - 3c_\alpha s_\alpha^2) v_s - 4 s_\alpha^3 v_h\right)^2}{16 \left(-\left(M_{H_1}^2 - M_{H_2}^2\right) v_s^2 c_\alpha^6 + M_{H_1}^2 v_s^2 c_\alpha^4 + \left(M_{H_1}^2 - M_{H_2}^2\right) s_\alpha^4 v_h c_\alpha^2 + 2 \left(M_{H_1}^2 - M_{H_2}^2\right) s_\alpha^3 v_s v_h c_\alpha^3 + M_{H_2}^2 s_\alpha^4 v_h^2\right)} \\[4pt]
& + \delta M_{H_1 H_2}^2 \times \frac{2 c_\alpha s_\alpha \left(c_\alpha^4 v_s^2 - c_\alpha s_\alpha v_h v_s + 2 c_\alpha^3 s_\alpha v_h v_s - s_\alpha^4 v_h^2\right)}{-\left(M_{H_1}^2 - M_{H_2}^2\right) v_s^2 c_\alpha^6 + M_{H_1}^2 v_s^2 c_\alpha^4 + \left(M_{H_1}^2 - M_{H_2}^2\right) s_\alpha^4 v_h c_\alpha^2 + 2 \left(M_{H_1}^2 - M_{H_2}^2\right) s_\alpha^3 v_s v_h c_\alpha^3 + M_{H_2}^2 s_\alpha^4 v_h^2} \\[4pt]
& - \delta Z_{H_1 H_2} \times \frac{c_\alpha s_\alpha \left(-c_\alpha \left(M_{H_1}^2 + 3M_{H_2}^2\right) v_s + \left(M_{H_1}^2 - M_{H_2}^2\right) \left(c_\alpha^3 - 3c_\alpha s_\alpha^2\right) v_s + 2 s_\alpha \left(M_{H_1}^2 - M_{H_2}^2\right) \left(c_\alpha^2 - s_\alpha^2\right) v_h\right) (c_\alpha v_s + s_\alpha v_h)}{2 \left(-\left(M_{H_1}^2 - M_{H_2}^2\right) v_s^2 c_\alpha^6 + M_{H_1}^2 v_s^2 c_\alpha^4 + 2 \left(M_{H_1}^2 - M_{H_2}^2\right) s_\alpha^3 v_s v_h c_\alpha^3 + M_{H_2}^2 s_\alpha^4 v_h^2\right)} \\[4pt]
& + \delta Z_{H_2 H_2} \times 2,
\end{aligned}
$$

$$(\text{A.20.5})$$

$$
\begin{aligned}
\delta C_{H_1 H_1 \varphi_S \varphi_S} = {}& -\delta t_{H_1} \times \frac{c_\alpha^2 v_\mathrm{h}}{v_\mathrm{s}\left(\left(\left(M_{H_2}^2 - M_{H_1}^2\right) v_\mathrm{h} c_\alpha^3 - M_{H_2}^2 v_\mathrm{h} c_\alpha + \left(M_{H_2}^2 - M_{H_1}^2\right) s_\alpha^3 v_\mathrm{s}\right)\right)} \\
&+ \delta t_{H_2} \times \frac{c_\alpha v_\mathrm{h} s_\alpha}{v_\mathrm{s}\left(\left(\left(M_{H_2}^2 - M_{H_1}^2\right) v_\mathrm{h} c_\alpha^3 - M_{H_2}^2 v_\mathrm{h} c_\alpha + \left(M_{H_2}^2 - M_{H_1}^2\right) s_\alpha^3 v_\mathrm{s}\right)\right)} \\
&+ \delta v_\mathrm{s} \times \frac{\left(2\left(M_{H_1}^2 - M_{H_2}^2\right) v_\mathrm{h} c_\alpha^3 + 2 M_{H_2}^2 v_\mathrm{h} c_\alpha + \left(M_{H_1}^2 - M_{H_2}^2\right) s_\alpha^3 v_\mathrm{s}\right)}{v_\mathrm{s}\left(\left(M_{H_2}^2 - M_{H_1}^2\right) v_\mathrm{h} c_\alpha^3 - M_{H_2}^2 v_\mathrm{h} c_\alpha + \left(M_{H_2}^2 - M_{H_1}^2\right) s_\alpha^3 v_\mathrm{s}\right)} \\
&+ \delta v_\mathrm{h} \times \frac{\left(s_\alpha v_\mathrm{s} - c_\alpha v_\mathrm{h}\right) s_\alpha^2}{v_\mathrm{h}\left(\left(M_{H_1}^2 - M_{H_2}^2\right) v_\mathrm{h} c_\alpha^3 + M_{H_2}^2 v_\mathrm{h} c_\alpha + \left(M_{H_1}^2 - M_{H_2}^2\right) s_\alpha^3 v_\mathrm{s}\right)} \\
&+ \delta M_{H_1}^2 \times \frac{1}{M_{H_1}^2 - M_{H_2}^2} + \frac{c_\alpha M_{H_2}^2 v_\mathrm{h}}{v_\mathrm{h} c_\alpha^3 + s_\alpha^3 v_\mathrm{s}} \\
&+ \delta M_{H_2}^2 \times \frac{\left(2 c_\alpha^2 s_\alpha v_\mathrm{h} - \dfrac{\left(2 c_\alpha^2 - 1\right) s_\alpha^2 v_\mathrm{s}}{c_\alpha}\right)}{\left(M_{H_2}^2 - M_{H_1}^2\right) v_\mathrm{h} c_\alpha^3 - M_{H_2}^2 v_\mathrm{h} c_\alpha + \left(M_{H_2}^2 - M_{H_1}^2\right) s_\alpha^3 v_\mathrm{s}} \\
&+ \delta M_{H_1 H_2}^2 \times \frac{\left(v_\mathrm{h} M_{H_2}^2 + c_\alpha \left(M_{H_1}^2 - M_{H_2}^2\right)\left(c_\alpha v_\mathrm{h} - s_\alpha v_\mathrm{s}\right)\right) s_\alpha}{\left(M_{H_2}^2 - M_{H_1}^2\right) v_\mathrm{h} c_\alpha^3 - M_{H_2}^2 v_\mathrm{h} c_\alpha + \left(M_{H_2}^2 - M_{H_1}^2\right) s_\alpha^3 v_\mathrm{s}} + \delta Z_{H_1 H_1} + \delta Z_H,
\end{aligned}
$$

$$
\begin{aligned}
\delta C_{H_1 H_1 \varphi_\mathrm{h} \varphi_\mathrm{h}} = {}& \delta t_{H_1} \times \frac{s_\alpha^2 v_\mathrm{s}}{v_\mathrm{h}\left(\left(\left(M_{H_1}^2 - M_{H_2}^2\right) v_\mathrm{h} c_\alpha^3 + \left(\left(M_{H_2}^2 - M_{H_1}^2\right) c_\alpha^2 + M_{H_1}^2\right) s_\alpha v_\mathrm{s}\right)\right)} \\
&+ \delta t_{H_2} \times \frac{s_\alpha v_\mathrm{s} c_\alpha}{v_\mathrm{h}\left(\left(\left(M_{H_1}^2 - M_{H_2}^2\right) v_\mathrm{h} c_\alpha^3 + \left(\left(M_{H_2}^2 - M_{H_1}^2\right) c_\alpha^2 + M_{H_1}^2\right) s_\alpha v_\mathrm{s}\right)\right)} \\
&+ \delta v_\mathrm{s} \times \frac{\left(M_{H_1}^2 - M_{H_2}^2\right) v_\mathrm{h} c_\alpha^3}{v_\mathrm{s}\left(\left(\left(M_{H_2}^2 - M_{H_1}^2\right) v_\mathrm{h} c_\alpha^3 + \left(M_{H_1}^2 - M_{H_2}^2\right) s_\alpha v_\mathrm{s} c_\alpha^2 - M_{H_1}^2 s_\alpha v_\mathrm{s}\right)\right)} \\
&+ \delta v_\mathrm{h} \times \frac{\left(-M_{H_1}^2 v_\mathrm{h} c_\alpha^3 + M_{H_2}^2 v_\mathrm{h} c_\alpha^3 + 2 M_{H_1}^2 s_\alpha v_\mathrm{s} c_\alpha^2 - 2 M_{H_2}^2 s_\alpha v_\mathrm{s} c_\alpha^2 - 2 M_{H_1}^2 s_\alpha v_\mathrm{s}\right)}{v_\mathrm{h}\left(M_{H_1}^2 v_\mathrm{h} c_\alpha^3 - M_{H_2}^2 v_\mathrm{h} c_\alpha^3 - M_{H_1}^2 s_\alpha v_\mathrm{s} c_\alpha^2 + M_{H_2}^2 s_\alpha v_\mathrm{s} c_\alpha^2 + M_{H_1}^2 s_\alpha v_\mathrm{s}\right)} \\
&+ \delta M_{H_1}^2 \times \frac{\left(v_\mathrm{h} c_\alpha^3 + s_\alpha^3 v_\mathrm{s}\right)}{\left(M_{H_1}^2 - M_{H_2}^2\right) v_\mathrm{h} c_\alpha^3 + \left(\left(M_{H_2}^2 - M_{H_1}^2\right) c_\alpha^2 + M_{H_1}^2\right) s_\alpha v_\mathrm{s}} \\
&+ \delta M_{H_2}^2 \times \frac{1}{\dfrac{s_\alpha v_\mathrm{s} M_{H_1}^2}{c_\alpha^2\left(s_\alpha v_\mathrm{s} - c_\alpha v_\mathrm{h}\right)} - M_{H_1}^2 + M_{H_2}^2} \\
&+ \delta M_{H_1 H_2}^2 \times \frac{\left(2 v_\mathrm{s} s_\alpha^3 + c_\alpha \left(2 c_\alpha^2 - 1\right) v_\mathrm{h}\right) c_\alpha}{s_\alpha\left(\left(M_{H_1}^2 - M_{H_2}^2\right) v_\mathrm{h} c_\alpha^3 + \left(M_{H_2}^2 - M_{H_1}^2\right) s_\alpha v_\mathrm{s} c_\alpha^2 + M_{H_1}^2 s_\alpha v_\mathrm{s}\right)} \\
&+ \delta Z_{H_1 H_2} \times \frac{\left(M_{H_1}^2 v_\mathrm{s} - c_\alpha \left(M_{H_1}^2 - M_{H_2}^2\right)\left(s_\alpha v_\mathrm{h} + c_\alpha v_\mathrm{s}\right)\right) c_\alpha}{\left(M_{H_1}^2 - M_{H_2}^2\right) v_\mathrm{h} c_\alpha^3 + \left(\left(M_{H_2}^2 - M_{H_1}^2\right) c_\alpha^2 + M_{H_1}^2\right) s_\alpha v_\mathrm{s}} + \delta Z_{H_1 H_1} + \delta Z_{\chi'},
\end{aligned}
\tag{A.20.6}
$$

$$
\begin{aligned}
\delta C_{H_2 H_2 \varphi_s \varphi_s} = \delta t_{H_1} \times {} & \frac{s_\alpha v_h c_\alpha}{v_s \left(\left(\left(M_{H_1}^2 - M_{H_2}^2 \right) v_s c_\alpha^3 + \left(\left(M_{H_2}^2 - M_{H_1}^2 \right) c_\alpha^2 + M_{H_2}^2 \right) s_\alpha v_h \right) \right)} \\
& + \delta t_{H_2} \times \frac{s_\alpha^2 v_h}{v_s \left(\left(M_{H_2}^2 - M_{H_1}^2 \right) v_s c_\alpha^3 + \left(- \left(M_{H_1}^2 - M_{H_2}^2 \right) c_\alpha^2 - M_{H_2}^2 \right) s_\alpha v_h \right)} \\
& + \delta v_s \times \frac{\left(\left(M_{H_2}^2 - M_{H_1}^2 \right) v_s c_\alpha^3 + 2 \left(M_{H_2}^2 - M_{H_1}^2 \right) s_\alpha v_h c_\alpha^2 - 2 M_{H_2}^2 s_\alpha v_h \right)}{\left(M_{H_1}^2 - M_{H_2}^2 \right) v_s c_\alpha^3} \\
& - \delta v_h \times \frac{\left(M_{H_1}^2 - M_{H_2}^2 \right) v_s c_\alpha^3}{v_h \left(\left(M_{H_1}^2 - M_{H_2}^2 \right) v_s c_\alpha^3 + \left(M_{H_1}^2 - M_{H_2}^2 \right) s_\alpha v_h c_\alpha^2 + M_{H_2}^2 s_\alpha v_h \right)} \\
& + \delta M_{H_2}^2 \times \frac{1}{M_{H_1}^2 - M_{H_2}^2 + \frac{M_{H_2}^2 s_\alpha v_h}{c_\alpha^2 \left(s_\alpha v_h + c_\alpha v_s \right)}} \\
& + \delta M_{H_2}^2 \times \frac{\left(s_\alpha^3 v_h - c_\alpha^3 v_s \right)}{v_h \left(\left(M_{H_1}^2 - M_{H_2}^2 \right) v_s c_\alpha^3 + \left(\left(M_{H_1}^2 - M_{H_2}^2 \right) c_\alpha^2 + M_{H_2}^2 \right) s_\alpha v_h \right)} \\
& + \delta M_{H_1 H_2}^2 \times \frac{\left(\frac{c_\alpha \left(2 c_\alpha^2 - 1 \right) v_s}{s_\alpha} - 2 s_\alpha^2 v_h \right) c_\alpha}{\left(M_{H_1}^2 - M_{H_2}^2 \right) v_s c_\alpha^3 + \left(\left(M_{H_1}^2 - M_{H_2}^2 \right) c_\alpha^2 + M_{H_2}^2 \right) s_\alpha v_h} \\
& + \delta M_{H_1 H_2}^2 \times \frac{c_\alpha \left(M_{H_1}^2 - M_{H_2}^2 \right) \left(s_\alpha v_s - c_\alpha v_h \right) - M_{H_2}^2 v_h \right) c_\alpha}{\left(M_{H_1}^2 - M_{H_2}^2 \right) v_s c_\alpha^3 + \left(\left(M_{H_1}^2 - M_{H_2}^2 \right) c_\alpha^2 + M_{H_2}^2 \right) s_\alpha v_h} + \delta Z_{H_2 H_2} + \delta Z_{H_1},
\end{aligned}
$$

$$\text{(A.20.7)}$$

$$
\begin{aligned}
\delta C_{H_2 H_2 \varphi_h \varphi_h} = \delta t_{H_1} \times {} & \frac{s_\alpha v_s c_\alpha}{v_h \left(\left(M_{H_2}^2 - M_{H_1}^2 \right) v_s c_\alpha^3 + M_{H_1}^2 v_s c_\alpha + \left(M_{H_1}^2 - M_{H_2}^2 \right) s_\alpha^3 v_h \right)} \\
& + \delta t_{H_2} \times \frac{v_s c_\alpha^2}{v_h \left(\left(M_{H_2}^2 - M_{H_1}^2 \right) v_s c_\alpha^3 + M_{H_1}^2 v_s c_\alpha + \left(M_{H_1}^2 - M_{H_2}^2 \right) s_\alpha^3 v_h \right)} \\
& + \delta v_s \times \frac{\left(M_{H_1}^2 - M_{H_2}^2 \right) v_h}{v_s \left(\left(M_{H_1}^2 - M_{H_2}^2 \right) \left(\frac{c_\alpha^3 v_s}{s_\alpha^3} - v_h \right) - \frac{c_\alpha M_{H_1}^2 v_s}{s_\alpha^3} \right)} \\
& + \delta v_h \times \frac{\left(2 \left(M_{H_1}^2 - M_{H_2}^2 \right) v_s c_\alpha^3 - 2 M_{H_1}^2 v_s c_\alpha + \left(M_{H_2}^2 - M_{H_1}^2 \right) s_\alpha^3 v_h \right)}{v_h \left(\left(M_{H_2}^2 - M_{H_1}^2 \right) v_s c_\alpha^3 + M_{H_1}^2 v_s c_\alpha + \left(M_{H_1}^2 - M_{H_2}^2 \right) s_\alpha^3 v_h \right)} \\
& + \delta M_{H_2}^2 \times \frac{1}{\frac{c_\alpha v_s M_{H_1}^2}{c_\alpha^3 v_s - s_\alpha^3 v_h} - M_{H_1}^2 + M_{H_2}^2} \\
& + \delta M_{H_2}^2 \times \frac{s_\alpha^2 \left(s_\alpha v_h + c_\alpha v_s \right)}{\left(M_{H_2}^2 - M_{H_1}^2 \right) v_s c_\alpha^3 + M_{H_1}^2 v_s c_\alpha + \left(M_{H_1}^2 - M_{H_2}^2 \right) s_\alpha^3 v_h} \\
& + \delta M_{H_1 H_2}^2 \times \frac{s_\alpha \left(2 v_s c_\alpha^2 + \frac{\left(2 c_\alpha^2 - 1 \right) s_\alpha v_h}{c_\alpha} \right)}{\left(M_{H_2}^2 - M_{H_1}^2 \right) v_s c_\alpha^3 + M_{H_1}^2 v_s c_\alpha + \left(M_{H_1}^2 - M_{H_2}^2 \right) s_\alpha^3 v_h} \\
& + \delta M_{H_1 H_2}^2 \times \frac{s_\alpha \left(M_{H_1}^2 v_s - c_\alpha \left(M_{H_1}^2 - M_{H_2}^2 \right) \left(s_\alpha v_h + c_\alpha v_s \right) \right)}{\left(M_{H_2}^2 - M_{H_1}^2 \right) v_s c_\alpha^3 + M_{H_1}^2 v_s c_\alpha + \left(M_{H_1}^2 - M_{H_2}^2 \right) s_\alpha^3 v_h} + \delta Z_{H_2 H_2} + \delta Z_\chi,
\end{aligned}
$$

$$
\begin{aligned}
\delta C_{H_1 H_2 \varphi_s \varphi_s} = {}& \delta t_{H_1} \times \frac{c_\alpha v_{\mathrm h}}{v_{\mathrm s}\left(v_{\mathrm h}M_{H_2}^2 + c_\alpha\left(M_{H_1}^2 - M_{H_2}^2\right)(c_\alpha v_{\mathrm h} - s_\alpha v_{\mathrm s})\right)} - \delta t_{H_2} \times \frac{s_\alpha v_{\mathrm h}}{v_{\mathrm s}\left(v_{\mathrm h}M_{H_2}^2 + c_\alpha\left(M_{H_1}^2 - M_{H_2}^2\right)(c_\alpha v_{\mathrm h} - s_\alpha v_{\mathrm s})\right)} \\
&+ \delta v_{\mathrm s} \times \frac{\left(c_\alpha\left(M_{H_1}^2 - M_{H_2}^2\right)(s_\alpha v_{\mathrm s} - 2c_\alpha v_{\mathrm h}) - 2M_{H_2}^2 v_{\mathrm h}\right)}{v_{\mathrm s}\left(v_{\mathrm h}M_{H_2}^2 + c_\alpha\left(M_{H_1}^2 - M_{H_2}^2\right)(c_\alpha v_{\mathrm h} - s_\alpha v_{\mathrm s})\right)} + \delta v_{\mathrm h} \times \frac{c_\alpha\left(M_{H_2}^2 - M_{H_1}^2\right)s_\alpha v_{\mathrm s}}{v_{\mathrm h}\left(c_\alpha\left(M_{H_1}^2 - M_{H_2}^2\right)(s_\alpha v_{\mathrm s} - c_\alpha v_{\mathrm h}) - M_{H_2}^2 v_{\mathrm h}\right)} \\
&+ \delta M_{H_1}^2 \times \frac{1}{M_{H_1}^2 - M_{H_2}^2 + c_\alpha\frac{M_{H_2}^2 v_{\mathrm h}}{(c_\alpha v_{\mathrm h} - s_\alpha v_{\mathrm s})}} + \delta M_{H_2}^2 \times \frac{s_\alpha\left(c_\alpha v_{\mathrm h} - s_\alpha v_{\mathrm s}\right)}{v_{\mathrm h}M_{H_2}^2 + c_\alpha\left(M_{H_1}^2 - M_{H_2}^2\right)(c_\alpha v_{\mathrm h} - s_\alpha v_{\mathrm s})} \\
&+ \delta M_{H_1 H_2}^2 \times \frac{\left(2c_\alpha s_\alpha v_{\mathrm h} + \left(2c_\alpha^2 - 1\right)v_{\mathrm s}\right)}{c_\alpha\left(M_{H_1}^2 - M_{H_2}^2\right)(s_\alpha v_{\mathrm s} - c_\alpha v_{\mathrm h}) - M_{H_2}^2 v_{\mathrm h}} - \delta Z_{H_1 H_2} \times \frac{\left(\frac{s_\alpha v_{\mathrm h}M_{H_2}^2}{c_\alpha} + c_\alpha\left(M_{H_1}^2 - M_{H_2}^2\right)(s_\alpha v_{\mathrm h} + c_\alpha v_{\mathrm s})\right)}{\left(M_{H_1}^2 + M_{H_2}^2\right)v_{\mathrm h} + \left(M_{H_1}^2 - M_{H_2}^2\right)\left(\left(2c_\alpha^2 - 1\right)v_{\mathrm h} - 2c_\alpha s_\alpha v_{\mathrm s}\right)} \\
&- \delta Z_{H_1 H_2} \times \frac{\left(M_{H_1}^2 - M_{H_2}^2\right)v_{\mathrm s}s_\alpha^2 + \frac{c_\alpha\left(\left(M_{H_1}^2 - M_{H_2}^2\right)c_\alpha^2 + M_{H_2}^2\right)v_{\mathrm h}}{s_\alpha}}{\left(M_{H_1}^2 + M_{H_2}^2\right)v_{\mathrm h} + \left(M_{H_1}^2 - M_{H_2}^2\right)\left(\left(2c_\alpha^2 - 1\right)v_{\mathrm h} - 2c_\alpha s_\alpha v_{\mathrm s}\right)} \\
&+ \delta Z_{H_1 H_1} \times \frac{1}{2} + \delta Z_{H_2 H_2} \times \frac{1}{2} + \delta Z_{H},
\end{aligned}
$$

$$
\begin{aligned}
\delta C_{H_1 H_2 \varphi_h \varphi_h} = {}& -\delta t_{H_1} \times \frac{s_\alpha v_{\mathrm s}}{v_{\mathrm h}\left(c_\alpha\left(M_{H_1}^2 - M_{H_2}^2\right)(s_\alpha v_{\mathrm h} + c_\alpha v_{\mathrm s}) - M_{H_1}^2 v_{\mathrm s}\right)} - \delta t_{H_2} \times \frac{c_\alpha v_{\mathrm s}}{v_{\mathrm h}\left(c_\alpha\left(M_{H_1}^2 - M_{H_2}^2\right)(s_\alpha v_{\mathrm h} + c_\alpha v_{\mathrm s}) - M_{H_1}^2 v_{\mathrm s}\right)} \\
&+ \delta v_{\mathrm s} \times \frac{c_\alpha\left(M_{H_2}^2 - M_{H_1}^2\right)s_\alpha v_{\mathrm h}}{v_{\mathrm s}\left(c_\alpha\left(M_{H_1}^2 - M_{H_2}^2\right)(s_\alpha v_{\mathrm h} + c_\alpha v_{\mathrm s}) - M_{H_1}^2 v_{\mathrm s}\right)} + \delta v_{\mathrm h} \times \frac{\left(2M_{H_1}^2 v_{\mathrm s} - c_\alpha\left(M_{H_1}^2 - M_{H_2}^2\right)(s_\alpha v_{\mathrm h} + 2c_\alpha v_{\mathrm s})\right)}{v_{\mathrm h}\left(c_\alpha\left(M_{H_1}^2 - M_{H_2}^2\right)(s_\alpha v_{\mathrm h} + c_\alpha v_{\mathrm s}) - M_{H_1}^2 v_{\mathrm s}\right)} \\
&+ \delta M_{H_1}^2 \times \frac{s_\alpha\left(c_\alpha v_{\mathrm h} + c_\alpha v_{\mathrm s}\right)}{c_\alpha\left(M_{H_1}^2 - M_{H_2}^2\right)(s_\alpha v_{\mathrm h} + c_\alpha v_{\mathrm s}) - M_{H_1}^2 v_{\mathrm s}} + \delta M_{H_2}^2 \times \frac{1}{\frac{v_{\mathrm s}M_{H_1}^2}{c_\alpha(s_\alpha v_{\mathrm h} + c_\alpha v_{\mathrm s})} - M_{H_1}^2 + M_{H_2}^2} \\
&+ \delta M_{H_1 H_2}^2 \times \frac{\left(\left(2c_\alpha^2 - 1\right)v_{\mathrm h} - 2c_\alpha s_\alpha v_{\mathrm s}\right)}{c_\alpha\left(M_{H_1}^2 - M_{H_2}^2\right)(s_\alpha v_{\mathrm h} + c_\alpha v_{\mathrm s}) - M_{H_1}^2 v_{\mathrm s}} - \delta Z_{H_1 H_2} \times \frac{\frac{s_\alpha v_{\mathrm s}M_{H_1}^2}{c_\alpha} + c_\alpha\left(M_{H_1}^2 - M_{H_2}^2\right)(c_\alpha v_{\mathrm h} - s_\alpha v_{\mathrm s})}{\left(-M_{H_1}^2 - M_{H_2}^2\right)v_{\mathrm s} + \left(M_{H_1}^2 - M_{H_2}^2\right)\left(2c_\alpha s_\alpha v_{\mathrm h} + \left(2c_\alpha^2 - 1\right)v_{\mathrm s}\right)} \\
&+ \delta Z_{H_1 H_2} \times \left(\frac{c_\alpha}{2s_\alpha} + \frac{\left(M_{H_2}^2 - M_{H_1}^2\right)v_{\mathrm h}}{\left(-M_{H_1}^2 - M_{H_2}^2\right)v_{\mathrm s} + \left(M_{H_1}^2 - M_{H_2}^2\right)\left(2c_\alpha s_\alpha v_{\mathrm h} + \left(2c_\alpha^2 - 1\right)v_{\mathrm s}\right)}\right) \\
&+ \delta Z_{H_1 H_1} \times \frac{1}{2} + \delta Z_{H_2 H_2} \times \frac{1}{2} + \delta Z_\chi,
\end{aligned}
$$

$$
\begin{aligned}
\delta C_{\varphi_{\mathrm{s}}\varphi_{\mathrm{s}}\varphi_{\mathrm{s}}\varphi_{\mathrm{s}}} = {}& \delta t_{H_1} \times \frac{c_\alpha}{v_{\mathrm{s}}\left(c_\alpha^2\left(M_{H_1}^2 - M_{H_2}^2\right) + M_{H_2}^2\right)} + \delta t_{H_2} \times \frac{s_\alpha}{c_\alpha^2\left(M_{H_2}^2 - M_{H_1}^2\right)v_{\mathrm{s}} - M_{H_2}^2 v_{\mathrm{s}}} - \delta v_{\mathrm{s}} \times \frac{2}{v_{\mathrm{s}}} \\
& + \delta M_{H_1}^2 \times \frac{c_\alpha^2}{c_\alpha^2\left(M_{H_1}^2 - M_{H_2}^2\right) + M_{H_2}^2} - \delta M_{H_2}^2 \times \frac{s_\alpha^2}{c_\alpha^2\left(M_{H_2}^2 - M_{H_1}^2\right) - M_{H_2}^2} + \delta M_{H_1 H_2}^2 \times \frac{2c_\alpha s_\alpha}{c_\alpha^2\left(M_{H_2}^2 - M_{H_1}^2\right) - M_{H_2}^2} + \delta Z_H \times 2, \\[2ex]
\delta C_{\varphi_{\mathrm{h}}\varphi_{\mathrm{h}}\varphi_{\mathrm{h}}\varphi_{\mathrm{h}}} = {}& -\delta t_{H_1} \times \frac{s_\alpha}{c_\alpha^2 v_{\mathrm{h}}\left(M_{H_1}^2 - M_{H_2}^2\right) - v_{\mathrm{h}} M_{H_1}^2} - \delta t_{H_2} \times \frac{c_\alpha}{c_\alpha^2 v_{\mathrm{h}}\left(M_{H_1}^2 - M_{H_2}^2\right) - v_{\mathrm{h}} M_{H_2}^2} - \delta v_{\mathrm{h}} \times \frac{2}{v_{\mathrm{h}}} \\
& + \delta M_{H_1}^2 \times \frac{s_\alpha^2}{c_\alpha^2\left(M_{H_2}^2 - M_{H_1}^2\right) + M_{H_1}^2} + \delta M_{H_2}^2 \times \frac{c_\alpha^2}{c_\alpha^2\left(M_{H_2}^2 - M_{H_1}^2\right) + M_{H_1}^2} + \delta M_{H_1 H_2}^2 \times \frac{2c_\alpha s_\alpha}{c_\alpha^2\left(M_{H_2}^2 - M_{H_1}^2\right) + M_{H_1}^2} + \delta Z_\chi \times 2, \\[2ex]
\delta C_{\varphi_{\mathrm{s}}\varphi_{\mathrm{s}}\varphi_{\mathrm{h}}\varphi_{\mathrm{h}}} = {}& -\delta v_{\mathrm{s}} \times \frac{1}{v_{\mathrm{s}}} - \delta v_{\mathrm{h}} \times \frac{1}{v_{\mathrm{h}}} + \delta M_{H_1}^2 \times \frac{1}{M_{H_1}^2 - M_{H_2}^2} + \delta M_{H_2}^2 \times \frac{1}{M_{H_2}^2 - M_{H_1}^2} + \delta M_{H_1 H_2}^2 \times \frac{\left(\frac{c_\alpha}{s_\alpha} - \frac{s_\alpha}{c_\alpha}\right)}{M_{H_1}^2 - M_{H_2}^2} + \delta Z_H + \delta Z_\chi, \\[2ex]
\delta C_{\phi^+\phi^-\phi^+\phi^-} = {}& \delta t_{H_1} \times \frac{c_\alpha}{v_{\mathrm{s}}\left(c_\alpha^2\left(M_{H_1}^2 - M_{H_2}^2\right) + M_{H_2}^2\right)} + \delta t_{H_2} \times \frac{s_\alpha}{c_\alpha^2\left(M_{H_2}^2 - M_{H_1}^2\right)v_{\mathrm{s}} - M_{H_2}^2 v_{\mathrm{s}}} - \delta v_{\mathrm{s}} \times \frac{2}{v_{\mathrm{s}}} \\
& + \delta M_{H_1}^2 \times \frac{c_\alpha^2}{c_\alpha^2\left(M_{H_1}^2 - M_{H_2}^2\right) + M_{H_2}^2} - \delta M_{H_2}^2 \times \frac{s_\alpha^2}{c_\alpha^2\left(M_{H_2}^2 - M_{H_1}^2\right) - M_{H_2}^2} + \delta M_{H_1 H_2}^2 \times \frac{2c_\alpha s_\alpha}{c_\alpha^2\left(M_{H_2}^2 - M_{H_1}^2\right) - M_{H_2}^2} + \delta Z_H \times 2, \\[2ex]
\delta C_{\varphi_{\mathrm{s}}\varphi_{\mathrm{s}}\phi^+\phi^-} = {}& \delta t_{H_1} \times \frac{c_\alpha}{v_{\mathrm{s}}\left(c_\alpha^2\left(M_{H_1}^2 - M_{H_2}^2\right) + M_{H_2}^2\right)} + \delta t_{H_2} \times \frac{s_\alpha}{c_\alpha^2\left(M_{H_2}^2 - M_{H_1}^2\right)v_{\mathrm{s}} - M_{H_2}^2 v_{\mathrm{s}}} - \delta v_{\mathrm{s}} \times \frac{2}{v_{\mathrm{s}}} \\
& + \delta M_{H_1}^2 \times \frac{c_\alpha^2}{c_\alpha^2\left(M_{H_1}^2 - M_{H_2}^2\right) + M_{H_2}^2} - \delta M_{H_2}^2 \times \frac{s_\alpha^2}{c_\alpha^2\left(M_{H_2}^2 - M_{H_1}^2\right) - M_{H_2}^2} + \delta M_{H_1 H_2}^2 \times \frac{2c_\alpha s_\alpha}{c_\alpha^2\left(M_{H_2}^2 - M_{H_1}^2\right) - M_{H_2}^2} + \delta Z_H \times 2, \\[2ex]
\delta C_{\varphi_{\mathrm{h}}\varphi_{\mathrm{h}}\phi^+\phi^-} = {}& -\delta v_{\mathrm{s}} \times \frac{1}{v_{\mathrm{s}}} - \delta v_{\mathrm{h}} \times \frac{1}{v_{\mathrm{h}}} + \delta M_{H_1}^2 \times \frac{1}{M_{H_1}^2 - M_{H_2}^2} + \delta M_{H_2}^2 \times \frac{1}{M_{H_2}^2 - M_{H_1}^2} + \delta M_{H_1 H_2}^2 \times \frac{\left(\frac{c_\alpha}{s_\alpha} - \frac{s_\alpha}{c_\alpha}\right)}{M_{H_1}^2 - M_{H_2}^2} + \delta Z_H + \delta Z_\chi,
\end{aligned}
$$

(A.20.9)

$$
\begin{aligned}
\delta C_{H_1 H_1 \phi^+ \phi^-} = {} & -\delta t_{H_1} \times \frac{c_\alpha^2 v_{\mathrm h}}{v_{\mathrm s}\left(\left(M_{H_2}^2 - M_{H_1}^2\right) v_{\mathrm h} c_\alpha^3 - M_{H_2}^2 v_{\mathrm h} c_\alpha + \left(M_{H_2}^2 - M_{H_1}^2\right) s_\alpha^3 v_{\mathrm s}\right)} \\[4pt]
& + \delta t_{H_2} \times \frac{c_\alpha v_{\mathrm h} s_\alpha}{v_{\mathrm s}\left(\left(M_{H_2}^2 - M_{H_1}^2\right) v_{\mathrm h} c_\alpha^3 - M_{H_2}^2 v_{\mathrm h} c_\alpha + \left(M_{H_2}^2 - M_{H_1}^2\right) s_\alpha^3 v_{\mathrm s}\right)} \\[4pt]
& + \delta v_{\mathrm s} \times \frac{2\left(M_{H_1}^2 - M_{H_2}^2\right) v_{\mathrm h} c_\alpha^3 + 2 M_{H_2}^2 v_{\mathrm h} c_\alpha + \left(M_{H_1}^2 - M_{H_2}^2\right) s_\alpha^3 v_{\mathrm s}}{v_{\mathrm s}\left(\left(M_{H_2}^2 - M_{H_1}^2\right) v_{\mathrm h} c_\alpha^3 - M_{H_2}^2 v_{\mathrm h} c_\alpha + \left(M_{H_2}^2 - M_{H_1}^2\right) s_\alpha^3 v_{\mathrm s}\right)} \\[4pt]
& + \delta v_{\mathrm h} \times \frac{\left(M_{H_2}^2 - M_{H_1}^2\right) v_{\mathrm s} s_\alpha^3}{v_{\mathrm h}\left(\left(M_{H_1}^2 - M_{H_2}^2\right) v_{\mathrm h} c_\alpha^3 + M_{H_2}^2 v_{\mathrm h} c_\alpha + \left(M_{H_1}^2 - M_{H_2}^2\right) s_\alpha^3 v_{\mathrm s}\right)} \\[4pt]
& + \delta M_{H_1}^2 \times \frac{1}{M_{H_1}^2 - M_{H_2}^2 + \dfrac{c_\alpha M_{H_2}^2 v_{\mathrm h}}{v_{\mathrm h} c_\alpha^3 + s_\alpha^3 v_{\mathrm s}}} \\[4pt]
& + \delta M_{H_2}^2 \times \frac{\left(2 c_\alpha s_\alpha v_{\mathrm h} - \dfrac{\left(2 c_\alpha^2 - 1\right) s_\alpha^2 v_{\mathrm s}}{c_\alpha}\right)\left(s_\alpha v_{\mathrm s} - c_\alpha v_{\mathrm h}\right) s_\alpha^2}{\left(M_{H_2}^2 - M_{H_1}^2\right) v_{\mathrm h} c_\alpha^3 - M_{H_2}^2 v_{\mathrm h} c_\alpha + \left(M_{H_2}^2 - M_{H_1}^2\right) s_\alpha^3 v_{\mathrm s}} \\[4pt]
& + \delta M_{H_1 H_2}^2 \times \frac{\left(v_{\mathrm h} M_{H_2}^2 + c_\alpha\left(M_{H_1}^2 - M_{H_2}^2\right)\left(c_\alpha v_{\mathrm h} - s_\alpha v_{\mathrm s}\right)\right) s_\alpha}{\left(M_{H_2}^2 - M_{H_1}^2\right) v_{\mathrm h} c_\alpha^3 - M_{H_2}^2 v_{\mathrm h} c_\alpha + \left(M_{H_2}^2 - M_{H_1}^2\right) s_\alpha^3 v_{\mathrm s}} \\[4pt]
& + \delta Z_{H_1 H_2} \times \frac{s_\alpha v_{\mathrm h}}{\left(M_{H_2}^2 - M_{H_1}^2\right) v_{\mathrm h} c_\alpha^3 - M_{H_2}^2 v_{\mathrm h} c_\alpha + \left(M_{H_2}^2 - M_{H_1}^2\right) s_\alpha^3 v_{\mathrm s}} + \delta Z_{H_1 H_1} + \delta Z_H,
\end{aligned}
$$

$$
\begin{aligned}
\delta C_{H_1 H_2 \phi^+ \phi^-} = {} & \delta t_{H_1} \times \frac{c_\alpha v_{\mathrm h}}{v_{\mathrm s}\left(v_{\mathrm h} M_{H_2}^2 + c_\alpha\left(M_{H_1}^2 - M_{H_2}^2\right)\left(c_\alpha v_{\mathrm h} - s_\alpha v_{\mathrm s}\right)\right)} \\[4pt]
& - \delta t_{H_2} \times \frac{s_\alpha v_{\mathrm h}}{v_{\mathrm s}\left(v_{\mathrm h} M_{H_2}^2 + c_\alpha\left(M_{H_1}^2 - M_{H_2}^2\right)\left(c_\alpha v_{\mathrm h} - s_\alpha v_{\mathrm s}\right)\right)} \\[4pt]
& + \delta v_{\mathrm s} \times \frac{c_\alpha\left(M_{H_1}^2 - M_{H_2}^2\right)\left(s_\alpha v_{\mathrm s} - 2 c_\alpha v_{\mathrm h}\right) - 2 M_{H_2}^2 v_{\mathrm h}}{v_{\mathrm s}\left(v_{\mathrm h} M_{H_2}^2 + c_\alpha\left(M_{H_1}^2 - M_{H_2}^2\right)\left(s_\alpha v_{\mathrm s} - c_\alpha v_{\mathrm h}\right) - M_{H_2}^2 v_{\mathrm h}\right)} \\[4pt]
& + \delta v_{\mathrm h} \times \frac{c_\alpha\left(M_{H_1}^2 - M_{H_2}^2\right)\left(c_\alpha v_{\mathrm h} - s_\alpha v_{\mathrm s}\right) s_\alpha}{v_{\mathrm h}\left(c_\alpha\left(M_{H_1}^2 - M_{H_2}^2\right)\left(s_\alpha v_{\mathrm s} - c_\alpha v_{\mathrm h}\right) - M_{H_2}^2 v_{\mathrm h}\right)} \\[4pt]
& + \delta M_{H_1}^2 \times \frac{1}{M_{H_1}^2 - M_{H_2}^2 + \dfrac{M_{H_2}^2 v_{\mathrm h}}{c_\alpha\left(c_\alpha v_{\mathrm h} - s_\alpha v_{\mathrm s}\right)}} \\[4pt]
& + \delta M_{H_2}^2 \times \frac{s_\alpha\left(s_\alpha v_{\mathrm h} + c_\alpha v_{\mathrm s}\right)}{v_{\mathrm h} M_{H_2}^2 + c_\alpha\left(M_{H_1}^2 - M_{H_2}^2\right)\left(c_\alpha v_{\mathrm h} - s_\alpha v_{\mathrm s}\right)} \\[4pt]
& + \delta M_{H_1 H_2}^2 \times \frac{\left(2 c_\alpha s_\alpha v_{\mathrm h} + \left(2 c_\alpha^2 - 1\right) v_{\mathrm s}\right)}{c_\alpha\left(M_{H_1}^2 - M_{H_2}^2\right)\left(s_\alpha v_{\mathrm s} - c_\alpha v_{\mathrm h}\right) - M_{H_2}^2 v_{\mathrm h}} \\[4pt]
& - \delta Z_{H_1 H_2} \times \frac{\left(\dfrac{s_\alpha v_{\mathrm h} M_{H_2}^2}{c_\alpha} + c_\alpha\left(M_{H_1}^2 - M_{H_2}^2\right)\left(s_\alpha v_{\mathrm h} + c_\alpha v_{\mathrm s}\right)\right)}{\left(M_{H_1}^2 + M_{H_2}^2\right) v_{\mathrm h} + \left(M_{H_1}^2 - M_{H_2}^2\right)\left(\left(2 c_\alpha^2 - 1\right) v_{\mathrm h} - 2 c_\alpha s_\alpha v_{\mathrm s}\right)} \\[4pt]
& - \delta Z_{H_1 H_2} \times \frac{c_\alpha\left(\left(M_{H_1}^2 - M_{H_2}^2\right) c_\alpha^2 + M_{H_2}^2\right) v_{\mathrm h}}{s_\alpha\left(\left(M_{H_1}^2 + M_{H_2}^2\right) v_{\mathrm h} + \left(M_{H_1}^2 - M_{H_2}^2\right)\left(\left(2 c_\alpha^2 - 1\right) v_{\mathrm h} - 2 c_\alpha s_\alpha v_{\mathrm s}\right)\right)} \\[4pt]
& + \delta Z_{H_1 H_1} \times \frac{1}{2} + \delta Z_{H_2 H_2} \times \frac{1}{2} + \delta Z_H,
\end{aligned}
$$

$$\text{(A.20.10)}$$

$$
\begin{aligned}
\delta C_{H_2 H_2 \phi^+ \phi^-} = {}& \delta t_{H_1} \times \frac{s_\alpha v_{\mathrm{h}} c_\alpha}{v_{\mathrm{s}}\left(\left(M_{H_1}^2 - M_{H_2}^2\right)v_{\mathrm{s}} c_\alpha^3 + \left(\left(M_{H_1}^2 - M_{H_2}^2\right)c_\alpha^2 + M_{H_2}^2\right)s_\alpha v_{\mathrm{h}}\right)} \\
&+ \delta t_{H_2} \times \frac{s_\alpha^2 v_{\mathrm{h}}}{v_{\mathrm{s}}\left(\left(M_{H_2}^2 - M_{H_1}^2\right)v_{\mathrm{s}} c_\alpha^3 + \left(-\left(M_{H_1}^2 - M_{H_2}^2\right)c_\alpha^2 - M_{H_2}^2\right)s_\alpha v_{\mathrm{h}}\right)} \\
&+ \delta v_{\mathrm{s}} \times \frac{\left(M_{H_1}^2 v_{\mathrm{s}} c_\alpha^3 - M_{H_2}^2 v_{\mathrm{s}} c_\alpha^3 + 2M_{H_1}^2 s_\alpha v_{\mathrm{h}} c_\alpha^2 - 2M_{H_2}^2 s_\alpha v_{\mathrm{h}} c_\alpha^2 + 2M_{H_2}^2 s_\alpha v_{\mathrm{h}}\right)}{v_{\mathrm{s}}\left(-M_{H_1}^2 v_{\mathrm{s}} c_\alpha^3 + M_{H_2}^2 v_{\mathrm{s}} c_\alpha^3 - M_{H_1}^2 s_\alpha v_{\mathrm{h}} c_\alpha^2 + M_{H_2}^2 s_\alpha v_{\mathrm{h}} c_\alpha^2 - M_{H_2}^2 s_\alpha v_{\mathrm{h}}\right)} \\
&- \delta v_{\mathrm{h}} \times \frac{\left(s_\alpha^3 v_{\mathrm{h}} - c_\alpha^3 v_{\mathrm{s}}\right)}{v_{\mathrm{h}}\left(\left(M_{H_1}^2 - M_{H_2}^2\right)v_{\mathrm{s}} c_\alpha^3 + \left(\left(M_{H_1}^2 - M_{H_2}^2\right)c_\alpha^2 + M_{H_2}^2\right)s_\alpha v_{\mathrm{h}}\right)} \\
&+ \delta M_{H_1}^2 \times \frac{1}{M_{H_1}^2 - M_{H_2}^2 + \frac{M_{H_2}^2 s_\alpha v_{\mathrm{h}}}{c_\alpha^2 \left(s_\alpha v_{\mathrm{h}} + c_\alpha v_{\mathrm{s}}\right)}} + \delta M_{H_2}^2 \times \frac{\left(M_{H_1}^2 - M_{H_2}^2\right)}{\left(M_{H_1}^2 - M_{H_2}^2\right)v_{\mathrm{s}} c_\alpha^3 + \left(\left(M_{H_1}^2 - M_{H_2}^2\right)c_\alpha^2 + M_{H_2}^2\right)s_\alpha v_{\mathrm{h}}} \\
&+ \delta M_{H_1 H_2}^2 \times \frac{\left(\frac{c_\alpha\left(2c_\alpha^2 - 1\right)v_{\mathrm{s}}}{s_\alpha} - 2s_\alpha^2 v_{\mathrm{h}}\right)c_\alpha}{\left(M_{H_1}^2 - M_{H_2}^2\right)v_{\mathrm{s}} c_\alpha^3 + \left(\left(M_{H_1}^2 - M_{H_2}^2\right)c_\alpha^2 + M_{H_2}^2\right)s_\alpha v_{\mathrm{h}}} \\
&+ \delta Z_{H_1 H_2} \times \frac{\left(c_\alpha\left(M_{H_1}^2 - M_{H_2}^2\right)\left(s_\alpha v_{\mathrm{s}} - c_\alpha v_{\mathrm{h}}\right) - M_{H_2}^2 v_{\mathrm{h}}\right)c_\alpha}{\left(M_{H_1}^2 - M_{H_2}^2\right)v_{\mathrm{s}} c_\alpha^3 + \left(\left(M_{H_1}^2 - M_{H_2}^2\right)c_\alpha^2 + M_{H_2}^2\right)s_\alpha v_{\mathrm{h}}} + \delta Z_{H_2 H_2} + \delta Z_H .
\end{aligned}
$$

$$(\text{A.20.11})$$

B

$\mathrm{U}(1)_{Y_\mathrm{h}}$ Ward identities

Here we list a set of Ward identities resulting from the case of a global $\mathrm{U}(1)_{Y_\mathrm{h}}$ symmetry of the (quantized) Lagrangian $\mathcal{L}_{\mathrm{EHS}}$ (cf. Chapter 3). It consists of relations between scalar n-point vertex functions $\Gamma_{\mathrm{X}_1\ldots\mathrm{X}_n}$ with $n \leq 5$ and $\mathrm{X}_i = H_1, H_2, \varphi_\mathrm{s}, \varphi_\mathrm{h}, \phi^\pm$. These generally apply to the EHSG model − but also to the EHSL model if the global $\mathrm{U}(1)_{Y_\mathrm{h}}$ is unbroken.[1] Our renormalization scheme does not introduce any symmetry-restoring counterterms (cf. Chapter 5). As a consequence, at the one-loop order all these Ward identities separately apply to the respective renormalized vertex functions, unrenormalized vertex functions and vertex counterterms.

B.1 Conventions

Under the infinitesimal global $\mathrm{U}(1)_{Y_\mathrm{h}}$ transformation $\delta\theta_\mathrm{h} = \frac{Y_\mathrm{h}}{2}\delta\theta^{Y_\mathrm{h}}$ the scalar fields behave as

$$
\begin{aligned}
\frac{\delta H_1(x)}{\delta\theta_\mathrm{h}} &= s_\alpha\varphi_\mathrm{h}(x), & \frac{\delta\varphi_\mathrm{s}(x)}{\delta\theta_\mathrm{h}} &= \frac{\delta\phi^\pm(x)}{\delta\theta_\mathrm{h}} = 0, \\
\frac{\delta H_2(x)}{\delta\theta_\mathrm{h}} &= c_\alpha\varphi_\mathrm{h}(x), & \frac{\delta\varphi_\mathrm{h}(x)}{\delta\theta_\mathrm{h}} &= -v_\mathrm{h} - s_\alpha H_1(x) - c_\alpha H_2(x),
\end{aligned}
\tag{B.1.1}
$$

according to (3.3.4). Due to the global $\mathrm{U}(1)_{Y_\mathrm{h}}$ symmetry the variation of the corresponding vertex functional $\Gamma\left(H_1, H_2, \varphi_\mathrm{s}, \varphi_\mathrm{h}, \phi\right)$ under $\delta\theta_\mathrm{h}$ vanishes, i.e.

$$
\begin{aligned}
\mathcal{S}(\Gamma) = \frac{\delta\Gamma}{\delta\theta_\mathrm{h}} = \int d^4x \Bigg\{ & s_\alpha\varphi_\mathrm{h}(x)\frac{\delta\Gamma}{\delta H_1(x)} + c_\alpha\varphi_\mathrm{h}(x)\frac{\delta\Gamma}{\delta H_2(x)} \\
& - \left[v_\mathrm{h} + s_\alpha H_1(x) + c_\alpha H_2(x)\right]\frac{\delta\Gamma}{\delta\varphi_\mathrm{h}(x)} \Bigg\} = 0.
\end{aligned}
\tag{B.1.2}
$$

After the appropriate functional differentiation of $\mathcal{S}(\Gamma)$ the fields are set to zero which is denoted by the label $\phi = 0$. Consequently, we obtain various relations between

---

[1]Note that we fix the non-standard gauge parameters of the EHSL model according to the 't Hooft-Feynman gauge (cf. Sect. 3.2) such that here the associated global $\mathrm{U}(1)_{Y_\mathrm{h}}$ is broken.

different vertex functions

$$\Gamma_{X_1\ldots X_n}(x_1,\ldots,x_n) = \frac{\delta^{(n)}\Gamma}{\delta X_1(x_1)\ldots\delta X_n(x_n)}\bigg|_{\phi=0} \tag{B.1.3}$$

in configuration space. The relations listed below are obtained by subsequently transforming to momentum space. Here, the momenta are assigned according to the notation $\Gamma_{abc\ldots}(p_a, p_b, p_c, \ldots)$. Moreover, we use the short notation $p_{1\ldots m} = -\sum_{i=1}^{m} p_i$. All momenta are considered as incoming.

B.2   Relations between vertex functions

Relations involving n-point functions with $n > 5$ are omitted since these are independent of the related counterterm structure at the one-loop level. The same holds for relations which do not involve any of the existing tree-level vertex functions.

$$\frac{\delta\mathcal{S}(\Gamma)}{\delta\varphi_{\mathrm{h}}(a)}\bigg|_{\phi=0} = 0 :$$

$$\longrightarrow\ 0 = -s_\alpha\Gamma_{H_1}(0) - c_\alpha\Gamma_{H_2}(0) + v_{\mathrm{h}}\Gamma_{\varphi_{\mathrm{h}}\varphi_{\mathrm{h}}}(0,0), \tag{B.2.1}$$

$$\frac{\delta^2\mathcal{S}(\Gamma)}{\delta H_1(a)\delta\varphi_{\mathrm{h}}(b)}\bigg|_{\phi=0} = 0 :$$

$$\longrightarrow\ 0 = -s_\alpha\Gamma_{H_1 H_1}(-p, p) - c_\alpha\Gamma_{H_1 H_2}(-p, p) + s_\alpha\Gamma_{\varphi_{\mathrm{h}}\varphi_{\mathrm{h}}}(-p, p) + v_{\mathrm{h}}\Gamma_{\varphi_{\mathrm{h}} H_1 \varphi_{\mathrm{h}}}(0, -p, p),$$

$$\tag{B.2.2}$$

$$\frac{\delta^2\mathcal{S}(\Gamma)}{\delta H_2(a)\delta\varphi_{\mathrm{h}}(b)}\bigg|_{\phi=0} = 0 :$$

$$\longrightarrow\ 0 = -c_\alpha\Gamma_{H_2 H_2}(-p, p) - s_\alpha\Gamma_{H_2 H_1}(-p, p) + c_\alpha\Gamma_{\varphi_{\mathrm{h}}\varphi_{\mathrm{h}}}(-p, p) + v_{\mathrm{h}}\Gamma_{\varphi_{\mathrm{h}} H_2 \varphi_{\mathrm{h}}}(0, -p, p),$$

$$\tag{B.2.3}$$

$$\left.\frac{\delta^3 \mathcal{S}(\Gamma)}{\delta H_1(a)\delta H_1(b)\delta\varphi_{\mathrm{h}}(c)}\right|_{\phi=0} = 0 :$$

$$\longrightarrow \; 0 = -s_\alpha \Gamma_{H_1 H_1 H_1}(p_{12}, p_1, p_2) - c_\alpha \Gamma_{H_1 H_1 H_2}(p_{12}, p_1, p_2) + s_\alpha \Gamma_{H_1 \varphi_{\mathrm{h}} \varphi_{\mathrm{h}}}(p_{12}, p_1, p_2)$$
$$+ s_\alpha \Gamma_{\varphi_{\mathrm{h}} H_1 \varphi_{\mathrm{h}}}(p_{12}, p_1, p_2) + v_{\mathrm{h}} \Gamma_{\varphi_{\mathrm{h}} H_1 H_1 \varphi_{\mathrm{h}}}(0, p_{12}, p_1, p_2),$$

$$(\mathrm{B}.2.4)$$

$$\left.\frac{\delta^3 \mathcal{S}(\Gamma)}{\delta H_1(a)\delta H_2(b)\delta\varphi_{\mathrm{h}}(c)}\right|_{\phi=0} = 0 :$$

$$\longrightarrow \; 0 = -s_\alpha \Gamma_{H_1 H_2 H_1}(p_{12}, p_1, p_2) - c_\alpha \Gamma_{H_1 H_2 H_2}(p_{12}, p_1, p_2) + c_\alpha \Gamma_{H_1 \varphi_{\mathrm{h}} \varphi_{\mathrm{h}}}(p_{12}, p_1, p_2)$$
$$+ s_\alpha \Gamma_{\varphi_{\mathrm{h}} H_2 \varphi_{\mathrm{h}}}(p_{12}, p_1, p_2) + v_{\mathrm{h}} \Gamma_{\varphi_{\mathrm{h}} H_1 H_2 \varphi_{\mathrm{h}}}(0, p_{12}, p_1, p_2),$$

$$(\mathrm{B}.2.5)$$

$$\left.\frac{\delta^3 \mathcal{S}(\Gamma)}{\delta H_2(a)\delta H_2(b)\delta\varphi_{\mathrm{h}}(c)}\right|_{\phi=0} = 0 :$$

$$\longrightarrow \; 0 = -s_\alpha \Gamma_{H_2 H_2 H_1}(p_{12}, p_1, p_2) - c_\alpha \Gamma_{H_2 H_2 H_2}(p_{12}, p_1, p_2) + c_\alpha \Gamma_{H_2 \varphi_{\mathrm{h}} \varphi_{\mathrm{h}}}(p_{12}, p_1, p_2)$$
$$+ c_\alpha \Gamma_{\varphi_{\mathrm{h}} H_2 \varphi_{\mathrm{h}}}(p_{12}, p_1, p_2) + v_{\mathrm{h}} \Gamma_{\varphi_{\mathrm{h}} H_2 H_2 \varphi_{\mathrm{h}}}(0, p_{12}, p_1, p_2),$$

$$(\mathrm{B}.2.6)$$

$$\left.\frac{\delta^3 \mathcal{S}(\Gamma)}{\delta\varphi_{\mathrm{s}}(a)\delta\varphi_{\mathrm{s}}(b)\delta\varphi_{\mathrm{h}}(c)}\right|_{\phi=0} = 0 :$$

$$\longrightarrow \; 0 = -s_\alpha \Gamma_{\varphi_{\mathrm{s}} \varphi_{\mathrm{s}} H_1}(p_{12}, p_1, p_2) - c_\alpha \Gamma_{\varphi_{\mathrm{s}} \varphi_{\mathrm{s}} H_2}(p_{12}, p_1, p_2) + v_{\mathrm{h}} \Gamma_{\varphi_{\mathrm{h}} \varphi_{\mathrm{s}} \varphi_{\mathrm{s}} \varphi_{\mathrm{h}}}(0, p_{12}, p_1, p_2),$$

$$(\mathrm{B}.2.7)$$

$$\left.\frac{\delta^3 \mathcal{S}(\Gamma)}{\delta\varphi_{\mathrm{h}}(a)\delta\varphi_{\mathrm{h}}(b)\delta\varphi_{\mathrm{h}}(c)}\right|_{\phi=0} = 0 :$$

$$\longrightarrow \; 0 = -s_\alpha \Gamma_{\varphi_{\mathrm{h}} \varphi_{\mathrm{h}} H_1}(p_{12}, p_1, p_2) - s_\alpha \Gamma_{\varphi_{\mathrm{h}} H_1 \varphi_{\mathrm{h}}}(p_{12}, p_1, p_2) - s_\alpha \Gamma_{H_1 \varphi_{\mathrm{h}} \varphi_{\mathrm{h}}}(p_{12}, p_1, p_2)$$
$$- c_\alpha \Gamma_{\varphi_{\mathrm{h}} \varphi_{\mathrm{h}} H_2}(p_{12}, p_1, p_2) - c_\alpha \Gamma_{\varphi_{\mathrm{h}} H_2 \varphi_{\mathrm{h}}}(p_{12}, p_1, p_2) - c_\alpha \Gamma_{H_2 \varphi_{\mathrm{h}} \varphi_{\mathrm{h}}}(p_{12}, p_1, p_2)$$
$$+ v_{\mathrm{h}} \Gamma_{\varphi_{\mathrm{h}} \varphi_{\mathrm{h}} \varphi_{\mathrm{h}} \varphi_{\mathrm{h}}}(0, p_{12}, p_1, p_2),$$

$$(\mathrm{B}.2.8)$$

$$\frac{\delta^3 \mathcal{S}(\Gamma)}{\delta\varphi_h(a)\delta\phi^+(b)\delta\phi^-(c)}\bigg|_{\phi=0} = 0 :$$

$$\longrightarrow 0 = -s_\alpha \Gamma_{H_1\phi^+\phi^-}(p_{12}, p_1, p_2) - c_\alpha \Gamma_{H_2\phi^+\phi^-}(p_{12}, p_1, p_2) + v_h \Gamma_{\varphi_h\varphi_h\phi^+\phi^-}(0, p_{12}, p_1, p_2),$$

$$(B.2.9)$$

$$\frac{\delta^4 \mathcal{S}(\Gamma)}{\delta H_1(a)\delta H_1(b)\delta H_1(c)\delta\varphi_h(d)}\bigg|_{\phi=0} = 0 :$$

$$\longrightarrow 0 = -s_\alpha \Gamma_{H_1 H_1 H_1 H_1}(p_{123}, p_1, p_2, p_3) - c_\alpha \Gamma_{H_1 H_1 H_1 H_2}(p_{123}, p_1, p_2, p_3)$$
$$+ s_\alpha \Gamma_{H_1 H_1 \varphi_h \varphi_h}(p_{123}, p_1, p_2, p_3) + s_\alpha \Gamma_{H_1 \varphi_h H_1 \varphi_h}(p_{123}, p_1, p_2, p_3)$$
$$+ s_\alpha \Gamma_{\varphi_h H_1 H_1 \varphi_h}(p_{123}, p_1, p_2, p_3) + v_h \Gamma_{\varphi_h H_1 H_1 H_1 \varphi_h}(0, p_{123}, p_1, p_2, p_3),$$

$$(B.2.10)$$

$$\frac{\delta^4 \mathcal{S}(\Gamma)}{\delta H_1(a)\delta H_1(b)\delta H_2(c)\delta\varphi_h(d)}\bigg|_{\phi=0} = 0 :$$

$$\longrightarrow 0 = -s_\alpha \Gamma_{H_1 H_1 H_2 H_1}(p_{123}, p_1, p_2, p_3) - c_\alpha \Gamma_{H_1 H_1 H_2 H_2}(p_{123}, p_1, p_2, p_3)$$
$$+ c_\alpha \Gamma_{H_1 H_1 \varphi_h \varphi_h}(p_{123}, p_1, p_2, p_3) + s_\alpha \Gamma_{H_1 \varphi_h H_2 \varphi_h}(p_{123}, p_1, p_2, p_3)$$
$$+ s_\alpha \Gamma_{\varphi_h H_1 H_2 \varphi_h}(p_{123}, p_1, p_2, p_3) + v_h \Gamma_{\varphi_h H_1 H_1 H_2 \varphi_h}(0, p_{123}, p_1, p_2, p_3),$$

$$(B.2.11)$$

$$\frac{\delta^4 \mathcal{S}(\Gamma)}{\delta H_1(a)\delta H_2(b)\delta H_2(c)\delta\varphi_h(d)}\bigg|_{\phi=0} = 0 :$$

$$\longrightarrow 0 = -s_\alpha \Gamma_{H_1 H_2 H_2 H_1}(p_{123}, p_1, p_2, p_3) - c_\alpha \Gamma_{H_1 H_2 H_2 H_2}(p_{123}, p_1, p_2, p_3)$$
$$+ c_\alpha \Gamma_{H_1 H_2 \varphi_h \varphi_h}(p_{123}, p_1, p_2, p_3) + c_\alpha \Gamma_{H_1 \varphi_h H_2 \varphi_h}(p_{123}, p_1, p_2, p_3)$$
$$+ s_\alpha \Gamma_{\varphi_h H_2 H_2 \varphi_h}(p_{123}, p_1, p_2, p_3) + v_h \Gamma_{\varphi_h H_1 H_2 H_2 \varphi_h}(0, p_{123}, p_1, p_2, p_3),$$

$$(B.2.12)$$

$$\frac{\delta^4 \mathcal{S}(\Gamma)}{\delta H_2(a)\delta H_2(b)\delta H_2(c)\delta\varphi_{\rm h}(d)}\bigg|_{\phi=0} = 0 :$$

$$\begin{aligned}
\longrightarrow 0 = &-s_\alpha \Gamma_{H_2 H_2 H_2 H_1}(p_{123}, p_1, p_2, p_3) - c_\alpha \Gamma_{H_2 H_2 H_2 H_2}(p_{123}, p_1, p_2, p_3) \\
&+ c_\alpha \Gamma_{H_2 H_2 \varphi_{\rm h} \varphi_{\rm h}}(p_{123}, p_1, p_2, p_3) + c_\alpha \Gamma_{H_2 \varphi_{\rm h} H_2 \varphi_{\rm h}}(p_{123}, p_1, p_2, p_3) \\
&+ c_\alpha \Gamma_{\varphi_{\rm h} H_2 H_2 \varphi_{\rm h}}(p_{123}, p_1, p_2, p_3) + v_{\rm h} \Gamma_{\varphi_{\rm h} H_2 H_2 \varphi_{\rm h}}(0, p_{123}, p_1, p_2, p_3),
\end{aligned}$$

$$\text{(B.2.13)}$$

$$\frac{\delta^4 \mathcal{S}(\Gamma)}{\delta H_1(a)\delta\varphi_{\rm s}(b)\delta\varphi_{\rm s}(c)\delta\varphi_{\rm h}(d)}\bigg|_{\phi=0} = 0 :$$

$$\begin{aligned}
\longrightarrow 0 = &-s_\alpha \Gamma_{H_1 \varphi_{\rm s} \varphi_{\rm s} H_1}(p_{123}, p_1, p_2, p_3) - c_\alpha \Gamma_{H_1 \varphi_{\rm s} \varphi_{\rm s} H_2}(p_{123}, p_1, p_2, p_3) \\
&+ s_\alpha \Gamma_{\varphi_{\rm h} \varphi_{\rm s} \varphi_{\rm s} \varphi_{\rm h}}(p_{123}, p_1, p_2, p_3) + v_{\rm h} \Gamma_{\varphi_{\rm h} H_1 \varphi_{\rm s} \varphi_{\rm s} \varphi_{\rm h}}(0, p_{123}, p_1, p_2, p_3),
\end{aligned}$$

$$\text{(B.2.14)}$$

$$\frac{\delta^4 \mathcal{S}(\Gamma)}{\delta H_2(a)\delta\varphi_{\rm s}(b)\delta\varphi_{\rm s}(c)\delta\varphi_{\rm h}(d)}\bigg|_{\phi=0} = 0 :$$

$$\begin{aligned}
\longrightarrow 0 = &-s_\alpha \Gamma_{H_2 \varphi_{\rm s} \varphi_{\rm s} H_1}(p_{123}, p_1, p_2, p_3) - c_\alpha \Gamma_{H_2 \varphi_{\rm s} \varphi_{\rm s} H_2}(p_{123}, p_1, p_2, p_3) \\
&+ c_\alpha \Gamma_{\varphi_{\rm h} \varphi_{\rm s} \varphi_{\rm s} \varphi_{\rm h}}(p_{123}, p_1, p_2, p_3) + v_{\rm h} \Gamma_{\varphi_{\rm h} H_2 \varphi_{\rm s} \varphi_{\rm s} \varphi_{\rm h}}(0, p_{123}, p_1, p_2, p_3),
\end{aligned}$$

$$\text{(B.2.15)}$$

$$\frac{\delta^4 \mathcal{S}(\Gamma)}{\delta H_1(a)\delta\varphi_{\rm h}(b)\delta\varphi_{\rm h}(c)\delta\varphi_{\rm h}(d)}\bigg|_{\phi=0} = 0 :$$

$$\begin{aligned}
\longrightarrow 0 = &-s_\alpha \Gamma_{H_1 \varphi_{\rm h} \varphi_{\rm h} H_1}(p_{123}, p_1, p_2, p_3) - c_\alpha \Gamma_{H_1 \varphi_{\rm h} \varphi_{\rm h} H_2}(p_{123}, p_1, p_2, p_3) \\
&- s_\alpha \Gamma_{H_1 \varphi_{\rm h} H_1 \varphi_{\rm h}}(p_{123}, p_1, p_2, p_3) - c_\alpha \Gamma_{H_1 \varphi_{\rm h} H_2 \varphi_{\rm h}}(p_{123}, p_1, p_2, p_3) \\
&- s_\alpha \Gamma_{H_1 H_1 \varphi_{\rm h} \varphi_{\rm h}}(p_{123}, p_1, p_2, p_3) - c_\alpha \Gamma_{H_1 H_2 \varphi_{\rm h} \varphi_{\rm h}}(p_{123}, p_1, p_2, p_3) \\
&+ s_\alpha \Gamma_{\varphi_{\rm h} \varphi_{\rm h} \varphi_{\rm h} \varphi_{\rm h}}(p_{123}, p_1, p_2, p_3) + v_{\rm h} \Gamma_{\varphi_{\rm h} H_1 \varphi_{\rm h} \varphi_{\rm h} \varphi_{\rm h}}(0, p_{123}, p_1, p_2, p_3),
\end{aligned}$$

$$\text{(B.2.16)}$$

$$\left. \frac{\delta^4 \mathcal{S}(\Gamma)}{\delta H_2(a) \delta \varphi_h(b) \delta \varphi_h(c) \delta \varphi_h(d)} \right|_{\phi=0} = 0 :$$

$$
\begin{aligned}
\longrightarrow \quad 0 = &-s_\alpha \Gamma_{H_2 \varphi_h \varphi_h H_1}(p_{123}, p_1, p_2, p_3) - c_\alpha \Gamma_{H_2 \varphi_h \varphi_h H_2}(p_{123}, p_1, p_2, p_3) \\
&-s_\alpha \Gamma_{H_2 \varphi_h H_1 \varphi_h}(p_{123}, p_1, p_2, p_3) - c_\alpha \Gamma_{H_2 \varphi_h H_2 \varphi_h}(p_{123}, p_1, p_2, p_3) \\
&-s_\alpha \Gamma_{H_2 H_1 \varphi_h \varphi_h}(p_{123}, p_1, p_2, p_3) - c_\alpha \Gamma_{H_2 H_2 \varphi_h \varphi_h}(p_{123}, p_1, p_2, p_3) \\
&+c_\alpha \Gamma_{\varphi_h \varphi_h \varphi_h \varphi_h}(p_{123}, p_1, p_2, p_3) + v_h \Gamma_{\varphi_h H_2 \varphi_h \varphi_h}(0, p_{123}, p_1, p_2, p_3),
\end{aligned}
$$

$$\text{(B.2.17)}$$

$$\left. \frac{\delta^4 \mathcal{S}(\Gamma)}{\delta H_1(a) \delta \phi^+(b) \delta \phi^-(c) \delta \varphi_h(d)} \right|_{\phi=0} = 0 :$$

$$
\begin{aligned}
\longrightarrow \quad 0 = &-s_\alpha \Gamma_{H_1 \phi^+ \phi^- H_1}(p_{123}, p_1, p_2, p_3) - c_\alpha \Gamma_{H_1 \phi^+ \phi^- H_2}(p_{123}, p_1, p_2, p_3) \\
&+s_\alpha \Gamma_{\varphi_h \phi^+ \phi^- \varphi_h}(p_{123}, p_1, p_2, p_3) + v_h \Gamma_{\varphi_h H_1 \phi^+ \phi^- \varphi_h}(0, p_{123}, p_1, p_2, p_3),
\end{aligned}
$$

$$\text{(B.2.18)}$$

$$\left. \frac{\delta^4 \mathcal{S}(\Gamma)}{\delta H_2(a) \delta \phi^+(b) \delta \phi^-(c) \delta \varphi_h(d)} \right|_{\phi=0} = 0 :$$

$$
\begin{aligned}
\longrightarrow \quad 0 = &-s_\alpha \Gamma_{H_2 \phi^+ \phi^- H_1}(p_{123}, p_1, p_2, p_3) - c_\alpha \Gamma_{H_2 \phi^+ \phi^- H_2}(p_{123}, p_1, p_2, p_3) \\
&+c_\alpha \Gamma_{\varphi_h \phi^+ \phi^- \varphi_h}(p_{123}, p_1, p_2, p_3) + v_h \Gamma_{\varphi_h H_2 \phi^+ \phi^- \varphi_h}(0, p_{123}, p_1, p_2, p_3).
\end{aligned}
$$

$$\text{(B.2.19)}$$

As already mentioned, these identities apply to the renormalized and unrenormalized vertex functions. Consequently, we obtain relations between the corresponding vertex counterterms and between the associated renormalization constants. The renormalization constant δv_h drops out in each of these relations. Remarkably enough, the identities (B.2.2)−(B.2.9) imply that $\delta Z_\chi = 0$ is required in the renormalization scheme of the EHSG model. The transition (5.3.34) from the local to the global here generally follows from symmetry. This can be deduced by introducing the explicit expressions of the corresponding vertex counterterms according to Apps. A.10, A.11, A.19 and A.20 whilst taking into account (5.3.12) and (5.3.13).

Appendix C

Appended numerical results

In this appendix, further numerical results for the H_1-decay observables are collected, in completion of those discussed in Chapter 7. We refer to the latter for more information about the interpretation of the following results.
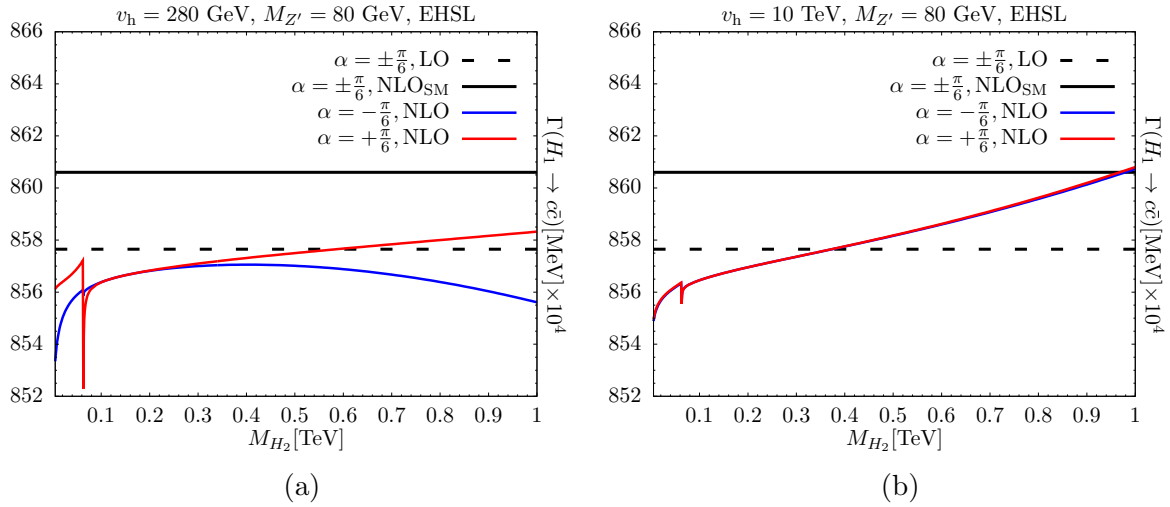
Figure C.1: EHSL predictions for the partial width $\Gamma(H_1 \to c\bar{c})$ for $v_\mathrm{h} = 280$ GeV (left side) and $v_\mathrm{h} = 10$ TeV (right side), with $M_{Z'} = 80$ GeV and $\alpha = \pm\pi/6$.
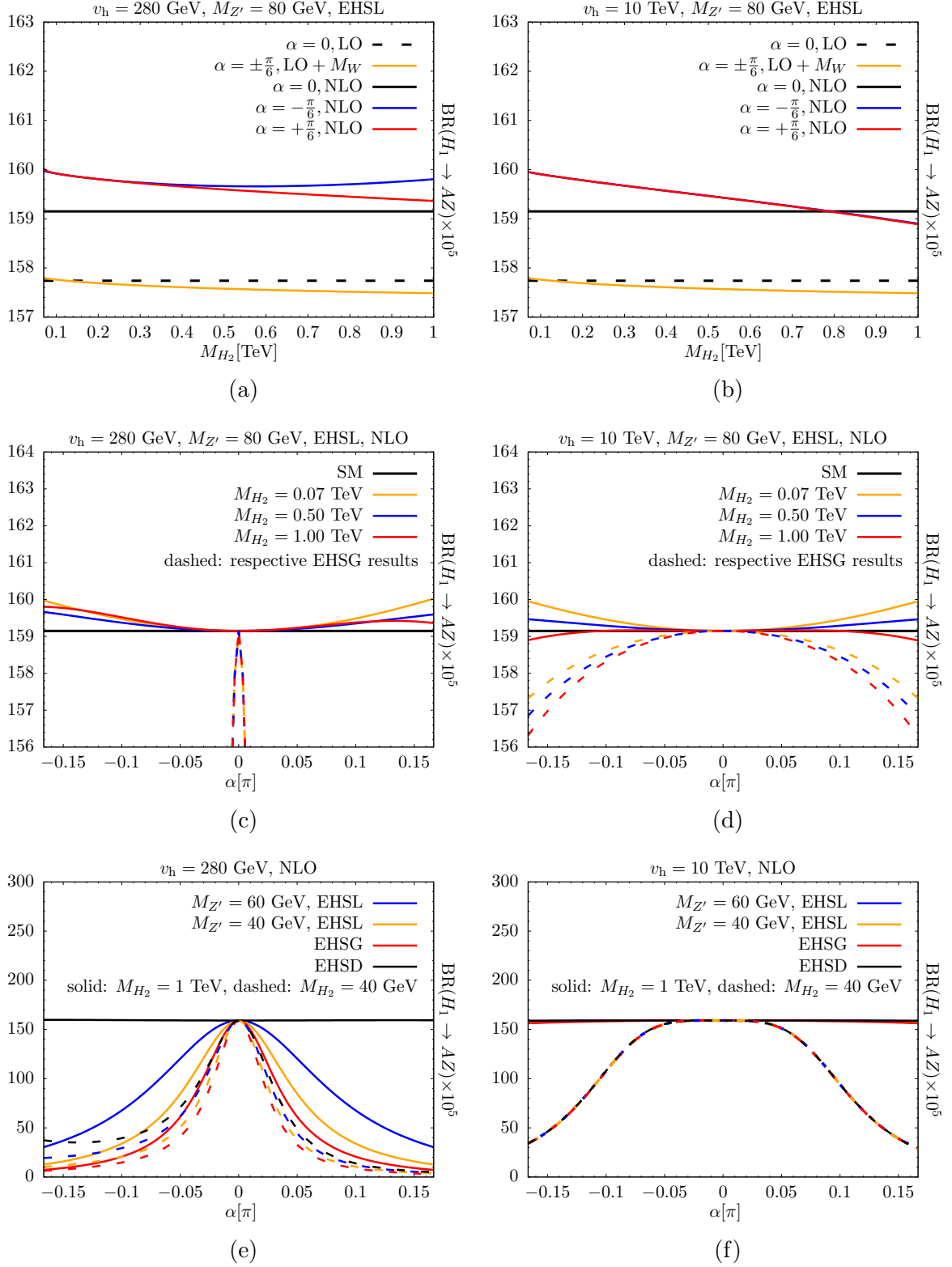
Figure C.2: Predictions for $\mathrm{BR}(H_1 \to AZ)$ in the EHSL, EHSG and EHSD models.
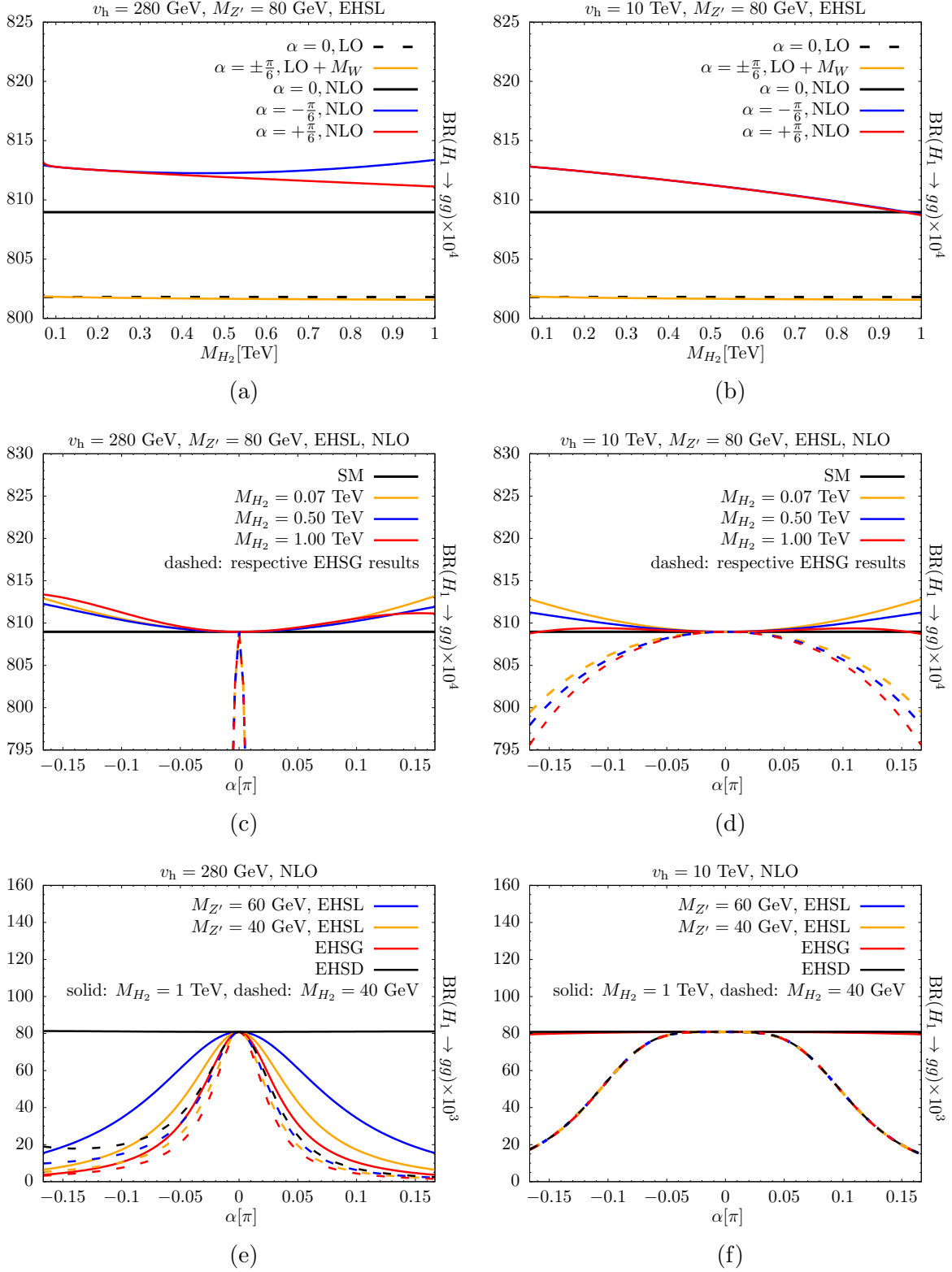
Figure C.3: Predictions for $\mathrm{BR}(H_1 \to gg)$ in the EHSL, EHSG and EHSD models.
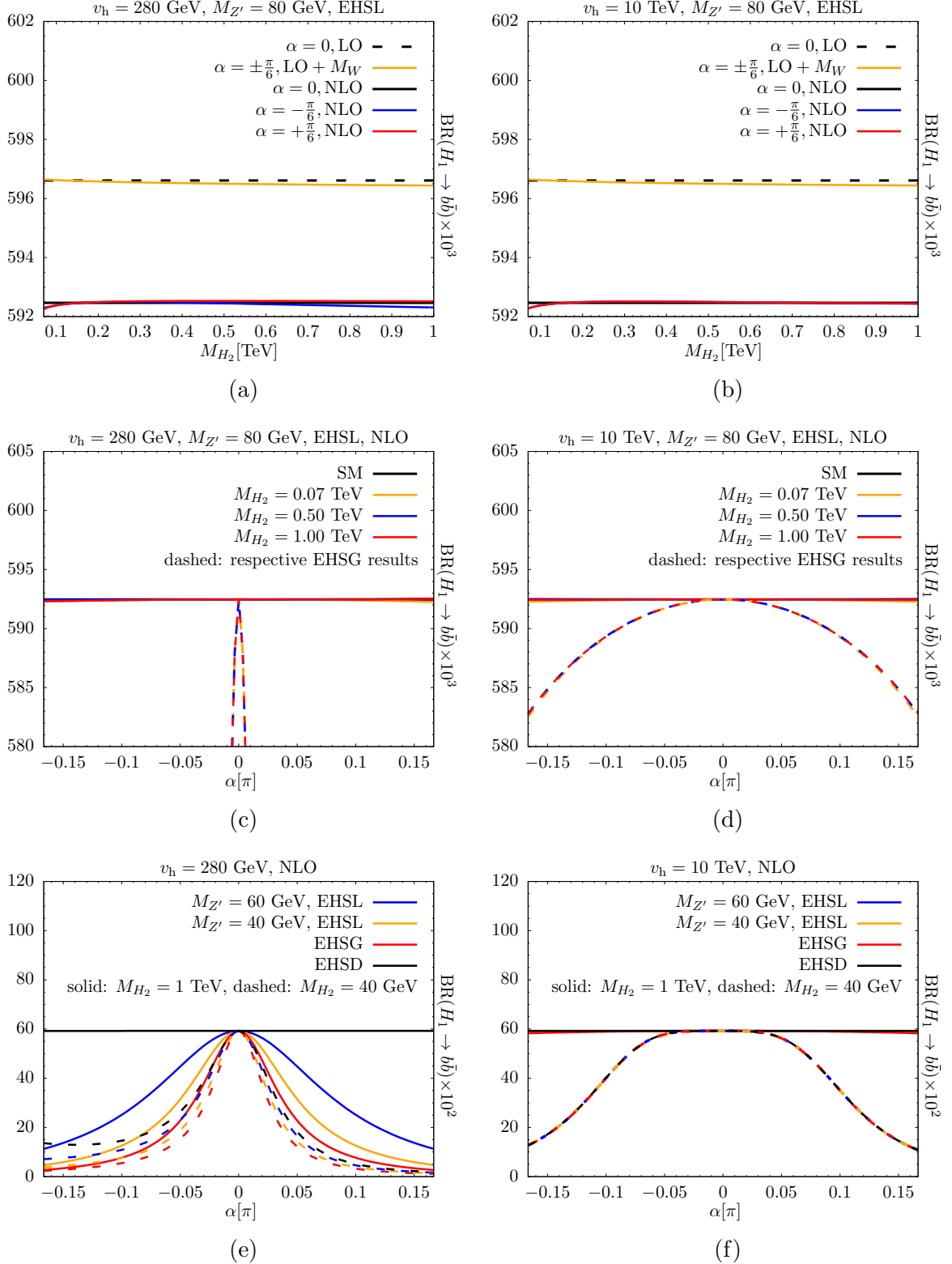
Figure C.4: Predictions for $\mathrm{BR}(H_1 \to b\bar{b})$ in the EHSL, EHSG and EHSD models.
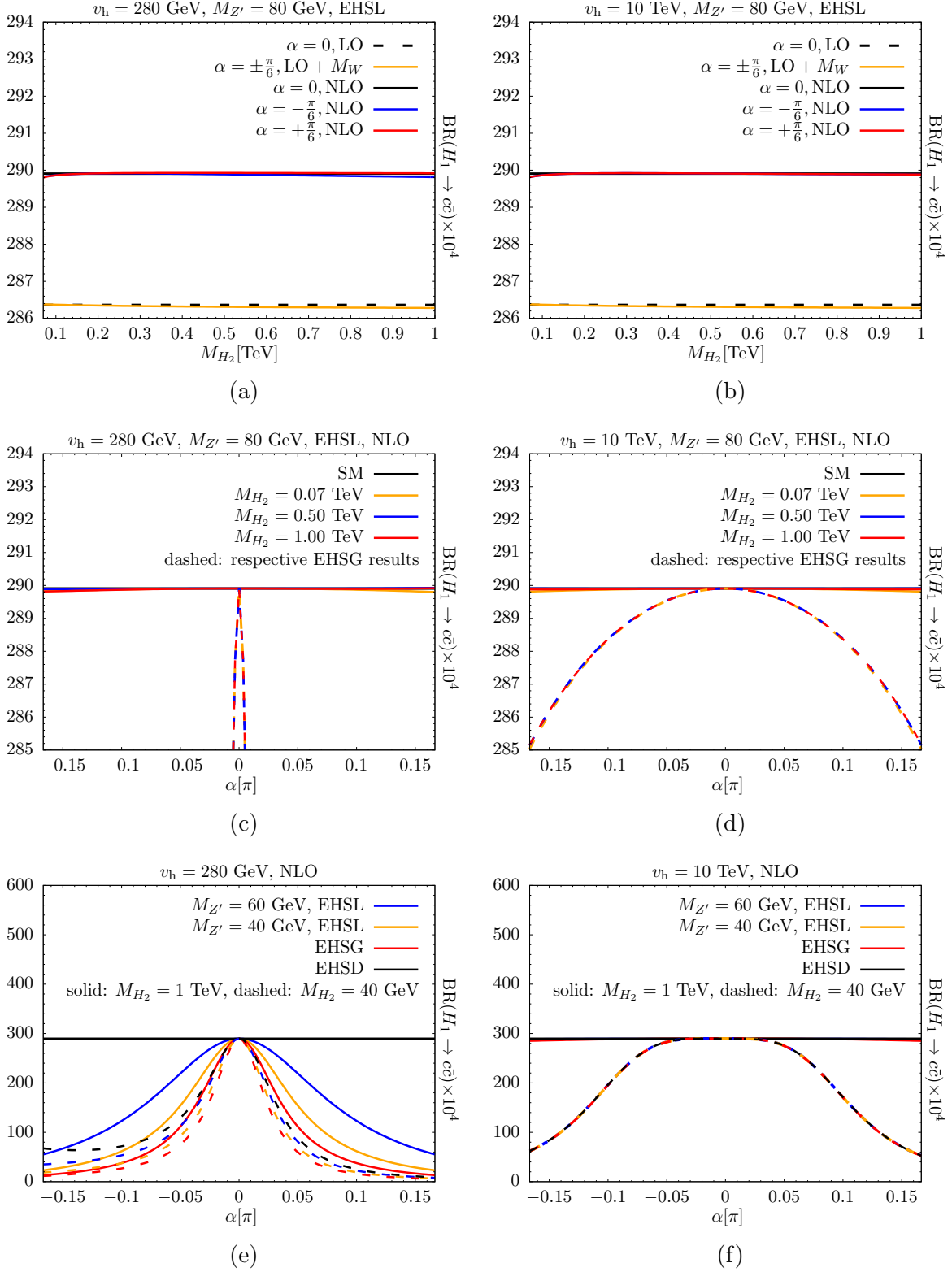
Figure C.5: Predictions for $\mathrm{BR}(H_1 \to c\bar{c})$ in the EHSL, EHSG and EHSD models.

Bibliography

[1] D.J. Gross and F. Wilczek. Ultraviolet Behavior of Non-Abelian Gauge Theories. *Phys. Rev. Lett.* **30**, pp. 1343-1346, 1973.

[2] D.J. Gross and F. Wilczek. Asymptotically Free Gauge Theories. I. *Phys. Rev.* ***D*8**, pp. 3633-3652, 1973.

[3] H.D. Politzer. Reliable Perturbative Results for Strong Interactions? *Phys. Rev. Lett.* **30**, pp. 1346-1349, 1973.

[4] H. Fritzsch, M. Gell-Mann and H. Leutwyler. Advantages of the color octet gluon picture. *Phys. Lett.* **47*B***, pp. 365-368, 1973.

[5] S.L. Glashow. Partial-symmetries of weak interactions. *Nucl. Phys.* **22**, pp. 579-588, 1961.

[6] S. Weinberg. A Model of Leptons. *Phys. Rev. Lett.* **19**, pp. 1264-1266, 1967.

[7] A. Salam. Weak and Electromagnetic Interactions. Elementary Particle Theory: Relativistic Groups and Analyticity, ed. N. Svartholm (Almqvist and Wiksell, Stockholm). *Proceedings of the 8th Nobel Symposium*, pp. 367-377, 1968.

[8] S.L. Glashow, J. Iliopoulos and L. Maiani. Weak Interactions with Lepton-Hadron Symmetry. *Phys. Rev.* ***D*2**, pp. 1285-1292, 1970.

[9] N. Cabibbo. Unitary Symmetry and Leptonic Decays. *Phys. Rev. Lett.* **10**, pp. 531-533, 1963.

[10] M. Kobayashi and T. Maskawa. CP Violation in the Renormalizable Theory of Weak Interaction. *Prog. Theor. Phys.* **49**, pp. 652-657, 1973.

[11] V.A. Bednyakov and N.D. Giokaris. On the Higgs mass generation mechanism in the Standard Model. *Phys. Part. Nucl.* **39**, pp. 13-36, 2008, hep-ph/0703280.

[12] P.W. Higgs. Broken symmetries, massless particles and gauge fields. *Phys. Lett.* **12**, pp. 132-133, 1964.

[13] F. Englert and R. Brout. Broken Symmetry and the Mass of Gauge Vector Mesons. *Phys. Rev. Lett.* **13**, pp. 321-323, 1964.

[14] T.W.B. Kibble. Symmetry Breaking in Non-Abelian Gauge Theories. *Phys. Rev.* **155**, pp. 1554-1561, 1967.

[15] G.S. Guralnik, C.R. Hagen and T.W.B. Kibble. Global Conservation Laws and Massless Particles. *Phys. Rev. Lett.* **13**, pp. 585-587, 1964.

[16] G. Aad and others. Observation of a new particle in the search for the Standard Model Higgs boson with the ATLAS detector at the LHC. *Phys. Lett.* **B716**, pp. 1-29, 2012, hep-ex/1207.7214.

[17] S. Chatrchyan and others. Observation of a new boson at a mass of 125 GeV with the CMS experiment at the LHC. *Phys. Lett.* **B716**, pp. 30-61, 2012, hep-ex/1207.7235.

[18] J. de Blas and others. Electroweak precision observables and Higgs-boson signal strengths in the Standard Model and beyond: present and future. *JHEP* **12**, p. 135, 2016, hep-ph/1608.01509.

[19] G. Aad and others. Combined Measurement of the Higgs Boson Mass in pp Collisions at $\sqrt{s} = 7$ and 8 TeV with the ATLAS and CMS Experiments. *Phys. Rev. Lett.* **114**, p. 191803, 2015, hep-ex/1503.07589.

[20] L. Canetti, M. Drewes and M. Shaposhnikov. Matter and antimatter in the universe. *New J. Phys.* **14**, p. 095012, 2012, hep-ph/1204.4186.

[21] T. Mannel. Theory and Phenomenology of CP Violation. *Nucl. Phys. Proc. Suppl.* **167**, pp. 115-119, 2007.

[22] F. Zwicky. Die Rotverschiebung von extragalaktischen Nebeln. *Helv. Phys. Acta* **6**, pp. 110-127, 1933.

[23] F. Zwicky. On the Masses of Nebulae and of Clusters of Nebulae. *Astrophys. J.* **86**, pp. 217-246, 1937.

[24] P.J.E. Peebles and B. Ratra. The cosmological constant and dark energy. *Rev. Mod. Phys.* **75**, pp. 559-606, 2003, astro-ph/0207347.

[25] D. Buttazzo and others. Investigating the near-criticality of the Higgs boson. *JHEP* **12**, p. 089, 2013, hep-ph/1307.3536.

[26] G. Cynolter, E. Lendvai and G. Pocsik. Note on Unitarity Constraints in a Model for a Singlet Scalar Dark Matter Candidate. *Acta Phys. Polon.* **B36**, pp. 827-832, 2005, hep-ph/0410102.

[27] R. Schabinger and J.D. Wells. A minimal spontaneously broken hidden sector and its impact on Higgs boson physics at the CERN Large Hadron Collider. *Phys. Rev.* **D72**, p. 093007, 2005, hep-ph/0509209.

[28] B. Patt and F. Wilczek. Higgs-field Portal into Hidden Sectors. 2006, hep-ph/0605188.

[29] M. Bowen, Y. Cui and J.D. Wells. Narrow trans-TeV Higgs bosons and $H \rightarrow hh$ decays: two LHC search paths for a hidden sector Higgs boson. *JHEP* **03**, p. 036, 2007, hep-ph/0701035.

[30] G. Bhattacharyya, G.C. Branco and S. Nandi. Universal doublet-singlet Higgs couplings and phenomenology at the CERN Large Hadron Collider. *Phys. Rev.* **D77**, p. 117701, 2008, hep-ph/0712.2693.

[31] S. Bock, R. Lafaye, T. Plehn, M. Rauch, D. Zerwas and others. Measuring hidden Higgs and strongly-interacting Higgs scenarios. *Phys. Lett.* **B694**, pp. 44-53, 2010, hep-ph/1007.2645.

[32] C. Englert, T. Plehn, D. Zerwas and P.M. Zerwas. Exploring the Higgs portal. *Phys. Lett.* **B703**, pp. 298-305, 2011, hep-ph/1106.3097.

[33] R.S. Gupta and J.D. Wells. Higgs boson search significance deformations due to mixed-in scalars. *Phys. Lett.* **B710**, pp. 154-158, 2012, hep-ph/1110.0824.

[34] C. Englert, T. Plehn, M. Rauch, D. Zerwas and P.M. Zerwas. LHC: Standard Higgs and hidden Higgs. *Phys. Lett.* **B707**, pp. 512-516, 2012, hep-ph/1112.3007.

[35] O. Lebedev. On stability of the electroweak vacuum and the Higgs portal. *Eur. Phys. J.* **C72**, p. 2058, 2012, hep-ph/1203.0156.

[36] M.J. Dolan, C. Englert and M. Spannowsky. New physics in LHC Higgs boson pair production. *Phys. Rev.* **D87**, p. 055002, 2013, hep-ph/1210.8166.

[37] Y. Farzan and A.R. Akbarieh. VDM: a model for vector dark matter. *JCAP* **1210**, p. 026, 2012, hep-ph/1207.4272.

[38] S. Baek, P. Ko, W.-I. Park and E. Senaha. Higgs portal vector dark matter: revisited. *JHEP* **05**, p. 036, 2013, hep-ph/1212.2131.

[39] G.M. Pruna and T. Robens. Higgs singlet extension parameter space in the light of the LHC discovery. *Phys. Rev.* **D88**, p. 115012, 2013, hep-ph/1303.1150.

[40] S. Baek, P. Ko and W.-I. Park. Invisible Higgs decay width vs. dark matter direct detection cross section in Higgs portal dark matter models. *Phys. Rev.* **D90**, p. 055014, 2014, hep-ph/1405.3530.

[41] R. Costa, M. Mühlleitner, M.O.P. Sampaio and R. Santos. Singlet extensions of the standard model at LHC Run 2: benchmarks and comparison with the NMSSM. *JHEP* **06**, p. 034, 2016, hep-ph/1512.05355.

[42] W. Chao. First order electroweak phase transition triggered by the Higgs portal vector dark matter. *Phys. Rev.* **D92**, p. 015025, 2015, hep-ph/1412.3823.

[43] M. Duch, B. Grzadkowski and M. McGarrie. A stable Higgs portal with vector dark matter. *JHEP* **09**, p. 162, 2015, hep-ph/1506.08805.

[44] V. Barger, P. Langacker, M. McCaskey, M.J. Ramsey-Musolf and G. Shaughnessy. CERN LHC phenomenology of an extended standard model with a real scalar singlet. *Phys. Rev.* **D77**, p. 035005, 2008, hep-ph/0706.4311.

[45] W. Guo and Y. Wu. The real singlet scalar dark matter model. *JHEP* **10**, p. 083, 2010, hep-ph/1006.2518.

[46] S. Kanemura, S. Matsumoto, T. Nabeshima and H. Taniguchi. Testing Higgs portal dark matter via Z fusion at a linear collider. *Phys. Lett.* **B701**, pp. 591-596, 2011, hep-ph/1102.5147.

[47] C. Englert, J. Jaeckel, E. Re and M. Spannowsky. Evasive Higgs maneuvers at the LHC. *Phys. Rev.* **D85**, p. 035008, 2012, hep-ph/1111.1719.

[48] P.J. Fox, D. Tucker-Smith and N. Weiner. Higgs friends and counterfeits at hadron colliders. *JHEP* **06**, p. 127, 2011, hep-ph/1104.5450.

[49] D. Bertolini and M. McCullough. The social Higgs. *JHEP* **12**, p. 118, 2012, hep-ph/1207.4209.

[50] C.-Y. Chen, S. Dawson and I.M. Lewis. Exploring resonant di-Higgs boson production in the Higgs singlet model. *Phys. Rev.* **D91**, p. 035015, 2015, hep-ph/1410.5488.

[51] F. Bojarski, G. Chalons, D. López-Val and T. Robens. Heavy to light Higgs boson decays at NLO in the singlet extension of the Standard Model. *JHEP* **02**, p. 147, 2016, hep-ph/1511.08120.

[52] D. López-Val and T. Robens. Δr and the W-boson mass in the singlet extension of the standard model. *Phys. Rev.* **D90**, p. 114018, 2014, hep-ph/1406.1043.

[53] A. Falkowski, C. Gross and O. Lebedev. A second Higgs from the Higgs portal. *JHEP* **05**, p. 057, 2015, hep-ph/1502.01361.

[54] S. Kanemura, M. Kikuchi and K. Yagyu. Radiative corrections to the Higgs boson couplings in the model with an additional real singlet scalar field. *Nucl. Phys.* **B907**, pp. 286-322, 2016, hep-ph/1511.06211.

[55] S. Ghosh, A. Kundu and S. Ray. Potential of a singlet scalar enhanced standard model. *Phys. Rev.* **D93**, p. 115034, 2016, hep-ph/1512.05786.

[56] S. Kanemura, M. Kikuchi and K. Yagyu. One-loop corrections to the Higgs self-couplings in the singlet extension. *Nucl. Phys.* **B917**, pp. 154-177, 2017, hep-ph/1608.01582.

[57] T. Robens and T. Stefaniak. LHC benchmark scenarios for the real Higgs singlet extension of the standard model. *Eur. Phys. J.* ***C76***, p. 268, 2016, hep-ph/1601.07880.

[58] A. Cuoco, B. Eiteneuer, J. Heisig and M. Krämer. A global fit of the γ-ray galactic center excess within the scalar singlet Higgs portal model. *JCAP* **1606**, p. 050, 2016, hep-ph/1603.08228.

[59] J. Armando Arroyo and S. Ramos-Sanchez. One-loop corrections for Higgs-portal dark matter. *J. Phys. Conf. Ser.* **761**, p. 012014, 2016, hep-ph/1608.00791.

[60] S. He and S. Zhu. One-Loop radiative correction to the triple Higgs coupling in the Higgs singlet model. *Phys. Lett.* ***B764***, pp. 31-37, 2017, hep-ph/1607.04497.

[61] W. Chao. Hiding Scalar Higgs Portal Dark Matter. 2016, hep-ph/1601.06714.

[62] N. Darvishi and M. Krawczyk. CP violation in the Standard Model with a complex singlet. 2016, hep-ph/1603.00598.

[63] P. Ko and H. Yokoya. Search for Higgs portal DM at the ILC. *JHEP* **08**, p. 109, 2016, hep-ph/1603.04737.

[64] H. Han, J.M. Yang, Y. Zhang and S. Zheng. Collider signatures of Higgs-portal scalar dark matter. *Phys. Lett.* ***B756***, pp. 109-112, 2016, hep-ph/1601.06232.

[65] F.S. Sage and R. Dick. Gamma ray signals of the annihilation of Higgs-portal singlet dark matter. 2016, astro-ph.HE/1604.04589.

[66] K. Assamagan and others. The Higgs Portal and Cosmology. 2016, hep-ph/1604.05324.

[67] K. Hashino, M. Kakizaki, S. Kanemura, P. Ko and T. Matsui. Gravitational waves and Higgs boson couplings for exploring first order phase transition in the model with a singlet scalar field. *Phys. Lett.* ***B766***, pp. 49-54, 2017, hep-ph/1609.00297.

[68] V. Vaskonen. Electroweak baryogenesis and gravitational waves from a real scalar singlet. *Phys. Rev.* ***D95***, p. 123515, 2017, hep-ph/1611.02073.

[69] C. Balazs, A. Fowlie, A. Mazumdar and G.A. White. Gravitational waves at aLIGO and vacuum stability with a scalar singlet extension of the standard model. *Phys. Rev.* ***D95***, p. 043505, 2017, hep-ph/1611.01617.

[70] G. Arcadi, C. Gross, O. Lebedev, S. Pokorski and T. Toma. Evading direct dark matter detection in Higgs portal models. *Phys. Lett.* ***B769***, pp. 129-133, 2017, hep-ph/1611.09675.

[71] G. Chalons, D. López-Val, T. Robens and T. Stefaniak. The Higgs singlet extension at LHC Run 2. *PoS ICHEP2016*, p. 1180, 2016, hep-ph/1611.03007.

[72] I.M. Lewis and M. Sullivan. Benchmarks for double Higgs production in the singlet-extended standard model at the LHC. 2017, hep-ph/1701.08774.

[73] T. Kamon, P. Ko and J. Li. Characterizing Higgs portal dark matter models at the ILC. 2017, hep-ph/1705.02149.

[74] G. Kurup and M. Perelstein. Dynamics of electroweak phase transition in singlet-scalar extension of the standard model. 2017, hep-ph/1704.03381.

[75] G. Ria and D. Meloni. Radiative corrections of heavy scalar decays to gauge bosons in the singlet extension of the Standard Model. 2017, hep-ph/1705.11126.

[76] A. Fradette and M. Pospelov. BBN for the LHC: Constraints on lifetimes of the Higgs portal scalars. *Phys. Rev.* **D96**, p. 075033, 2017, hep-ph/1706.01920.

[77] A. Beniwal, M. Lewicki, J.D. Wells, M. White and A.G. Williams. Gravitational wave, collider and dark matter signals from a scalar singlet electroweak baryogenesis. *JHEP* **08**, p. 108, 2017, hep-ph/1702.06124.

[78] T. Hahn. Generating Feynman diagrams and amplitudes with FeynArts 3. *Comput. Phys. Commun.* **140**, pp. 418-431, 2001, hep-ph/0012260.

[79] C. Patrignani and others. Review of Particle Physics (RPP). *Chin. Phys.* **C40**, p. 100001, 2016 and 2017 update.

[80] W. Hollik. Quantum field theory and the Standard Model. 2010, hep-ph/1012.3883.

[81] W. Hollik. Electroweak Theory. 1995, hep-ph/9602380.

[82] A. Denner. Techniques for the calculation of electroweak radiative corrections at the one-loop level and results for W-physics at LEP200. *Fortsch. Phys.* **41**, pp. 307-420, 1993, hep-ph/0709.1075.

[83] M. Böhm, A. Denner and H. Joos. Gauge Theories of the Strong and Electroweak Interaction. *Teubner (Stuttgart, Germany)*, 2001.

[84] L.D. Faddeev and V.N. Popov. Feynman diagrams for the Yang-Mills field. *Phys. Lett.* **25B**, pp. 29-30, 1967.

[85] G. 't Hooft. Renormalization of massless Yang-Mills fields. *Nucl. Phys.* **B33**, pp. 173-199, 1971.

[86] G. 't Hooft. Renormalizable Lagrangians for massive Yang-Mills fields. *Nucl. Phys.* **B35**, pp. 167-188, 1971.

[87] C. Becchi, A. Rouet and R. Stora. The abelian Higgs Kibble model, unitarity of the S-operator. *Phys. Lett.* **B52**, pp. 344-346, 1974.

[88] C. Becchi, A. Rouet and R. Stora. Renormalization of the abelian Higgs-Kibble model. *Commun. Math. Phys.* **42**, pp. 127-162, 1975.

[89] C. Becchi, A. Rouet and R. Stora. Renormalization of gauge theories. *Ann. Phys.* **98**, pp. 287-321, 1976.

[90] G. 't Hooft and M.J.G. Veltman. Combinatorics of gauge fields. *Nucl. Phys.* **B50**, pp. 318-353, 1972.

[91] B.W. Lee and J. Zinn-Justin. Spontaneously Broken Gauge Symmetries. I. Preliminaries. *Phys. Rev.* **D5**, pp. 3121-3137, 1972.

[92] B.W. Lee and J. Zinn-Justin. Spontaneously Broken Gauge Symmetries. IV. General Gauge Formulation. *Phys. Rev.* **D7**, pp. 1049-1056, 1973.

[93] J.C. Taylor. Ward identities and charge renormalization of the Yang-Mills field. *Nucl. Phys.* **B33**, pp. 436-444, 1971.

[94] A.A. Slavnov. Ward identities in gauge theories. *Theor. Math. Phys.* **10**, pp. 99-107, 1972.

[95] T. Kugo and I. Ojima. Manifestly Covariant Canonical Formulation of Yang-Mills Field Theories. I. The Case of Yang-Mills Fields of Higgs-Kibble Type in Landau Gauge. *Prog. Theor. Phys.* **60**, pp. 1869-1889, 1978.

[96] T. Kugo and I. Ojima. Manifestly Covariant Canonical Formulation of Yang-Mills Field Theories. II. The Case of Pure Yang-Mills Theories without Spontaneous Symmetry Breaking in General Covariant Gauges. *Prog. Theor. Phys.* **61**, pp. 294-314, 1979.

[97] T. Kugo and I. Ojima. Local Covariant Operator Formalism of Non-Abelian Gauge Theories and Quark Confinement Problem. *Prog. Theor. Phys. Suppl.* **66**, pp. 1-130, 1979.

[98] B.W. Lee, C. Quigg and H.B. Thacker. Weak interactions at very high energies: The role of the Higgs-boson mass. *Phys. Rev.* **D16**, p. 1519, 1977.

[99] A. Arhrib. Unitarity constraints on scalar parameters of the Standard and Two Higgs Doublets Model. 2000, hep-ph/0012353.

[100] T. van Ritbergen and R.G. Stuart. Hadronic contributions to the muon lifetime. *Phys. Lett.* **B437**, pp. 201-208, 1998, hep-ph/9802341.

[101] T. van Ritbergen and R.G. Stuart. Complete 2-Loop Quantum Electrodynamic Contributions to the Muon Lifetime in the Fermi Model. *Phys. Rev. Lett.* **82**, pp. 488-491, 1999, hep-ph/9808283.

[102] B.W. Lee and J. Zinn-Justin. Spontaneously Broken Gauge Symmetries. II. Perturbation Theory and Renormalization. *Phys. Rev.* **D5**, pp. 3137-3155, 1972. [Erratum: Phys. Rev. **D8**, p. 4654, 1973].

[103] G. 't Hooft and M.J.G. Veltman. Regularization and renormalization of gauge fields. *Nucl. Phys.* **B44**, pp. 189-213, 1972.

[104] T. Hahn and M. Perez-Victoria. Automated one-loop calculations in four and D dimensions. *Comput. Phys. Commun.* **118**, pp. 153-165, 1999, hep-ph/9807565.

[105] C.G. Bollini and J.J. Giambiagi. Lowest order "divergent" graphs in ν-dimensional space. *Phys. Lett.* **40B**, pp. 566-568, 1972.

[106] E.C.G. Stueckelberg and A. Petermann. La normalisation des constantes dans la théorie des quanta. *Helv. Phys. Acta* **26**, pp. 499-520, 1953.

[107] M. Gell-Mann and F.E. Low. Quantum Electrodynamics at Small Distances. *Phys. Rev.* **95**, pp. 1300-1312, 1954.

[108] H. Lehmann, K. Symanzik and W. Zimmermann. Zur Formulierung quantisierter Feldtheorien. *Nuovo Cim.* **1**, pp. 205-225, 1955.

[109] W. Zimmermann. One particle singularities of green functions in quantum field theory. *Nuovo Cim.* **13**, pp. 503-521, 1959.

[110] K. Symanzik. On the Many-Particle Structure of Green's Functions in Quantum Field Theory. *J. Math. Phys.* **1**, pp. 249-273, 1960.

[111] K. Symanzik. Many-Particle Structure of Green's Functions. *Symposia on theoretical physics, Vol. 3, ed A. Ramakrishnan, New York*, pp. 121-170, 1967.

[112] D.A. Ross and J.C. Taylor. Renormalization of a unified theory of weak and electromagnetic interactions. *Nucl. Phys.* **B51**, pp. 125-144, 1973. [Erratum: Nucl. Phys. **B58**, p. 643, 1973].

[113] A. Sirlin. Radiative corrections in the $\mathrm{SU}(2)_L \times \mathrm{U}(1)$ theory: A simple renormalization framework. *Phys. Rev.* **D22**, pp. 971-981, 1980.

[114] W.J. Marciano and A. Sirlin. Radiative corrections to neutrino-induced neutral-current phenomena in the $\mathrm{SU}(2)_L \times \mathrm{U}(1)$ theory. *Phys. Rev.* **D22**, pp. 2695-2717, 1980. [Erratum: Phys. Rev. **D31**, p. 213, 1985].

[115] A. Sirlin and W.J. Marciano. Radiative corrections to $\nu_\mu + \mathrm{N} \to \mu^- + \mathrm{X}$ and their effect on the determination of ρ^2 and $\sin^2 \theta_\mathrm{W}$. *Nucl. Phys.* **B189**, pp. 442-460, 1981.

[116] D.Y. Bardin, P.K. Khristova and O.M. Fedorenko. On the lowest order electroweak corrections to spin-12 fermion scattering: (I). The one-loop diagrammar. *Nucl. Phys.* **B175**, pp. 435-461, 1980.

[117] D.Y. Bardin, P.K. Khristova and O.M. Fedorenko. On the lowest order electroweak corrections to spin-12 fermion scattering: (II). The one-loop amplitudes. *Nucl. Phys.* **B197**, pp. 1-44, 1982.

[118] J. Fleischer and F. Jegerlehner. Radiative corrections to Higgs-boson decays in the Weinberg-Salam model. *Phys. Rev.* **D23**, pp. 2001-2026, 1981.

[119] S. Sakakibara. Radiative corrections to the neutral-current interactions in the Weinberg-Salam model. *Phys. Rev.* **D24**, pp. 1149-1168, 1981.

[120] K.-I. Aoki, Z. Hioki, R. Kawabe, M. Konuma and T. Muta. One-Loop Corrections to ν-e Scattering in Weinberg-Salam Theory: Neutral Current Processes. *Prog. Theor. Phys.* **64**, pp. 707-710, 1980.

[121] K.-I. Aoki, Z. Hioki, R. Kawabe, M. Konuma and T. Muta. Electroweak Radiative Corrections to High Energy νe Scatterings. *Prog. Theor. Phys.* **65**, pp. 1001-1025, 1981.

[122] K.-I. Aoki, Z. Hioki, R. Kawabe, M. Konuma and T. Muta. Electroweak Theory: Framework of On-Shell Renormalization and Study of Higher-Order Effects. *Prog. Theor. Phys. Suppl.* **73**, pp. 1-225, 1982.

[123] M. Böhm, W. Hollik and H. Spiesberger. On the 1-Loop Renormalization of the Electroweak Standard Model and its Application to Leptonic Processes. *Fortsch. Phys.* **34**, pp. 687-751, 1986.

[124] M. Sperling, D. Stöckinger and A. Voigt. Renormalization of vacuum expectation values in spontaneously broken gauge theories. *JHEP* **07**, p. 132, 2013, hep-ph/1305.1548.

[125] D.Y. Bardin, W. Hollik and G. Passarino. Reports of the Working Group on precision calculations for the Z resonance. *CERN-95-03*, 1995.

[126] M. Steinhauser. Leptonic contribution to the effective electromagnetic coupling constant up to three loops. *Phys. Lett.* **B429**, pp. 158-161, 1998, hep-ph/9803313.

[127] F. Jegerlehner. Hadronic contributions to the photon vacuum polarization and their role in precision physics. *J. Phys.* **G29**, pp. 101-110, 2003, hep-ph/0104304.

[128] M. Awramik, M. Czakon, A. Freitas and G. Weiglein. Precise prediction for the W-boson mass in the standard model. *Phys. Rev.* **D69**, p. 053006, 2004, hep-ph/0311148.

[129] D.Y. Bardin, P. Christova, M. Jack, L. Kalinovskaya, A. Olchevski and others. ZFITTER v.6.21: A semi-analytical program for fermion pair production in $e^{+}e^{-}$ annihilation. *Comput. Phys. Commun.* **133**, pp. 229-395, 2001, hep-ph/9908433.

[130] A.B. Arbuzov, M. Awramik, M. Czakon, A. Freitas, M.W. Grünewald and others. ZFITTER: a semi-analytical program for fermion pair production in $e^{+}e^{-}$ annihilation, from version 6.21 to version 6.42. *Comput. Phys. Commun.* **174**, pp. 728-758, 2006, hep-ph/0507146.

[131] M.W. Grünewald. Combined electroweak analysis. *J. Phys. Conf. Ser.* **110**, p. 042008, 2008, hep-ph/0709.3744.

[132] LEP Electroweak Working Group, ALEPH Coll., CDF Coll., D0 Coll., DELPHI Coll., L3 Coll., OPAL Coll., SLD Coll., SLD Electroweak and Heavy Flavour Groups and Tevatron Electroweak Working Group. Precision Electroweak Measurements and Constraints on the Standard Model. 2010, hep-ex/1012.2367.

[133] ATLAS Collaboration. Study of the Higgs boson properties and search for high-mass scalar resonances in the $H \to ZZ^* \to 4\ell$ decay channel at $\sqrt{s} = 13$ TeV with the ATLAS detector. 2016.

[134] CMS Collaboration. Measurements of properties of the Higgs boson and search for an additional resonance in the four-lepton final state at $\sqrt{s} = 13$ TeV. 2016.

[135] R. Barate and others. Search for the Standard Model Higgs boson at LEP. *Phys. Lett.* **B565**, pp. 61-75, 2003, hep-ex/0306033.

[136] A. Djouadi and C. Verzegnassi. Virtual very heavy top effects in LEP/SLC precision measurements. *Phys. Lett.* **B195**, pp. 265-271, 1987.

[137] A. Djouadi. $O(\alpha\alpha_s)$ vacuum polarization functions of the standard-model gauge bosons. *Nuovo Cim.* **A100**, pp. 357-371, 1988.

[138] B.A. Kniehl. Two-loop corrections to the vacuum polarizations in perturbative QCD. *Nucl. Phys.* **B347**, pp. 86-104, 1990.

[139] F. Halzen and B.A. Kniehl. Δr beyond one loop. *Nucl. Phys.* **B353**, pp. 567-590, 1991.

[140] B.A. Kniehl and A. Sirlin. Dispersion relations for vacuum-polarization functions in electroweak physics. *Nucl. Phys.* **B371**, pp. 141-148, 1992.

[141] B.A. Kniehl and A. Sirlin. Effect of the $t\bar{t}$ threshold on electroweak parameters. *Phys. Rev.* **D47**, pp. 883-893, 1993.

[142] A. Djouadi and P. Gambino. Electroweak gauge boson self-energies: Complete QCD corrections. *Phys. Rev.* **D49**, pp. 3499-3511, 1994, hep-ph/9309298. [Erratum: Phys. Rev. **D53**, p. 4111, 1996].

[143] L. Avdeev, J. Fleischer, S. Mikhailov and O. Tarasov. $O(\alpha\alpha_s^2)$ correction to the electroweak ρ parameter. *Phys. Lett.* **B336**, pp. 560-566, 1994, hep-ph/9406363. [Erratum: Phys. Lett. **B349**, p. 597, 1995].

[144] K.G. Chetyrkin, J.H. Kühn and M. Steinhauser. Corrections of order $O(G_F M_t^2 \alpha_s^2)$ to the ρ parameter. *Phys. Lett.* **B351**, pp. 331-338, 1995, hep-ph/9502291.

[145] K.G. Chetyrkin, J.H. Kühn and M. Steinhauser. QCD Corrections from the Top Quark to Relations between Electroweak Parameters to Order α_s^2. *Phys. Rev. Lett.* **75**, pp. 3394-3397, 1995, hep-ph/9504413.

[146] K.G. Chetyrkin, J.H. Kühn and M. Steinhauser. Three-loop polarization function and $O(\alpha_s^2)$ corrections to the production of heavy quarks. *Nucl. Phys.* **B482**, pp. 213-240, 1996, hep-ph/9606230.

[147] Y. Schröder and M. Steinhauser. Four-loop singlet contribution to the electroweak ρ parameter. *Phys. Lett.* **B622**, pp. 124-130, 2005, hep-ph/0504055.

[148] K.G. Chetyrkin, M. Faisst, J.H. Kühn, P. Maierhöfer and C. Sturm. Four-Loop QCD Corrections to the Electroweak ρ Parameter. *Phys. Rev. Lett.* **97**, p. 102003, 2006, hep-ph/0605201.

[149] R. Boughezal and M. Czakon. Single scale tadpoles and $\mathcal{O}(G_F m_t^2 \alpha_s^3)$ corrections to the ρ parameter. *Nucl. Phys.* **B755**, pp. 221-238, 2006, hep-ph/0606232.

[150] A. Freitas, W. Hollik, W. Walter and G. Weiglein. Complete fermionic two-loop results for the $M_W - M_Z$ interdependence. *Phys. Lett.* **B495**, pp. 338-346, 2000, hep-ph/0007091. [Erratum: Phys. Lett. **B570**, p. 265, 2003].

[151] A. Freitas, W. Hollik, W. Walter and G. Weiglein. Electroweak two-loop corrections to the $M_W - M_Z$ mass correlation in the Standard Model. *Nucl. Phys.* **B632**, pp. 189-218, 2002, hep-ph/0202131. [Erratum: Nucl. Phys. **B666**, p. 305, 2003].

[152] M. Awramik and M. Czakon. Complete two loop electroweak contributions to the muon lifetime in the Standard Model. *Phys. Lett.* **B568**, pp. 48-54, 2003, hep-ph/0305248.

[153] M. Awramik and M. Czakon. Complete Two Loop Bosonic Contributions to the Muon Lifetime in the Standard Model. *Phys. Rev. Lett.* **89**, p. 241801, 2002, hep-ph/0208113.

[154] M. Awramik and M. Czakon. Two loop electroweak bosonic corrections to the muon decay lifetime. *Nucl. Phys. Proc. Suppl.* **116**, pp. 238-242, 2003, hep-ph/0211041.

[155] A. Onishchenko and O. Veretin. Two-loop bosonic electroweak corrections to the muon lifetime and $M_Z - M_W$ interdependence. *Phys. Lett.* **B551**, pp. 111-114, 2003, hep-ph/0209010.

[156] M. Awramik, M. Czakon, A. Onishchenko and O. Veretin. Bosonic corrections to Δr at the two-loop level. *Phys. Rev.* **D68**, p. 053004, 2003, hep-ph/0209084.

[157] M. Faisst, J.H. Kühn, T. Seidensticker and O. Veretin. Three loop top quark contributions to the ρ parameter. *Nucl. Phys.* **B665**, pp. 649-662, 2003, hep-ph/0302275.

[158] M. Awramik, M. Czakon and A. Freitas. Electroweak two-loop corrections to the effective weak mixing angle. *JHEP* **11**, p. 048, 2006, hep-ph/0608099.

[159] G. Aad and others. Measurements of the Higgs boson production and decay rates and constraints on its couplings from a combined ATLAS and CMS analysis of the LHC *pp* collision data at $\sqrt{s} = 7$ and 8 TeV. *JHEP* **08**, p. 045, 2016, hep-ex/1606.02266.

[160] ATLAS Collaboration. Projections for measurements of Higgs boson signal strengths and coupling parameters with the ATLAS detector at a HL-LHC. 2014, ATL-PHYS-PUB-2014-016.

[161] CMS Collaboration. Projected Performance of an Upgraded CMS Detector at the LHC and HL-LHC: Contribution to the Snowmass Process. 2013, hep-ex/1307.7135.

[162] M. Bicer and others. First look at the physics case of TLEP. *JHEP* **01**, p. 164, 2014, hep-ex/1308.6176.

[163] H. Abramowicz and others. Higgs physics at the CLIC electron-positron linear collider. *Eur. Phys. J.* **C77**, p. 475, 2017, hep-ex/1608.07538.

[164] K. Fujii and others. Physics Case for the 250 GeV Stage of the International Linear Collider. 2017, hep-ex/1710.07621.

[165] K. Peters. Prospects for beyond Standard Model Higgs boson searches at future LHC runs and other machines. *PoS CHARGED2016*, p. 028, 2017, hep-ex/1701.05124.

[166] T. Hahn. CUBA − a library for multidimensional numerical integration. *Comput. Phys. Commun.* **168**, pp. 78-95, 2005, hep-ph/0404043.

[167] A. Djouadi. The anatomy of electroweak symmetry breaking: Tome I: The Higgs boson in the Standard Model. *Phys. Rept.* **457**, pp. 1-216, 2008, hep-ph/0503172.

[168] J. Kalinowski A. Djouadi and M. Spira. HDECAY: a program for Higgs boson decays in the Standard Model and its supersymmetric extension. *Comput. Phys. Commun.* **108**, pp. 56-74, 1998, hep-ph/9704448.

[169] M. Spira, A. Djouadi, D. Graudenz and P.M. Zerwas. Higgs boson production at the LHC. *Nucl. Phys.* **B453**, pp. 17-82, 1995, hep-ph/9504378.

[170] A. Dabelstein and W. Hollik. Electroweak corrections to the fermionic decay width of the standard Higgs boson. *Z. Phys.* **C53**, pp. 507-516, 1992.

[171] B.A. Kniehl. Higgs phenomenology at one loop in the standard model. *Phys. Rept.* **240**, pp. 211-300, 1994.

[172] A. Bredenstein, A. Denner, S. Dittmaier and M.M. Weber. Precise predictions for the Higgs-boson decay $H \to WW/ZZ \to 4$ leptons. *Phys. Rev.* **D74**, p. 013004, 2006, hep-ph/0604011.

[173] A. Bredenstein, A. Denner, S. Dittmaier and M.M. Weber. Precision calculations for the Higgs decays $H \to ZZ/WW \to 4$ leptons. *Nucl. Phys. Proc. Suppl.* **160**, pp. 131-135, 2006, hep-ph/0607060.

[174] A. Bredenstein, A. Denner, S. Dittmaier and M.M. Weber. Radiative corrections to the semileptonic and hadronic Higgs-boson decays $H \to WW/ZZ \to 4$ fermions. *JHEP* **02**, p. 080, 2007, hep-ph/0611234.

[175] G.J. Gounaris, R. Kögerler and H. Neufeld. Relationship between longitudinally polarized vector bosons and their unphysical scalar partners. *Phys. Rev.* **D34**, pp. 3257-3259, 1986.

[176] K.G. Chetyrkin, J.H. Kühn and M. Steinhauser. RunDec: a Mathematica package for running and decoupling of the strong coupling and quark masses. *Comput. Phys. Commun.* **133**, pp. 43-65, 2000, hep-ph/0004189.

[177] T. van Ritbergen, J.A.M. Vermaseren and S.A. Larin. The four-loop β-function in quantum chromodynamics. *Phys. Lett.* **B400**, pp. 379-384, 1997, hep-ph/9701390.

[178] K.G. Chetyrkin, B.A. Kniehl and M. Steinhauser. Strong Coupling Constant with Flavor Thresholds at Four Loops in the Modified Minimal-Subtraction Scheme. *Phys. Rev. Lett.* **79**, pp. 2184-2187, 1997, hep-ph/9706430.

[179] K.G. Chetyrkin. Quark mass anomalous dimension to $O(\alpha_s^4)$. *Phys. Lett.* **B404**, pp. 161-165, 1997, hep-ph/9703278.

[180] J.A.M. Vermaseren, S.A. Larin and T. van Ritbergen. The 4-loop quark mass anomalous dimension and the invariant quark mass. *Phys. Lett.* **B405**, pp. 327-333, 1997, hep-ph/9703284.

[181] K.G. Chetyrkin, B.A. Kniehl and M. Steinhauser. Decoupling relations to $O(\alpha_s^3)$ and their connection to low-energy theorems. *Nucl. Phys.* **B510**, pp. 61-87, 1998, hep-ph/9708255.

[182] G. Rodrigo and A. Santamaria. QCD matching conditions at thresholds. *Phys. Lett.* **B313**, pp. 441-446, 1993, hep-ph/9305305.

[183] G. Rodrigo, A. Pich and A. Santamaria. $\alpha_s(m_Z)$ from τ decays with matching conditions at three loops. *Phys. Lett.* **B424**, pp. 367-374, 1998, hep-ph/9707474.

[184] G. Aad and others. Constraints on the off-shell Higgs boson signal strength in the high-mass ZZ and WW final states with the ATLAS detector. *Eur. Phys. J.* **C75**, p. 335, 2015, hep-ex/1503.01060.

[185] V. Khachatryan and others. Limits on the Higgs boson lifetime and width from its decay to four charged leptons. *Phys. Rev.* **D92**, p. 072010, 2015, hep-ex/1507.06656.

[186] V. Khachatryan and others. Search for Higgs boson off-shell production in proton-proton collisions at 7 and 8 TeV and derivation of constraints on its total decay width. *JHEP* **09**, p. 051, 2016, hep-ex/1605.02329.

Acknowledgments

My heartfelt gratefulness goes to my lovely grandparents Ruth and Gerhard Pietsch. From my early childhood on they always supported me in many ways. Thank you so much for everything!

The same I would like to say to my maternal grandparents Ina and Heinz Gerhard Kahle. For me you always set an example for high-mindedness, subtlety and a lot more. May you rest in peace.

Staying with my family which I hold in high regard, best wishes and warm thanks of course also go to my lovely aunts and uncles Elke and Rüdiger Jakob, Lucile Bertrand and Eckhard Kahle, Violandi Vratsanou and Martin Kahle as well as to my dear cousins Eleni and Leonid Kahle.

Finally, I would like to take the opportunity to say thank you to all of my friends. It is always a great pleasure to spend time together with you! I would particularly like to thank Andreas Heger, Tom Vermaaten, Alexander Rohloff, Christoph Erdle, Jacob Schäfer, Clemens Feigl, Ulrich Schütz, David Tartaglini $^{*\text{May you rest in peace}*}$ and Patrick Tartaglini for the deep friendship which grew from youth or childhood on. Also, I would particularly like to thank Erich Erdle for his support and advice during my studies.

I wish you all the very best!